Letter from the Editors

Dear readers of *Acta Naturae*!

We are delighted to bring you the last issue of 2014. What have we been able to accomplish by year 2015? For one, there is no doubt that we offer undeniable benefits to our authors: we translate and publish open-access full-text articles with colored illustrations, free of charge. A strict peer review process (at least two reviews by experts), as well as indexing in PubMed, Scopus, Web of Science, and the Russian Science Citation Index, has yielded good results. We have already reported that our journal's impact factor has reached 0.872. This year, *Acta Naturae* received the Thomson Reuters Awards MIPT for Increase in Scientific Productivity in Rising Star nomination. Of course, this fact imposes certain obligations on us. We do not strive to artificially boost the journal's impact factor. Improving the quality of our peer review and article selection processes are our only weapons. As we have mentioned, preliminary review by the Editorial Board prior to sending the article to two experts is now a routine, and this practice has yielded results. This year, we have also decided to move closer to the scientific community and to our young readers, in particular. We are planning to award diplomas to young scientists who have won the best poster competitions carried out at Russian conferences in the fields relevant to those featured in our journal. The winners of the competition at the IV International Scientific and Practice Conference Post-Genome Methods of Analysis in Biology and Laboratory and Clinical Medicine, held in Kazan (Russia) on October 29–November 1, 2014, have already received their diplomas. Let us take this opportunity to thank the organizers of the competition, Marina Viktorovna Tretyak and Vadim Markovich Govorun, for their hard work. The winners have been invited to publish their studies in the Short Reports section, which will certainly be peer-reviewed. The winners work in different Russian cities: Moscow, Nizhny Novgorod, Kazan, and Novosibirsk. We wish the young scientists success, and we are looking forward to publishing their articles.

This issue begins with a review devoted to the mechanism of activation of voltage-gated potassium channels (Grizel *et al.*) and it's followed by a research article that delves into the same subject matter (Vigont *et al.*). This subject matter resonates with other research articles published in the current issue (Efimova *et al.*, Chelombitko *et al.*, and Gaidukov *et al.*). We remained committed to highlighting issues of innate immunity, with allowance for a possible pharmaceutical orientation (Bagaev *et al.* and Shamova *et al.*). Two articles in the field of pharmacology are devoted to fluorescence imaging (Grebenik *et al.* and Terekhov *et al.*). An interesting synthetic study devoted to phosphoryl guanidines also found its way into this issue (Kupryushkin *et al.*). A new actinoporin family is reported in the study by Leychenko *et al.* The NMR and calculation studies are presented in high quality (Lyukmanova *et al.*).

We sincerely wish you a New Year 2015 filled with new research accomplishments! ●

Editorial Board

INNOVATION RUSSIA

Discussion club

We create a dialogue between all socially active groups of people: students, scientists, lecturers, businessmen, managers, innovators, investors, designers, art critics, architects, photographs.

Learn more at WWW.STRF.RU

Everyone with something to say and ideas to share is welcome to visit our events

Tel.: +7 (495) 930-87-07, 930-88-50
E-mail: seminar@strf.ru

Regulation of the Target Protein (Transgene) Expression in the Adenovirus Vector Using Agonists of Toll-Like Receptors

A. V. Bagaev, A. V. Pichugin, E. S. Lebedeva, A. A. Lysenko, M. M. Shmarov, D. Yu. Logunov, B. S. Naroditsky, R. I. Ataullakhanov, R. M. Khaitov, A. L. Gintsburg

Toll-like receptor (TLR) agonists (namely, TLR2, 4, 5, 7, 8 and 9) are shown to enhance production of the target protein in cells transduced with recombinant adenoviral vector (rAd) encoding this target protein. Overexpression is observed in dendritic cells and macrophages expressing cytoplasmic, membrane, or secretory proteins. The role of the signaling pathways MyD88 → NF-kB and TRIF → IRF, respectively, in activation and suppression of production of protein encoded by the transgene in the context of rAd vector is discussed.

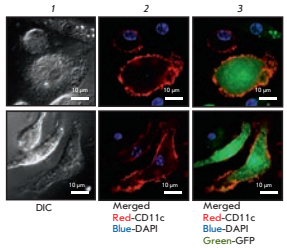

Confocal microscopy of dendritic cells transduced with rAd-GFP

Investigation of Channel-Forming Activity of Polyene Macrolide Antibiotics in Planar Lipid Bilayers in the Presence of Dipole Modifiers

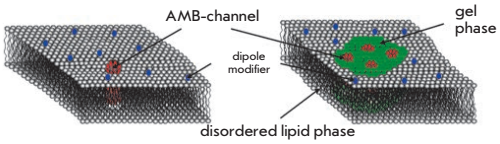

Schematic representation of the microenvironment of AMB channels in membranes with different concentrations of polyene antimycotics, corresponding to the functioning of single channels and the integral multi-channel current

S. S. Efimova, L. V. Shchagina, O. S. Ostroumova

The study is devoted to determining the role of various membrane components in the formation and functioning of ion-permeable nanopores formed by antifungal polyene macrolide antibiotics in model membranes. Dipole modifiers are used as tools for the study. The role of the membrane dipole potential, polyene-sterol and polyene-lipid interactions, as well as physicochemical properties of ordered membrane domains in polyene channel-forming activity of polyene macrolide antibiotics, is discussed.

A Cytofluorometric Study of Membrane Rafts in Human Monocyte Subsets in Atherosclerosis

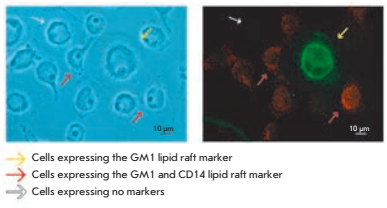

Immunocytochemical staining of cultured monocytes/macrophages from a healthy subject

M. A. Chelombitko, V. S. Shishkina, O. P. Il'inskya, A. I. Kaminnyi, T. O. Pavlunina, N. N. Samovilova, E. V. Gracheva, E. M. Tararak, N.V. Prokazova

A comparative study of membrane rafts of various monocyte subpopulations in the blood of atherosclerosis patients compared to healthy volunteers was conducted by flow cytofluorometry in order to elucidate the tentative mechanism of preactivation of circulating monocytes. It is suggested that peripheral blood monocytes in atherosclerosis accumulate gangliosides that are used to form membrane rafts during the macrophage differentiation after the migration of monocytes into the arterial intima.

ActaNaturae
OCTOBER–DECEMBER 2014 VOL. 6 № 4 (23)

Founders
Ministry of Education and
Science of the Russian Federation,
Lomonosov Moscow State University,
Park Media Ltd

Address: 119234 Moscow, Russia, Leninskiye Gory, Nauchny
Park MGU, vlad.1, stroeniye 75G.
Phone/Fax: +7 (495) 930 88 50
E-mail: vera.knorre@gmail.com, mmorozova@strf.ru,
actanaturae@gmail.com

Номер подписан в печать 21 ноября 2014 г.
Тираж 200 экз. Цена свободная.
Отпечатано в типографии «МЕДИА-ГРАНД»

Indexed in Pubmed, Web of Science, Scopus, and RISC

CONTENTS

Letter from the Editors 1

FORUM

A. E. Voinov, I. B. Khlebnikov,
Sh. A. Dzhabrailov
Reform of the Current Legislation Procedure for Importing and Exporting Research Materials . . 6

REVIEWS

A. V. Grizel, G. S. Glukhov, O. S. Sokolova
Mechanisms of Activation of Voltage-Gated Potassium Channels 10

RESEARCH ARTICLES

A. V. Bagaev, A. V. Pichugin, E. S. Lebedeva,
A. A. Lysenko, M. M. Shmarov, D. Yu.
Logunov, B. S. Naroditsky, R. I. Ataullakhanov,
R. M. Khaitov, A. L. Gintsburg
Regulation of the Target Protein (Transgene) Expression in the Adenovirus Vector Using Agonists of Toll-Like Receptors 27

V. A. Vigont, O. A. Zimina, L. N. Glushankova,
J. A. Kolobkova, M. A. Ryazantseva,
G. N. Mozhayeva, E. V. Kaznacheyeva
STIM1 Protein Activates Store-Operated Calcium Channels in Cellular Model of Huntington's Disease 40

E. A. Grebenik, A. N. Generalova,
A. V. Nechaev, E.V. Khaydukov, K. E. Gobova,
O. A. Stremovskiy, A. V. Zvyagin, S. M. Deyev
Specific Visualization of Tumor Cells Using Upconversion Nanophosphors 48

S. S. Terekhov, I. V. Smirnov, O. G. Shamborant, M. A. Zenkova, E. L. Chernolovskaya, D. V. Gladkikh, A. N. Murashev, I. A. Dyachenko, V. D. Knorre, A. A. Belogurov, N. A. Ponomarenko, S. M. Deyev, V. V. Vlasov, A. G. Gabibov

Excessive Labeling Technique Provides a Highly Sensitive Fluorescent Probe for Real-time Monitoring of Biodegradation of Biopolymer Pharmaceuticals *in vivo* 54

E. N. Lyukmanova, M. A. Shulepko, M. L. Bychkov, Z. O. Shenkarev, A. S. Paramonov, A. O. Chugunov, A. S. Arseniev, D. A. Dolgikh, M. P. Kirpichnikov

Human SLURP-1 and SLURP-2 Proteins Acting on Nicotinic Acetylcholine Receptors Reduce Proliferation of Human Colorectal Adenocarcinoma HT-29 Cells 60

S. S. Efimova, L. V. Schagina, O. S. Ostroumova

Investigation of Channel-Forming Activity of Polyene Macrolide Antibiotics in Planar Lipid Bilayers in the Presence of Dipole Modifiers 67

M. A. Chelombitko, V. S. Shishkina, O. P. Ilyinskaya, A. I. Kaminnyi, T. O. Pavlunina, N. N. Samovilova, E. V. Gracheva, E. M. Tararak, N. V. Prokazova

A Cytofluorometric Study of Membrane Rafts in Human Monocyte Subsets in Atherosclerosis 80

E. V. Leichenko, M. M. Monastirnaya, E. A. Zelepuga, E. S. Tkacheva, M. P. Isaeva, G. N. Likhatskaya, S. D. Anastyuk, E. P. Kozlovskaya

Hct-A Is a New Actinoporin Family from the *Heteractis Crispa* **Sea Anemone** 89

O. V. Shamova, D. S. Orlov, S. V. Balandin, E. I. Shramova, E. V. Tsvetkova, P. V. Panteleev, Yu. F. Leonova, A. A. Tagaev, V. N. Kokryakov, T. V. Ovchinnikova

Acipensins — Novel Antimicrobial Peptides from Leukocytes of the Russian Sturgeon *Acipenser gueldenstaedtii* 99

A. E. Gaydukov, P. O. Bogacheva, E. O. Tarasova, O. P. Balezina

The Mechanism of Choline-Mediated Inhibition of Acetylcholine Release in Mouse Motor Synapses 110

SHORT REPORTS

M. S. Kupryushkin, D. V. Pyshnyi, D. A. Stetsenko

Phosphoryl Guanidines: A New Type of Nucleic Acid Analogues 116

Guidelines for Authors 119

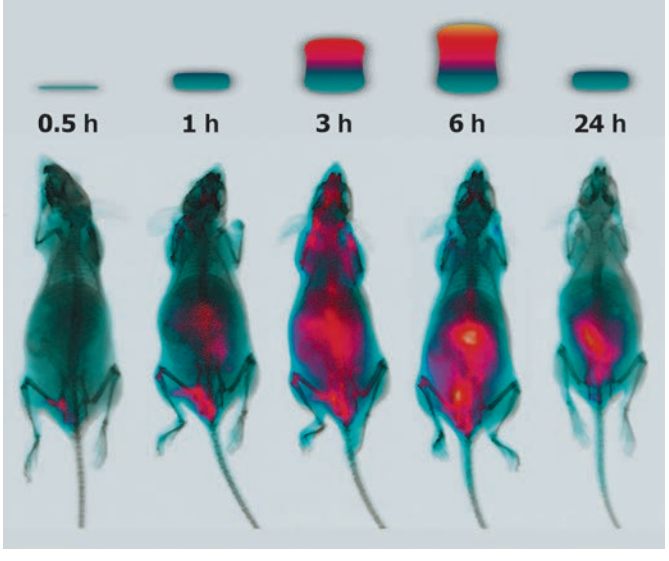

IMAGE ON THE COVER PAGE
See the article by Terekhov *et al.*

Reforming Current Legislation On the Import and Export of Research Materials

A. E. Voinov, I. B. Khlebnikov, Sh. A. Dzhabrailov*
Autonomous Non-Profit Organization for Higher Education "Skolkovo Institute of Science and Technology"
*E-mail: s.jabrailov@skoltech.ru

The current procedure for importing and exporting materials for research and development activity prevents their prompt delivery, which leads to a decrease in the effectiveness of research and development activity conducted by Russian scientific and educational organizations. A simplified procedure for importing and exporting research materials (issuing a uniform permit required for importing and exporting research materials into and from the Russian Federation) is proposed at the legislative level.

As Russia proceeds to an innovation-driven economic development model, reforms aimed at stimulating research and development activity (hereinafter referred to as R&D) and improving R&D performance are currently underway. Along with other factors, the possibility of prompt delivery of the materials and equipment required for organizing and conducting R&D is among the key factors that predicate the success and effectiveness of R&D. Leading Russian scientists and experts continue to insist that the current procedure for importing and exporting research materials does not allow one to ensure prompt delivery: thus, it hampers the effectiveness of the R&D conducted by Russian scientific and educational organizations and curtails the ability of Russian scientists to participate in international research projects. One of the major problems is the overbearing legislative control (multiple legal norms concerning the same issues) that accompany the importing and exporting of biological materials, including human materials, reagents, and laboratory animals (hereinafter referred to as research materials), which requires going through a large number of approval processes to obtain the permit documents required to import/export research materials (permits, veterinary certificates, etc.).

At the current stage, the working group of the Skolkovo Institute of Science and Technology (hereinafter referred to as the working group) has developed recommendations on improving the current rules and regulations governing the import/export of research materials.

It seems reasonable to regulate the import/export of research materials based on a comprehensive approach. This approach involves the establishment of a simplified procedure for importing/exporting research materials by issuing a uniform permit for importing/exporting research materials into and from the Russian Federation, which would be valid for an unlimited period of time with respect to the types of research materials specified in it and their hazard (pathogenicity) classes; expedited customs clearance of these research materials; application of special simplified procedures foreseen in article 197 of the Customs Code of the Customs Union [1] to certain categories of research materials (a simplified declaration procedure for research materials in accordance with article 178 of the Customs Code of the Customs Union); application of a simplified declaration procedure to research materials, identical to that foreseen in articles 279 and 283 of the Federal Law On Customs Regulation in the Russian Federation [2] for commercial and research samples.

Furthermore, subsequent control over the targeted use of research materials imported into the Russian Federation in compliance with the simplified procedure by scientific and educational organizations needs to be established. In this connection, it is reasonable to provide control mechanisms that would include the following components:

- state accreditation of organizations entitled to use the simplified procedure for importing/exporting research materials and establishing a registry of the accredited scientific and educational organizations, imposing requirements on these organizations, including the requirements concerning the development and implementation of in-house pro-

grams for controlling the use of research materials at these organizations;
- imposing reporting requirements on the accredited scientific and educational organizations and establishing mechanisms for controlling the targeted use of research materials by the authorized federal executive bodies;
- identifying new research materials, characterizing research materials into hazard (pathogenicity) classes, and establishing a registry of research materials; and
- establishing penalties for the non-targeted use of research materials.

The order of using the simplified procedure for importing/exporting research materials into/from the Russian Federation by scientific and educational organizations is suggested to be as follows:
- The authorized federal executive body (hereinafter referred to as AFEB) shall organize state accreditation of scientific and educational organizations participating in import and export, which have established in-house programs for controlling the use of research materials; shall issue the uniform permit for importing/exporting research materials for the purposes of conducting R&D into/from the Russian Federation (hereinafter referred to as uniform permit); and shall keep the registry of accredited organizations;
- The AFEB shall render a decision on state accreditation of scientific and educational organizations based on their applications if they comply with the requirements. The AFEB shall issue a uniform permit for importing/exporting research materials according to the simplified procedure to the accredited scientific or educational organizations (material type and hazard class being specified);
- the accredited scientific or educational organizations are entitled to import/export research materials into/from the Russian Federation based on the uniform permit, without the need to provide any additional permitting documents (except for licenses and permits issued in accordance with the legislation of the Russian Federation concerning narcotic drugs, psychoactive substances and their precursors (except for the precursors listed in Table III of Registry IV [3]), as well as veterinary and phytosanitary certificates);
- scientific and educational organizations shall undertake the obligation to use research materials only for R&D, without the right to transfer the material to third parties, either for compensation or free of charge (except for the transferring of research materials under research collaboration, while retaining control over targeted use of these materials);
- scientific and educational organizations entitled to use the simplified procedure for importing/exporting research materials shall report on all materials that have been imported/exported and their consumption to the AFEB. The AFEB shall perform a regular inspection of the control over the targeted use of materials (if needed, with the assistance of other appropriate federal executive bodies).

It is also reasonable that the federal data resource devoted to the import/export of research materials into/from the Russian Federation be established, which would contain thorough and well-structured information on rules and regulations in the field of import/export of research materials into/from the Russian Federation, including the title and matter of the legal acts; the edition they have been published; the information on the procedure of assigning code numbers of the Foreign Economic Activity Commodity Nomenclature of the Customs Union to research materials; and other legal, reference, and analytical information related to the import/export of research materials into/from the Russian Federation.

An overhaul of the current legislation for importing/exporting research materials based on the proposed recommendations would significantly expedite the import/export of research materials and, therefore, increase the effectiveness and performance of R&D conducted by Russian scientific and educational organizations, and broaden opportunities for Russian scientists to participate in international collaborative R&D projects. ●

REFERENCES

1. The Customs Code of the Customs Union (Appendix to the Agreement on the Customs Code of the Customs Union approved by Decree of the Interstate Council of the Eurasian Economic Community No. 17 dated November 27, 2009).
2. The Federal Law No. 311-FZ dated November 27, 2010 (revised June 4, 2014) On Customs Regulation in the Russian Federation.
3. Decree No. 681 of the RF Government dated June 30, 1998, On Approval of the List of Narcotic Drugs, Psychotropic Substances and Their Precursors Subject to Control in the Russian Federation (amended and revised).

A COMMENT ON THE INFORMATION PRESENTED BY THE WORKING GROUP OF THE SKOLKOVO INSTITUTE OF SCIENCE AND TECHNOLOGY

Acta Naturae focuses again on the problem of customs handling of research materials (AN 2010, vol. 2, No. 2(5)).

The debate-provoking article presented by the Skolkovo Institute of Science and Technology (Skoltech) provides a rather detailed overview of the "possible formalization" of customs clearance of research materials and equipment. Since the very first publication in our journal and my speech at the meeting chaired by D.A. Medvedev on March 11, 2011, the number of problems associated with exporting high-tech products for Russian scientists has increased. It is absolutely clear that a Russian researcher has to buy reagents and equipment abroad with an extra charge (50, and sometimes even 100%) and wait for them to be delivered for 1–2 months. It is a systemic problem. The Russian market is rather small, and prominent players in the research industry usually find it unprofitable to keep large warehouses in Russia. How can the state help Russian researchers who are not involved in commercial activity and the research companies deriving profits from their research activity (it should be mentioned that these companies have not been paid due attention in Skoltech's publication)?. The information presented in the article seems to be excessively formalized to me. There is a well-defined problem related to customs code numbers. All high-tech goods contributing to the development of the country's potential should be indicated with a special mark in the customs reference books. It is a large amount of work, and qualified experts are needed to have it done. Verification is rather simple: relatively small quantities of these groups of goods are imported, and the use of the code numbers for "research goods" to import regular commodity goods can be avoided. Special attention should be paid to products requiring special storage conditions, such as deep freezing (e.g., cell lines). These products should be given a special status in the customs reference books and have the proper legal requirements for conditions and duration of customs clearance. Failure to comply with these requirements should imply a penalty for the customs officers responsible for the violation in accordance with the established procedure. As for the certificates for hazardous chemical or biological materials, one-stop shop service should be established at customs terminals. Specially trained experts who can make adequate decisions according to the established procedure should work in this service. Certificates complying with the international regulations and preventing ambiguous interpretation should be elaborated. A terminal lacking such services should be temporarily closed. This measure would prevent getting the runaround and make customs clearance of research materials a much faster procedure. What about the "scientific export" (in other words, sending genetic constructs, or proteins, or samples to one's foreign colleagues to conduct joint studies)? It is clear that a non-bureaucratic structure of customs certification needs to be established, involving the Federal Agency for Scientific Organizations, the Ministries of Healthcare and Education, and Federal universities. The issued certificate should constitute grounds for export customs clearance. The key is to work with qualified experts at all stages rather than with people who try to wall themselves off from the existing problem because of lack of knowledge or understanding of the situation. One should be aware, however, that there still will be some violations, but it is a problem that law enforcement authorities are supposed to deal with. ●

Aleksandr Gabibov

The editorial board of *Acta Naturae* has invited representatives of Sigma-Aldrich to comment on the article by Voinov *et al*. from the Skolkovo Institute of Science and Technology. Sigma-Aldrich is among the key importers of self-produced materials for chemical and biological research into Russia. The representatives of Sigma-Aldrich have commented on such aspects as excessive legislative control over the import (exporting) of biological materials, the lenght of the customs clearance process, etc.

Leading Russian scientists and experts keep saying that the current procedure for importing and exporting research materials does not allow one to ensure prompt delivery, thus reducing the effectiveness of the research conducted by Russian scientific and educational establishments and limits the chances of Russian scientists to participate in international research projects.

Today, if no additional permits are required, the customs clearance of research materials takes 1–2 days.

One of the major problems is the excessive legislative control (multiple legal norms concerning the same issues) in importing and exporting biological materials, including human materials, reagents, and laboratory animals.

The "excess" legislative control in this field is needed to prevent importing or exporting of hazardous materials. It is a high-risk commodity group, and the requirement to provide a large number of permits is more than

justified. Furthermore, preferences are provided in description to certain code numbers of the Commodity Classifier for Foreign Economic Activities. Thus, a product with the specification "for laboratory studies" can be imported without any additional permits.

At the current stage, the working group of the Skolkovo Institute of Science and Technology (hereinafter referred to as the working group) has elaborated recommendations for improving the current procedure of importing (exporting) materials for research and diagnostics.

Issuing a uniform permit seems infeasible, since the list of research materials is too long and is continuously being updated (e.g., Sigma-Aldrich catalogue contains over 300,000 items). They can be classified into absolutely different commodity groups and are regarded as potentially high-risk goods requiring special attention when being imported into the Russian Federation.

State accreditation of organizations entitled to use the simplified procedure for importing (exporting) research materials and establishing a registry of accredited scientific and educational institutions, imposing requirements to these organizations, including the requirements concerning the development and implementation of in-house programs for controlling research materials at these organizations.

Research materials are typically imported by commercial companies rather than by research institutions. As research institutions are not foreign trade operators, they buy these materials from importers. Therefore, I would rather be speaking about establishment of state accreditation for the importers of research materials.

The certified federal executive agency (hereinafter referred to as CFEA) shall render a decision on state accreditation of scientific and educational institutions based on applications if they comply with the requirements. The CFEA shall issue a uniform permit for importing (exporting) research materials according to the simplified procedure to the accredited scientific or educational institutions (material type and hazard class being specified).

It is impossible to use a single import permit to embrace the catalogue including 300,000 research items, which is constantly updated. The permit for a uniform code number will make it extremely difficult and almost infeasible to monitor the fate of these materials in Russia in order to determine their targeted (non-targeted) use. Furthermore, it may facilitate criminal intent.

Scientific and educational institutions shall undertake an obligation to use materials only for research and experimental developments, without the right to transfer the material to third parties, either for a compensation or free of charge (except for transferring research materials under research collaboration, while retaining the control over targeted use of these materials).

Unification would make control infeasible for the reasons described above.

It is also reasonable that a federal data resource devoted to import/export of research materials into/from the Russian Federation be established.

This data resource is available at any customs office, any customs station and any customs declarant has it as a part of specialized customs software. It provides comprehensive data on the Commodity Classifier for Foreign Economic Activities and regulatory acts of foreign economic activities. In addition, it is used as a database of all the imported and exported goods. If needed, the data can be copied from this resource to a separate website. ●

Andrey Zubkov, foreign economic activity and logistics director, Sigma-Aldrich Russia

Mechanisms of Activation of Voltage-Gated Potassium Channels

A. V. Grizel[1], G. S. Glukhov[2], O. S. Sokolova[2]*
[1]Saint Petersburg State University, 7-9, Universitetskaya nab., 199034, St. Petersburg, Russia
[2]Biological Faculty of Moscow State MV Lomonosov University, 1, Leninskie Gory, Bld. 12, 119991, Moscow, Russia
*E-mail: sokolova@mail.bio.msu.ru

ABSTRACT **Voltage-gated potassium ion channels (Kv) play an important role in a variety of cellular processes, including the functioning of excitable cells, regulation of apoptosis, cell growth and differentiation, the release of neurotransmitters and hormones, maintenance of cardiac activity, etc. Failure in the functioning of Kv channels leads to severe genetic disorders and the development of tumors, including malignant ones. Understanding the mechanisms underlying Kv channels functioning is a key factor in determining the cause of the diseases associated with mutations in the channels, and in the search for new drugs. The mechanism of activation of the channels is a topic of ongoing debate, and a consensus on the issue has not yet been reached. This review discusses the key stages in studying the mechanisms of functioning of Kv channels and describes the basic models of their activation known to date.**

KEYWORDS **activation; potassium ion channels; modeling; structure.**

ABBREVIATIONS **Kv – voltage-gated potassium channel; aa – amino acid residue; VSD, voltage-sensing domain; SHM – sliding-helix model; TM – transport model; PM, paddle model; CMH, model of coordinated movement of helices; CM – consensus model; MCT – model of charge transfer; MKD – model of Kv deactivation; MMd – mechanistic model of Kv activation/deactivation; FRET – Förster resonance energy transfer; MM – molecular modeling; CTC – charge transfer center, MD – molecular dynamics; GC – gate channel.**

INTRODUCTION

Membrane proteins account for ~30% of the total proteome of an organism, with about half of this number being carrier proteins and ion channels. Potassium ion channels represent the most diverse and widespread class of membrane proteins [1]. Depending on the functioning principle and based on the primary structure of a channel-forming subunit, these proteins are subdivided into inwardly rectifying channels (Kir), Ca^{2+}-activated channels (KCa), two-pore domain (K2P), and voltage-gated (Kv) channels. Kv channels form the most diverse group (*Fig. 1*), represented by 12 families (Kv1-Kv12) [2].

All Kv channels play an important regulatory role in various cellular processes. These proteins participate in the functioning of excitable cells [3–5], regulation of apoptosis [6], as well as cell differentiation and growth [7]. Correct functioning of Kv channels is necessary for the release of neurotransmitters [8] and hormones [9, 10], for maintenance of cardiac activity [11], etc.

Mutations in the genes of Kv channels can lead to various severe hereditary disorders [12], including deafness, epilepsy [13], and certain types of cardiac rhythm disorders [11]. They are also involved in the pathogenesis of multiple sclerosis and the pain syndrome [14]. Kv channels are also linked to the processes of tumor onset and development, including in malignant tumors [15].

Functioning of Kv channels can be modulated by using activators and blockers [16]; therefore, they represent perspective drug targets [17, 18]: hence, studying the structure and function of Kv channels is an important task.

QUATERNARY STRUCTURE OF Kv CHANNELS

All Kv channels have a high level of similarity. Each Kv channel gene encodes one α-subunit (Kvα). Four α-subunits are required to form a functional channel (*Fig. 2*) [19, 20]. Kv channels usually have a homotetrameric structure (with all Kvα being identical) [19, 20]; however, some channels can be heterotetrameric (with two or more non-identical Kvα subunits).

The transmembrane domain of the Kv channel α-subunit consists of six helices: S1–S6 (*Fig. 2A,B*). These helices form two structurally and functionally different parts of the tetrameric channel: 1) a potassium ion-conducting domain (pore domain) – helices S5–S6 located in the channel center, and 2) a domain

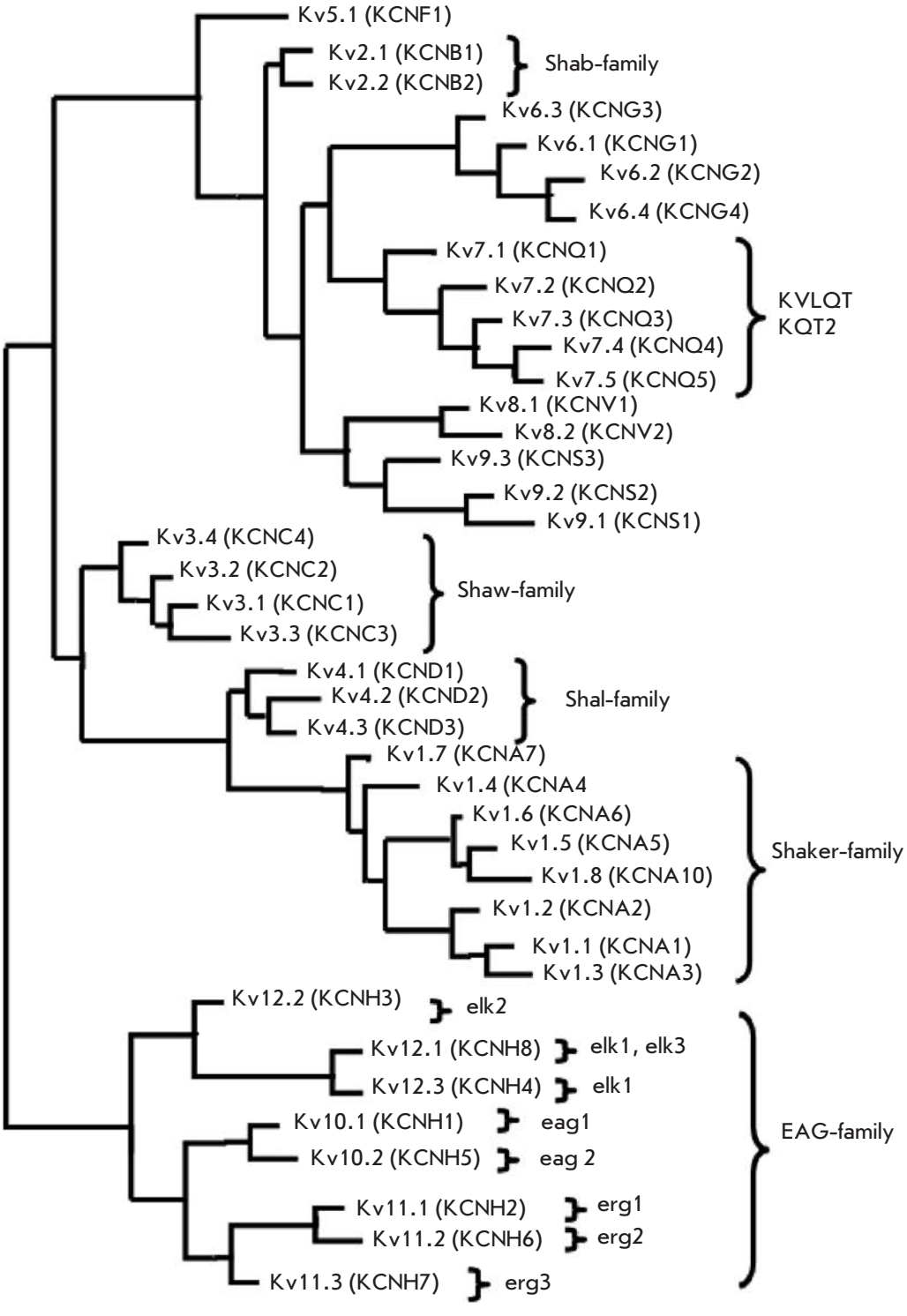

Fig. 1. The phylogenetic tree of Kv channels based on the alignment of amino acid sequences. Braces combine channels belonging to the same family. Names are given according to the system of the International Union of Pure and Applied Chemistry (IUPAC) (alternative names according to the Gene Nomenclature Committee of the Human Genome Organization [2] are given in brackets)

sensible to changes in the membrane potential (voltage-sensing domain, VSD) – helices S1–S4 located on the channel periphery (*Fig. 2B,C*).

The pore part includes a channel gate and a selective filter that does not allow ions other than K^+ to penetrate through the channel. The channel gate is formed by crossing C-termini of the S6 helices that block passage of ions when the channel is closed [22-24]. A conserved fragment (P-region) and a S5–S6 loop participate in the formation of the selectivity filter of the channel (*Fig. 2*).

It is known that VSD and the pore domain are covalently bound by the S4–S5 linker, an amphiphylic helix

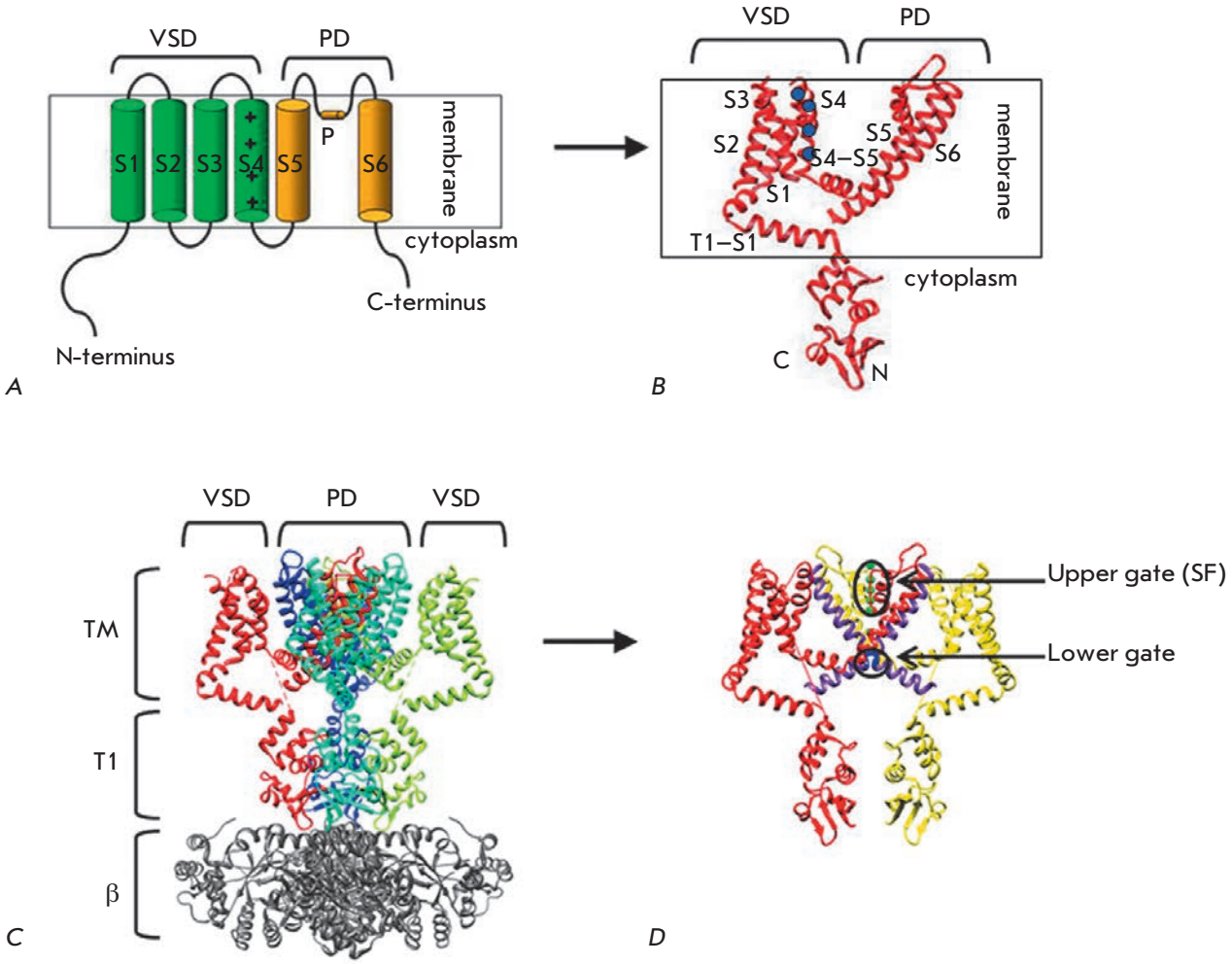

Fig. 2. Structure of Kv channels. A. Scheme of a single α-subunit of the Kv channel. Transmembrane segments S1–S6 and pore-forming P-loop are marked. Charged Arg of the membrane voltage sensor S4 are marked with "+" signs. PD – pore domain. B. Crystal structure of a single α-subunit of the Kv1.2 channel [21]. S1–S6 segments, cytoplasmic domain T1, linker connecting the transmembrane portion with the T1 domain (T1–S1), as well as N- and C-termini are marked. Charged Arg residues of the membrane voltage sensor S4 are indicated by blue circles. C. Crystal structure of the Kv1.2 channel in a complex with the β-subunit (marked as β, grey colored) (modified from [21]). TM – transmembrane region. D. Gate of the Kv2.1 channel. Only two opposite subunits of Kvα are shown for clarity reasons. The S6 helix is shown in purple, the blue color denotes a highly conserved portion of $S6_T$ – PXP helix (Pro-Val-Pro in Kv2.1), a key component of the lower gate. Green spheres mark K^+ ions in the selectivity filter (P-loop), which represents the upper gate of the channel

connected to the C-terminus of S6 helix ($S6_T$) and the next subunit [21, 25–30]. The highly conserved region of the $S6_T$ helix plays an important role in the opening/closing of the channel gates and consists of two Pro residues usually separated by Val or another amino acid, PXP (*Fig. 2D*). This region is flexible, which allows the channel to open [21]. Kv channels have two gates: (1) the lower gate (LG) formed by crossing the S6 helices on the intracellular side, and (2) the upper gate (UG) formed by the P-loop of the selectivity filter on the extracellular side (*Fig. 2D*). In the Kv channels, as well as in the majority of other potassium channels, LG are the main activation gates controlled by external stimuli, such as the membrane potential. Inner S6 helices intercross, similarly to the blades in the iris diaphragm of a photographic camera, and they open/close in a similar manner.

Besides the transmembrane part, Kv channels have a cytoplasmic part formed by N- and C-termini (*Fig. 2*). The cytoplasmic part does not contain highly conserved regions and is different for Kv channels from different families [31].

In cells, Kv channels function in the form of large macromolecular complexes comprising ion-conducting α-subunits, auxiliary cytoplasmic and/or transmembrane β-subunits, as well as regulatory and supporting proteins [32] (*Fig. 2C*). The assembly of pore-forming α-subunits and the auxiliary subunits of Kv channels in mammals takes place in the endoplasmic reticulum, where they form a stable complex [33]. α-Subunits form the ion pore, while β-subunits (*Fig. 2B,C*) and other auxiliary subunits modulate the properties and functions of α-subunits. This complexity of the structural forms determines the wide variety of the properties and functions of Kv channels [34].

ACTIVATION OF Kv CHANNELS

All Kv channels share a similar mechanism of activation. They can be present in three functional states: quiescent state (closed conformation) ↔ activated state (open conformation) ↔ inactivated state (*Fig. 3*).

The channel does not conduct the ions in the quiescent state. Depolarization of the membrane results in positive charge of its intracellular part, causing conformational rearrangements of Kv channels and making an open conformation energetically favorable. This rearrangement is termed the activation of channel [36]. In case the membrane remains depolarized, the majority of Kv channels switch to the inactivated non-conducting state. Two basic inactivation types termed N and C have been described so far (*Fig. 3*). Fast N-type inactivation is mediated by an inactivation peptide folded into a globule and attached by a linker to the N-terminus of either an α-subunit (α-ball) or a β-subunit (β-ball) [3, 37]. The inactivation peptide enters the open pore of the channel and blocks ion traffic [3, 38, 39]. In case of slow inactivation (C-type), the selectivity filter acts as the second gate and closes, preventing the entry of ions [4, 40–42]. The channels completely return to the closed conformation after the inactivation when the potential drops to the resting potential level.

The mechanism of channel activation remains a topic of debate. Knowledge of the atomic structure of the channel in various functional states and in at least two final conformations (open and closed) is necessary for a comprehensive understanding of this issue. The majority of the crystal structures of Kv channels [21, 43, 44] have been obtained in the open state; therefore, the models of Kv channels activation are often created on the basis of structural information acquired by various experimental approaches and molecular modeling (MM) [43, 45–53]. These models form the basis for reasonable interpretations of the obtained results and design of further experiments. As of today, an extensive amount of data pointing to the features of the Kv channels structure in the open and closed conformations has been collected. The modern models of activation largely converge to a single consensus model of channel opening [54–57]. All these models are based on earlier key experiments and activation models.

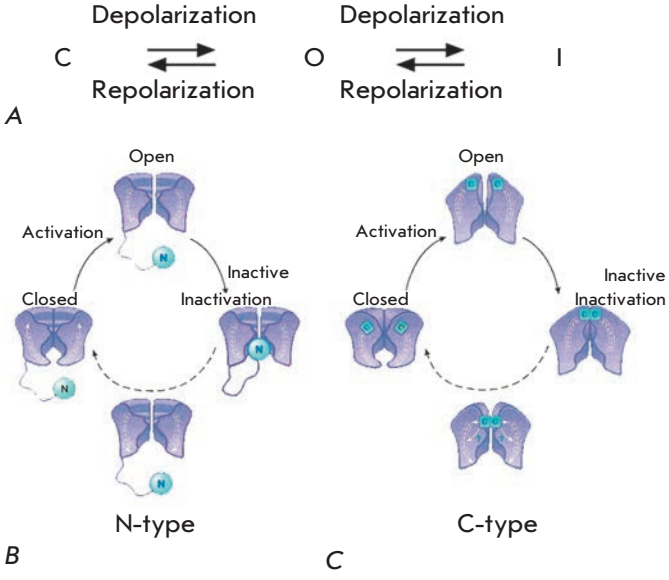

Fig. 3. A. Scheme of the conformational transitions in Kv channels: C – closed channel; O – open channel; I – inactivated channel. B. N-type inactivation. The inactivation peptide enters the pore and physically blocks the transfer of ions after the activation of the channel. C. C-type inactivation. The selectivity filter acts as the second gate and closes, preventing the penetration of ions. The channels completely return to the closed conformation when the potential drops to the resting potential level (modified from [35])

EXPERIMENTAL DATA FOR THE MODELING OF ACTIVATION OF Kv CHANNELS

It was suggested in the very first models of Kv channels activation that the change in the transmembrane potential during the activation of the channel caused the voltage sensor S4 to move upstream of the channel that was connected to the external and internal solutions [58]. Later on, experimental data on the functioning of Kv channels were accumulated, allowing one to refine the available models of activation. The fundamental data important for deciphering the activation mechanism of Kv channels are as follows:

(1) *S4 segment contains a conserved repeated motif of three amino acid residues: (+, X1, X2, +, X1, X2 …).*

Mutational and electrophysiological analyses allowed researchers to identify the most significant (HI – high-impact) and least significant (LI – low-impact) residues for the process of channel activation/

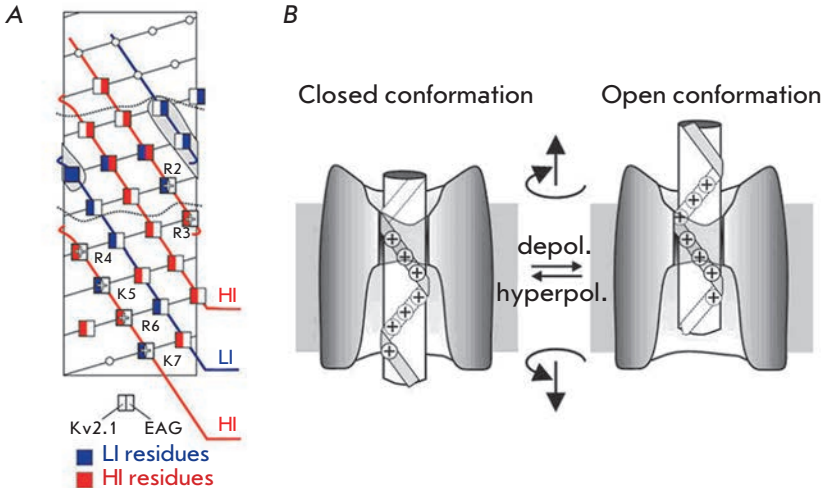

Fig. 4. A. Schematic arrangement of S4 helix residues in the Kv10 and Kv2.1 channels. The distribution of residues with high impact (HI) and low impact (LI) on the opening/closing process is shown. Three parallel stripes along the S4 helix (HI charged residues, HI hydrophobic residues, LI hydrophobic residues) are continuous for both channels and form a three-step coil [59]. B. Kv channel activation scheme according to the SHM model [59] – screw rotation and motion of S4 helix (white cylinder) in a fixed gate channel (GC)

deactivation [59]. The voltage sensor S4 contains the conserved sequence (+, X1, X2, +, X1, X2 ...), where (+) is a positively charged HI (significant) residue, (X1) is a hydrophobic HI residue, and (X2) is a hydrophobic LI (non-significant) residue (*Fig. 3A*) [60, 61]. X1 residues are located in a protein environment where their mutations may lead to a disruption in protein folding and, consequently, to disruption in the channel opening/closing process. X2 residues are exposed in the lipid or water environment, and their impact on channel functioning is insignificant. The repeat (+, X1, X2, +, X1, X2 ...) forms three parallel left-handed coils with a small inclination along the right-handed S4 helix.

(2) *Each subunit possesses approximately three gate charges located on the R1–R4 residues of the S4 helix.*

The movement of the voltage sensor S4 can be detected by measuring the gate currents resulting from the movement of the electrostatic charges of the S4 helix relative to the electric field. The transition of the *Shaker* channel from the quiescent to the activated state is accompanied by the transfer of ~3.2–3.4 charges per subunit [62–64]. The method of alternate neutralization of the negative charges of S2/S3 helices and the positive charges of S4 allowed researchers to identify the amino acid residues responsible for the transfer of the gate charge [63, 64] as R1, R2, R3 and R4 [65, 66].

(3) *10 amino acid residues of the S4 segment are located in the membrane.*

Substitution of certain amino acid residues of the *Shaker* channel for Cys showed that the sequence of ~10 aa is inaccessible to both intracellular and extracellular solvents while the channel remains in the quiescence state [67, 68]. This sequence corresponds to ~13.5 Å of the α-helix and can include only two or three positive charges of S4 (*Fig. 3B,C*). Accordingly, there are deep water antechambers on both sides of the membrane and only a small portion of S4 is located in a short GC (gate channel) (*Fig. 3B,C*).

(4) *The S4 helix is able to move in a water-filled cleft called gate channel (GC) with a very narrow barrier between the external and internal solutions.*

The three "sides" of the GC are formed by S2/S3 helices, the pore domain, and lipids. An interaction between three conserved negative amino acid residues in the S2 and S3 helices and the positive residues in S4 indicates that S2 and S3 are located on one side of the GC [63, 69–71].

According to fluorescent and mutational analysis data, the pore domain is located on the other side of GC [72, 73]. This is supported by the fact that the R1 and R2 residues of the S4 helix approach E418 of the pore domain during activation [74, 75], while Cys inserted in S4 can form a bond with Cys introduced in the pore domain [45, 59].

The third side of GC is apparently formed by lipids, corresponding to the hydrophobic nature of a residue of the S4 helix at the X2 position. A weak relationship between the mutations in these residues and channel activation also points to this fact [60, 61].

(5) *Activation leads to a shift of the S4 segment by 9 amino acid residues.*

The fluorescence measurement method shows that the activation process is connected to the movement of ~9 aa of S4 from GC into the external solution [61, 67, 68, 76, 77]. At the same time, the sequence of ~9 aa disappears from the inner water antechamber [67, 68].

(6) *The S4 helix rotates during activation.*

It has been established using the FRET method that S4 rotates by ~180° during the activation of the channel [78, 79].

(7) *The membrane voltage sensor S4 has a stable intermediate state.*

Two phases in the movement of gate charges [80] and two consecutive movements of gate charges in the external direction with an intermediate transmembrane position of S4 [68] were established by kinetic studies.

(8) *The channel can form a proton pore.*

A substitution of R1 or R4 for His allows the channel to conduct protons (omega-current) [65, 66]. Consequently, the channel may contain a water channel that serves as a bridge between the internal and external solutions, while R1H forms the proton pore in the quiescent state and R4H – in the activated state.

FUNDAMENTAL MODELS OF ACTIVATION OF KV CHANNELS

(1) A sliding-helix model (SHM) [59] was proposed basing on the key facts reviewed above. The pore domain in a model of the Kv channel was reconstructed on the basis of the structure of the homologous potassium channel KcsA, while the location of VSD helices remained unknown at that time. The SHM model describes in details only the relative position of some amino acid residues of S1-S4 helices. According to this model, the rather short (~13.5 Å) GC channel has large antechambers filled with water on both the outer and inner sides. Due to this space, the electric field focuses on the small S4 portion, minimizing contact between several charged amino acids and the dielectric environment and providing a large gate charge. The activation is accompanied by a screw motion of S4 perpendicularly to the membrane surface in three separate steps. The screw motion during the activation can be stopped in stable intermediated states, in which the basic charges (R1-R4) move to the position occupied by the previous charge (*Fig. 4A*). The positively charged R1-R4 residues form consecutive ionic pairs with the negatively charged amino acid residues of neighbor helices. Each step is accompanied by the transfer of 1/3 of the total charge (~3) per subunit; i.e., 1 charge in general (*Fig. 4*) [59].

(2) *A paddle model (PM)* is a completely different activation model that emerged after the deciphering of the crystal structure of the bacterial channel KvAP [43, 81].

S3-S4 helices in the crystal structure of the KvAP channel are located close to the intracellular surface of the membrane and perpendicular to the pore axis (*Fig. 4B*). It has been shown that the S3 helix consists of two fragments (S3a and S3b) connected by the S3 loop (*Fig. 3B*). The S3b segment and N-terminal part of the S4 helix are oriented in antiparallel strictly opposite each other, forming a hydrophobic element with an helix-loop-helix structure that is attached to the pore domain via the flexible loop of the S3 helix and S4-S5 linker (*Fig. 3B*). This S3b-S4 element was termed the "paddle" [43], giving its name to the concerned model.

According to the PM, the positively charged paddles of the channel in closed conformation are located near the intracellular surface of the membrane; they are held in this position by a large electrical field, while the membrane resting potential is negative. In response to depolarization, the paddles move simultaneously through the membrane towards the external side, pulling along the S4-S5 linker that in turn pulls the S5 helix away from the pore axis.

This model conforms to some experimental data [46, 81] that point to a possible long-distance movement of a paddle of the potential sensor (about 20 Å). However, later experiments have shown that the used crystal structure of KvAP [43] possesses a non-native conformation [82].

Acquisition of new structural data [65, 67–69, 71, 73, 83–86] allowed researchers to propose *(3) an advanced SHM model* [87]. It was created on the basis of the data on the sequence of the *Shaker* channel and the crystal structure of the KvAP channel [43]. Similar to the previous model [59, 88], the new model suggests that the movement between the open and closed conformations of the channel includes three consecutive screw motions, when S4 moves by ~13.5 Å along the axis and rotates by 180°. At the same time, the positively charged S4 groups remain in the polar environment where they can interact with the negatively charged residues of S1-S3 helices, with other polar atoms, negatively charged lipid heads, and water. There is a single barrier dividing the amino acid residues of S4 into ones accessible from outside and inside (*Fig. 4B*) in this model. It provides a more detailed description of the interaction of the different amino acids of VSD with each other and includes a modeling of the channel pore part.

Later data of FRET [78] and potentiometric studies [89] showed that S4 virtually does not move towards the transmembrane direction [48], which contradicts both SHM and, especially, PM. Moreover, in the open state, the upper part of the S4 sensor interacts with the pore domain, which is impossible according to PM. Those data as well as earlier studies [45, 84, 89, 90] gave rise to *(4) a transport model (TM)* of activation [48, 84, 91] (*Fig. 5A,B*).

According to the TM model, similar to the SHM, the channel has deep water cavities on both sides of the membrane, divided by a small area of the channel in the middle of the membrane; the electric field focuses exactly on this spot, and thus the transfer of gate charges from one side of the membrane to another does not require big S4 movements. S4 changes its position during channel activation, tilting by 45°, but at the same time moving perpendicularly to the membrane surface to a small distance (less than 2 Å), while

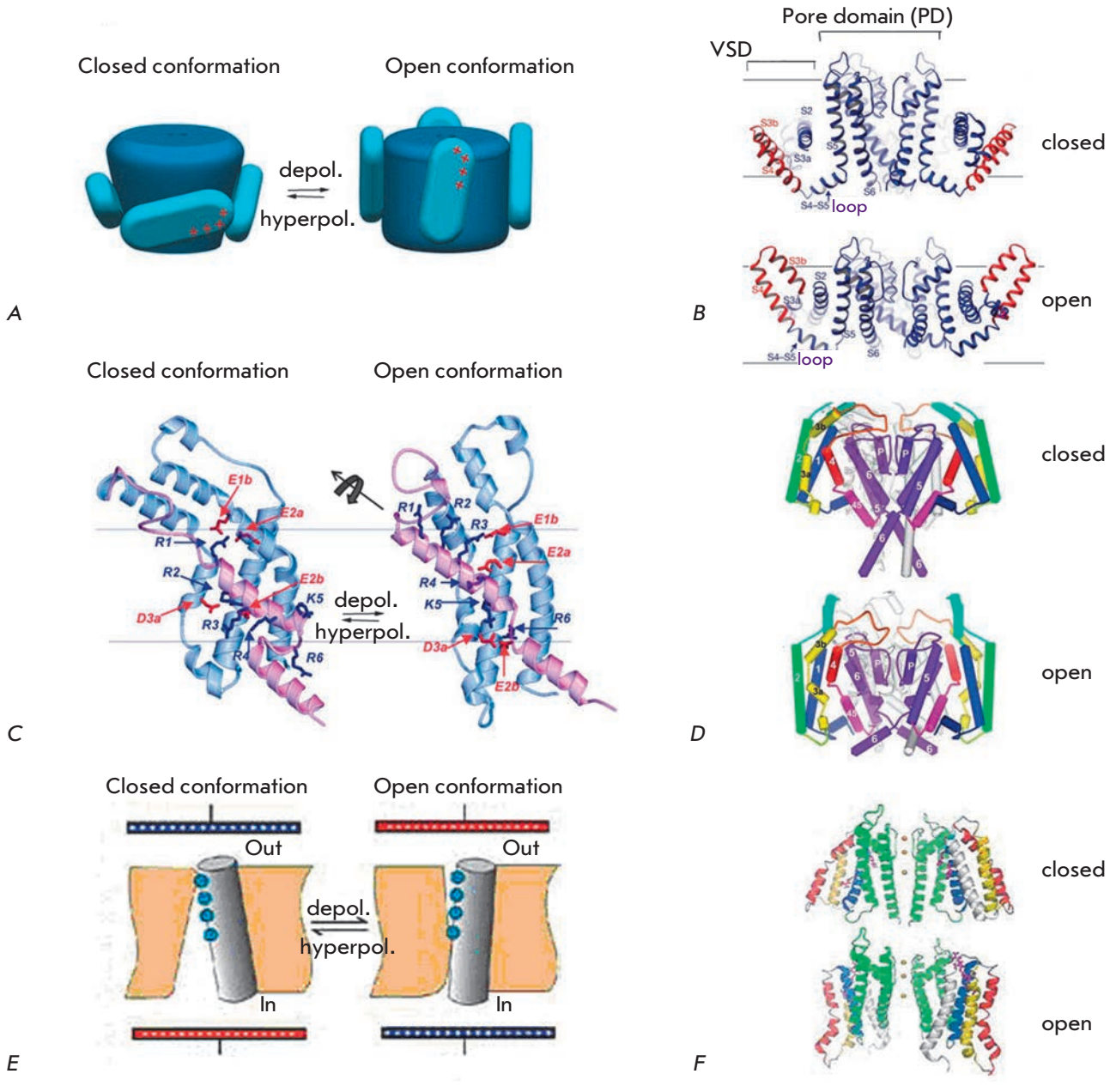

Fig. 5. Various models of Kv channels activation. All channels and their parts are shown in lateral orientation: the extracellular space is at the top, and the cytoplasm is at the bottom. A. Scheme of the paddle model (PM) of Kv activation. The movement of the paddles (blue ovals) is shown. Red "+" signs mark Arg in the S4 helix. B. PM based on the crystal structure of KvAP [92] in open and closed conformation. Paddle S3b–S4 is shown in red. S1–S4 helices are marked. The channel is shown as a frontal section. C. Sliding-helix model (SHM). The changes in the VSD domain of the *Shaker* channel are shown. Movable S4 segments and the S4–S5 loop are purple-colored. Positively charged side chains of the S4 helix and negatively charged side chains of the S1–S3 helices interacting with each other are colored blue and red, respectively [83]. D. SHM. The full-sized channels are given in closed and open conformations. S1–S6 helices are numbered. Helices of the VSD domain are shown in different colors. Helices of the pore domain (S5–S6) are purple-colored [83] E. Scheme of S4 helix movement (grey cylinder) during the activation of the Kv channel, according to the transport model (TM), showing how depolarization changes the availability of Arg residues (shown as blue circles) from the inner and outer aqueous cavities [48]. F. TM of Kv channels activation – closed and open conformations of the *Shaker* channel are shown. Transmembrane helices are color-coded: S1 – white, S2 – yellow, S3 – red, S4 – blue; pore domain is shown in green; Arg in S4 are shown in purple [48]

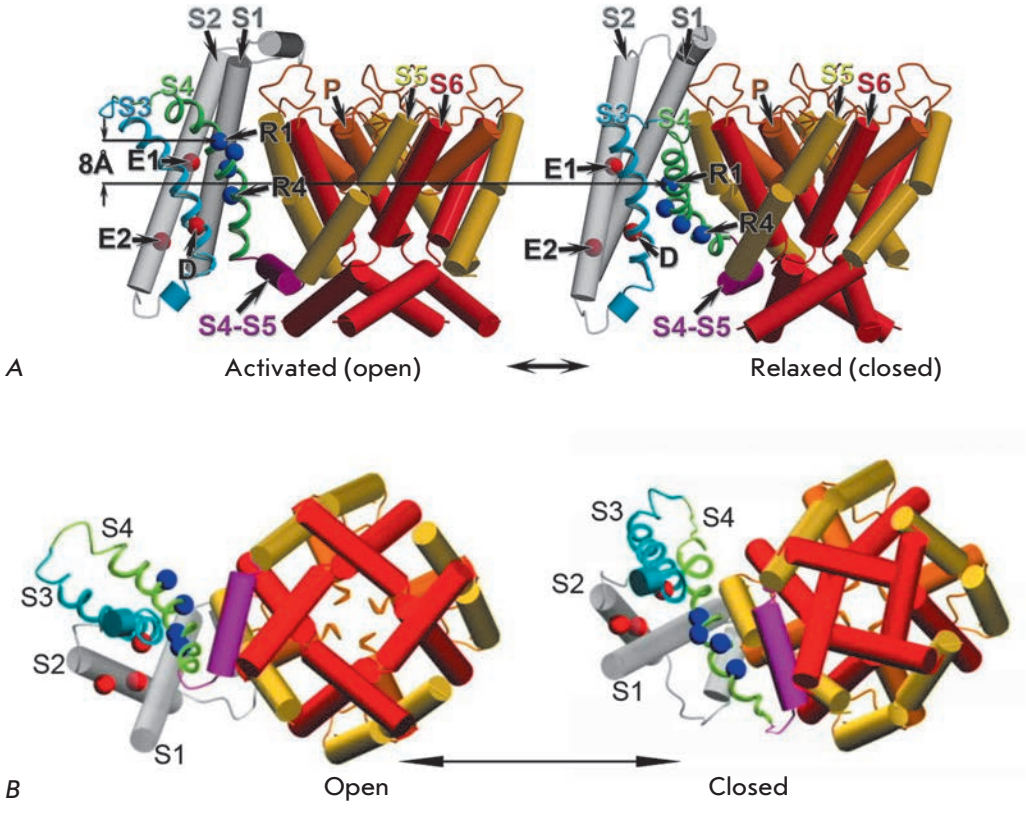

Fig. 6. Comparison of Kv1.2 channel models [53] in the activated (open) state (left) and in the rested (closed) state (right). All transmembrane helices are shown as cylinders, except for S3 and S4 shown as spirals. Only one VSD domain is shown. S1 and S2 helices are shown in grey; the S4– S5 linker is purple-colored. The positions of Cα carbon atoms of Arg in the S4 helix are marked as R1 and R4 and highlighted in blue. The amino acid residue E226 of the S2 helix is marked as E1; E236 of the S2 helix, as E2; and residue D259 of the S3 helix, as D; these amino acids are highlighted in red. A. Lateral view. B. View from the extracellular space

Arg on this helix move from the deep aqueous cavity on the intracellular side to the cavity on the outer side of the membrane. This relocation of Arg is possible due to two barriers that control the accessibility of S4 amino acid residues to water from the inner and outer sides (*Fig. 5*). The movement of the S4 helix combines rotation and inclination, and the helix always stays in the polar environment (*Fig. 5A,B*). In the TM model, S4 may be qualitatively compared to a transporter that has its binding site accessibility changing between the inner and outer sides in each cycle. This evolutionarily conserved mechanism is sufficient for the transfer of a large amount of charge through the electric field without movement of S4 through the membrane. The TM model conforms to much of the experimental data [47, 60, 72, 73, 78, 89, 93].

The biggest difference between the fundamental models consists in the amplitude of the S4 segment movement, which may be a consequence of the simplifications adopted in these models. For example, the movement of S4 in the SHM model is basically represented as the motion of a rigid body; however, it has been shown that S4 can transit from the α-helix conformation to a 3_{10} helix [44, 54, 94-97]. The PM model assumes that the S3-S4 paddle moves as a single entity, but experiments demonstrate that these two helices move independently [98].

MODERN MODELS OF Kv CHANNELS ACTIVATION

New data on the open conformation of the Kv channel became available after the crystal structures of the eukaryotic channel Kv1.2 (*Fig. 2C*) [21] and Kv1.2/Kv2.1 chimera [44] were determined, with the first one being improved later on [99]. The advances in computer software and methods allowed researchers to compute more complicated molecular models and to study the functioning mechanisms by means of molecular dynamics. This led to the emergence of several new models and hypotheses regarding Kv channel activation, including *(5) a model of coordinated movement of helices (CMH)* [53].

A molecular model of the eukaryotic channel Kv2.1 in the closed state and the CMH model of activation for this channel were created using the data of an X-ray structural analysis (*Fig. 2C*) [53]. *De novo* modeling (Rosetta method), the molecular dynamics method (MD), and voltage-clamp fluorometry (VCF) data were used for that purpose.

According to the CMH model, during depolarization of the membrane, S4 moves as an inclining screw that rotates by ~180° clockwise (on the extracellular side), ascending vertically by 6-8 Å and changing its inclination angle from ~ 60° to ~35°. The amplitude of S4 vertical movements varies from ~0 Å for S308 to ~14 Å for S289. As this takes place, the S1, S2, and S3 helices

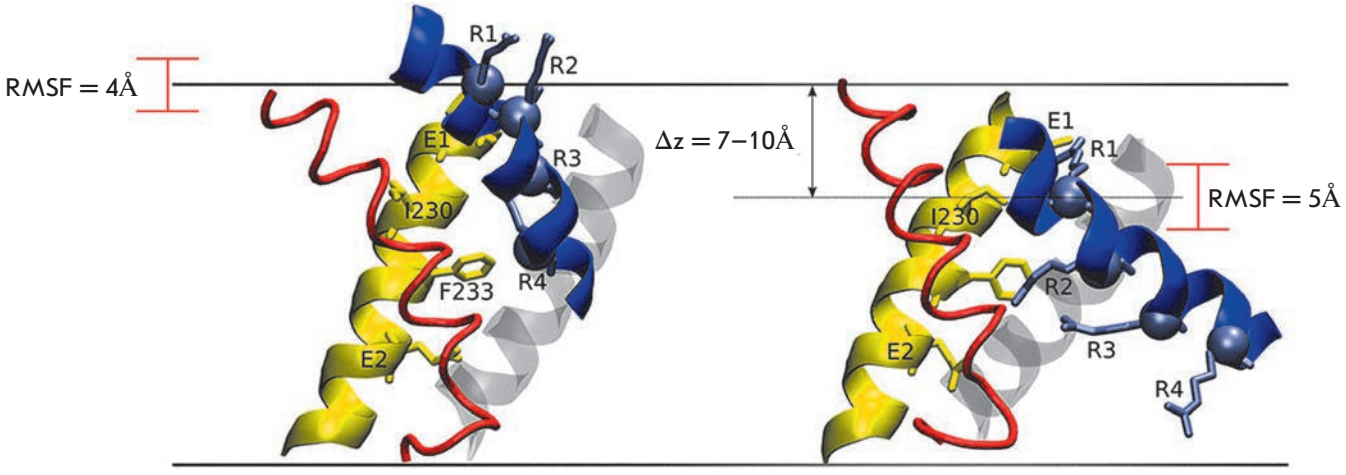

Fig. 7. Comparison of Kv1.2 VSD domain models in the open (left) [21] and closed (right) conformations according to the consensus model (CM). The S1 helix is shown in grey; S2,in yellow; S3, in red; and S4, in blue. Cα atoms of the R294 residue move in the vertical direction by 7-10 Å. The values of the root mean square fluctuations (RMSF) reflect the variation in the vertical *z* coordinate calculated for a Cα atom. The blue spheres with lateral radicals represent the basic charged amino acid residues of the S4 helix (R1–R4) that interact with amino acid residues in other helices (their side chains are marked) [55]

rotate around S4 clockwise, conforming to earlier data [49] (*Fig. 6*).

Results of omega-current measurements [100] indicate that a salt bridge is formed between R1 in the S4 helix (R294 in Kv1.2) and E226 (in Kv2.1) in the S2 helix (*Fig. 6A*) in the closed channel state, stabilizing this state and preventing the penetration of ions from the extracellular aqueous antechamber to the inner one [53]. A substitution of R1 for a small non-polar amino acid causes the salt bridge's destruction and formation of a through pore that allows protons to pass; this gives rise to the omega-current [100] confirmed by electrophysiological experiments [101, 102].

The obtained data indicate that Kv channels activation is linked to two basic types of conformational changes: (1) independent movement of VSD domains with a transition from the quiescent state to the "closed activated" state that keeps the pore domain gate closed [103-105]; and (2) cooperative transition of all VSD domains and the pore domain to the open state, when the pore domain gate is open for ion entry [104-106].

The role of gate-opening in the CMH model is attributed to the intracellular region of the S6 helix, while S5 initially rotates by ~7 Å around the pore domain. Thus, the second basic rearrangement involves inclinations of the S4 helix that promote the inclination of the intracellular half of S5. This counterclockwise movement (on the extracellular membrane side) allows S4-S5 linkers and S6 helices in all four subunits to move together and to open the intracellular gate (*Fig. 6*).

The CMH models of closed and open channel demonstrate the following molecular details of the Kv channel activation mechanism (*Fig. 6*):

(1) The S4 helix moves vertically by ~6-8 Å. The magnitude of S4 vertical movements in published structural models of the VSD domain transmembrane region in the open and/or closed states differs significantly: ~2–4 [48], ~3 [49] and 10–13 Å [87, 100]. The model of the KvAP channel in the quiescent state that was published earlier [46, 81] suggested an amplitude of S4 vertical movements of ~15-20 Å.

(2) The S3 helix moves relative to the S1, S2, and S4 helices. No significant movements of the S3 helix relative to all other segments of the VSD domain were noted in the previous publications.

(3) Coordinated movements of the S4 and S5 helices, the S4-S5 linker and S6 in all four subunits during the final opening of the channel. The mechanism of cooperative movements during channel opening had not been shown in any of the activation models published prior.

The CMH model conformity with the wide set of data that were previously considered as contradictory [47, 60, 72, 73, 93, 100, 107] allowed researchers to eliminate many contradictons in the discussion of the conformational rearrangements underlying the activation of Kv channels. Similar to the SHM model [108], the main movement in the CMH model is the axial rotation of S4 by ~180°. Like in the TM [48], the dielectric cavity contributes to the focusing of the transmembrane field,

thus increasing the gate charge that links the VSD domain to the membrane potential energetically.

The CMH model was further improved using a full-atom molecular dynamics method in the membrane environment with an evident solvent [55, 109]. It was shown that the S4 α-helix spontaneously transits to the dexiotropic 3_{10} helix in the closed state of the Kv1.2 channel. This S4 helix conformation orients Arg towards the aqueous cavity in the VSD domain and allows salt bridge formation with the negatively charged amino acid residues along the S2 and S3 helices. The tendency of S4 to assume the 3_{10} helix conformation matches the crystal structures of the channels [44, 94] in which the inner part of S4 (~11 AA) forms the 3_{10} helix.

(6) A consensus model (CM) was developed by Vargas *et al.* [55] based on an improved CMH model [54]. They used data on the basic interactions between the amino acid residues of the VSD domain helices in the closed channel. Four key interactions (R294 and I177; R294 and I230; I230 and F267; F233 and R294 in Kv1.2 channel) were modeled using the MD method. The resulting four independent models were further averaged to create the CM of closed Kv1.2 conformation (*Fig. 7*).

The CM model conformed to all the experimental results that were used as the basis for the earlier models (SHM, TM, PM) [46, 84, 89, 110–113]. CM demonstrates that S4 moves in the vertical direction approximately by 7-10 Å (*Fig. 7*) [55].

However, the CMH and the CM models cannot explain all the aspects of channel opening/closing. One of the reasons for that is the absence of information on intermediate Kv channel conformations. In this connection, attempts to determine the quantity of intermediate conformations and their structure by experimental methods and MM were made.

MacKinnon *et al.* [114] found a highly conserved site in the VSD domain (*Fig. 8A*) formed by two negatively charged amino acid residues (D259, E236 – in *Shaker* channel) and one highly conserved (F233) that represented a "catalyst" for the transfer of each of the VSD domain basic amino acids (R1-R4, K5) through the membrane field.

This site is termed a charge transfer center (CTC) [114]. During the S4 movement, each of its charged residues sequentially binds to this center; as a result, the whole activation/inactivation process divides into five consecutive stages (open channel, three intermediate stages, and closed channel), when the charged amino acids of the S4 helix (R1-R4, K5) sequentially bind to CTC (*Fig. 8B*). A group of French researchers [115] used the MD method and experimental data to study the VSD domain structure at different intermediate stages

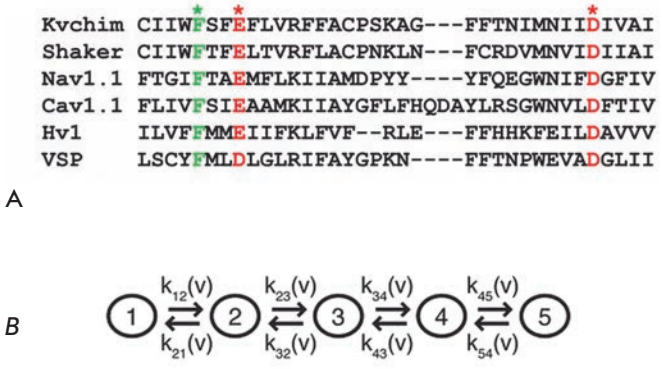

Fig. 8. A. The charge transfer center (CTC) is highly conserved among VSD-containing proteins. The alignment of the sequences of the chimeric channel Kv1.2/2.1 (GI: 160877792), *Shaker* (GI: 13432103), human channel Nav1.1 (GI: 115583677), human channel Cav1.1 (GI: 110349767), human channel Hv1 (GI: 91992155), and VSP (GI: 76253898) is shown. Only CTC-forming portions of the S2 and S3 segments are given. The highly conserved residues forming the site are marked: F – green; E and D – red. F corresponds to Phe233 in the chimeric channel Kv1.2/2.1. B. The five-stage model of Kv channel activation with four steps of VSD movement. At each stage, different, positively charged residues of the S4 helix (R1–R5, indicated by numbers) consistently occupy the CTC (shown as a circle). When all four sensors reach stage 5, the pore opens [114]

for a Kv1.2 channel placed on a lipid bilayer with an applied hyperpolarization potential. These five stages (states) are termed as follows: initial upper position, α; three intermediate positions, β, γ, δ; and lower closed position, ε (*Fig. 9*). During channel deactivation, the basic charged amino acid residues of S4 move from the external to the internal binding sites that represent the negatively charged residues of the S1-S3 segments (E183, E226, D259 and E236) as well as PO_4^- groups of lipids. At the same time, the mass center of R1-R4 residues moves in the intracellular direction approximately by 12 Å [78, 79]. Moreover, each of the four relocations is accompanied by the transition of one residue (K5, R4, R3 and R2) through the CTC area (*Fig. 9*). As a result, *(7) a model of charge transfer (MCT)* has been proposed.

In case process is observed from the external membrane side, the movement of S4 is accompanied by a slight inclination (~15°); S4 has a bigger inclination towards the membrane at the ε stage compared to the α stage. Earlier experiments [78, 79] demonstrated a moderate helical rotation of S4 clockwise (~45°) and a significant helical twisting counterclockwise (~90°) (*Fig. 9*). This model lacks significant (compared to other

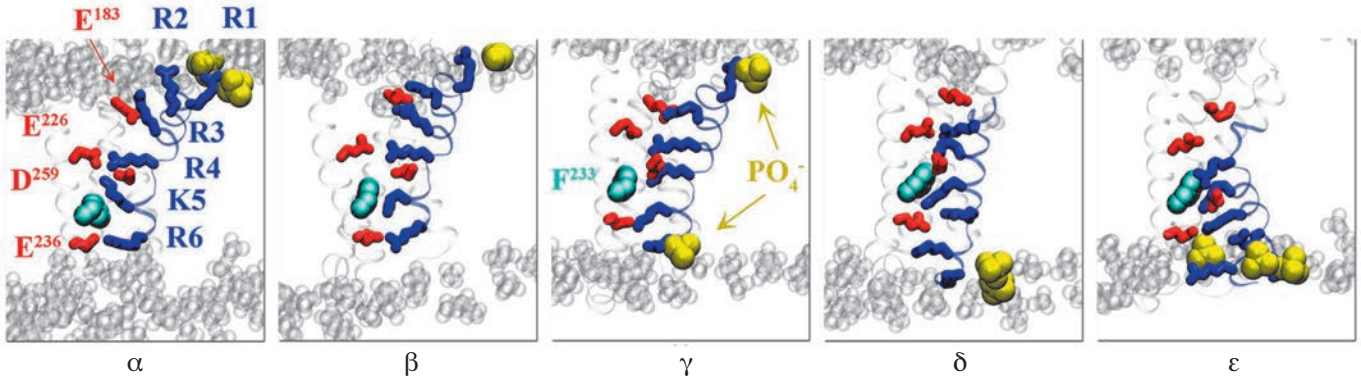

Fig. 9. Five key intermediate stages of the Kv1.2 channel VSD domain, according to the model of charge transfer (MCT): initial upper position – α; three intermediate positions – β, γ, δ; and lower closed position – ε. The basic residues of the S4 helix are shown as blue sticks; amino acid residues and lipid PO_4^- group that form salt bridges with R1–R5 are indicated by red sticks and yellow spheres, respectively. The highly conserved residue F233 of the S2 helix is shown as blue spheres [115]

models) movement of the S4 helix until its top turns [50, 53, 96]. This model takes into account the data on the CTC presence [114]: the CTC site binds the basic residues K5, R4, R3, R2, and R1 in the conformations α, β, γ, δ, and ε, respectively. The CTC position in each conformation is preserved within the frames of the lipid bilayer central part [115].

The results of experiments on the creation of metal-ion (Cd^{2+}) bridges later served as the basis for the identification of 20 new sites of interaction between the helices of the VSD domain [116]. These data were used for the modeling (by Rosetta method) of different intermediate conformations of the *Shaker* channel and for the creation of *(8) a model of Kv deactivation (MKD)* [116]. According to the MKD model, channel deactivation comprises five stages: O – open channel, C1-C2 – intermediate states, C3 – closed conformation, and C4 – deep closed state, which occurs under strong hyperpolarization (*Fig. 10*). The C3 stage corresponds to the CM of the closed conformation of the Kv channel [55].

In the MKD model, S4 moves fast in the intracellular direction during the deactivation, sliding along the S3 helix by at least 12 Å (*Fig. 10*) [116]. As this takes place, the short region of the S4 helix (~10 aa) has the 3_{10} helix conformation. At the open channel stage (O), the 3_{10} helix is positioned in the middle of S4; as S4 moves down, the 3_{10} helix moves along the S4 segment, always staying in the center of the membrane. The 3_{10} part is limited by two out of five charged amino acids (R1-R4, K5) on either side, with its central part located opposite the CTC (F290). At the C4 stage, the last R1 residue passes below the hydrophobic lock formed by F290 and cannot form a salt bridge with E283; as a result, the structure of S4 relaxes into an α-helix. The C4 stage is difficult to achieve and is possible only under significant hyperpolarization [117]. The S4 segment must move by 17 Å in order to reach the C4 stage [116]. The existence of C4 is confirmed by experimental data [114, 118].

ELECTROMECHANICAL COUPLING OF THE PORE AND VSD DOMAINS

It is still unknown how the VSD movement causes the opening of the channel pore; i.e., how the electromechanical coupling of VSD and the pore domains is implemented. It is known that the S4-S5 linker plays a major role in this process [31, 56], but the structural data are missing. In order to explain the functioning of the Kv channel and reveal the mechanism of electromechanical coupling of the pore and VSD domains, a group of researchers [56] studied the crystal structure of the open state of the Kv1.2/Kv2.1 channel [44, 119] using the MD method.

An integral and detailed *(9) mechanistic model of Kv activation/deactivation (MMd)* (*Fig. 11*) was created. This model describes many previously unknown features of the process [56].

The channel deactivation causes a decrease in the ion transport that is accompanied by the exit of water from the hydrophobic cavity of the pore and a concurrent closing of the pore (pore collapse), explaining the osmotic dependence of the whole process of channel functioning [17, 18]. Next, the following steps take place: (1) full relaxation of VSD domains – movement of S4 inwards by ~15 Å relative to the more stationary S1-S3a helices; (2) S4 rotation by ~120° that allows the charged amino acid residues to stay directed towards the VSD cavity; and (3) lateral detachment of VSD and

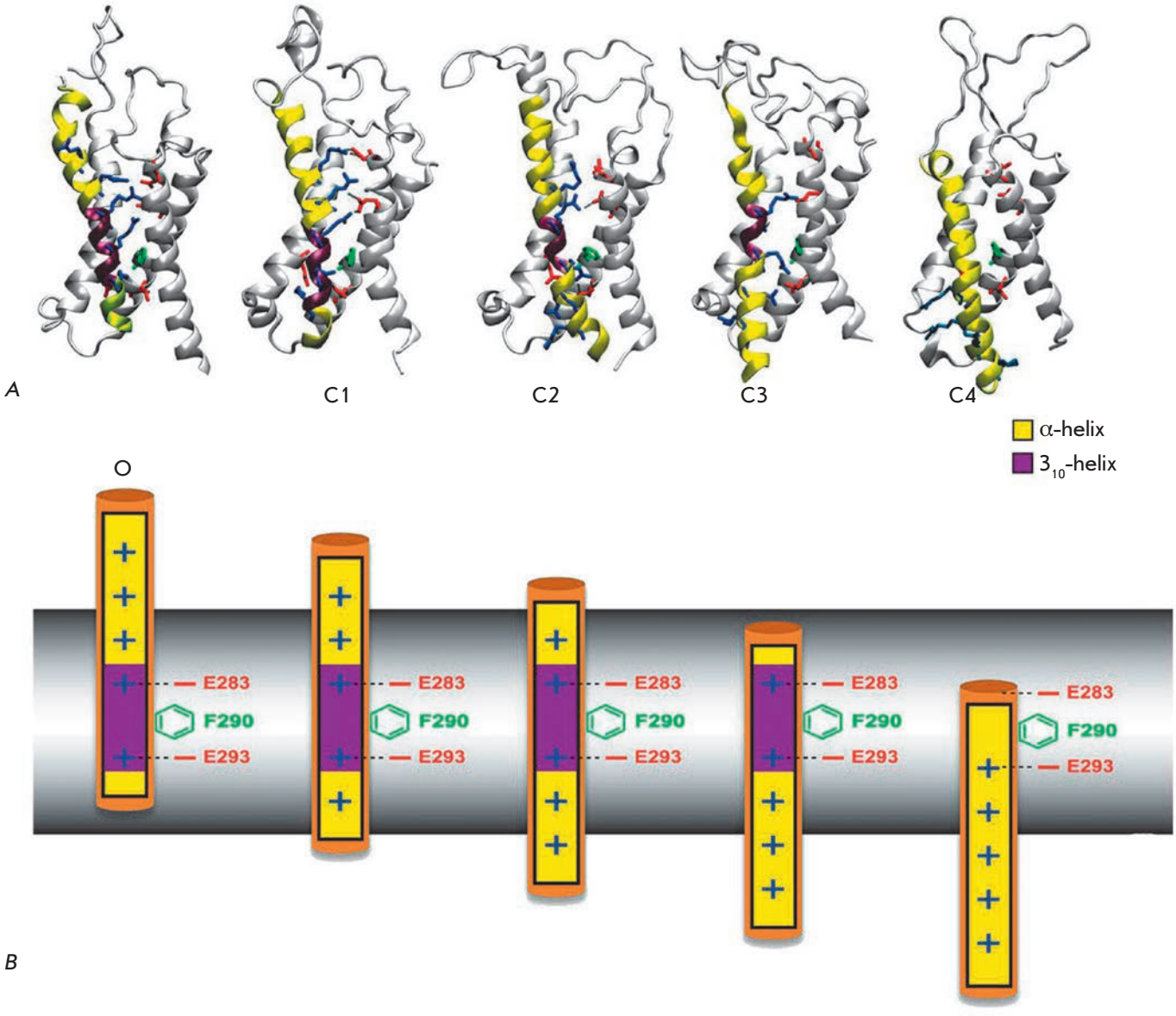

Fig. 10. Model of Kv deactivation (MKD). Intermediate stages that the VSD domain of the *Shaker* channel passes during deactivation [116]. A. Molecular models of the VSD domain: O – open channel, C1-C2 – intermediate states, C3 – closed conformation, C4 – deep closed state, which occurs under special conditions. At each stage, the side chain of one of the Arg residues of the S4 helix (blue sticks) passes through the CTC (F290, green stick), while the Arg side chains located close to the CTC form salt bridges with the negatively charged residues of the S1-S3 helices (red sticks; E247 in S1 and E283 in S2 above F290; and E293 in S2 and 316D in S3 below F290). At all the stages, the portion of the S4 helix situated opposite F290 transits into a 3_{10} helix (purple), but at the C4 stage this portion is relaxed into an α-helix (yellow). Thus, the portion of the 3_{10} helix slides along the S4 segment without energy consumption, which prevents the rotation of this segment during the activation/deactivation of the channel. B. Schematic, demonstrating the movements of the S4 helix. Color coding as in *Fig. 10A*

the pore domains due to VSD rotation and movement outwards relative to the pore, allowing the pore to remain closed. During the activated state of the channel, the R4 residue is located in the membrane center, in a point of the peak transmembrane electric field, and serves as an initiator of movement for the gate charges. The CTC is the central hydrophobic residue F233 that divides the external and internal hydrated cavities of the VSD domain. The R2 and R3 residues move sequentially, while S4 movement inward usually stops when R1(Q) reaches F233. Several salt bridges are formed in the VSD domain, but S4 mainly interacts with the

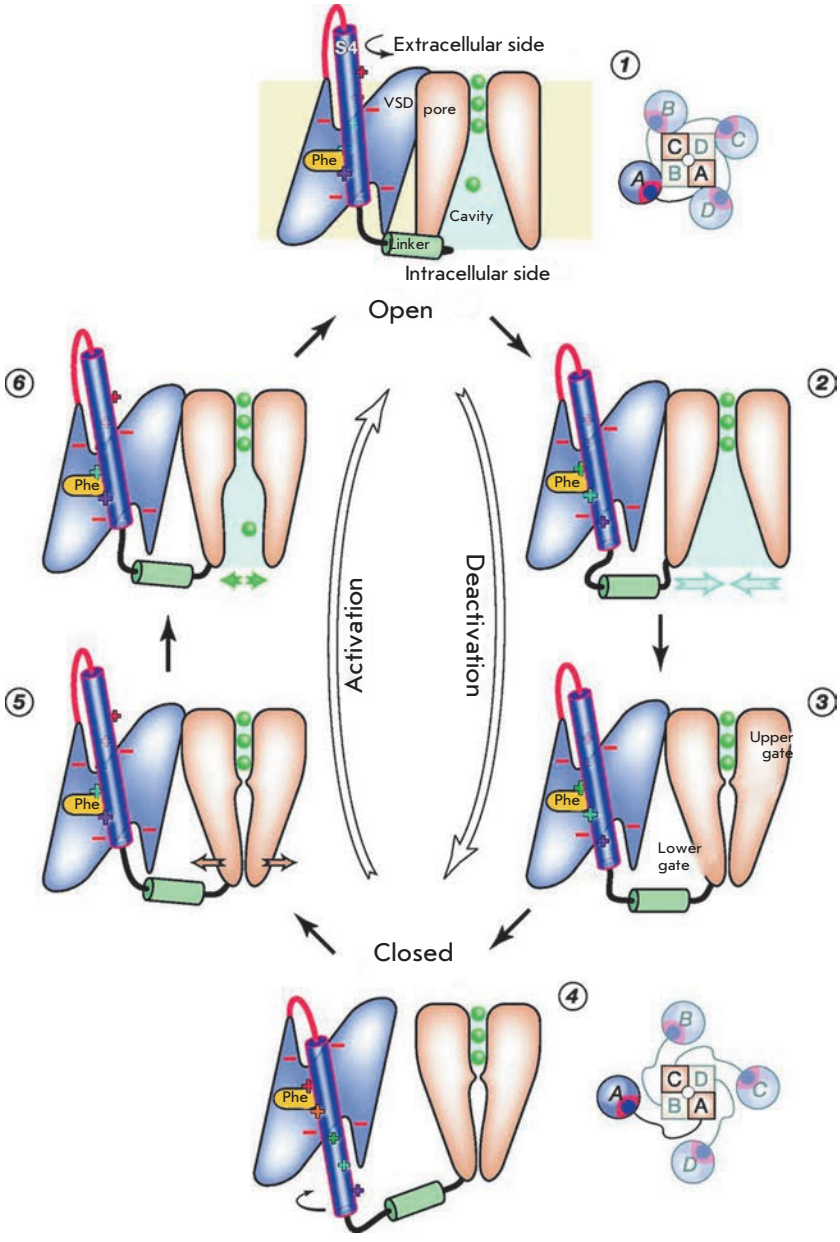

Fig. 11. Mechanistic model of Kv activation/deactivation (MMd) [56]. Effect of the hyperpolarization potential on the activated channel (1) initiates the inward movement of the S4 helix and weakens the bond between VSD and the pore domains. As a result, a depletion of ion transport in the pore cavity (2) and subsequent hydrophobic collapse of the pore occur. Closure of the upper (Ile402 in Kv1.2) and the lower gates [PVP motif; Leu331 (S5)–Pro405 (S6)] stops the ion current (3). The S4 helix continues to move inwardly; as soon as the S4 movement stops, the S4–S5 linker lowers completely and VSD domains are removed from the pore; the channel transits into the closed state (4). The impact of the depolarization potential on the closed channel leads to the movement of the S4 helix in an outward direction. The lower gate destabilizes when all four segments of the S4 and S4-S5 linker rise (5) and all VSD domains approach the pore again; the transition 4 => 5 represents the rate-limiting step of channel activation. Fluctuation of the lower gate causes opening of the pore and its partial rehydration. This allows potassium ions to enter into the pore and to initiate the channel conductance (6); the transition 5 => 6 is potential-independent. The presence of ions promotes complete rehydration of the pore leading to the complete opening of the upper and lower gates and returning the channel to the open state (1). Distribution of VSD domains (circles) relative to the pore domain (squares) is shown schematically (view from the extracellular side) [56]

phosphate groups of the lipids. These data conform to those on the functional interaction of the VSD domain with lipids [13, 120].

The channel follows the same steps during the activation, but in the reverse order (*Fig. 11*): S4 swiftly moves outside by ~5-10 Å. In the first step, the gate charges move fast because the majority of the salt bridges between S4 and the other segment of the VSD domain in the closed state are disrupted; these salt bridges are temporarily restored, while S4 moves outward, leading to the gradual slowdown of S4 movement. The VSD domains approach the characteristic state of an activated channel as soon as the S4 movement approaches its termination. A key difference as opposed to the deactivation is that all four VSD domains must be raised before the full opening of the channel pore; the channel with fully raised S4 segments breaks the packing of the S4-S5 linker together with S6 helix, allowing water and exiting ions to enter the pore again and restore the conductivity. The side chains of L331 (S5) and P405 (S6) move into a position that allows them to interact [17]. These rearrangements favor the binding of the S6 helix to the PVP motif, leading to the expansion at the intracellular side and full hydration of the pore. This is accompanied by the opening of the upper (hydrophobic) gate

(I402) that allows the S5 site of the selectivity filter to fill up with K^+ ions [121], and the channel transits to the fully open state. The S6 helix and S4-S5 linker adopt a closely packed configuration that stabilizes the pore opening.

We arrive at the conclusion that the opening and closing of the Kv channel is an energetically asymmetric process [56]. As far as the pore is more stable in the dehydrated closed state [17, 122] due to the hydrophobicity of its cavity [17], its closing does not require strong pressure by the S4 helix on the S4-S5 linker. On the contrary, channel activation requires the application of the depolarization work that stimulates the movement of the S4 helix through the membrane. Finally, S4 strongly pulls the S4-S5 linker, causing disruption of the S4-S5/S6 interaction and pore opening. Rather strong destabilization of the closed pore occurs only when all charged amino acid residues of the gate and S4-S5 linker are in the raised position. As a result, the fluctuations of the lower gate due to the disruption of linker interaction with the S6 helix allow partial (and then full) hydration of the pore cavity. The S4-S5 linker is strained during the activated channel state and relaxed in the quiescent state; this probably explains the conservatism of the linker length: a shorter linker inhibits channel closing, because S4 cannot move by a sufficient distance, while a longer linker inhibits the opening, because even complete outward relocation of S4 cannot efficiently pull the S6 helix using the S4-S5 linker [56].

Thus, the MMd model demonstrates that the S4-S5 linker and C-terminus of the S6 helix govern the process of channel opening/closing independently of the mechanism that raises and lowers the VSD domain [56]. The fact that it is possible to substitute the S3b-S4 paddle for a homologous sequence with the chimeric channel preserving the properties of the native channel [123, 124] indicates that this paddle is a key mechanic element in the process of channel activation/deactivation. The natural variability of the sequence of this functional region (S3b-S4 paddle and interacting region of the S4-S5 linker with the S6 helix) explains the differences in the activation parameters of Kv channels.

CONCLUSIONS

A large number of models starting with the fundamental ones (SHM, PM and TM) and ending with modern ones (CMH, CM, MCT, MKD, MMd) [53, 54, 56, 115, 116] were proposed during the long history of studying the mechanism of Kv channels activation based on crystallography, mutational analysis, as well as MM and biophysical data. Such a synthesis of different methods and approaches allowed researchers to solve a very complicated problem: to identify the processes underlying the Kv channel activation without using the direct structural data on its closed conformation and intermediate states.

At present, researchers largely agree on a united model of Kv channel activation. The groups of scientists [53, 54, 56, 115, 116] has been able to obtain similar results, but the number of stages, the amplitudes of movements, and their directions still differ in different models. The estimation of the vertical translocation of S4 depends on how it is aligned relative to the open structure of the channel, as well as on the significant fluctuations due to the dynamic nature of the intermediate conformations [55].

A comparison of all available models of the VSD domains of the channel in the closed conformation [53, 54, 56, 115, 116] shows that all of them lay in a limit of ~3.5 Å RMSD relative to the position of the Cα atoms [125]. Only one contradiction remains, which consists in determining the position of the R1 residue side chain. In some models [53, 55], this residue interacts with E226, while in others [56, 115] it interacts with D283. Each group of researchers asserts that their data are experimentally verified [50, 114, 118, 126]. It is possible that both conformations exist simultaneously in the case when a hyperpolarization potential is present [127].

The activation models consider two or three intermediate stages [53, 54, 56, 115, 116]. It should be noted that the intermediate conformations are unstable and hardly separable from each other [116]; therefore, different authors may well consider the same activation steps. Thus, in the MCT and MMd models [56, 115], three intermediate stages are considered, while in the MKD model [116] there are two stages, but all these models attempt to describe very similar processes. Probably, all models consider the same process, but they choose different intermediate points. Despite the slight differences in the models [53, 54, 56, 115, 116], all of them describe satisfactorily the generalized process of Kv channel activation and explain the basic principles of its functioning. The MMd model [56] is the most developed one. According to these principles, each VSD domain of the channel has deep aqueous cavities on both sides of the membrane, divided by a thin isthmus that contains a conserved Phe serving as a catalyst for moving the S4 gate charges. The positive basic amino acid residues of S4 are stabilized, interacting in pairs with the negative charges in the S1-S3 helices located along the S4 surface [49, 69, 71]. During activation, the positive charges "jump" from one negative charge to the next, leading to conformational change in the VSD. The S4 movement represents the combination of several processes: 1) inclination of the S4 helix in the membrane,

2) rotation on its axis, and 3) vertical and radial translocation. This movement displaces the S4-S5 linker and thus leads to the pore opening. The inner part of the S4 helix extends, while its two termini undergo screw-like rotation. The channel opening occurs after all VSD domains displace, while the channel closing requires displacement of only one of these domains. In order to reveal the precise mechanism of activation/deactivation, especially the process of electromechanical coupling of the domains, it is necessary to elucidate the atomic structure of the Kv channel not only in the two final conformations (open and closed), but also in the intermediate states. This represents a very complicated problem, because these conditions are unstable and short-lived compared to the whole activation process timeframe. ●

The authors are grateful to Prof. G.V. Maksimov (Moscow State University) for fruitful discussions. This work was in part funded by a grant from the Seventh Framework Program of the European Union (EDICT #201924). A.V. Grizel is supported by the Development Program of St. Petersburg State University (#1.50.1038.2014).

REFERENCES

1. Yu F.H., Yarov-Yarovoy V., Gutman G.A., Catterall W.A. // Pharmacol. Rev. 2005. V. 57. P. 387–395.
2. Gutman G.A., Chandy K.G., Grissmer S., Lazdunski M., McKinnon D., Pardo L.A., Robertson G.A., Rudy B., Sanguinetti M.C., Stühmer W., Wang X. // Pharmacol. Rev. 2005. V. 57. P. 473–508.
3. Hoshi T., Zagotta W.N., Aldrich R.W. // Science. 1990. V. 250. P. 533–538.
4. Yellen G. // Nature. 2002. V. 419. P. 35–42.
5. Bosma M.M., Hille B. // Endocrinology. 1992. V. 130. P. 3411–3420.
6. Pal S.K., Takimoto K., Aizenman E., Levitan E.S. // Cell Death. Differ. 2006. V. 13. P. 661–667.
7. Deutsch C., Chen L.Q. // Proc. Natl. Acad. Sci. USA. 1993. V. 90. P. 10036–10040.
8. Singer-Lahat D., Sheinin A., Chikvashvili D., Tsuk S., Greitzer D., Friedrich R., Feinshreiber L., Ashery U., Benveniste M., Levitan E.S., et al. // J. Neurosci. 2007. V. 27. P. 1651–1658.
9. MacDonald P.E., Sewing S., Wang J., Joseph J.W., Smukler S.R., Sakellaropoulos G., Saleh M.C., Chan C.B., Tsushima R.G., Salapatek A.M., et al. // J. Biol. Chem. 2002. V. 277. P. 44938–44945.
10. Kim S.J., Widenmaier S.B., Choi W.S., Nian C., Ao Z., Warnock G., McIntosh C.H. // Cell Death. Differ. 2012. V. 19. P. 333–344.
11. Wang Q., Curran M.E., Splawski I., Burn T.C., Millholland J.M., VanRaay T.J., Shen J., Timothy K.W., Vincent G.M., de Jager T., et al. // Nat. Genet. 1996. V. 12. P. 17–23.
12. Wray D. // Eur. Biophys. J. 2009. V. 38. P. 271–272.
13. Watanabe H., Nagata E., Kosakai A., Nakamura M., Yokoyama M., Tanaka K., Sasai H. // J. Neurochem. 2000. V. 75. P. 28–33.
14. Beekwilder J.P., O'Leary M.E., van den Broek L.P., van Kempen G.T., Ypey D.L., van den Berg R.J. // J. Pharmacol. Exp. Ther. 2003. V. 304. P. 531–538.
15. Camacho J. // Cancer Lett. 2006. V. 233. P. 1–9.
16. Milescu M., Lee H.C., Bae C.H., Kim J.I., Swartz K.J. // J. Gen. Physiol. 2013. V. 141. P. 203–216.
17. Thomas D., Wimmer A.B., Wu K., Hammerling B.C., Ficker E.K., Kuryshev Y.A., Kiehn J., Katus H.A., Schoels W., Karle C.A. // Naunyn Schmiedebergs Arch. Pharmacol. 2004. V. 369. P. 462–472.
18. Ikeda M., Tomita Y., Mouri A., Koga M., Okochi T., Yoshimura R., Yamanouchi Y., Kinoshita Y., Hashimoto R., Williams H.J., et al. // Biol. Psychiatry. 2010. V. 67. P. 263–269.
19. Sokolova O. // FEBS Lett. 2004. V. 564. P. 251–256.
20. Carrington J.C., Freed D.D. // J. Virol. 1990. V. 64. P. 1590–1597.
21. Long S.B., Campbell E.B., Mackinnon R. // Science. 2005. V. 309. P. 897–903.
22. Brandt F., Etchells S.A., Ortiz J.O., Elcock A.H., Hartl F.U., Baumeister W. // Cell. 2009. V. 136. P. 261–271.
23. Myasnikov A.G., Afonina Z.A., Klaholz B.P. // Ultramicroscopy. 2013. V. 126. P. 33–39.
24. Doyle D.A., Morais Cabral J., Pfuetzner R.A., Kuo A., Gulbis J.M., Cohen S.L., Chait B.T., MacKinnon R. // Science. 1998. V. 280. P. 69–77.
25. Lu Z., Klem A.M., Ramu Y. // J. Gen. Physiol. 2002. V. 120. P. 663–676.
26. Lu Z., Klem A.M., Ramu Y. // Nature. 2001. V. 413. P. 809–813.
27. Labro A.J., Raes A.L., Grottesi A., van Hoorick D., Sansom M.S., Snyders D.J. // J. Gen. Physiol. 2008. V. 132. P. 667–680.
28. Barghaan J., Bahring R. // J. Gen. Physiol. 2009. V. 133. P. 205–224.
29. Batulan Z., Haddad G.A., Blunck R. // J. Biol. Chem. 2010. V. 285. P. 14005–14019.
30. Haddad G.A., Blunck R. // J. Gen. Physiol. 2011. V. 137. P. 455–472.
31. Pischalnikova A.V., Sokolova O.S. // J. Neuroimmune Pharmacol. 2009. V. 4. P. 71–82.
32. Leicher T., Bahring R., Isbrandt D., Pongs O. // J. Biol. Chem. 1998. V. 273. P. 35095–35101.
33. Shi G., Nakahira K., Hammond S., Rhodes K. J., Schechter L.E., Trimmer J.S. // Neuron. 1996. V. 16. P. 843–852.
34. Wray D. // Eur. Biophys. J. 2004. V. 33. P. 194–200.
35. Rasmusson R.L., Morales M.J., Wang S., Liu S., Campbell D.L., Brahmajothi M.V., Strauss H.C. // Circ. Res. 1998. V. 82. P. 739–750.
36. Sigworth F.J. // Q. Rev. Biophys. 1994. V. 27. P. 1–40.
37. Rettig J., Heinemann S.H., Wunder F., Lorra C., Parcej D.N., Dolly J.O., Pongs O. // Nature. 1994. V. 369. P. 289–294.
38. Armstrong C.M., Bezanilla F. // J. Gen. Physiol. 1977. V. 70. P. 567–590.
39. Zagotta W.N., Hoshi T., Aldrich R.W. // Science. 1990. V. 250. P. 568–571.
40. Blunck R., Cordero-Morales J.F., Cuello L.G., Perozo E., Bezanilla F. // J. Gen. Physiol. 2006. V. 128. P. 569–581.
41. Cordero-Morales J.F., Cuello L.G., Zhao Y., Jogini V., Cortes D.M., Roux B., Perozo E. // Nat. Struct. Mol. Biol. 2006. V. 13. P. 311–318.

42. Cordero-Morales J.F., Cuello L.G., Perozo E. // Nat. Struct. Mol. Biol. 2006. V. 13. P. 319–322.
43. Jiang Y., Lee A., Chen J., Ruta V., Cadene M., Chait B.T., MacKinnon R. // Nature. 2003. V. 423. P. 33–41.
44. Long S.B., Tao X., Campbell E.B., MacKinnon R. // Nature. 2007. V. 450. P. 376–382.
45. Laine M., Lin M.C., Bannister J.P., Silverman W.R., Mock A.F., Roux B., Papazian D.M. // Neuron. 2003. V. 39. P. 467–481.
46. Ruta V., Chen J., MacKinnon R. // Cell. 2005. V. 123. P. 463–475.
47. Posson D.J., Ge P., Miller C., Bezanilla F., Selvin P.R. // Nature. 2005. V. 436. P. 848–851.
48. Chanda B., Asamoah O.K., Blunck R., Roux B., Bezanilla F. // Nature. 2005. V. 436. P. 852–856.
49. Yarov-Yarovoy V., Baker D., Catterall W.A. // Proc. Natl. Acad. Sci. USA. 2006. V. 103. P. 7292–7297.
50. Campos F.V., Chanda B., Roux B., Bezanilla F. // Proc. Natl. Acad. Sci. USA. 2007. V. 104. P. 7904–7909.
51. Grabe M., Lai H.C., Jain M., Jan Y.N., Jan L.Y. // Nature. 2007. V. 445. P. 550–553.
52. Lewis A., Jogini V., Blachowicz L., Laine M., Roux B. // J. Gen. Physiol. 2008. V. 131. P. 549–561.
53. Pathak M.M., Yarov-Yarovoy V., Agarwal G., Roux B., Barth P., Kohout S., Tombola F., Isacoff E.Y. // Neuron. 2007. V. 56. P. 124–140.
54. Khalili-Araghi F., Jogini V., Yarov-Yarovoy V., Tajkhorshid E., Roux B., Schulten K. // Biophys. J. 2010. V. 98. P. 2189–2198.
55. Vargas E., Bezanilla F., Roux B. // Neuron. 2011. V. 72. P. 713–720.
56. Jensen M.O., Jogini V., Borhani D.W., Leffler A.E., Dror R.O., Shaw D.E. // Science. 2012. V. 336. P. 229–233.
57. Yarov-Yarovoy V., DeCaen P.G., Westenbroek R.E., Pan C.Y., Scheuer T., Baker D., Catterall W.A. // Proc. Natl. Acad. Sci. USA. 2012. V. 109. P. E93–102.
58. Goldstein S.A., Miller C. // Biophys. J. 1992. V. 62. P. 5–7.
59. Gandhi C.S., Isacoff E.Y. // J. Gen. Physiol. 2002. V. 120. P. 455–463.
60. Li-Smerin Y., Hackos D.H., Swartz K.J. // Neuron. 2000. V. 25. P. 411–423.
61. Schonherr R., Mannuzzu L.M., Isacoff E.Y., Heinemann S.H. // Neuron. 2002. V. 35. P. 935–949.
62. Schoppa N.E., McCormack K., Tanouye M.A., Sigworth F.J. // Science. 1992. V. 255. P. 1712–1715.
63. Seoh S.A., Sigg D., Papazian D.M., Bezanilla F. // Neuron. 1996. V. 16. P. 1159–1167.
64. Aggarwal S.K., MacKinnon R. // Neuron. 1996. V. 16. P. 1169–1177.
65. Starace D.M., Stefani E., Bezanilla F. // Neuron. 1997. V. 19. P. 1319–1327.
66. Starace D.M., Bezanilla F. // J. Gen. Physiol. 2001. V. 117. P. 469–490.
67. Larsson H.P., Baker O.S., Dhillon D.S., Isacoff E.Y. // Neuron. 1996. V. 16. P. 387–397.
68. Baker O.S., Larsson H.P., Mannuzzu L.M., Isacoff E.Y. // Neuron. 1998. V. 20. P. 1283–1294.
69. Papazian D.M., Shao X.M., Seoh S.A., Mock A.F., Huang Y., Wainstock D.H. // Neuron. 1995. V. 14. P. 1293–1301.
70. Tiwari-Woodruff S.K., Schulteis C.T., Mock A.F., Papazian D.M. // Biophys. J. 1997. V. 72. P. 1489–1500.
71. Tiwari-Woodruff S.K., Lin M.A., Schulteis C.T., Papazian D.M. // J. Gen. Physiol. 2000. V. 115. P. 123–138.
72. Li-Smerin Y., Hackos D.H., Swartz K.J. // J. Gen. Physiol. 2000. V. 115. P. 33–50.
73. Gandhi C.S., Clark E., Loots E., Pralle A., Isacoff E.Y. // Neuron. 2003. V. 40. P. 515–525.
74. Elinder F., Mannikko R., Larsson H.P. // J. Gen. Physiol. 2001. V. 118. P. 1–10.
75. Elinder F., Arhem P., Larsson H.P. // Biophys. J. 2001. V. 80. P. 1802–1809.
76. Mannuzzu L.M., Moronne M.M., Isacoff E.Y. // Science. 1996. V. 271. P. 213–216.
77. Yusaf S.P., Wray D., Sivaprasadarao A. // Pflugers Arch. 1996. V. 433. P. 91–97.
78. Cha A., Ruben P.C., George A.L., Jr., Fujimoto E., Bezanilla F. // Neuron. 1999. V. 22. P. 73–87.
79. Glauner K.S., Mannuzzu L.M., Gandhi C.S., Isacoff E.Y. // Nature. 1999. V. 402. P. 813–817.
80. Bezanilla F., Perozo E., Stefani E. // Biophys. J. 1994. V. 66. P. 1011–1021.
81. Jiang Y., Ruta V., Chen J., Lee A., MacKinnon R. // Nature. 2003. V. 423. P. 42–48.
82. Lee S.Y., Lee A., Chen J., MacKinnon R. // Proc. Natl. Acad. Sci. USA. 2005. V. 102. P. 15441–15446.
83. Yang N., George A.L., Jr., Horn R. // Neuron. 1996. V. 16. P. 113–122.
84. Starace D.M., Bezanilla F. // Nature. 2004. V. 427. P. 548–553.
85. Ahern C.A., Horn R. // J. Gen. Physiol. 2004. V. 123. P. 205–216.
86. Gonzalez C., Rosenman E., Bezanilla F., Alvarez O., Latorre R. // Proc. Natl. Acad. Sci. USA. 2001. V. 98. P. 9617–9623.
87. Durell S.R., Shrivastava I.H., Guy H.R. // Biophys. J. 2004. V. 87. P. 2116–2130.
88. Durell S.R., Hao Y., Guy H.R. // J. Struct. Biol. 1998. V. 121. P. 263–284.
89. Asamoah O.K., Wuskell J.P., Loew L.M., Bezanilla F. // Neuron. 2003. V. 37. P. 85–97.
90. Islas L.D., Sigworth F.J. // J. Gen. Physiol. 2001. V. 117. P. 69–89.
91. Bezanilla F. // Physiol. Rev. 2000. V. 80. P. 555–592.
92. Jiang Q.X., Wang D.N., MacKinnon R. // Nature. 2004. V. 430. P. 806–810.
93. Neale E.J., Elliott D.J., Hunter M., Sivaprasadarao A. // J. Biol. Chem. 2003. V. 278. P. 29079–29085.
94. Clayton G.M., Altieri S., Heginbotham L., Unger V.M., Morais-Cabral J.H. // Proc. Natl. Acad. Sci. USA. 2008. V. 105. P. 1511–1515.
95. Villalba-Galea C.A., Sandtner W., Starace D.M., Bezanilla F. // Proc. Natl. Acad. Sci. USA. 2008. V. 105. P. 17600–17607.
96. Bjelkmar P., Niemela P.S., Vattulainen I., Lindahl E. // PLoS Comput. Biol. 2009. V. 5. P. e1000289.
97. Vieira-Pires R.S., Morais-Cabral J.H. // J. Gen. Physiol. 2010. V. 136. P. 585–592.
98. Broomand A., Elinder F. // Neuron. 2008. V. 59. P. 770–777.
99. Chen X., Wang Q., Ni F., Ma J. // Proc. Natl. Acad. Sci. USA. 2010. V. 107. P. 11352–11357.
100. Tombola F., Pathak M.M., Gorostiza P., Isacoff E.Y. // Nature. 2007. V. 445. P. 546–549.
101. Ramsey I.S., Mokrab Y., Carvacho I., Sands Z.A., Sansom M.S., Clapham D.E. // Nat. Struct. Mol. Biol. 2010. V. 17. P. 869–875.
102. Wood M.L., Schow E.V., Freites J.A., White S.H., Tombola F., Tobias D.J. // Biochim. Biophys. Acta. 2012. V. 1818. P. 286–293.
103. Horn R., Ding S., Gruber H.J. // J. Gen. Physiol. 2000. V. 116. P. 461–476.
104. del Camino D., Kanevsky M., Yellen G. // J. Gen. Physiol. 2005. V. 126. P. 419–428.

105. Pathak M., Kurtz L., Tombola F., Isacoff E. // J. Gen. Physiol. 2005. V. 125. P. 57–69.
106. Zagotta W.N., Hoshi T., Aldrich R.W. // J. Gen. Physiol. 1994. V. 103. P. 321–362.
107. Schmidt D., Jiang Q.X., MacKinnon R. // Nature. 2006. V. 444. P. 775–779.
108. Guy H.R., Seetharamulu P. // Proc. Natl. Acad. Sci. USA. 1986. V. 83. P. 508–512.
109. Khalili-Araghi F., Jogini V., Yarov-Yarovoy V., Tajkhorshid E., Roux B., Schulten K. // Biophys. J. 2010. V. 98. P. 2189–2198.
110. Ahern C.A., Horn R. // Neuron. 2005. V. 48. P. 25–29.
111. Freites J.A., Tobias D.J., White S.H. // Biophys. J. 2006. V. 91. P. L90–92.
112. Sands Z.A., Sansom M.S. // Structure. 2007. V. 15. P. 235–244.
113. Jogini V., Roux B. // Biophys. J. 2007. V. 93. P. 3070–3082.
114. Tao X., Lee A., Limapichat W., Dougherty D.A., MacKinnon R. // Science. 2010. V. 328. P. 67–73.
115. Delemotte L., Tarek M., Klein M.L., Amaral C., Treptow W. // Proc. Natl. Acad. Sci. USA. 2011. V. 108. P. 6109–6114.
116. Henrion U., Zumhagen S., Steinke K., Strutz-Seebohm N., Stallmeyer B., Lang F., Schulze-Bahr E., Seebohm G. // Cell Physiol. Biochem. 2012. V. 29. P. 809–818.
117. Cole K.S., Moore J.W. // Biophys. J. 1960. V. 1. P. 1–14.
118. Lin M.C., Hsieh J.Y., Mock A.F., Papazian D.M. // J. Gen. Physiol. 2011. V. 138. P. 155–163.
119. Tao X., MacKinnon R. // J. Mol. Biol. 2008. V. 382. P. 24–33.
120. Madin K., Sawasaki T., Kamura N., Takai K., Ogasawara T., Yazaki K., Takei T., Miura K. I., Endo Y. // FEBS Lett. 2004. V. 562. P. 155–159.
121. Jensen M.O., Borhani D.W., Lindorff-Larsen K., Maragakis P., Jogini V., Eastwood M.P., Dror R.O., Shaw D.E. // Proc. Natl. Acad. Sci. USA. 2010. V. 107. P. 5833–5838.
122. Schwarz T.L., Tempel B.L., Papazian D.M., Jan Y.N., Jan L.Y. // Nature. 1988. V. 331. P. 137–142.
123. Zhou Y., Morais-Cabral J.H., Kaufman A., MacKinnon R. // Nature. 2001. V. 414. P. 43–48.
124. Berneche S., Roux B. // Proc. Natl. Acad. Sci. USA. 2003. V. 100. P. 8644–8648.
125. Vargas E., Yarov-Yarovoy V., Khalili-Araghi F., Catterall W.A., Klein M.L., Tarek M., Lindahl E., Schulten K., Perozo E., Bezanilla F., et al. // J. Gen. Physiol. 2012. V. 140. P. 587–594.
126. Delemotte L., Treptow W., Klein M.L., Tarek M. // Biophys. J. 2010. V. 99. P. L72–74.
127. Tarek M., Delemotte L. // Acc. Chem. Res. 2013. V. 46. P. 2755–2762.

Regulation of the Target Protein (Transgene) Expression in the Adenovirus Vector Using Agonists of Toll-Like Receptors

A. V. Bagaev[1], A. V. Pichugin[1], E. S. Lebedeva[1], A. A. Lysenko[2], M. M. Shmarov[2], D. Yu. Logunov[2], B. S. Naroditsky[2], R. I. Ataullakhanov[1*], R. M. Khaitov[1], A. L. Gintsburg[2]

[1]National Research Center – Institute of Immunology Federal Medical-Biological Agency of Russia; Kashirskoye shosse, 24, corpus 2, 115478, Moscow, Russia

[2]N.F. Gamaleya Research Institute of Epidemiology and Microbiology, Ministry of Health of the Russian Federation; Gamaleya Str., 18, 123098, Moscow, Russia

Received 27.08.2014

*E-mail: ravshan.ataullakhanov@gmail.com

ABSTRACT **Replication-defective adenoviral vectors are effective molecular tools for both gene therapy and gene vaccination. Using such vectors one can deliver and express target genes in different epithelial, liver, hematopoietic and immune system cells of animal and human origin. The success of gene therapy and gene vaccination depends on the production intensity of the target protein encoded by the transgene. In this work, we studied influence of Toll-like receptors (TLR) agonists on transduction and expression efficacy of adenoviral vectors in animal and human antigen-presenting cells. We found that agonists of TLR2, 4, 5, 7, 8 and 9 significantly enhance a production of the target protein in cells transduced with adenoviral vector having the target gene insert. The enhancement was observed in dendritic cells and macrophages expressing cytoplasmic (GFP), membrane (HA) or secretory (SEAP) proteins encoded by the respective rAd-vectors. Experiments in mice showed that enhancement of the transgene expression can be achieved in the organism of animals using a pharmaceutical-grade TLR4-agonist. In contrast to other TLR-agonists, the agonist of TLR3 substantially suppressed the expression of transgene in cells transduced with adenoviral vectors having insert of GFP or SEAP target genes. We propose that the enhancement of transgene expression is linked to the activation of MyD88→ NF-kB, while the inhibition of transgene expression depends on TRIF→ IRF signaling pathways. Both of these pathways jointly exploited by TLR4-agonists lead to the enhancement of transgene expression due to the dominant role of the MyD88→ NF-kB signaling.**

KEYWORDS **gene therapy, gene vaccination, recombinant replication-defective adenovirus vectors, transgene expression, Toll-like receptor agonists.**

ABBREVIATIONS **rAd – replication-defective recombinant adenovirus vector; TLR – Toll-like receptor; PFU – plaque-forming unit; CM – complete culture medium; BSA – bovine serum albumin; PBS – phosphate buffered saline; LTA – lipoteichoic acid; Poly [I:C] – polyinosinic : polycytidylic acid; LPS – lipopolysaccharide; MPL-A – monophosphoryl derivative of lipid A; TNF-α – tumor necrosis factor alpha; GM-CSF – granulocyte macrophage colony stimulating factor; CLI-095 – also known as TAK-242, a specific inhibitor of TLR4-signaling; SEAP – secreted embryonic alkaline phosphatase; GFP – green fluorescent protein; DAPI – 4',6-diamidino-2-phenylindole dihydrochloride; HA – H1N1 influenza virus hemagglutinin; CMV – *Cytomegalovirus*; IL – interleukin.**

INTRODUCTION

Replication-defective adenovirus vectors (rAd) are used for transgene expression in different tissues. Depending on the transgene inserted rAd are used for gene therapy (tumor suppressor genes, growth factors, etc) or gene immunization (genes encoding infection-specific antigens). In the case of in vivo immunization, the transgene is expressed in transduced cells during 2-3 weeks, which leads to a potent immune response. Effective vaccines against tuberculosis, malaria, influenza, and other important infectious diseases have been designed as rAd. The majority of rAd-based medical preparations are currently in various stages of clinical trials [1–5], and only one therapeutic agent has

been licensed and approved for use [6]. There is a large body of evidence demonstrating that rAd-derived immunogens and viccines are safe and efficacious.

The immune response to the rAd-expressed antigen could be enhanced by Toll-like receptor agonists (TLR) [3]. We engineered a rAd-based vaccine encoding the surface antigens of the influenza virus in combination with a synthetic TLR4 agonist – Immunomax® [7–9], a plant-derived water soluble polysaccharide of a molecular weight of over 1 MDa [10]. The use of Immunomax as an adjuvant enhances the T-cell response to Influenza virus antigens and increases rAd-vaccine protectivity. In addition, this adjuvant allows a 3- to 10-fold reduction in the dosage of rAd, encoding influenza virus antigens, without compromising immunogenicity and protective efficacy of the vaccine.

Immunomax has no direct influence on T-cells. It stimulates antigen-presenting cells, particularly dendritic cells and macrophages. In dendritic cells, Immunomax induces the expression of co-stimulatory molecules such as CD80, CD86, CD40, and the MHC class II and the release of immunostimulatory cytokines such as IL1β, TNF-α, IL6, IL8, and IL12 [10]. Although these events in antigen-presenting cells are sufficient for the immunostimulatory response elicited by Immunomax, it is likely that Immunomax also increases the expression of antigen encoded by rAd.

Following administration of rAd, the antigen is produced in antigen-presenting cells, which allows one to suppose that Immunomax, alongside co-stimulatory molecules and cytokines, could also promote the expression of rAd-encoded antigen. Such stimulatory activity of the preparation could contribute to an enhanced response of T-cells, recognizing antigens on the surface of the antigen-presenting dendritic cells.

In the present study, we examined the expression levels of the rAd-encoded antigens in dendritic cells and macrophages treated with Immunomax and agonists of other TLRs. The findings demonstrate that under influence of Immunomax the expression of rAd-encoded antigens in dendritic cells and macrophages is elevated 2- to 11-times. The increased expression was observed with rAd-encoded membrane-bound, cytoplasmic, and secretory proteins. Similarly to Immunomax, another TLR4-agonist --- an *Escherichia coli* Lipopolysaccharide --- also up-regulated the expression of rAd-encoded transgenic proteins. In addition, agonists of other TLRs, in particular TLR2, 5, 7, 8 and 9, increased the expression levels of rAd-encoded proteins, whereas the TLR3 agonist down-regulated it. Comparison of the intracellular signaling pathways linked to different TLRs suggested that the pathway beginning from MyD88 and ending with NF-κB does enhance expression, but the pathway beginning from TRIF and ending with the IRF-3 and IRF-7 transcription factors inhibits the expression of rAd-encoded proteins. The pathway started by MyD88 dominates over the one started by TRIF. Therefore, transgene expression is increased under influence of TLR4 agonist, when both pathways are operational (MyD88 and TRIF).

EXPERIMENTAL SECTION

Antibodies and reagents

The following monoclonal antibodies were used: CD11b-BD Horizon V450, Ly-6G APC-Cy7 (BD Pharmingen™), CD11c PE, CD19 eFluo450 (eBiosciences), F4/80 APC (BioLegend), Anti Mouse MHC II (I-A)-FITC (eBiosciences). Monoclonal antibodies to H1N1 influenza virus (HA) were a courtesy of A.A. Kushch (Ivanovskii Institute of Virology, Ministry of Health of the Russian Federation). The following Toll-like receptor agonists were used: lipoteichoic acid (LTA, TLR2 ligand), a synthetic analog of double-stranded RNA – polyinosinic:polycytidylic acid (Poly[I:C], TLR3 ligand), monophosphoryl lipid A (MPL-A, TLR4 ligand), flagellin (TLR5 ligand), imiquimod (TLR7/8 ligand), synthetic oligonucleotide ODN-CpG 1826 (TLR9 ligand), all obtained from InvivoGen; lipopolysaccharide from *E. coli* serotype 055:B5 (LPS, TLR4 ligand, Sigma, L-2880). In addition, a recombinant tumor necrosis factor alpha was used (TNF-α, Sigma, T7539). In some experiments CLI-095 (InvivoGen), a specific inhibitor of the TLR4-dependent pathway, DAPI dihydrochloride (Sigma), was used as a nuclear counterstain.

Animals

Eight- to ten-week-old BALB/c mice were obtained from the breeder Stolbovaya and fed standard rodent food under standard animal house conditions in the vivarium of the National Research Center Institute of Immunology FMBA.

Cell cultures

All cell cultures were incubated in a complete medium (CM) based on DMEM with 25 mM HEPES supplemented with a cocktail of nonessential amino acids, 10% fetal bovine serum (FBS), 2 mM L- glutamine, 1 mM sodium pyruvate, 50 μM β-mercaptoethanol and 10 μg/ml gentamycin (all reagents obtained from PanEco) at 37°C in a 5% CO_2 humidified atmosphere.

The cell line 293/TLR4-MD2-CD14 (InvivoGen), stably transfected with the TLR4 and CD14 and MD-2 co-receptors, was maintained *in vitro* in the presence of the selective antibiotics blasticidin and hygromycin according to the manufacture's instructions. For the assessment of NF-κB activity, the cells were transduced with a lentivirus vector (Cleveland BioLabs) bearing a

reporter β- galactosidase gene under the control of the NF-κB-dependent promoter. Thereafter, the cells were cultured following the manufacturer's protocol in the presence of another selective antibiotic – puromycin.

Primary cell suspensions from the spleen, bone marrow, and peritoneal cavity were made as described elsewhere. Dendritic cells were obtained *in vitro* by culturing bone marrow cells of BALB/c mice with a granulocyte-macrophage colony-stimulating factor (GM-CSF). Bone marrow was washed out from the femurs and the tibias, erythrocytes removed by osmotic shock, nuclear cells washed twice in PBS (Amresco, E404), followed by cultivation in a complete medium supplemented with 10 ng/ml GM-CSF (Sigma) for 7 days as described [4]. After 7 days of culture, the non-adherent cells contained 70–75% of dendritic cells. The adherent cells comprised 95% of macrophages. After removed of non-adherent cells and washing the remaining confluent cells with PBS (0.5% FBS), macrophages were detached by incubation in a Versen solution (PanEco) for 1 h at 4°C. Then cells were gently washed off in PBS (0.5% FBS).

Peritoneal macrophages were obtained by washing of the peritoneal cavity of BALB/c mice with PBS supplemented with 1% glucose, 10 mM HEPES, and 0.5% FBS. The cells were pelleted by centrifugation, resuspended in CM, and cultured for 18–20 h at 37°C in a humidified atmosphere of 5% CO_2. Then non-adhesive cells were gently washed away with the medium and PBS. The remaining adherent cells comprised over 90% of macrophages.

Recombinant replication-defective adenovirus vector with a gene insert

Replication-defective adenovirus vectors rAd-SEAP, rAd-GFP, and rAd-HA carrying the gene of secreted embryonic alkaline phosphatase (SEAP), green fluorescent protein (GFP), or H1N1 influenza virus hemagglutinin (HA) were constructed based on the pShuttle-CMV plasmid according to the manufacturer's instruction for the AdEasy Adenoviral vector system (Stratagene, cat. 240009), using the plasmids pGREEN (Carolina Biological Supply Company), p310D (pRc-CMV-SEAP, produced in-house) and pAL-HA (produced in-house). The GFP, SEAP, and HA inserts in the corresponding constructs pShuttle-CMV-GFP, pShuttle-CMV-SEAP, and pShuttle-CMV-HA were verified by restriction analysis using EcoRI, NotI and EcoRV endonucleases, and PCR.

The presence of the genes GFP, SEAP, and HA in rAd was confirmed by PCR. The effective titer of the rAd-GFP, rAd-SEAP, and rAd-HA preparations was estimated using the plaque-forming assay in the HEK-293 cell culture [11].

Transduction of cells with recombinant replication-defective adenovirus vectors

The cell cultures were transduced with rAd-SEAP, rAd-GFP, or rAd-HA at a dose of 7–200 PFU/cell in a 50 μl OpTmizer™ serum-free medium ("GIBCO") for 1 h, 150 μl of CM was then added to the cells. The transduced cells were cultured in the presence or absence of the TLR4 agonist Immunomax (10 μg/ml) for 1–6 days. When other TLR agonists were studied, the cells were incubated in the presence of LTA (1 μg/ml), Poly[I:C] (10 μg/ml), LPS (10 μg/ml), MPL-A (5 μg/ml), flagellin (0.1 μg/ml), imiquimod (1 μg/ml), or ODN-CpG 1826 (10 ng/ml). In addition, for cell activation, bypassing the TLR pathway, TNF-α (10 ng/ml) was used. TLR4-associated signaling was inhibited using CLI-095 (1 μg/ml).

In vivo transduction with recombinant replication-incompetent adenovirus vectors

For *in vivo* transduction, BALB/c mice were intraperitoneally injected with rAd-SEAP at a dose of 10^8 PFU in 200 μl of a physiological saline without or together with 10 μg Immunomax (four mice in each group).

Transgene expression rate was evaluated by the serum level of SEAP protein. On day 3 post-injection, blood was sampled from the retro-orbital sinus of rAd-SEAP-injected mice and serum level of SEAP was measured.

Measurement of production intensity of the SEAP, GFP, and HA proteins encoded by rAd.

The expression rates of SEAP in the serum or culture medium was assessed as described in [12] with minor modifications. Samples were clarified by centrifugation at 14,000 g for 2 min, followed by heating at 65°C for 5 min. The substrate p-nitrophenyl-phosphate was added in the reaction buffer (0.5 M $CaCO_3$, 0.5 mM $MgCl_2$, pH 9.8); and the absorbance was measured at 405 nm. The SEAP activity was expressed as mU/ml, given that 1 mU/ml corresponds to an increase in absorbance of 0.04 U/min.

Intracellular GFP accumulation was estimated by flow cytometry on FACS Aria II (BD Biosciences). Fluorescence was excited with the 488 nm laser, and emission intensity was measured between 515 and 545 nm. Cell populations were identified using fluorochrome-conjugated antibodies to the surface proteins CD11b , CD11c, CD19, Ly6G, F4/80; followed by analysis on a FACS Aria II flow cytometer. In addition, accumulation of GFP in dendritic cells and macrophages labeled with CD11c or F4/80 antibodies, respectively, was confirmed by confocal microscopy.

Expression of membrane-bound HA was examined by staining cells with HA-specific monoclonal antibod-

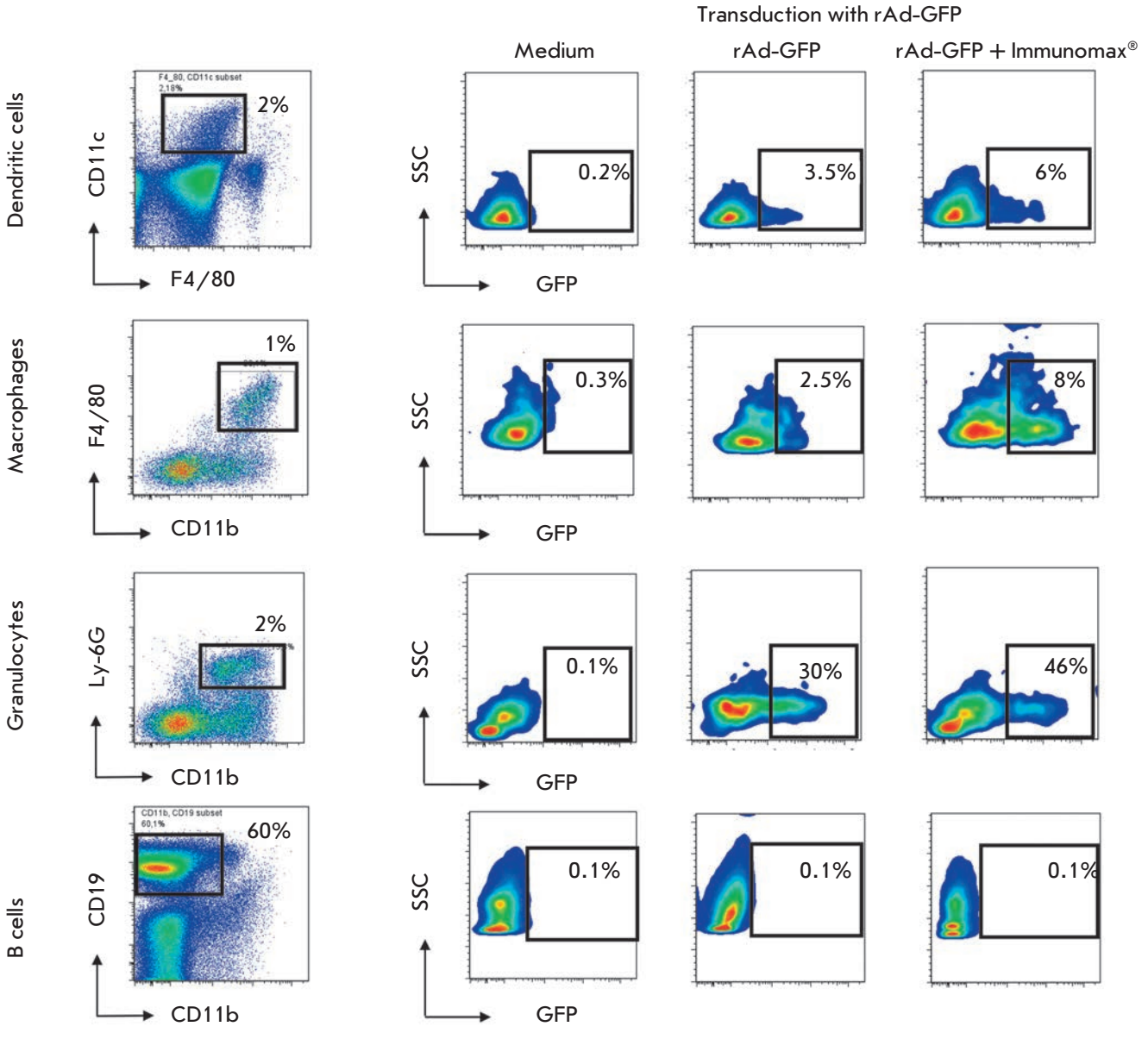

Fig. 1. Influence of the TLR4-agonist (Immunomax) on the transduction and expression of rAd-GFP in different cell types of mouse spleen cells. Mouse splenocytes were transduced with rAd-GFP ($5x10^5$ PFU/ml) and incubated for 3 days in the presence of Immunomax (10 μg/ml) or its absence. Then cells were labeled with fluorochrome-conjugated antibodies and analyzed using a FACS Aria II flow cytometer. The left vertical – gating of $CD11c^+$ dendritic cells, $F4/80^+$ macrophages, $CD11b^+$ $Ly6G^+$ granulocytes and $CD19^+$ B-cells with the indication of the cell type content (percent) in the total population of splenocytes. Respective horizontal lines represent the contents of GFP-positive dendritic cells, macrophages, granulocytes, and B cells after transduction with rAd-GFP and further cultivation with Immunomax or without. The negative control (medium) represents spleen cell cultures without transduction

ies, followed by flow cytometry on a FACS Aria II flow cytometer.

Confocal microscopy

The cell cultures in CM were incubated on culture slides (SPL Life Sciences Ltd., S. Korea) suitable for the following microscopy. After incubation, the cells were fixed for 20 min in PBS containing 3.7% paraformaldehyde (Sigma), washed in PBS with 0.5% FBS, and then stained with antibodies for 1 h. After an extra wash with PBS, the cells were stained with DAPI (1 μg/ml) in PBS for confocal microscopy on a Axio Observer. Z1 microscope (Carl Zeiss, Germany) with a QuantEM 512SC camera (Photometrics, UK).

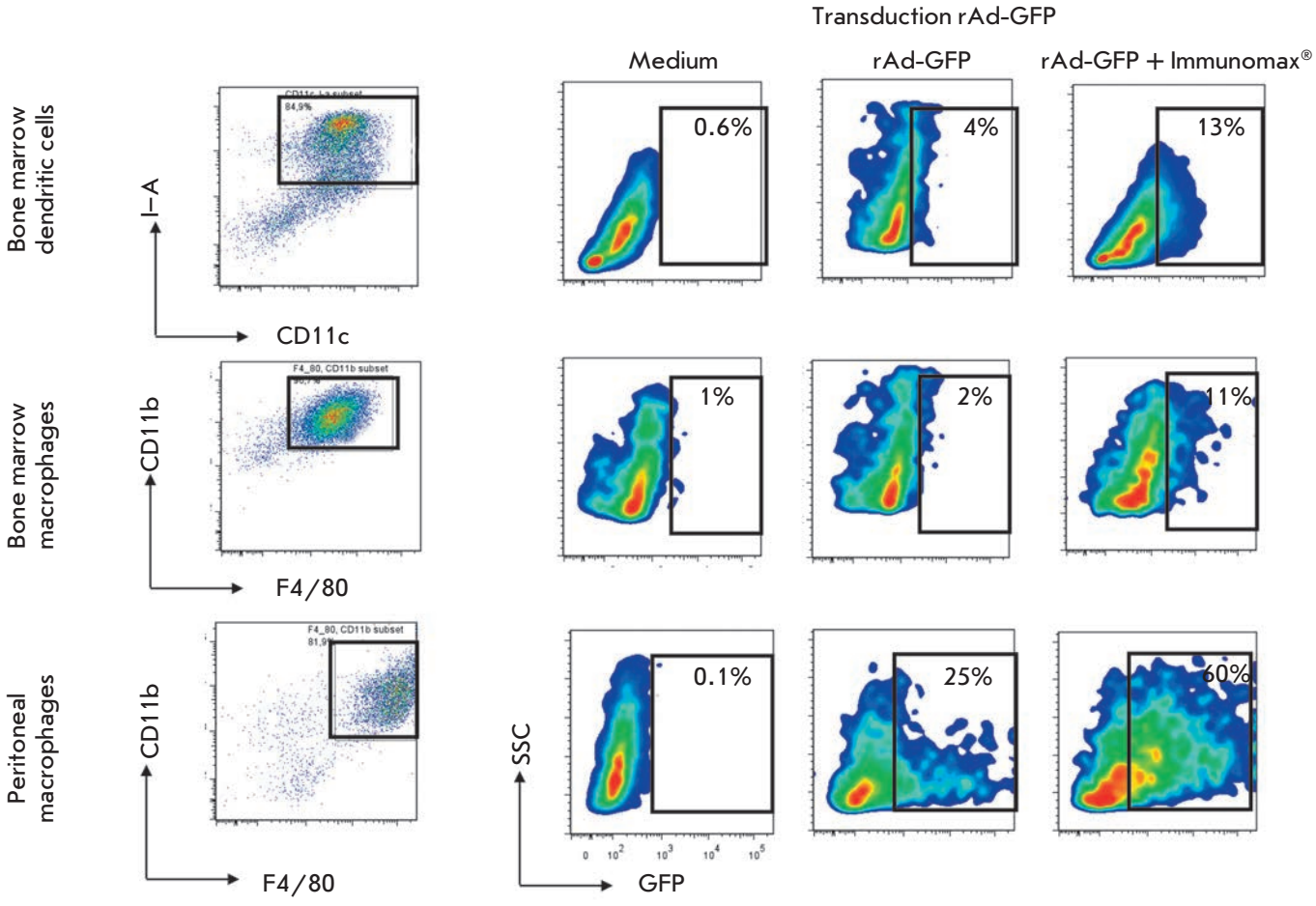

Fig. 2. Influence of the TLR4-agonist (Immunomax) on the transduction and expression of rAd-GFP in dendritic cells obtained by the *in vitro* differentiation of mouse bone marrow cells, and also in mouse peritoneal macrophages. The cells were transduced with rAd-GFP ($5x10^5$ PFU/ml) and incubated for 4 days in the presence of Immunomax (10 μg/ml) or its absence. Then, the cells were labeled with fluorochrome-conjugated antibodies and analyzed using a FACS Aria II flow cytometer. The left vertical – gating of $CD11c^+I\text{-}A^+$ dendritic cells and $CD11b^+F4/80^+$ bone marrow macrophages, and $CD11b^+F4/80^+$ peritoneal macrophages with the indication of these cell types percent in the total population. Respective horizontal lines represent the contents of GFP-positive dendritic cells and macrophages after transduction with rAd-GFP and further cultivation with Immunomax or without. The negative control (medium) represents cell cultures without transduction

Statistical analysis

Data are presented as means ± SD. Statistical analysis of the data was performed using Student's t-test

RESULTS

Immunomax enhances expression of the protein encoded by rAd

Replication-defective rAd readily transduce epithelial cells and transgene is efficiently expressed in this type of cells. For rAd-immunization purposes, it is critically important to achieve the target antigen expression within antigen-presenting cells, particularly dendritic cells and macrophages. In this study, we showed a substantial expression of rAd in murine primary dendritic cells and macrophages. Upon inoculation of rAd-GFP into cultures of spleen and bone marrow cells, as well as peritoneal macrophages, we observed the transgene expression in splenic dendritic cells, macrophages and granulocytes, and in bone marrow-derived macrophages and dendritic cells obtained in the presence of GM-CSF, and also in peritoneal macrophages (*Fig. 1 and 2*). No rAd expression was observed in lymphoid cells, in particular B-cells, CD4 and CD8 T-cells, and NK cells. The cell type expressing GFP was confirmed via staining with monoclonal antibodies to CD11c for dendritic cells, and F4/80 for macrophages, and Ly-6G for granulocytes. Figure 3A shows microphotographs

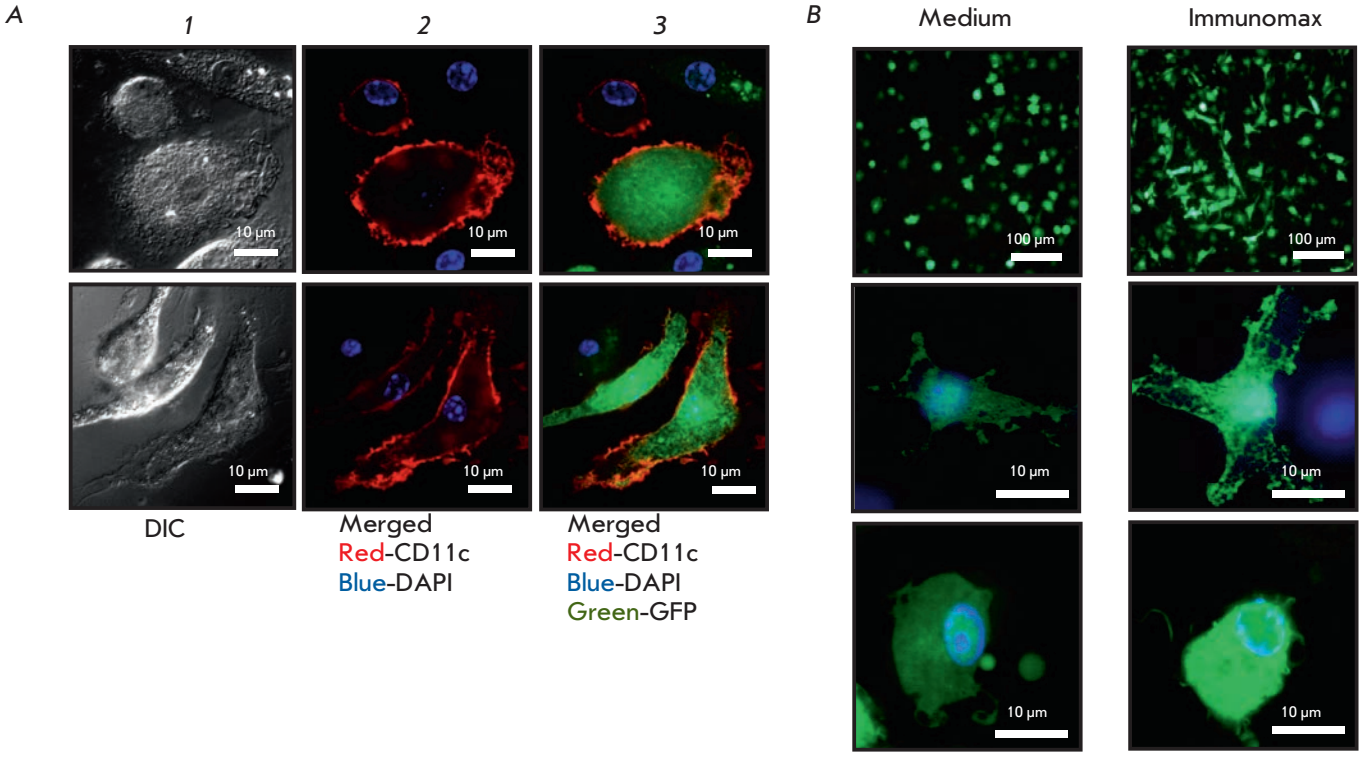

Fig. 3. Confocal microscopy of dendritic cells transduced with rAd-GFP in the presence of Immunomax or its absence. **A** - cultures of bone-marrow dendritic cells incubated in a complete medium containing rAd (30 PFU per a cell). In 24 hrs, the cells were fixed and stained with the CD11c-PE antibody. Microscopy was performed in PBS with DAPI (1 μg/ml) using a Axio Observer. Z1 (Zeiss, Germany) with QuantEM 512SC camera (Photometrics, UK), by the use of 405 nm, 488 nm, and 561 nm lasers. From left to right, cell images are shown: (1) DIC – differential interference contrast; (2) merging of anti-CD11c-PE (red) and DAPI (blue) channels; (3) merging of GFP (green), DAPI, and anti-CD11c-PE channels. **B** – the culture of bone-marrow dendritic cells 24 hrs after incubation in the presence of rAd-GFP with Immunomax (10 μg/ml) or without. Photographs show the merged images in GFP (green) and DAPI (blue) channels at 20x and 200x magnifications

of dendritic cells expressing CD11c molecules on their outer membrane and GFP in the cytosol.

Activation of dendritic cells with Immunomax, simultaneously with transduction by rAd-GFP, led to enhanced expression of the GFP protein, which could be observed by an increase in both the proportion of GFP-positive dendritic cells (*Fig. 1, 2, 4A*) and the intensity of GFP production (*Fig. 3B, 4B*). A similar elevation in rAd-GFP expression was also observed in macrophages. Enhanced expression was observed regardless of the tissue origin of dendritic cells and macrophages. It was pronounced in dendritic cells from the spleen and bone marrow as well as macrophages from the spleen, bone marrow, or the peritoneal cavity (*Fig. 1–4*).

No influence of Immunomax on rAd tropism for its target cell types

When studying rAd expression in mouse spleen or bone marrow cell cultures, we noticed that Immunomax increased transgene expression in only those cell types that exhibited the vector expression in the absence of Immunomax. Immunomax did not retarget the adenovirus vector to different cell types. In particular, rAd-GFP was expressed in dendritic cells and macrophages but not in CD4 or CD8 T-cells, B-cells and NK-cells. Immunomax increased rAd-GFP expression only in dendritic cells, macrophages, and granulocytes. In other cell types, the vector still showed no expression. As an example, Fig.1 illustrates B-cell studies (*Fig. 1*) in which rAd-GFP exhibited no expression both before and after activation with Immunomax.

No influence of Immunomax on rAd replication in HEK-293 cells

Enhanced expression of rAd-encoded transgene under the influence of Immunomax raises natural concern whether Immunomax can enhance also the replication of adenoviral particles. Since replication-defective

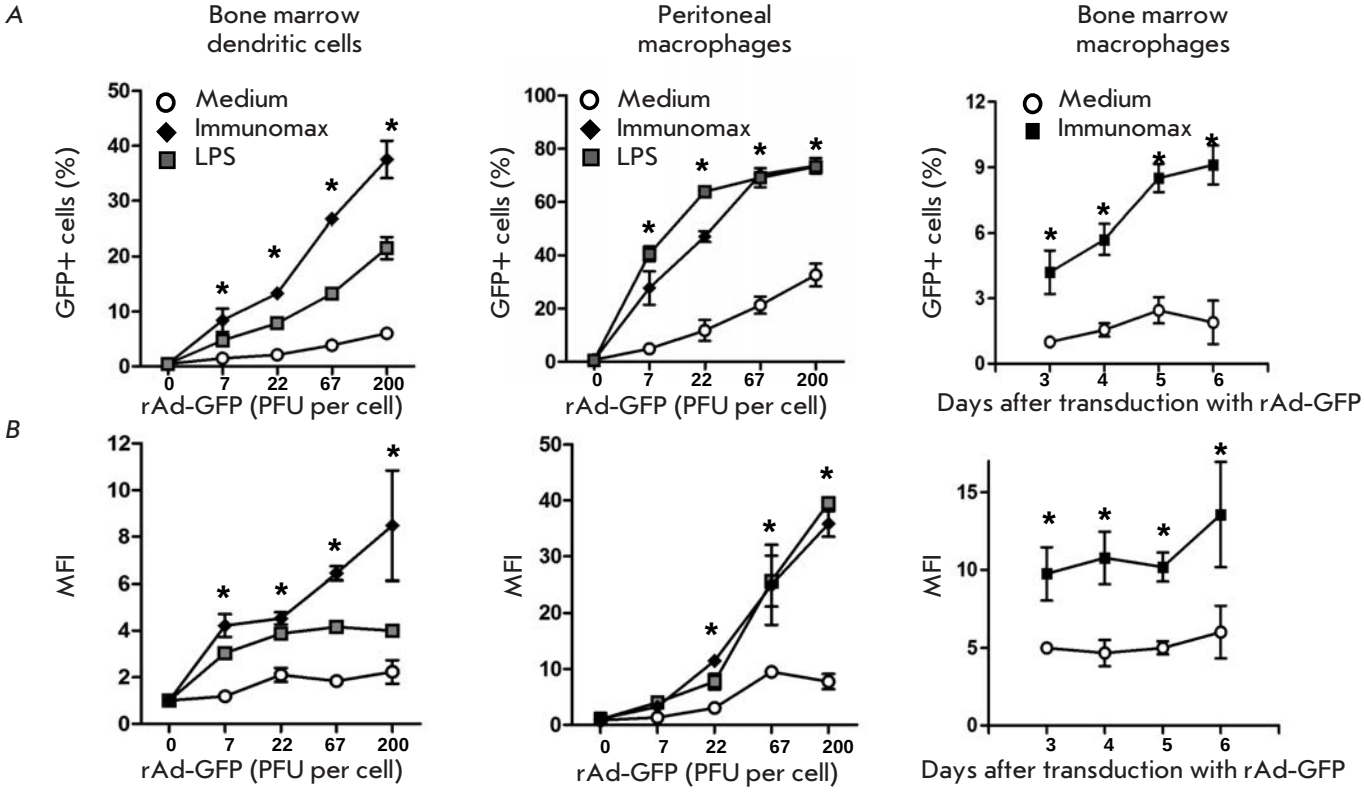

Fig. 4. Influence of the TLR4 agonist (Immunomax) on GFP-expression in dendritic cells and macrophages depending on the rAd-GFP dose or the time elapsed after the transduction of cells. Bone marrow dendritic cells and peritoneal macrophages were transduced with rAd-GFP and then incubated for 24 hrs in the presence of Immunomax (10 μg/ml), or LPS (3 μg/ml), or without activators (medium). Bone marrow macrophages were transduced with rAd-GFP in the presence of Immunomax (10 μg/ml) or without it, and then they were incubated for 6 days. Cell samples were taken on days 3, 4, 5, and 6. After staining with fluorochrome-conjugated antibodies, the cells were analyzed using flow cytometry on a FACS Aria II. *x*-axis – rAd-GFP dose used for the transduction of cells, or days after transduction (the right side vertical). *y*-axis – (**A**) percent of GFP-positive cells; (**B**) mean fluorescence intensity (MFI) normalized on the value of the control cultures without the activator. Mean values and standard deviations are shown based on data from three experiments. Significance for $P<0.05$ is shown using asterisk *

adenovirus vectors cannot replicate in common cells, their propagation is usually achieved in the specially constructed HEK-293 cell line bearing adenoviral E1-genes, which are deleted from adenovirus vectors.

We examined if Immunomax affects the replication capacity of rAd in a HEK-293-TLR4/MD2 cell culture. In our previous studies, we had demonstrated that Immunomax acts through the TLR4 pathway, triggering the synthesis of reporter protein in HEK-293-TLR4/MD2 cells. This effect of Immunomax is suppressed by CLI-095, a selective inhibitor of the TLR4-signal pathway. As with HEK-293 cells, HEK-293-TLR4/MD2 cells exhibit active rAd replication, resulting in cytopathic effects on days 2–4. The rAd-GFP vector was titrated on a HEK-293-TLR4/MD2 cell culture in the presence or absence of Immunomax. The rAd-GFP vector was added in three wells of a 96-well plate at 40–50% confluence of HEK-293-TLR4/MD2 cells. Virus titration was performed as 24 steps of 5-fold successive dilutions. Cell cultures positive for rAd replication displayed intracellular GFP accumulation and cell death within a few days. The rAd vector replicated starting from the highest concentration to the 13^{th} successive dilution. In the presence and absence of Immunomax (control cultures) the lowest rAd-GFP dilution at which GFP was expressed and cytopathic effects were observed was 5^{13}; i.e., Immunomax did not affect rAd replication in HEK-293-TLR4/MD2 cells carrying TLR4 receptors and triggering NF-κB activation in response to Immunomax.

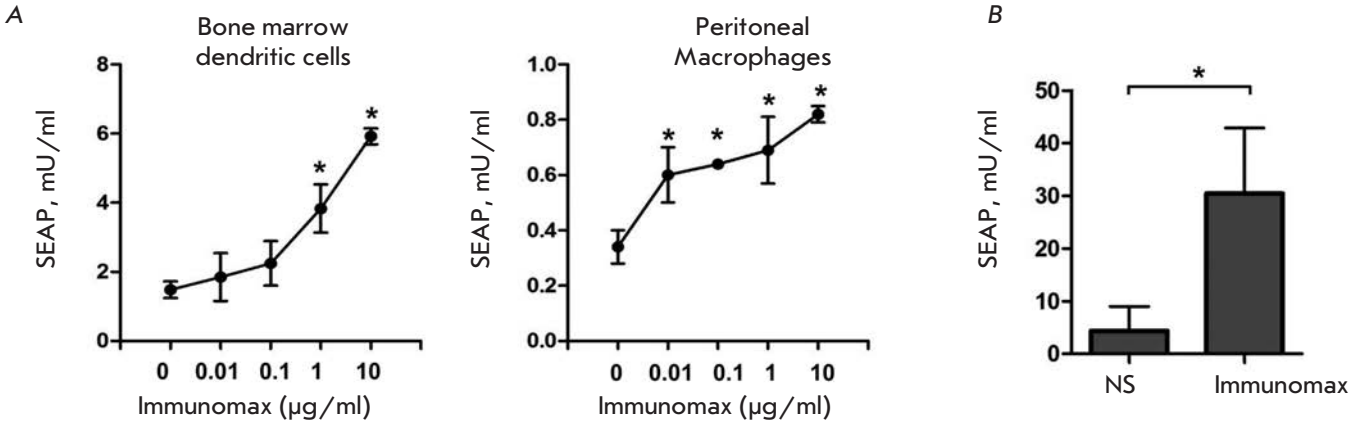

Fig. 5. Influence of the TLR4 agonist (Immunomax) on the expression of the rAd-encoded secretory target protein (SEAP) in the *in vitro* cell cultures and in the mouse organism. (**A**). Mouse bone marrow dendritic cells and peritoneal macrophages were transduced with rAd-SEAP ($5x10^5$ PFU/ml) and incubated during 4 days in the presence of the shown concentrations of Immunomax. Production intensity of the target protein was estimated according to the concentration of SEAP (mU/ml) in culture supernatants. (**B**). The SEAP target protein concentration in mouse blood 3 days after injection of rAd-SEAP with Immunomax or without it. The experimental mice (n=4) were intraperitoneally injected with rAd-SEAP (10^8 PFU/mouse) with Immunomax (10μg) in a volume of 200 μl physiological saline. The control mice (n=4) were injected with a 200 μl volume of physiological saline, instead of Immunomax. Three days later, the concentration of SEAP was measured in the blood serum of all mice. Significance for $P<0.05$ is shown using asterisk *

Immunomax enhances the expression of transgenes encoding cytoplasmic, secretory, or membrane-bound proteins.

It was shown above that Immunomax enhances the expression of transgene incorporated in rAd, which encoded the cytoplasmic protein GFP. Here we demonstrate that the expression of secretory and membrane-bound proteins is also up-regulated in response to Immunomax. For these experiments, we used rAd-SEAP and rAd-HA, which encode the embryonic alkaline phosphatase and the influenza virus hemagglutinin, respectively. SEAP expression was estimated by its concentration in the culture medium, and HA expression was measured on the cell surface using flow cytometry with HA-specific monoclonal antibodies.

Figure 5A shows the expression of rAd-SEAP *in* mouse dendritic cells and peritoneal macrophages. The findings indicate that Immunomax amplifies expression of the secretory protein SEAP encoded by rAd-SEAP. In studies of human monocytes transduced with rAd-HA, Immunomax also enhanced expression of the membrane-bound protein HA encoded by the vector. Of note, the increase in transgene expression was observed not only in mouse, but also in human cells.

Immunomax enhances expression of rAd not only *in vitro* but also *in vivo*

Our principal concern was to know whether the expression of rAd-encoded transgene could be enhanced *in vivo*. An increase in the target protein expression would be of great benefit to both immunization and gene therapy using rAd.

We investigated the influence of Immunomax on transgene expression in BALB/c mice that received rAd-SEAP intraperitoneally at a dose of 10^8 PFU in a 200 μl normal saline solution. The expression levels of SEAP were assessed by its blood concentration on day 3 post-injection. Experimental mice were injected with rAd-SEAP and Immunomax (10 μg/mouse). The control mice received rAd-SEAP with normal saline solution. The findings in *Fig. 5B* demonstrate that Immunomax caused a statistically significant increase in production of SEAP in mice injected with the rAd-SEAP vector.

Enhanced rAd-expression in antigen-presenting cells is induced by agonists of TLR2, 4, 5, 7/8 and 9. The TLR3 agonist suppresses rAd expression

Immunomax acts as a TLR4 agonist which up-regulates rAd transgene expression in dendritic cells and macrophages. We were curious if another TLR4 agonist, in particular LPS, could exhibit the same activity. In addition, it was worthwhile to study agonists of other TLRs by their possible effects on rAd-encoded transgene expression. Data presented in *Figures 4* and *6* confirm that, similarly to Immunomax, LPS amplifies the transgene expression. Interestingly, the monophosphoryl lipid A (MPL-A), a minimal immunostimulatory derivative of LPS, also enhanced rAd-GFP expression. In addition, agonists of TLR2, 5, 7/8, and 9, similarly to

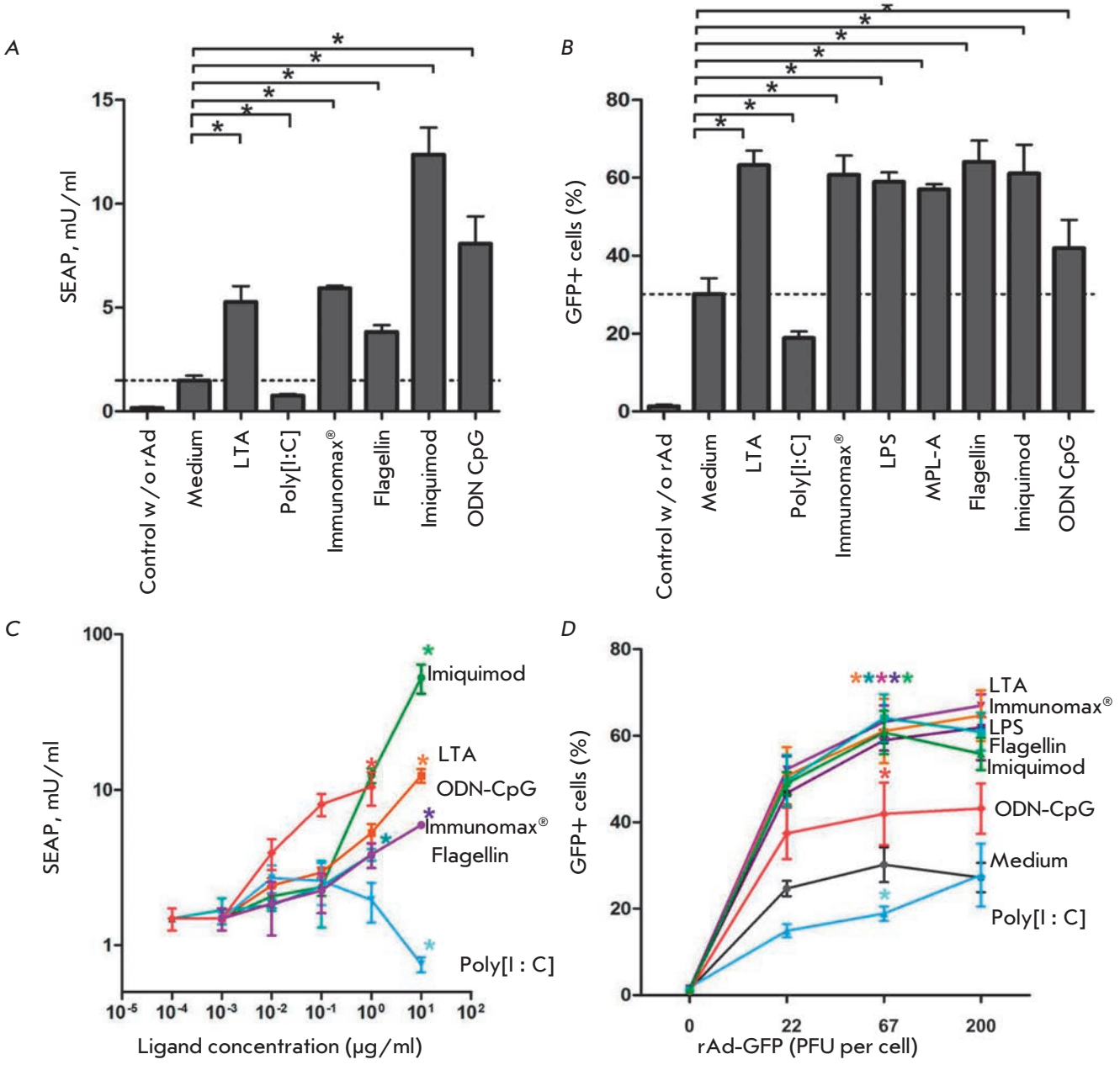

Fig. 6. Influence of different Toll-receptor agonists on the transduction and expression of rAd-SEAP and rAd-GFP in mouse macrophages. Mouse peritoneal macrophages were transduced with (**A**, **C**) rAd-SEAP $5x10^7$ PFU/ml, or (**B**) rAd-GFP $5x10^7$ PFU/ml, or (**D**) different concentrations of rAd-GFP, then the cells were incubated for 4 days in the presence of different TLR agonists. At the end of incubation, the concentration of SEAP in the culture supernatants (**A**, **C**), or percentage of GFP-positive cells (**B**, **D**) was determined. The following ligands were used in the experiments (**A**, **B**, **D**): LTA (1 μg/ml), poly[I:C] (10 μg/ml), LPS (10 μg/ml), MPL-A (5 μg/ml), flagellin (1 μg/ml), imiquimod (1 μg/ml), ODN-CpG 1826 (10 ng/ml), Immunomax (10 μg/ml). *x*-axis – the concentration of ligands in the experiments (**C**). Mean values and standard deviations are represented. Significance for $P<0.05$ is shown using asterisk *

agonists of TLR4, up-regulated the expression of *SEAP* and *GFP* genes comprised in rAd-SEAP and rAd-GFP, respectively (*Fig. 6*). The transgene expression increase caused by agonists of TLR2, 4, 5, 7/8, and 9 ranged in different experiments from 2- to 11-fold ($P < 0.05$).

Importantly, increased rAd expression induced by agonist of TLR was not attributed to the complex formation between rAd and the agonists or facilitated up-

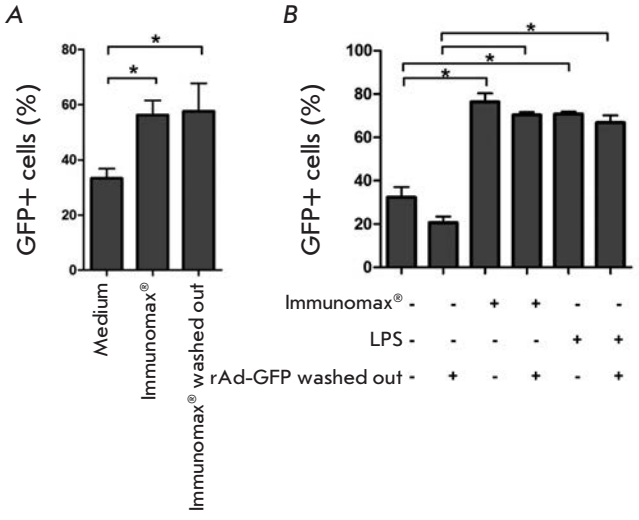

Fig. 7. Enhancement of rAd-GFP expression by the sequential (separate) use of the rAd-GFP and TLR4-agonists. (**A**). Peritoneal macrophages (2x10^4 per a well) were incubated during 4 hrs in a complete culture medium in the presence of Immunomax (10 μg/ml), then they were washed 3-times with PBS, transduced with rAd-GFP (70 PFU/cell), and transferred in the culture condition for further incubation under 37°C in 5% CO_2. After 24 hrs, the culture medium was replaced with a Versene solution (PanEco), the cultures were kept for 1 hr at 4°C, then the cells were carefully washed and harvested in PBS (0.5% BSA) and analyzed for GFP-positive cells using a FACS Aria II flow cytometer. (**B**) Peritoneal macrophages (2x10^4 per a well) were incubated during 2 hrs in a complete culture medium in the presence of rAd-GFP (70 PFU/cell). Then some of the wells were washed 3-times with PBS and re-filled with the complete culture medium with Immunomax (10 μg/ml) or LPS (3 μg/ml). Negative control cultures were washed and re-filled with the complete culture medium without activators. After 24 hrs, the cells were harvested using a Versene solution and analyzed for GFP-positive cells using a FACS Aria II flow cytometer

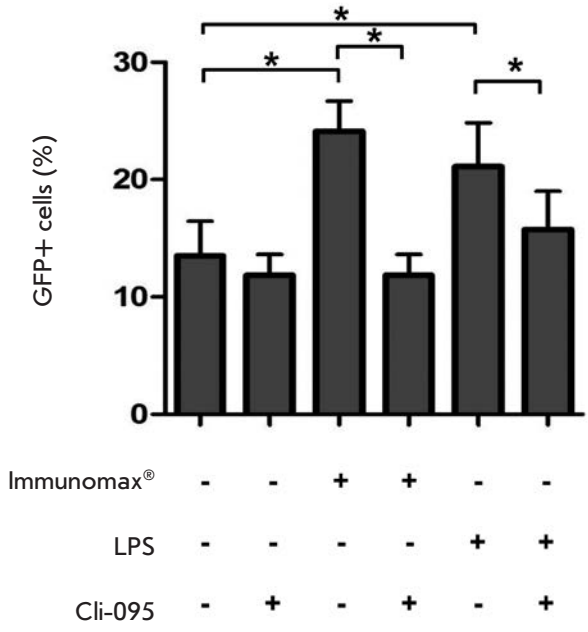

Fig. 8. A selective inhibitor of TLR4-signal (CLI-095) abrogates the enhancement of rAd-GFP expression by the TLR4-agonists. Peritoneal macrophages were incubated for 1 hr in a complete culture medium containing CLI-095 (1 μg/ml) or without it, then rAd-GFP (70 PFU/ml) and Immunomax (10 μg/ml), or LPS (3 μg/ml) were added into the culture medium. Control cultures were transduced with rAd-GFP without activators. After 24 hrs, the cells were harvested using a Versene solution and analyzed for GFP-positive cells using a FACS Aria II flow cytometer

take of rAd. This was shown in experiments in which rAd was washed prior to adding TLR4 agonists (Immunomax, LPS) over a cell monolayer, or *vice versa*, the TLR4 agonist was washed away prior to transduction of cells with rAd. In both cases, the increase in rAd expression was consistent with that observed for simultaneous use of rAd and a TLR agonists (*Fig. 7A,B*).

It was unexpectedly found that in contrast to agonists TLR2, 4, 5, 7/8, and 9, the agonist of TLR3 not only did the up-regulation of rAd-expression, but it suppressed the production of protein encoded by rAd. Agonist of TLR3 inhibited expression of rAd-SEAP and rAd-GFP (*Fig.6*).

NF-κB activation bypassing the TLR pathway also enhances transgene expression

All TLRs, except for TLR3, mediate the intracellular signal through an adaptor protein, MyD88, which ultimately leads to activation of NF-κB. We suggested that transgene expression is up-regulated by TLR agonists due to the activation of the MyD88 → NF-κB signaling axis. This suggestion was verified using two approaches: inhibition of the signal tranduction from TLR to MyD88 and activation of NF-κB without engagement of TLR. Signal transduction from TLR4 to MyD88 was blocked using a selective inhibitor: CLI-095. Activation of NF-κB, bypassing TLR, was performed with TNF-α, which activates NF-κB via TNF receptors.

The findings are given in *Figs. 8* and *9*. As anticipated, CLI-095 abrogated the enhancement of rAd-GFP expression caused by Immunomax or LPS (*Fig. 8*). Activation of peritoneal macrophages with recombinant TNF-α (10 ng/ml) induced increase in the expres-

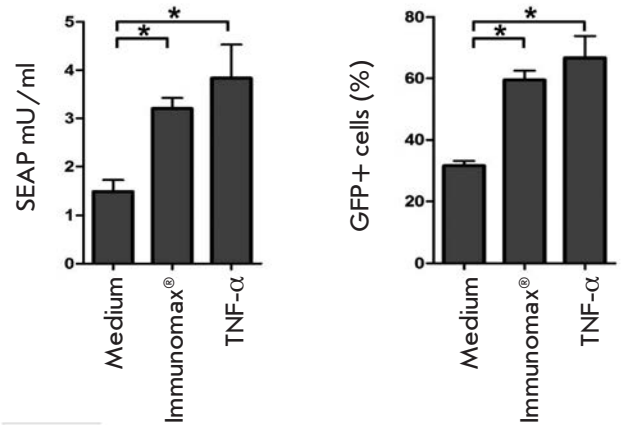

Fig. 9. TNF-α enhances the expression of target proteins in macrophages transduced with rAd with inserts of the GFP- or SEAP-target genes. Mouse peritoneal macrophages were transduced with rAd-SEAP ($5x10^7$ PFU/cell) or rAd-GFP ($5x10^7$ PFU/cell) then incubated during 4 days in the presence of Immunomax (10 μg/ml) or TNF-α (10 ng/ml). The control cultures were transduced with vectors in the absence of activators. At the end of incubation, the concentration of SEAP in the culture supernatants or percentage of GFP-positive cells was measured

sion of *SEAP* and *GFP* (*Fig. 9*), similar to that caused by Immunomax. The latter indicates that activation of TLR-pathways is not necessary, while activation of NF-κB is sufficient for the enhanced expression of transgene encoded by rAd.

DISCUSSION

Recombinant replication-defective adenovirus vectors transduce epithelial cells as well as dendritic cells and macrophages. The last two cell types are professional antigen-presenting cells, thus they are of interest in terms of rAd-based vaccines. Expression of rAd-encoded antigens in antigen-presenting cells ensures success of vaccines based on rAd. To elicit potent humoral and cell-mediated immune responses to the protein antigen at least two crucial requirements should be met. Firstly, the antigen-presenting cells should express target antigen peptide fragments bound to MHC class I and II molecules. Secondly, these cells also should express co-stimulatory CD80, CD86, and CD40 molecules on their surface, priming T-cells while encountering an antigen-presenting cell. The first requirement is met when the target antigen is produced by dendritic cells and macrophages transduced with rAd. To comply with the second requirement dendritic cells and macrophages must be activated through TLR receptors or other pathways.

In this work, we showed that the proteins encoded by rAd vectors are expressed in dendritic cells and macrophages (*Fig. 1–3*). Additional activation of antigen-presenting cells using the TLR4 agonist induces overexpression of the co-stimulatory molecules CD80, CD86, and CD40. In addition, as demonstrated in this study, the TLR4 agonist enhances the expression of the target protein (*Fig. 1–4*). An enhanced production of the protein antigen, together with expression of the co-stimulatory molecules CD80, CD86 and, CD40, could enhance efficacy of immune response when the combination of rAd and TLR4-agonist is used. We have previously reported that coadministration of rAd-HA encoding the influenza virus hemagglutinin and the pharmaceutical TLR4 agonist (Immunomax) allows one to increase efficacy of the vaccination against influenza viruses A and B [7].

Replication-defective adenovirus vectors could be used not only for vaccination, but also for gene therapy. In the latter case, administration of rAd with the transgene insert to a patient leads to the following production of the therapeutic protein during a period of 2-3 weeks. The possibility, shown in this study, for the increase of rAd-encoded protein production using combined administration of TLR4-agonist might be important for advancing effectiveness of rAd-based gene therapy. It is likely that the combination of rAd and TLR4-agonists enables one to obtain much higher concentrations of the therapeutic protein, as compared to rAd used alone, or substantially decrease the dose of rAd necessary to obtain the desired concentration of the protein.

TLR signaling has been the focus of much research for the last 15 years. These studies led to a good understanding of the intracellular signaling events triggered by ligands of TLR1/2, TLR2/6, TLR3, TLR4, TLR5, TLR7/8, and TLR9 in mouse and human cells [13, 14]. As was discovered, TLRs operate through two signaling pathways. One pathway is begun by the MyD88 key adaptor molecule and is ended by the activated NF-κB transcription factor. The other pathway is started by the TRIF key adaptor molecule and is ended by IRF transcription factors, in particular IRF3.

The signal pathway MyD88 → NF-κB comes into play when agonists act via TLR1/2, TLR2/6, TLR5, TLR7, TLR8 and TLR9 receptors. The signal pathway TRIF → IRF is employed during TLR3 activation. A unique feature of TLR4 is the use of both pathways. Immediately after ligation of the agonist, TLR4 signals from the outer cell membrane to the MyD88 → NF-κB pathway. Shortly, following endocytosis of the ligand-receptor complexes TLR4 initiates the second signal pathway TRIF → IRF.

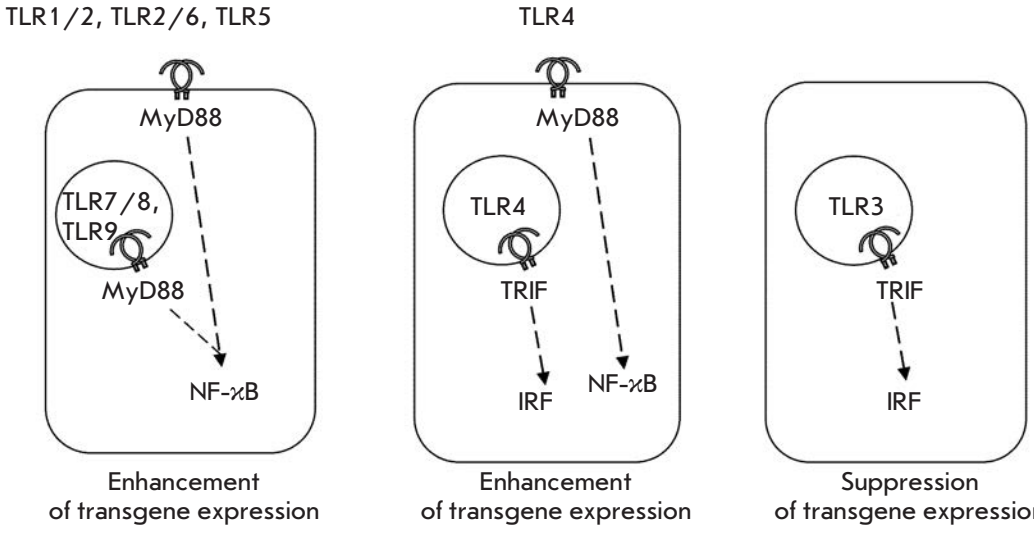

Fig. 10. A hypothetical mechanisms of enhancement and inhibition of Ad-vector encoded target protein expression by different TLR-agonists

In this study, we found that agonists of different TLRs enhance production of proteins encoded by rAd. Enhanced expression of transgene was observed following the use of the TLR2, TLR4, TLR5, TLR7/8 and TLR9 agonists (*Fig. 6A,B*). The TLR3 agonist acted opposite to the other agonists tested. Exposure of dendritic cells and macrophages to Poly[I : C] during their transduction with rAd-GFP or rAd-SEAP lead to a significant suppression of the GFP and SEAP production, respectively (*Fig. 6A,B*). Comparing various intracellular signaling pathways mediated by different TLRs, we suggested that the activation of NF-κB is responsible for up-regulation while the activation of IRF is involved in the down-regulation of the rAd-encoded protein synthesis.

A special case is the TLR4 agonist. Since TLR4 agonists enhance production of rAd-encoded proteins, we suggest that the MyD88 → NF-κB signaling axis dominates over the TRIF → IRF one (*Fig. 10*).

The suggestion of a stimulatory role for the MyD88 →NF-κB signaling axis is partially confirmed by our findings. CLI-095, a specific inhibitor of signal transduction from TLR4 to the adaptor molecule MyD88, abrogated enhancement induced by TLR4-agonists in production of rAd-encoded protein (*Fig. 8*). In turn, NF-κB activation bypassing TLR caused amplified expression of transgenes encoded by rAd. Activation of cells with TNF-α simultaneously with their transduction with rAd-SEAP or rAd-GFP enhanced the production of SEAP and GFP, respectively (*Fig. 9*). TNF-α signaling is known to operate through the TNFR1 and TNFR2 receptors. The intracellular signaling pathway is ended by NF-κB activation. Hence, NF-κB activation bypassing TLR receptors also enhances transgene expression, which does not confirm but bolsters our suggestion that up-regulation of the transgene-encoded protein production is dependent on NF-κB.

The rAd-GFP, rAd-SEAP, and rAd-HA constructs used in this study contained genes of corresponding proteins under the control of NF-kB-responsive CMV promoter having four recognition sites for NF-κB [15]. It is logical to hypothesize that additional activation of the NF-κB by TLR2, TLR4, TLR5, TLR7, TLR8, and TLR9 agonists could promote transcription of genes under the control of CMV-promoter.

In principle, TLR-mediated signaling can enhance production of a protein by affecting transcription, translation, and other essential cellular processes. The precise mechanisms by which the transgene expression is up-regulated upon activation of TLR2, TLR4, TLR5, TLR7, TLR8, TLR9 or reduced by the activation of TLR3 remain to be elucidated.

Replication-defective adenovirus vectors are used not only for immunization, but also in gene therapy. The effects of TLR agonists on rAd-transgene expression reported herein hold promise for a new approach to developing controlled transgene expression techniques *in vivo*. Ideally, advances in this field would allow to develop methods for controlled up-regulation or down-regulation of transgene expression *in patient*, depending on the purpose.

CONCLUSION

In our study, we examined the effects of Toll-like receptor agonists on the efficacy of transduction with and expression of rAd in the antigen-presenting cells of humans and animals. It is demonstrated that the agonist of TLR2, 4, 5, 7, 8, and 9 enhance production of the

protein encoded by rAd. The enhancement occurs in dendritic cells and macrophages producing cytoplasmic (GFP), membrane-bound (HA), or secretory (SEAP) proteins. Experiments in mice showed that target protein expression can be also enhanced in the animal organism with the use of a pharmaceutical TLR4 agonist. In contrast to other TLR agonists, the TLR3 agonist suppresses production of the protein (GFP or SEAP) in cells transduced with rAd having a corresponding gene insert.

The molecular mechanisms of the up- and down-regulation of rAd expression in antigen-presenting cells activated with various TLR agonists remain to be determined. In this paper, we reported on results that support the suggestion that the enhancement in rAd-transgene expression is due to the activation of the transcription factor NF-*k*B and that the suppression is attributed to the activation of IRF transcription factors. ●

REFERENCES

1. Arama C., Assefaw-Redda Y., Rodriguez A., Fernández C., Corradin G., Kaufmann S.H., Reece S.T., Troye-Blomberg M. // Vaccine. 2012. V. 30. No 27. P. 4040-4045.
2. Hoft D.F., Blazevic A., Stanley J., Landry B., Sizemore D., Kpamegan E., Gearhart J., Scott A., Kik S., Pau M.G., Goudsmit J., McClain J.B., Sadoff J. // Vaccine. 2012. V. 30. No 12. P. 2098-2108.
3. Scallan C.D., Tingley D.W., Lindbloom J.D., Toomey J.S., Tucker S.N. // Clin. Vaccine Immunol. 2013 V. 20. No 1. P. 85-94.
4. Sharma A., Tandon M., Bangari D.S., Mittal S.K. // Curr. Drug ther. 2009. V. 4. No 2. P. 117–138.
5. INGN 201: Ad-p53, Ad5CMV-p53, adenoviral p53, p53 gene therapy--introgen, RPR/INGN 201. // Drugs R. D. 2007. V. 8. No 3. P. 176-187. PMID: 17472413; [PubMed - indexed for MEDLINE] http://www.ncbi.nlm.nih.gov/pubmed/17472413
6. Pearson S., Jia H., Kandachi K. // Nat. Biotechnol. 2004. V. 22. No 1. P. 3-4.
7. Ataullakhanov R.R., Shmarov M.M., Sedova E.S., Logunov D.Yu., Pichugin A.V., Ataullakhanov R.I., Khaitov R.M. // Patent WO2013129961 A1 RU. C07K16 / 10, A61P31 / 16, C12N15 / 44, C07K14 / 11, A61K39 / 145. 2012.
8. Shmarov M.M., Sedova E.S., Verkhovskaya L.V., Rudneva I.A., Bogacheva E.A., Barykova Y.A., Shcherbinin D.N., Lysenko A.A., Tutykhina I.L., Logunov D.Y., Smirnov Y.A., Naroditsky B.S., Gintsburg A.L. // Acta Naturae. 2010. V. 2. No 1. P. 111-118.
9. Ataullakhanov R.I., Pichugin A.V., Shishkova N.M., Masternak T.B., Malkina E.Yu., Ulyanova L.I., Stetsenko O.N. // Immunologia. 2005. No 2, P. 111-120.
10. Melnikova T.M., Pichugin A.V., Ataullakhanov R.I., Khaitov R.M. // Patent Application RU 2013151824, priority date 21.11.2013.
11. Graham F.L., Prevec L. // Methods in Mol. Biol. 1991. V. 7. P. 109-127.
12. Berger J., Hauber J., Hauber R., Geiger R., Cullen B.R. // Gene. 1988. V. 66. No 1. P. 1-10.
13. Newton K., Dixit V.M. // Cold Spring Harb. Perspect. Biol. 2012. V. 4. No 3.
14. Lim K.H., Staudt L.M. // Cold Spring Harb. Perspect. Biol. 2013. V. 5 No 1.
15. Lee Y., Sohn W.J., Kim D.S., Kwon H.J. // Eur. J. Biochem. 2004. V. 271. No 6. P. 1094-105.

STIM1 Protein Activates Store-Operated Calcium Channels in Cellular Model of Huntington's Disease

V. A. Vigont, O. A. Zimina, L. N. Glushankova, J. A. Kolobkova, M. A. Ryazantseva, G. N. Mozhayeva, E. V. Kaznacheyeva*
E-mail: evkazn@incras.ru
Institute of Cytology, Russian Academy of Sciences, Tikhoretsky pr., 4, St. Petersburg, 194064, Russia
Received 22.05.2014

ABSTRACT **We have shown that the expression of full-length mutated huntingtin in human neuroblastoma cells (SK-N-SH) leads to an abnormal increase in calcium entry through store-operated channels. In this paper, the expression of the N-terminal fragment of mutated huntingtin (Htt138Q-1exon) is shown to be enough to provide an actual model for Huntington's disease. We have shown that Htt138Q-1exon expression causes increased store-operated calcium entry, which is mediated by at least two types of channels in SK-N-SH cells with different reversal potentials. Calcium sensor, STIM1, is required for activation of store-operated calcium entry in these cells. The results provide grounds for considering the proteins responsible for the activation and maintenance of the store-operated calcium entry as promising targets for developing novel therapeutics for neurodegenerative diseases.**

KEYWORDS **Huntington's disease, calcium, neurodegeneration, SOC, STIM1.**

ABBREVIATIONS **HD – Huntington's disease; I-V curves – current-voltage characteristic; PM – plasma membrane; ER – endoplasmic reticulum; Htt138Q-1exon – product of the 1st exon of the gene encoding mutated huntingtin or cells expressing this product; Htt138Q-1exon STIM1(-) – Htt138Q-1exon cells with suppression of STIM1 protein; IP_3 – inositol 1,4,5-trisphosphate, IP_3R1 – receptor of inositol 1,4,5-trisphosphate 1; GFP – green fluorescent protein; SK-N-SH – human neuroblastoma cells; STIM1 – stromal interaction molecule 1 (protein).**

INTRODUCTION

Abnormal calcium signaling has been detected in many diseases; in particular, destabilization of calcium ion channels of different types is associated with pathologies such as diabetes mellitus [1] or amyotrophic lateral sclerosis [2]. Many studies have demonstrated the involvement of impaired calcium signaling processes in neurodegeneration [3, 4].

Huntington's disease (HD) is an autosomal dominant neurodegenerative disease caused by an increased number of repeats encoding glutamine in the first exon of protein-coding in the huntingtin gene. The length of the polyglutamine repeat normally does not exceed 35 residues; in the case of the disease, the length of repeats can reach up to 90 or more glutamine residues. [5] HD affects striatal neurons first.

In cells, huntingtin acts as an adapter protein that provides co-localization of the proteins interacting with it and helps these proteins to perform their functions. Many proteins interact with huntingtin, their function varying from vesicular transport and endocytosis to the regulation of transcription and apoptosis [6].

One of the toxic functions of mutant huntingtin is destabilization of calcium signaling. It was previously shown that mutant huntingtin is capable of binding directly to the C-terminus of the inositol 1,4,5-trisphosphate 1 receptor (IP_3R1). Such binding increases IP_3R1 sensitivity to its ligand, which may activate the receptor and deplete the intracellular calcium stores in response to IP_3 basal concentration in cytosol [7]. It was also shown that expression of mutant huntingtin increases the function of NR2B-containing NMDA receptors [8] and affects the voltage-gated calcium channels [9]. All the pathways mentioned above cause an increased concentration of calcium ions in the cytosol and, as a consequence, abnormal accumulation of calcium in mitochondria [10, 11], activation of calpains [12], pathological initiation of calcium-dependent signaling pathways, and apoptotic activity of neuronal degeneration.

Previously, we detected an abnormal activation of store-operated calcium channels in human SK-N-SH neuroblastoma cells, expressing the full-length mutant huntingtin protein for the modeling of HD [13]. In addition, we demonstrated that the store-operated cal-

cium entry can be considered as a potential target for therapeutic intervention in the development of new approaches for treating HD. The hyperactivation of store-operated calcium entry in striatal neurons isolated from YAC128 mice, used as a model for HD, was demonstrated using the fluorescent method [14].

It is believed that HD is associated with cleavage of the N-terminal fragment of mutant huntingtin that contains the polyglutamine tract and is encoded by the first exon of the huntingtin gene. This process is accompanied by the accumulation of the cleaved fragments in the nucleus, whereas the wild-type huntingtin is mainly localized in cytosol [15, 16]. It was also shown that expression of only the N-terminal fragment of pathogenic huntingtin is sufficient for an increased sensitivity of IP_3R1 to IP_3 [7].

Therefore, the goal of our study was to investigate the changes in the operation of store-operated calcium channels in SK-N-SH cells expressing the first exon of the pathological huntingtin gene with 138 glutamine residues in the tract (Htt138Q-1exon) and to identify the role of the STIM1 protein in the activation of these channels.

MATERIALS AND METHODS

Cells

Human neuroblastoma SK-N-SH cells from the cell culture collection of the Institute of Cytology, RAS, were cultured on a DMEM medium supplemented with a 10% fetal calf serum and an antibiotic (80 mg/ml gentamicin). The cells were plated on 3 × 3 mm glass cover-slip fragments 2–3 days prior to the experiment. The cover glasses were coated with a 0.01% polylysine for better cell adhesion.

Infection of cells, transfection, and RNA interference

A shuttle vector encoding the N-terminal fragment of the Htt138Q-1exon protein (270 amino acids) conjugated with the HA-tag, HIV-1-8.9 (Δ8.9)packing vector and VSVG plasmids encoding the surface glycoproteins of the viral particle were kindly provided by Prof. I. B. Besprozvanny (UT Southwestern Medical Center, USA). Virus Lenti-Htt138Q-1exon was obtained by co-transfection of the shuttle vector with the HΔ8.9-packing vector and VSVG plasmids encoding the surface glycoproteins in the packing HEK293T cell line. Petri dishes with the cells were incubated for 24 h at 37 ˚C and then for 72 h at 32 ˚C after the addition of the transfection solution to the medium. During this time, the packed viruses were excreted by the cells in the medium. The medium with viruses was filtered (Ø 0.45 μm) after incubation, immediately frozen in liquid nitrogen, and stored at −80 ˚C.

Immunostaining with anti-HA-tag antibodies was used to determine the virus titer. The proportion of infected cells out of the total number of cells on the glass was determined visually using a Pascal microscope. Having estimated the efficiency of the infection based on the proportion of luminous cells, we chose the ratio between the virus-containing medium and the culture medium with a minimal efficiency of 90%.

The cells were infected the following day after plating. The culture medium with the amount of lentivirus providing the minimal transfection efficiency of 90% was added to the cells.

In the control experiments, the cells were infected with an empty expression vector (control vector) (SIGMA, USA).

In experiments with the suppression of STIM1 expression in addition to infection of Lenti-Htt138Q-1exon cells, we used co-transfection with plasmid encoding the siRNA against STIM1 (SIGMA, USA) and plasmid encoding a green fluorescent protein (GFP), with a 3:1 ratio.

In the control experiments, we used a co-transfection of plasmid with siRNA without a specific target (control siRNA) (SIGMA, USA) and plasmids encoding GFP with a 3:1 ratio.

Electrophoresis and immunoblotting

The cells were grown in 50-mm Petri dishes. After transfection, the cells were lysed in a buffer solution containing 10 mM Tris-HCl pH 7.5, 150 mM NaCl, 1% Triton X-100, 1% NP40 (Nonidet P40, non-ionic detergent nonylphenyl-polyethylene glycol), 2 mM EDTA, 0.2 mM PMSF (phenylmethanesulfonyl fluoride, a serine protease inhibitor) supplemented with protease inhibitors (PIC, Hoffmann-La Roche AG, Germany). Lysate proteins were separated by electrophoresis in a 8% polyacrylamide gel in a vertical chamber and transferred to a nitrocellulose membrane. Proteins were detected by immunoblotting using monoclonal anti-STIM1 antibodies (BD Bioscience, USA) diluted 1:250. The secondary antibodies were anti-mouse IgG produced in goat (1:30000). Proteins on immunoblots were detected using the Super Signal Chemiluminescent Substrate (PIERCE, USA). The experiments were repeated at least three times using different cell lysates. Specific monoclonal anti-α-tubulin antibodies (1:1000) (SIGMA, USA) were used to control equal loading. The percentage of protein content was compared using the standard program for comparing the color intensities of the scanned immunoblots.

Electrophysiological measurements

A patch clamp was used to detect ion currents for whole cell recordering [17]. All measurements were

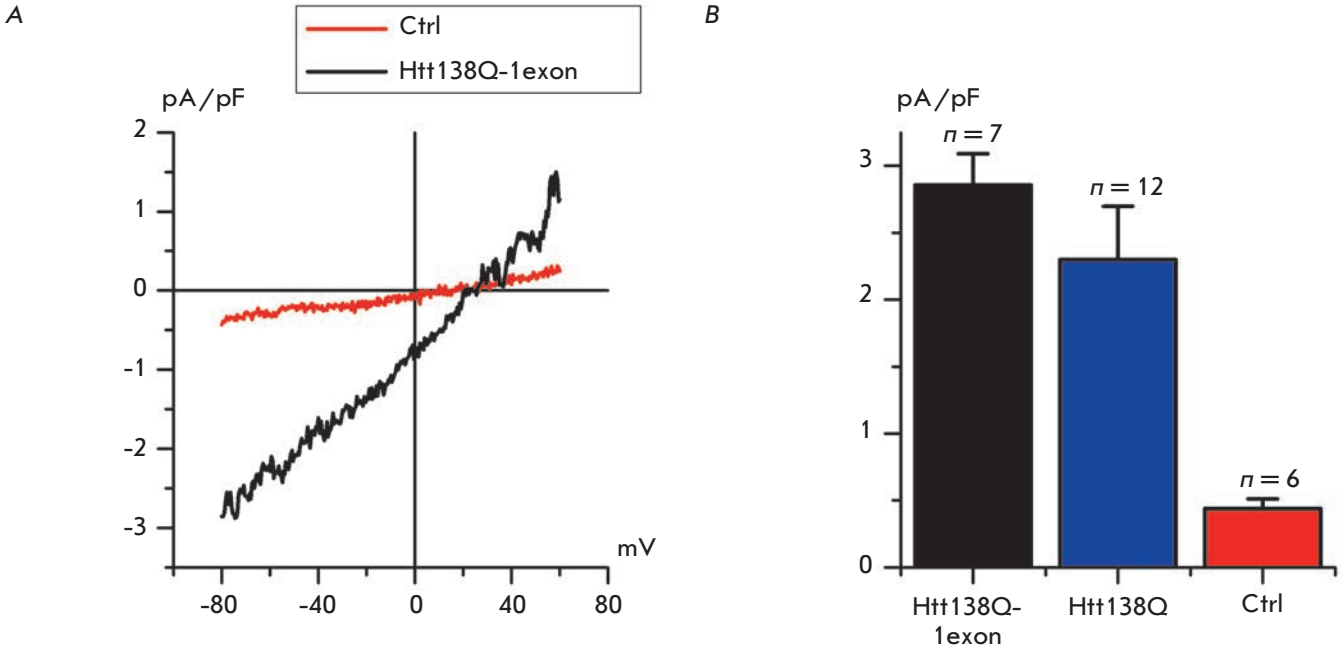

Fig. 1. Effect of the lentiviral expression of Htt138Q-1exon on the level of store-operated calcium currents in SK-N-SH cells. A – the average I-V curves of currents evoked by passive depletion of calcium stores by 1 mM Thapsigargin in SK-N-SH cells expressing the Htt138Q-1exon (*black line*), control SK-N-SH cells expressing the control empty vector (*red line*). I-V curves were recorded after full development of the store-operated currents. Each trace is an average based on the number of experiments as indicated in (*B*). B — The average amplitude of store-operated currents in control SK-N-SH cells (*red filling*) and in SK-N-SH transfected with full-length Htt138Q (*blue filling*) or infected with Htt138Q-1exon (*black filling*). For all groups of cells, the amplitude was determined at a potential of –80 mV and plotted as a mean ± SE (n = number of experiments). $p < 0.05$

performed using an Axopatch 200B amplifier (Axon Instruments, USA). Resistance of the microelectrodes was 5–15 MΩ. Series resistance was not compensated. The signal was amplified and pre-filtered using a two-pole Bessel filter built-in amplifier (cut off frequency 500 Hz). The signal was digitized at a frequency of 5000 Hz using an ADC board L305 (L-Card, Russia). The membrane potential was kept at –40 mV during the recording of integral currents within the cell. The membrane potential was changed to –100 mV (per 30 ms) periodically (every 5 s), and then the membrane potential was gradually changed to +100 mV at a constant rate of 1 mV/ms. The measurement interval was 0.5 mV. The recorded currents were normalized for cell capacity (10–30 pF). The records obtained prior to the activation of the investigated currents were used to subtract the leak current and currents via other channels.

Solutions

In the measurements made in the whole-cell configuration, the recording pipette solution contained (mM): 135 CsCl, 10 EGTA-Cs, 30 Hepes-Cs, 4.5 $CaCl_2$, 1.5 $MgCl_2$, 4 Na-ATP, 0.4 Na_2-GTP (pCa7), pH 7.3. The extracellular solution contained (mM): 130 NMDG-Asp, 10 $BaCl_2$, 20 Hepes-Cs, 0.01 nifedipine, pH 7.3.

Barium ions were selected as a current carrier to prevent calcium-dependent inactivation. Nifedipine was added to the solution of the experimental chamber in order to eliminate the possible contribution of integral L-type voltage-gated calcium channels to the inward current.

Thapsigargin (1 μM) was added to the extracellular solution to activate store-operated currents; the solution was supplied to the object by perfusion of the experimental chamber. The solution replacement time in the chamber was less than 1 s.

Calculation

Calculations of electrophysiological data and linearization of the current-voltage characteristics were performed using the OriginPro 8.0 software package.

RESULTS AND DISCUSSION

To simulate HD, SK-N-SH human neuroblastoma cells were infected with a lentivirus containing the construct

encoding the product of the first exon of the huntingtin gene with a polyglutamine tract consisting of 138 glutamine residues (Htt138Q-1exon).

Thapsigargin is an irreversible blocker of all SERCA (sarco/endoplasmic reticulum Ca_2^+-ATPase) isoforms that operate in the membranes of the endoplasmic reticulum (ER) as calcium pumps and control the pumping of calcium ions from the cytosol into the ER lumen. Thapsigargin (1 mM) was added to the solution to activate store-operated calcium channels. The recorded current can only be attributed to the operation of store-operated channels, since application of Thapsigargin leads to passive depletion of the stores and does not affect other cellular signaling pathways.

The analysis of electrophysiological experiments with the patch clamp technique in the whole-cell configuration, in response to the application of Thapsigargin (1 mM), demonstrated that store-operated entry of calcium was significantly higher in cells expressing the first exon of mutant huntingtin than in the control cells (ctrl) expressing the empty control vector (*Fig. 1A*). The amplitude of thapsigargin-induced currents in Htt138Q-1exon cells was 2.86 ± 0.24 pA/pF, whereas the amplitude of the same currents in the control cells was only 0.44 ± 0.07 pA/pF.

Based on a comparison with the data obtained earlier for SK-N-SH cells expressing full-length mutant huntingtin [13, 14], we could conclude that the expression of the full-length Htt138Q protein and the product of the first Htt138Q-1exon exon have almost the same effect on the level of store-operated calcium entry in SK-N-SH cells (*Fig. 1B*). The amplitude of store-operated calcium entry was 2.86 ± 0.24 pA/pF in SK-N-SH cells expressing the N-terminal fragment of pathogenic huntingtin; the amplitude for the expression of full-length pathogenic huntingtin was 2.30 ± 0.40 pA/pF (*Fig. 1B*). The difference in the amplitudes of store-operated calcium entry for various HD models on SK-N-SH cells was statistically insignificant ($p < 0.05$).

Thus, we have shown that the expression of the N-terminal fragment of mutant huntingtin in SK-N-SH cells is an adequate model for investigating the impairment of store-operated calcium channels in HD.

Another objective of this study was to investigate the role of the STIM1 protein in the activation of store-operated calcium channels in the lentiviral model of HD.

STIM1 is an integral membrane protein of ER and the plasma membrane (PM) with a single transmembrane domain. It is believed that STIM1 is mainly localized in the ER membranes, and only about 15–25% of STIM1 is localized on the PM of the cells [18].

In the cells, STIM1 acts as a calcium sensor in the lumenal space of the ER and an activator of the store-operated channels of PM [18]. Normally, when the intracellular calcium stores are filled, the STIM1 protein is localized in the ER membrane in a non-oligomerized state. Calcium store depletion causes a number of conformational changes resulting in the clustering of STIM1 and its transport to the puncta region, adjacent to the PM [18]. The presence of the proline-rich domain in the C-terminal region of the STIM1 protein suggests the possibility of protein–protein interactions between individual STIM1 molecules, as well as interaction with other proteins. Moreover, the localization of STIM1 in ER membranes located in close proximity to the PM enables direct interaction between STIM1 in the ER membrane proteins with the proteins of PM.

Various channel-forming proteins and the plasmatic pools of STIM1 proteins are among the proteins that interact with the endoplasmic STIM1. It was shown that STIM1 interacts with the proteins responsible for store-operated calcium entry into different types of cells: TRPC proteins [19] and the Orai1 protein [20].

Expression of STIM1 in Htt138Q-1exon cells was suppressed by small interfering RNA. The effectiveness of the suppression was confirmed by immunoblotting (*Fig. 2D*).

The results of electrophysiological experiments demonstrated that suppression of STIM1 leads to a marked decrease in the amplitude of thapsigargin-induced currents from 2.86 ± 0.24 pA/pF in Htt138Q-1exon cells to 0.91 ± 0.07 pA/pF in Htt138Q-1exon STIM1(–) cells (*Fig. 2A, B, C*). Thus, we can conclude that the STIM1protein is a key element in the activation of the store-operated calcium response in Htt138Q-1exon cells.

The reversal potential of the average current through the store-operated channels in Htt138Q-1exon STIM1(–) cells was not different from that in Htt138Q-1exon cells (*Fig. 2B*). However, the plotting of the current-voltage characteristics (I-V curves) of separate experiments on the same graph demonstrated that store-operated currents in Htt138Q-1exon STIM1(–) cells have a wide range of different reversal potentials, indicating the different selectivity of the channels that mediate the store-operated current (*Fig. 3A*). A detailed analysis of the individual I-V curves of registered store-operated currents in Htt138Q-1exon STIM1(–) cells and their linearization showed that the reversal potentials of these currents can be divided into three different groups (*Fig. 3B, C*). Some I-V curves had low reversal potentials (less than 5 mV), while the second group had mid-level reversal potentials of about 20 mV, and finally, the third group had high reversal potentials (more than 35 mV). Thus, it becomes clear that more than one type of store-operated channels with different selectivities for Ca^{2+} are involved

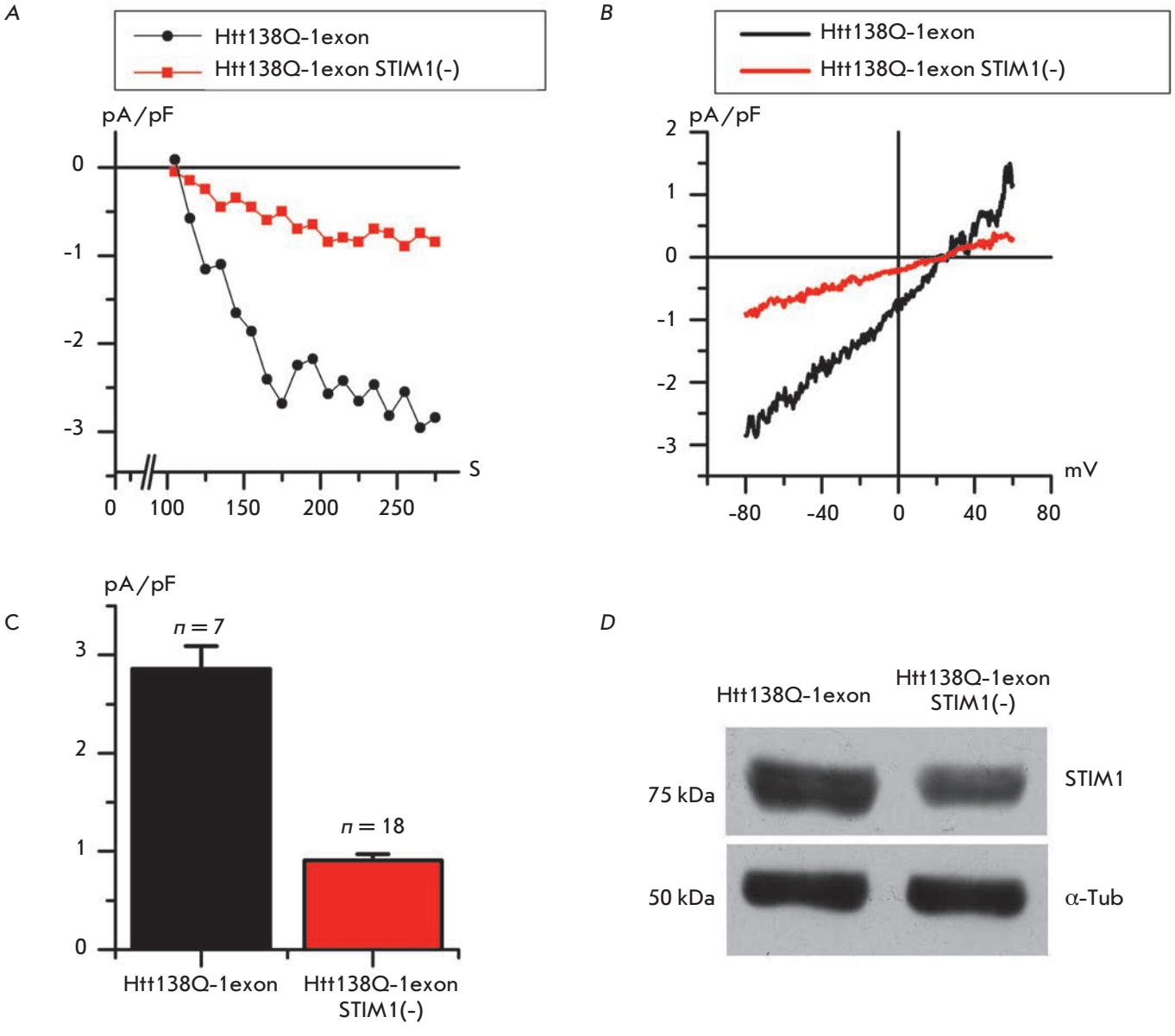

Fig. 2. Effect of STIM1 suppression on the store-operated calcium currents in SK-N-SH Htt138Q-1exon cells. A – the amplitude of store-operated currents recorded in whole-cell experiments is shown as a function of time after the application of 1 mM thapsigargin to Htt138Q-1exon cells transfected with the control GFP protein (Htt138Q-1exon) (*black circles*) or transfected with GFP and siRNA against STIM1 (Htt138Q-1exon STIM1(–)) (*red squares*). The amplitude of the currents for all groups of cells was measured every 10 s at a potential of –80 mV. Data from representative experiments are shown. B – the average I-V curves of currents evoked by passive depletion of calcium stores with 1 mM thapsigargin in Htt138Q-1exon cells transfected with the control GFP protein (Htt138Q-1exon) (*black trace*) or transfected with GFP and siRNA against STIM1 (Htt138Q-1exon STIM1(–)) (*red trace*). I-V curves were recorded after full development of the store-operated currents. Each trace is an average based on a number of experiments as indicated in (*C*). C – the average amplitude of store-operated currents in Htt138Q-1exon cells transfected with the control GFP protein (Htt138Q-1exon) (*black filling*) or transfected with GFP and siRNA against STIM1 (Htt138Q-1exon STIM1(–)) (*red filling*). For all groups of cells, the amplitude was determined at potential –80 mV and plotted as mean ± SE (n = number of experiments). $p < 0.05$. D – Western blot showing the levels of STIM1 expression in SK-N-SH Htt138Q-1exon cells transfected with the control GFP protein or transfected with GFP and siRNA against STIM1

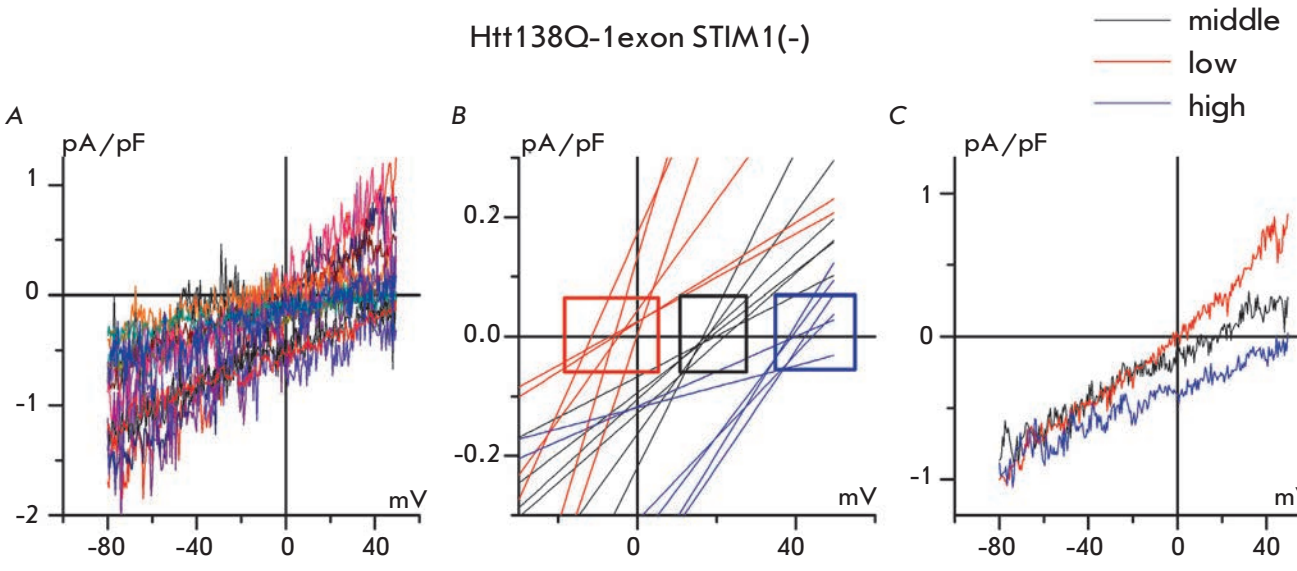

Fig. 3. Store-operated calcium currents in SK-N-SH Htt138Q-1exon cells with suppression of the STIM1 protein. A – the non-averaged I-V curves of currents evoked by the passive depletion of calcium stores with 1 mM thapsigargin in Htt138Q-1exon cells transfected with the control GFP protein and siRNA against STIM1. I-V curves were recorded after full development of the store-operated currents. (*Each colored line represents an independent experiment*) B – the fragments of linear fit of I-V curves from the (*A*) panel with a low (*red lines*), medium (*black lines*), and high (*blue lines*) reversal potential. C – the average I-V curves of currents evoked by the passive depletion of calcium stores with 1 mM thapsigargin in Htt138Q-1exon STIM1(–) cells with a low (*red trace*), medium (*black trace*), and high (*blue trace*) reversal potential. I-V curves were recorded after full development of the store-operated currents

in the store-operated calcium entry in Htt138Q-1exon STIM1(–) cells. The amplitudes of the currents with high, medium, and low reversal potentials were similar to each other at a potential of –80 mV (*Fig. 3B*) and were 0.88 ± 0.20, 0.87 ± 0.17 and 1.00 ± 0.28 pA/pF, respectively.

One hypothesis that explains these observations may be the assumption that there are two different types of channels in Htt138Q-1exon cells which are controlled by the store-operated mechanism and have similar amplitudes at a potential of –80 mV but different selectivities. In this case, when thapsigargin-induced currents are activated in Htt138Q-1exon cells, the I-V curves of integral currents are a superposition of two types of activated store-operated channels (*Fig. 2B*). As long as there is enough of the STIM1 protein responsible for the activation of store-operated entry in Htt138Q-1exon cells, the channels differing in their selectivity are activated to the same extent, producing averaged I-V curves with a reversal potential somewhere between the reversal potentials of each channel (*Fig. 2B, 4A*). When the STIM1 protein in Htt138Q-1exon STIM1(–) cells is suppressed, the equilibrium can be shifted toward the predominant activation of store-operated channels with a high (*Fig. 4B*) or low (*Fig. 4C*) reversal potential due to the lack of STIM1. Another possibility is the activation of an equal number of channels with different reversal potentials even when there is a lack of STIM1 (*Fig. 4D*), which can explain the experiments performed on Htt138Q-1exon STIM1(–) cells, when average values of the reversal potential were observed.

This is only one possible explanation, and the actual chain of events could be much more complicated. For example, store-operated currents in Htt138Q-1exon cells may represent a superposition of not two, but three or more, channels. In particular, we demonstrated in previously published studies the existence of four types of channels with completely different biophysical properties, which can be activated by store-operated mechanisms in human embryonic kidney epithelium cells (HEK293 cell line) [21]. Similar results were obtained for A431 human epidermoid carcinoma cells [22–24].

CONCLUSIONS

Thus, we have demonstrated that the expression of the N-terminal fragment of mutant huntingtin can

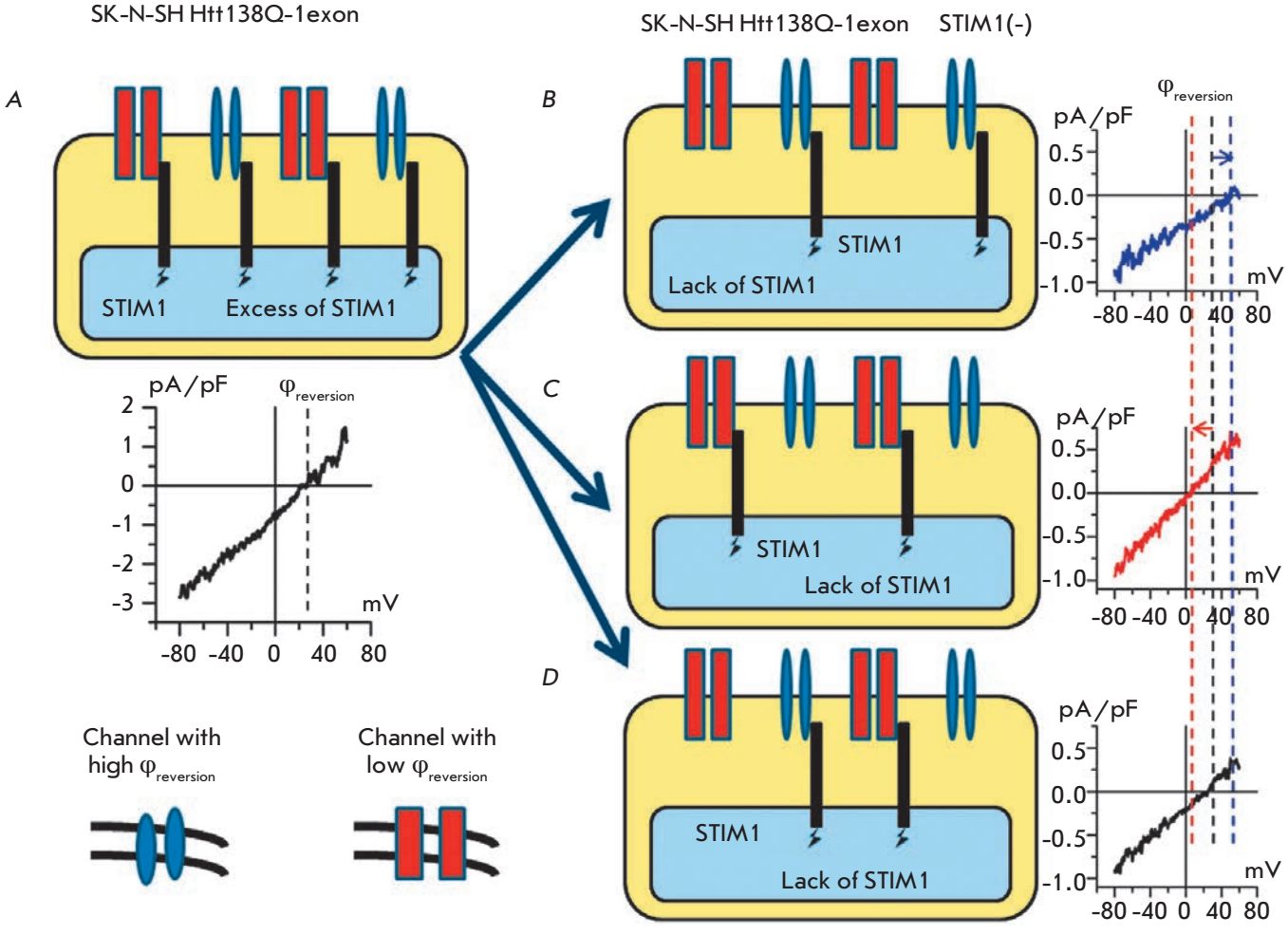

Fig. 4. Possible pathway of activation of the store-operated calcium channels with different reversal potentials in SK-N-SH Htt138Q-1exon STIM1 (-) cells. In this scheme, it is shown that activation of all types of store-operated channels could be observed under conditions of a large quantity of the STIM1 protein, resulting in average I-V curves of these currents with a medium reversal potential (*A*). Suppression of the STIM1 protein could lead to preferential activation of one type of store-operated channels with a high (*B*) or low (*C*) reversal potential. It also could lead to activation of an equal quantity of both channels with low and high reversal potentials (*D*). Channels with a high reversal potential are represented by blue ovals and a blue line on the plot. Channels with a low reversal potential are represented by red rectangles and a red line on the plot. Activation of both channel types is shown as black lines on the plots. Reversal potentials are shown by dotted lines of the corresponding colors

effectively simulate the earlier described changes in store-operated calcium entry in human neuroblastoma cells. We have also found that the activation of store-operated calcium channels in SK-N-SH cells requires the presence of a calcium sensor; the STIM1 protein. Furthermore, we established that store-operated calcium entry in SK-N-SH cells simulating DH is controlled by at least two different types of channels. ●

This work was supported by the Russian Science Foundation (grant № 14-14-00720 (V.V., J.K., M.R., E.K.), grants of the Russian Foundation for Basic Research, the program of the Presidium of the Russian Academy of Science Molecular and Cellular Biology, a grant from Era.NetRUS, and a scholarship of the President of the Russian Federation.

REFERENCES
1. Graham S., Yuan J.P., Ma R. // Exp Biol Med (Maywood). 2012. V. 237 № 2 P. 111–118.
2. Pieri M., Caioli S., Canu N., Mercuri N.B., Guatteo E., Zona C. // Exp. Neurol. 2012. V. 247. P. 349–358.
3. Wojda U., Salinska E., Kuznicki J. // IUBMB Life. 2008. V. 60. № 9. P. 575–590.
4. Bezprozvanny I. // Trends Mol Med. 2009. V. 15. № 3. P. 89–100.
5. Vonsattel J.P., Myers R.H., Stevens T.J., Ferrante R.J., Bird E.D., Richardson E.P. Jr. // J. Neuropathol. Exp. Neurol. 1985. V. 44. № 6. P. 559–577.
6. Harjes P., Wanker E.E. // Trends Biochem Sci. 2003. V. 28. № 8. P. 425–433.
7. Tang T.S., Tu H., Chan E.Y., Maximov A., Wang Z., Wellington C.L., Hayden M.R., Bezprozvanny I. // Neuron. 2003. V. 39. № 2. 227–239.
8. Zeron M.M., Hansson O., Chen N., Wellington C.L., Leavitt B.R., Brundin P., Hayden M.R., Raymond L.A // Neuron. 2002. V. 33. № 6. P. 849–860.
9. Kaltenbach L.S., Romero E., Becklin R.R., Chettier R., Bell R., Phansalkar A., Strand A., Torcassi C., Savage J., Hurlburt A., et al. // PLOS Genet. 2007. V. 3. № 5. E82.
10. Bossy-Wetzel E, Petrilli A, Knott A.B. // Trends Neurosci. 2008. V. 31. № 12. P. 609–616.
11. Panov A.V., Gutekunst C.A., Leavitt B.R., Hayden M.R., Burke J.R., Strittmatter W.J., Greenamyre J.T. // Nat. Neurosci. 2002. V. 5. № 8. P. 731–736.
12. Vosler P.S., Brennan C.S., Chen J. // Mol Neurobiol. 2008. V. 38. № 1. P. 78–100.
13. Glushankova L.N., Zimina O.A., Vigont V.A., Mozhaeva G.N., Bezprozvanny I.B., Kaznacheeva E.V. // Dokl Biol Sci. 2010. V. 433. P. 293–295.
14. Wu J., Shih H-P., Vigont V., Hrdlicka L., Diggins L., Singh C., Mahoney M., Chesworth R., Shapiro G., Ahlijanian M., et al. // Chemistry and Biology. 2011. V.18. №6. P. 777–793.
15. Davies S.W., Turmaine M., Cozens B.A., DiFiglia M., Sharp A.H., Ross C.A., Scherzinger E., Wanker E.E., Mangiarini L., Bates G.P. // Cell. 1997. V. 90. № 3. P. 537–548.
16. DiFiglia M., Sapp E., Chase K.O., Davies S.W., Bates G.P., Vonsattel J.P., Aronin N. // Science. 1997. V. 277. № 5334. P. 1990–1993.
17. Hamill O.P., Sakmann B. // Nature. 1981. V. 294. № 5840. P. 462–464.
18. Dziadek M.A., Johnstone L.S. // Cell Calcium. 2007. V. 42. № 2. 123–132.
19. Yuan J.P., Zeng W., Huang G.N., Worley P.F., Muallem S. // Nat Cell Biol. 2007. V. 9. № 6. P. 636–645.
20. Peinelt C., Vig M., Koomoa D.L., Beck A., Nadler M.J., Koblan-Huberson M., Lis A., Fleig A., Penner R., Kinet J.P. // Nat Cell Biol. 2006. V. 8. № 7. P. 771–773.
21. Bugaj V., Alexeenko V., Zubov A., Glushankova L., Nikolaev A., Wang Z., Kaznacheyeva E., Bezprozvanny I., Mozhayeva G.N. // J Biol Chem. 2005. V. 280. № 17. P. 16790–16797.
22. Kaznacheyeva E., Glushankova L., Bugaj V., Zimina O., Skopin A., Alexeenko V., Tsiokas L., Bezprozvanny I., Mozhayeva G.N. // J Biol Chem. 2007. V. 282. № 32. P. 23655–23562.
23. Gusev K., Glouchankova L., Zubov A., Kaznacheyeva E., Wang Z., Bezprozvanny I., Mozhayeva G.N. // J Gen Physiol. 2003. V. 122. № 1. P. 81-94.
24. Kaznacheyeva E., Zubov A., Gusev K., Bezprozvanny I., Mozhayeva G.N. // Proc Natl Acad Sci U S A. 2001. V. 98. № 1. P. 148–153.

Specific Visualization of Tumor Cells Using Upconversion Nanophosphors

E. A. Grebenik[1*], A. N. Generalova[1], A. V. Nechaev[2], E.V. Khaydukov[3], K. E. Mironova[1], O. A. Stremovskiy[1], E.N. Lebedenko[1], A. V. Zvyagin[1,4,5], S. M. Deyev[1,4]

[1]Shemyakin/Ovchinnikov Institute of Bioorganic Chemistry, Russian Academy of Sciences, Miklukho-Maklaya Str., 16/10, Moscow, 117997, Russia

[2]Lomonosov Moscow State University, GSP-1, Leninskie Gory, Moscow, 119991, Russia

[3]Institute of Laser and Information Technologies, Russian Academy of Sciences, Pionerskaya Str., 2, Troitsk, 142190, Russia

[4] Lobachevsky Nizhniy Novgorod State University, Gagarina Prospekt, 23, Nizhniy Novgorod, 603950, Russia

[5]Department of Physics and Astronomy, Macquarie University, Sydney, NSW 2109, Australia

*E-mail: katya.ivukina@rambler.ru

ABSTRACT **The development of targeted constructs on the basis of photoluminescent nanoparticles with a high photo- and chemical stability and absorption/emission spectra in the "transparency window" of biological tissues is an important focus area of present-day medical diagnostics. In this work, a targeted two-component construct on the basis of upconversion nanophosphors (UCNPs) and anti-tumor 4D5 scFv was developed for selective labeling of tumor cells overexpressing the HER2 tumor marker characteristic of a number of human malignant tumors. A high affinity barnase : barstar (Bn : Bs) protein pair, which exhibits high stability in a wide range of pH and temperatures, was exploited as a molecular adapter providing self-assembly of the two-component construct. High selectivity for the binding of the two-component 4D5 scFv-Bn : UCNP-Bs construct to human breast adenocarcinoma SK-BR-3 cells overexpressing HER2 was demonstrated. This approach provides an opportunity to produce similar constructs for the visualization of different specific markers in pathogenic tissues, including malignant tumors.**

KEYWORDS **upconversion nanophosphors; biomarker imaging; anti-tumor antibodies; self-assembly; HER2.**

ABBREVIATIONS **EDC – 1-ethyl-3-(3-dimethylaminopropyl)carbodiimide; HER2 – human epidermal growth factor receptor 2; PBS – phosphate buffered saline; scFv – single chain variable antibody fragment; sulfo-NHS – N-hydroxysulfosuccinimide; Bn – barnase; Bs – barstar; BSA – bovine serum albumin; UCNPs – upconversion nanophosphors; PAAG – polyacrylamide gel; PMAO – poly(maleic anhydride-*alt*-1-octadecene) amphiphilic polymer; TEM – transmission electron microscopy.**

INTRODUCTION

The use of modular constructs based on immunoglobulin superfamily proteins for targeted drug delivery and diagnosis is the current trend in molecular medicine referred to as theranostics [1–3]. In this case, special interest is generated by the problem of developing targeted constructs based on photoluminescent nanoparticles that have targeting modules that ensure their delivery to the target cells [4]. This approach enables the development of fundamentally new, highly efficient techniques for personalized optical diagnosis. These constructs, which accumulate in target cells, can contrast these cells against a background of healthy tissues due to photoluminescent response to excitation by light of a certain wavelength. In particular, the use of photoluminescent constructs capable of targeted binding to an appropriate cell cancer marker provides the most sensitive and noninvasive early diagnosis method for cancer.

Cell cancer markers such as the protein of the family of human epidermal growth factor receptors HER2 are abundant in tumor tissues, where they serve as effective targets for the detection and therapy of cancer. HER2 is overexpressed in many tumors, including tumors of the ovarian, uterine cervix, urinary bladder, rectum, stomach, esophagus, and breast, and the level of its expression is often correlated with poor prognosis and increased resistance to chemotherapy [5]. Consequently, the development of HER2-targeted photoluminescent constructs is one of the most promising approaches in the early-molecular diagnosis of cancer. Targeted delivery is provided by the use of a targeting module of protein nature, which is part of the construct. As the HER2-targeted module, a full-length humanized monoclonal antibody, 4D5, was used. It is widely utilized in clinical practice under the trade name Herceptin® [6]. The antibody was attached to a nanoparticle using

a variety of crosslinking agents or simple physical adsorption. In this study, a genetic engineering fragment of the antibody 4D5 scFv is used as a targeting module that is a single polypeptide chain in which the variable domains of light and heavy immunoglobulin chains are connected by short flexible linkers, and the constant domains are lacking [7]. The 4D5 scFv fragment, as the targeting module, attracts attention because it is also capable of effectively recognizing HER2 [8–10], but, unlike full length antibodies, it does not provide interaction with the receptors of immune system cells and complement system proteins [11].

To develop the targeted constructs, the principle of self-assembly through the system of barstar : barnase (Bs : Bn) protein adapters was suggested. It enables the combination of individual modules with different functionalities and the generation of constructs with a predetermined set of properties [12–15]. Bacterial ribonuclease Bn and its natural inhibitor Bs form a strong complex with a dissociation constant of ~ 10^{-14} M [16] and high individual stability in a wide range of pH and temperatures [17]. Furthermore, the feature of these proteins is their biotechnological producibility, and their use allows one to improve the properties of the targeted constructs. For example, Bn as a part of genetically encoded fusion proteins acts in some cases as an intramolecular chaperone providing correct folding of the composite domains comprising the targeting modules [18].

Upconversion nanophosphors (UCNPs) are inorganic photoluminescent nanoparticles whose photoluminescence is based on upconversion, which is the process of converting several photons of lower energy (longer wavelength) into a single photon with a higher energy (shorter wavelength). UCNPs are highly efficient contrasting agents with unique photoluminescence properties; they have a whole number of advantages compared to the fluorescent proteins and organic dyes traditionally used for optical diagnosis. These include their exceptional resistance to photodegradation and chemical degradation, excitation with wavelengths (typically 980 nm) falling into the "transparency window" of biological tissue, and long-term photoluminescence shifted to the shorter wavelengths, including visible and far-red light [19]. Moreover, long-term photoluminescence provides the possibility of delayed signal detection, which makes possible the elimination of tissue autofluorescence and the achievement of a significant increase in the image contrast at the individual nanoparticle level in a biological environment.

UCNP-based targeted constructs were used in a number of studies devoted to the visualization of cell and tissue structures [20], including cancer cells with HER2 overexpression. Targeting of UCNPs at HER2 by means of full-length antibodies attached to them was described in [21, 22]. In this paper, we offer a new approach to the development of targeted constructs on the basis of UCNP and 4D5 scFv specific to the HER tumor marker, by means of self-assembly through the system of Bs : Bn molecular adapters.

EXPERIMENTAL

Synthesis of UCNP

Hydrophobic UCNPs in the form of $NaYF_4$ crystals doped with Yb_3^+ and Er_3^+ and bearing a surface oleate anion were synthesized by the method described in [23]. Crystals of programmable size were grown from a solution of sodium salts and oleic acid in an oxygen-free atmosphere. A mixture of Y_2O_3 (0.78 mM), Yb_2O_3 (0.2 mM), and Er_2O_3 (0.02 mM) was refluxed in 70% trifluoroacetic acid (20 mL) for 6 h. The clear solution was then cooled to room temperature, and the solvent was evaporated. The resulting precipitate was dried under 0.1 mmHg vacuum for 3 h and triturated carefully in an agate mortar to a homogeneous state. This powder was mixed with sodium trifluoroacetate (2 mM), oleic acid (6 mL), and 1-octadecene (6 mL) at 100 ˚C in vacuum for 30 min.

The degased and dehydrated mixture was gradually heated to 290 ˚C at arate of 6 ˚C/min and held at this temperature for 45 min under argon. The temperature was then raised to 310 ˚C for 70 min. In the next step, the solution was cooled, suspended in isopropanol (130 mL), and centrifuged at 6,000 rpm for 30 min (Z206A centrifuge, Hermle, Germany). The resulting particles were washed four times in absolute ethanol and dried. The particles were then dissolved in chloroform (10 mL), precipitated with isopropanol (50 mL), and centrifuged twice at 4,000 rpm for 10 min. The desired product was dried at room temperature.

Preparation and characterization of proteins

The recombinant **4D5 scFv-Bn** protein consisting of Bn and 4D5 scFv connected by a flexible peptide linker was produced as previously described [7], with slight modifications. *Escherichia coli* cells of the SB536 strain [F-, WG1, Δ*fhuA* (ton Δ), Δ*hho*AB (SacII), *shh*] were transformed with the pSD4D5BnHis5 plasmid bearing the gene encoding the 4D5 scFv-Bn protein under the control of the *lac*-promoter and with the Bs gene, whose constitutive synthesis protects bacterial cells from the cytotoxic effect of Bn [24]. Transformants were grown in a nutrient YTPS broth (1% yeast extract, 1% tryptone, 150 mM NaCl, 40 mM K_2HPO_4, 10 mM KH_2PO_4, 2 mM $MgCl_2$, 0.1 g/L ampicillin, pH 7.5) at 37 ˚C until the optical density 0.6 at 560 nm; then, β-*D*-1-thiogalactopyranoside (1 mM) was added to induce the *lac*-promoter and transformants were incubated for more 5 h. The resulting biomass was collected by centrifugation (Allegra

21R centrifuge, Beckman Coulter, USA) and sonicated on ice in a lysis buffer with 5 mM Tris-HCl, 40 mM K_2HPO_4, and 500 mM NaCl, pH 8.2. The resulting extract was clarified by centrifugation and filtration through a membrane filter with a pore size of 0.22 μm and loaded onto the 1 mL HiTrap column with an affinity sorbent, Ni-nitrilotriacetic acid (Ni-NTA), (GE Healthcare Worldwide, USA). To free the target 4D5 scFv-Bn protein from the Bs inhibitor, the column was washed with 8 M urea, followed by refolding of 4D5 scFv-Bn with a linear urea gradient of 8–0 M. The target protein was eluted with 225 mM imidazole, transferred into a phosphate buffer (20 mM NaCl, 6.5 mM NaH_2PO_4, 41 mM Na_2HPO_4, pH 6.5) on the desalting PD-10 column (GE Healthcare Worldwide, USA), and subjected to final purification on the 1 mL HiTrap SP-Sepharose Fast Flow cation exchange column (GE Healthcare Worldwide, USA) that was eluted with a NaCl gradient; fractions were analyzed by electrophoresis in a 12.5% PAAG. According to the electrophoretic analysis in a 12.5% PAAG, the fraction of the target 4D5 scFv-Bn protein was eluted in 275 mM NaCl.

The cysteine-free **Bs (C40/82A)** barstar mutant was isolated from *E. coli* cells of the HB101 strain [F- Δ (*gpt-proA)62 leu B6 glnV44 ara-14 galK2 lacY1Δ(mcrC-mrr) rpsL20 (*Str^r*) xyl-5 mtl-1 recA13*] bearing the pMT641 plasmid [7]. The bacterial culture was grown in a YTPS broth to the stationary phase, and the cells were separated by centrifugation and re-suspended in a cold lysis buffer of the following composition: 0.05 M Tris-HCl, 0.1 M NaCl, 10 mM EDTA, 10 mM dithiothreitol, pH 8.0. The cells were disrupted by sonication on ice (30% saturation with $(NH_4)_2SO_4$), then nucleic acids were precipitated with polyethyleneimine. Proteins were precipitated from the resulting cell extract by adjusting the ammonium sulfate concentration to 70% saturation. The protein precipitate was dissolved in a buffer (0.1 M Tris-HCl, 10 mM EDTA, 10 mM dithiothreitol, pH 8.0) and size-fractionated on the Sephadex G-100 Super-Fine (C16/100) column equilibrated with a buffer: 0.02 M Tris-HCl, 0.02 M NaCl, 2 mM EDTA, 2 mM dithiothreitol, 0.05% Tween-20, pH 8.0. Final purification of Bs was performed on the 1mL HiTrap Q-Sepharose Fast Flow anion exchange column (GE Healthcare Worldwide, USA) equilibrated with a buffer: 0.2 M Tris-HCl, 2 mM dithiothreitol, 10% glycerol, pH 8.0. The target protein was eluted with a NaCl gradient; the fractions were analyzed by electrophoresis in 17% PAAG.

Ribonuclease activity of the recombinant 4D5 scFv-Bn protein

The ribonuclease activity of the recombinant 4D5 scFv-Bn protein was determined by the acid-insoluble RNA precipitate method [25]. 40 μL of the analyzed protein solution with a concentration of 30 to 0.015 nM in a 0.125 M Tris-HCl buffer, p H 8.5, was mixed with 160 μL of a yeast RNA solution (2 mg/mL) and incubated at 37 ˚C for 15 min. The RNAse reaction was quenched with 6% $HClO_3$ (200 μL), and the mixture was kept at 2 ˚C for 15 min. Unreacted RNA was separated by centrifugation. The concentration of the released nucleotides, which was directly proportional to the RNAse activity of the studied protein, was determined by optical absorption (OD_{260}).

To assess the binding of the Bs : Bn pair, different Bs dilutions were added to the Bn solution at a known concentration and RNAse activity was measured as described above. In the latter case, the Bs concentration was inversely proportional to OD_{260}.

Affinity of the 4D5 scFv-HER2/neu protein to the HER2 receptor

Affinity of the 4D5 scFv-HER2/neu protein to the HER2 receptor was assessed using polyclonal rabbit anti-human IgG antibodies. The p185$^{HER2\text{-}ESD}$ antigen (a recombinant protein that is an extracellular domain of the HER2 receptor) in a buffer (0.1 M Na_2CO_3, 0.1 M $NaHCO_3$, pH 9.2) was added into polystyrene flat bottom 96-well plates in the amount of 8 and 16 ng/well. After adsorption of the antigen for 1 h, the plates were washed with PBS and the unsaturated surface binding sites were blocked with a 5% solution of milk powder (Tesco, UK) in PBS, pH 7.4. The 4D5 scFv-Bn protein solution in PBS with 0.1% Tween-20 at different concentrations, beginning with 5 nM, was added to the wells and incubated for 1 h on a shaker, then washed. To detect the immobilized 4D5 scFv-Bn protein, the plates were treated with polyclonal rabbit anti-human IgG antibodies, followed by goat anti-rabbit IgG antibodies conjugated to horseradish peroxidase with washes between stages. For colorimetric measurement, the wells were added with 0.04% 1,2-diaminobenzene (Sigma-Aldrich, Germany) with 0.06% H_2O_2 in a citrate buffer (7.3 g/L citric acid, 11.86 g/L $Na_2HPO_4 \cdot 2H_2O$, pH 5). The reaction was stopped by adding 50 μL of 2 M H_2SO_4, and OD_{450} was measured, and on a tablet spectrophotometer (StatFax-2100, Awareness Technology, USA). The affinity constant, K_a, was calculated as described in [26], taking into account the monovalency of the studied mini-antibody according to the following equation:

$$K_a = (n - 1)/n[Ab']_t - [Ab]_t, \quad (1)$$

where $[Ab']_t$ and $[Ab]_t$ are total concentrations of the mini-antibody in wells with the values OD_{450}' and OD_{450} treated with the antigen at concentrations of [Ag'] (8 ng) and [Ag] (16 ng), respectively,

$$n = [Ag]_t/[Ag']_t. \quad (2)$$

Preparation of UCNP bioconjugates

UCNPs synthesized as described above were coated with an amphiphilic alternating copolymer of maleic anhydride and 1-octadecene (PMAO, Sigma-Aldrich, Germany) as described in [27] with minor modifications. To create a PMAO shell around the UCNP particles and to form cross links, 1,6-diaminohexane (Serva, Germany) was added. To attach the biomolecules to UCNP, the surface carboxyl groups of the resulting PMAO shell were activated with an excess of cross-linkers, 1-ethyl-3-(3-dimethylaminopropyl)carbodiimide hydrochloride (EDC) and N-hydroxysulfosuccinimide (sulfo-NHS) (Sigma-Aldrich, Germany), in a cold buffer with additional sonication. The resulting nanoparticles were then washed from the unreacted cross-linkers by centrifugation at 4 °C, re-suspended in a cold Bs protein solution, and incubated overnight for the attachment of Bs. Unbound Bs molecules were washed out in three cycles of centrifugation/re-suspension. The resulting nanoparticles were stored in PBS.

Transmission Electron Microscopy (TEM)

UCNP and UCNP-PMAO were dissolved in *n*-hexane and water, respectively, sonicated, and laid on copper TEM grids (300 mesh) coated with a 0.3% Pioloform® solution (Wacker Polymer Systems, Burghausen, Germany). Then the grids were dried at room temperature in a desiccator overnight and microscoped on a Philips CM10 TEM device (Philips, The Netherlands). The ImageJ software was used to analyze the UCNP fractional composition.

Infrared Spectroscopy

Free PMAO was carefully triturated with KBr in a mortar and compressed to form tablets. PMAO-modified UCNPs were dried using a Savant SpeedVac concentrator (France), then they were triturated with KBr and compressed to form tablets. IR spectra were recorded on a Varian 3100 spectrophotometer (USA).

Detection of the UCNP-PMAO emission spectra

The UCNP-PMAO powder was placed in a sample holder and irradiated by a laser with a wavelength of 978 nm through a multimodal optical fiber. An emission signal, passed through an emission filter with a bandwidth to 842 nm (Semrock, USA), was recorded in the transmitted light on a calibrated spectrophotometer (Ocean Optics, USA).

Cell labeling

Human breast adenocarcinoma SK-BR-3 cells and Chinese hamster ovary CHO-K1 cells (American Type Culture Collection, USA) were cultured in a RPMI-1640 culture medium (HyClone, USA) supplemented with *L*-glutamine and 10% fetal bovine serum (HyClone, USA). The cells were seeded onto 8-well glass slides at a concentration of 3×10^4 cells/mL and cultured at 37 °C in a CO_2 incubator (5% CO_2) for 24 h. The cells were inactivated by addition of 1% formaldehyde to prevent nonspecific internalization. To prevent nonspecific binding of the particles, the cover glasses were treated with 1% bovine serum albumin (BSA) (Bio-Rad, USA) in PBS for 1 h. Then, to create cell-surface sites for specific binding of an imaging agent, Bs-UCNP, the recombinant 4D5 scFv-Bn protein solution in PBS containing 0.1% BSA and 0.1% Tween-20 was laid on the glasses and incubated for 1 h. The cells were then washed with PBS and treated with a colloidal Bs-UCNP solution (100 μg/mL) for 20 min. This time was enough to complete the formation of 4D5 scFv-Bn : Bs-UCNP complexes due to the exceptionally high affinity constant of the Bs : Bn pair ~ K_d 10^{-14} M.

The cells were then washed several times from unbound Bs-UCNP, fixed in a 4% formaldehyde solution in PBS, and covered with a cover glass. In order to demonstrate that binding of UCNP is not a result of the nonspecific 4D5 scFv-Bn protein adsorption on the glasses, CHO cells were used as a negative control.

Photoluminescence cell microscopy

Photoluminescence cell microscopy was performed on an Olympus IX70 epi-luminescence inverted microscope (Japan) with excitation at 978 nm by a diode laser (LD980-01CW, CXCH-Photonics, China). To visualize the cells in visible light, a dry lens × 50, NA 0.45 (Olympus, Japan) was used.

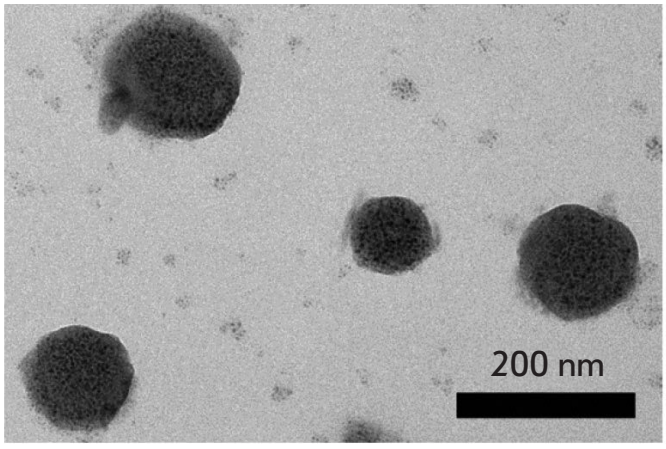

Fig. 1. Transmission electron microscopy imaging of UCNP-PMAO

RESULTS AND DISCUSSION

Hydrophobic UCNPs in the form of $NaYF_4$ crystals doped with Yb_3^+ and Er_3^+ and bearing oleate ani-

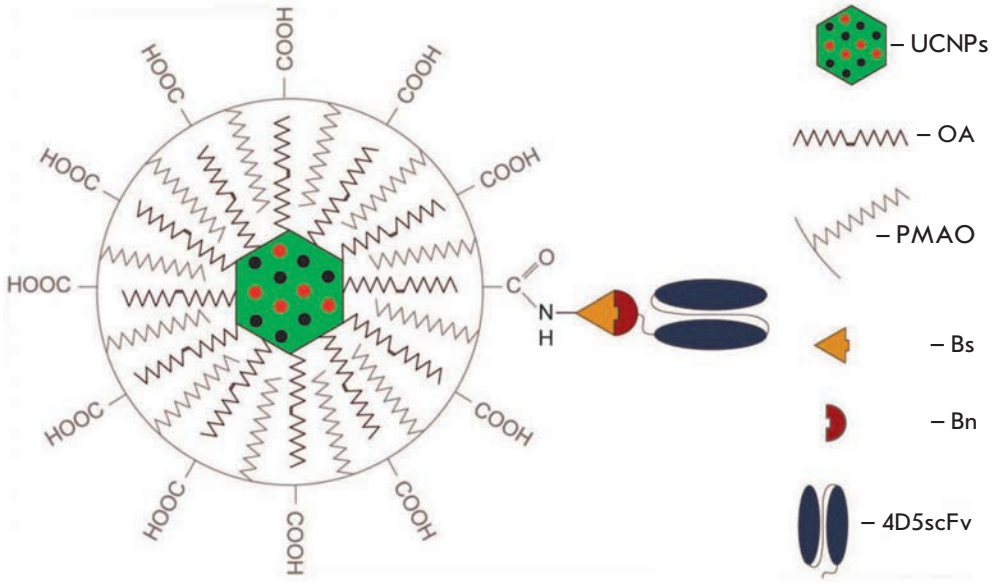

Fig. 2. Structural diagram of the targeted UCNP-PMAO-Bs : 4D5 scFv-Bn construct. UCNPs – upconversion nanophosphors, OA – oleate anion, PMAO – poly(maleic anhydride-*alt*-1-octadecene) amphiphilic polymer, Bs – barstar, Bn – barnase, 4D5 scFv – variable fragment of anti-HER2-antibody 4D5

ons on their surface were synthesized by the method described previously [23]. In order to impart hydrophilicity, the particles were further coated with the molecules of an alternating copolymer, poly(maleic anhydride-1-octadecene) (PMAO), interconnected by means of 1,6-diaminohexane (Serva, Germany). When the UCNP-PMAO particles are transferred from an organic solvent into water, the anhydride ring opens to form a carboxyl group exposed to the solution, which ensures the solubility of UCNP in water [27]. The UCNP-PMAO hydrodynamic diameter measured by dynamic light scattering was 130 ± 20 nm. *Figure 1* presents an image obtained by a transmission electron microscope of nanoparticles with the polymicellar PMAO structure on the UCNP surface. According to measurements using the calibrated integrating sphere, maximum efficiency of nanoparticle upconversion was achieved with a laser excitation power density of ~ 60 W/cm^2 and amounted to 1.2%.

Evaluation of the potential of UCNPs as agents for the optical imaging of target cells was carried out *in vitro* using human breast adenocarcinoma SK-BR-3 cells overexpressing the HER2 surface tumor marker. For this purpose, a targeted, two-component construct was developed that comprised contrasting and targeting modules capable of assembling by means of a system of molecular Bs : Bn adapters, as shown in *Figure 2*. The contrasting module was produced by conjugation of mutant Bs C40/82A with carboxyl groups of UCNP-PMAO using the crosslinking reagents 1-ethyl-3-(3-dimethylaminopropyl) carbodiimide hydrochloride and N-hydroxysuccinimide. The resulting conjugates retained the non-aggregated state and photoluminescence parameters. The targeting module capable of highly efficient binding to the external domain of the

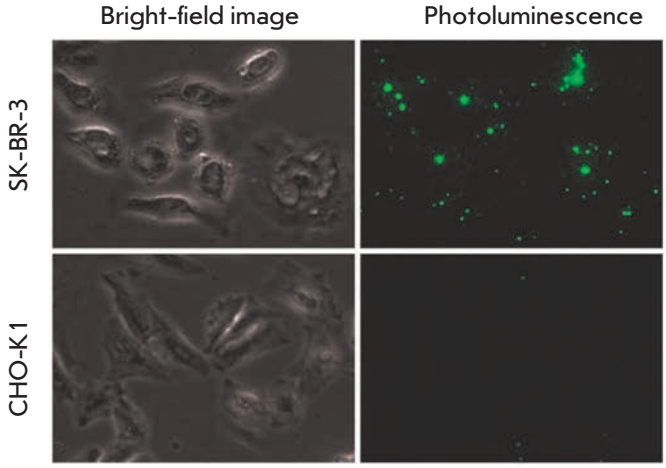

Fig. 3. Photoluminescence microscopy imaging of SK-BR-3 cells overexpressing the HER2 tumor marker, and CHO cells (negative control) after treatment with UCNP-PMAO-Bs and 4D5 scFv-Bn

HER2 receptor on the tumor cell surface was represented by the recombinant fusion 4D5 scFv-Bn protein described in [7]. It was produced by attachment of Bn to the C-terminal segment of the 4D5 scFv via a flexible peptide linker. Both polypeptides were proven [7] to preserve their functional properties – the ability to specifically recognize the HER2 receptor (4D5 scFv) and the ability to bind Bs with high affinity (Bn).

Highly sensitive visualization of SK-BR-3 cells using the described two-component construct was realized via two-stage delivery. To recognize the HER2 receptor, cells, grown on a scaffold and fixed with formaldehyde, were treated with the targeting 4D5 scFv-Bn module. Then, for visualization purpose, the cells were

added with a contrasting Bs-UCNP module that provided optical detection through binding to Bn, which was part of the 4D5 scFv-Bn module immobilized on HER2. After incubation, excess Bs-UCNP was removed by thorough washing of cells with a phosphate buffer. Chinese hamster ovary CHO cells lacking HER2 were used as a negative control. Based on photoluminescence microscopy of SK-BR-3 and CHO cells treated sequentially with the 4D5 scFv-Bn and Bs-UCNP modules, with the excitation of luminescence at 978 nm (*Figure 3*), it was demonstrated that the produced two-component 4D5 scFv-Bn : Bs-UCNP construct selectively binds to SK-BR-3 cells overexpressing the HER2 receptor and does not bind to control CHO cells lacking HER2. The total luminescence signal from the surface of tumor SK-BR-3 cells was 10 times higher than the signal from the surface of the control CHO cells.

CONCLUSION

The produced hybrid constructs consisting of targeting biopolymer molecules and inorganic photoluminescent nanocrystals are capable of highly specific visualization of the cancer marker on tumor cells. These nanoconstructs can serve as promising carriers for the targeted delivery of a wide variety of cytotoxic and imaging agents, which creates new opportunities for a highly accurate molecular diagnosis and effective therapy of tumor diseases. An important advantage of the UCNP-based constructs [28] is the possibility of their detection deep in the living tissue, which determines their particular potential for personalized optical diagnosis of malignant tumors. ●

This work was supported by Russian Science Foundation (grant 14-24-00106) - synthesis of bioconjugates with nanoparticles and study of their interaction with cancer cells; the program of the Presidium of the Russian Academy of Sciences "Molecular and Cell Biology" Ministry of Education of the Russian Federation (№14.578.21.0051, 14.Z50.31.0022) – preparation and characterization of recombinant proteins.

REFERENCES

1. Nikitin M.P., Shipunova V.O., Deyev S.M., Nikitin P.I. // Nat. Nanotechnol. 2014. V. 9. P. 716–722. doi: 10.1038/nnano.2014.156.
2. Mironova K.E., Proshkina G.M., Ryabova F.V., Stremovskiy O.A., Lukyanov S.A., Petrov R.V., Deyev S.M. // Theranostics. 2013. V. 3. № 11. P. 831–840.
3. Stepanov A.V., Belogurov A.A., Jr., Ponomarenko N.A., Stremovskiy O.A., Kozlov L.V., Bichucher A.M., Dmitriev S.E., Smirnov I.V., Shamborant O.G., Balabashin D.S., et al. // PLOS One. 2011. V. 6. e20991.
4. Generalova A.N., Sizova S.V., Zdobnova T.A., Zarifullina M.M., Artemyev M.V., Baranov A.V., Oleinikov V.A., Zubov V.P., Deyev S.M. // Nanomedicine (London). 2011. V. 6. P. 195–209.
5. Polanovski O.L., Lebedenko E.N., Deyev S.M. // Biochemistry (Moscow). 2012. V. 77. № 3. P. 227–245. .
6. Nahta R., Esteva F.J. // Cancer Lett. 2006. V. 232. P. 123–138.
7. Deyev S.M., Waibel R., Lebedenko E.N., Schubiger A.P., Plückthun A. // Nat. Biotechnol. 2003. V. 21. P. 1486–1492.
8. Zdobnova T.A., Dorofeev S.G., Tananaev P.N., Vasiliev R.B., Balandin T.G., Edelweiss E.F., Stremovskiy O.A., Balalaeva I.V., Turchin I.V., Lebedenko E.N., et al. // J. Biomed. Opt. 2009. V. 14. P. 021004.
9. Serebrovskaya E.O., Edelweiss E.F., Stremovskiy O.A., Lukyanov K.A., Chudakov D.M., Deyev S.M. // Proc. Natl. Acad. Sci. USA. 2009. V. 106. P. 9221–9225.
10. Balandin T.G., Edelweiss E., Andronova N.V., Treshalina E.M., Sapozhnikov A.M., Deyev S.M. // Invest. New Drugs. 2011. V. 29. P. 22–32.
11. Deyev S.M., Lebedenko E.N. // Acta Naturae. 2009. V. 1. № 1. P. 32–50.
12. Nikitin M.P., Zdobnova T.A., Lukash S.V., Stremovskiy O.A., Deyev S.M. // Proc. Natl. Acad. Sci. USA. 2010. V. 107. № 13. P. 5827–5832.
13. Zdobnova T.A., Stremovskiy O.A., Lebedenko E.N., Deyev S.M. // PLOS One. 2012. V. 7. e48248.
14. Glinka E.M., Edelweiss E.F., Sapozhnikov A.M., Deyev S.M. // Gene. 2006. V. 366. P. 97–103.
15. Sreenivasan V.K.A., Ivukina E.A., Deng W., Kelf T.A., Zdobnova T.A., Lukash S.V., Veryugin B.V., Stremovskiy O.A., Zvyagin A.V., Deyev S.M. // J. Mater. Chem. 2011. V. 21. P. 65–68.
16. Schreiber G., Fersht A.R. //. Nat. Struct. Biol. 1996. V. 3. № 5. P. 427–431.
17. Aghayeva U.F., Nikitin M.P., Lukash S.V., Deyev S.M. // ACS Nano. 2013. V. 7. № 2. P. 950–961.
18. Martsev S.P., Tsybovsky Y.I., Stremovsky O.A., Odincov S.G., Balandin T.G., Arosio P., Kravchuk Z.I., Deyev S.M. // Protein Engineering Design Selection. 2004. V. 17. P. 85–93.
19. Grebenik E.A., Nadort A., Generalova A.N., Nechaev A.V., Sreenivasan V.K., Khaydukov E.V., Semchishen V.A., Popov A.P., Sokolov V.I., Akhmanov A.S., et al. // J. Biomed. Opt. 2013. V. 18. P. 76004. doi: 10.1117/1.JBO.18.7.076004.
20. Xiong L., Chen Z., Tian Q., Cao T., Xu C., Li F. // Anal. Chem. 2009. V. 81. № 21. P. 8687–8694.
21. Dou Q., Idris N.M., Zhang Y. // Biomaterials. 2013. V. 34. № 6. P. 1722–1731.
22. Yi G., Peng Y., Gao Z. // Chem. Mater. 2011. V. 23. P. 2729–2734.
23. Mai H., Zhang Y., Sun L., Yan C. // J. Phys. Chem. C. 2007. V. 111. P. 13721–13729.
24. Yazynin S.A., Deyev S.M., Jucovic M., Hartley R.W. // Gene. 1996. V. 169. № 2. P. 131–132.
25. Rushizky G.W., Greco A.E., Hartley R.W., Jr., Sober H.A. // Biochemistry. 1963. V. 2. № 4. P. 787–793.
26. Zhan Q., Qian J., Liang H., Somesfalean G., Wang D., He S., Zhang Z., Andersson-Engels S. // ACS Nano. 2011. V. 5. № 5. P. 3744–3757.
27. Pellegrino T., Manna L., Kudera S., Liedl T., Koktysh D., Rogach A.L., Keller S., Rädler J., Natile G., Parak W.J. // Nano Lett. 2004. V. 4. P. 703–707.
28. Chen G., Qiu H., Prasad P.N., Chen X. // Chem. Rev. 2014. V. 114. № 10. P. 5161–5214.

Excessive Labeling Technique Provides a Highly Sensitive Fluorescent Probe for Real-time Monitoring of Biodegradation of Biopolymer Pharmaceuticals *in vivo*

S. S. Terekhov[1*], I. V. Smirnov[1,4], O. G. Shamborant[1], M. A. Zenkova[2], E. L. Chernolovskaya[2], D. V. Gladkikh[2], A. N. Murashev[3], I. A. Dyachenko[3], V. D. Knorre[1], A. A. Belogurov[1,4,5], N. A. Ponomarenko[1], S. M. Deyev[1], V. V. Vlasov[2], A. G. Gabibov[1,4,5]

[1]Shemyakin-Ovchinnikov Institute of Bioorganic Chemistry, Russian Academy of Sciences, Miklukho-Maklaya Str., 16/10, GSP-7, Moscow, Russia, 117997

[2]Institute of Chemical Biology and Fundamental Medicine, Siberian Branch of the Russian Academy of Sciences, Lavrentiev Ave., 8, 630090, Novosibirsk, Russia

[3]Branch of the Shemyakin-Ovchinnikov Institute of Bioorganic Chemistry, Russian Academy of Sciences, Pushchino, 142290, Moscow region, Russia

[4]Kazan Federal University, Kremlevskaya str. 18, 420008, Kazan, Republic of Tatarstan, Russia

[5]Institute of Gene Biology, Russian Academy of Sciences, Vavilova Str., 34/5, 119334, Moscow, Russia

*E-mail: sterekhoff@mail.ru

ABSTRACT **Recombinant proteins represent a large sector of the biopharma market. Determination of the main elimination pathways raises the opportunities to significantly increase their half-lives *in vivo*. However, evaluation of biodegradation of pharmaceutical biopolymers performed in the course of pre-clinical studies is frequently complicated. Noninvasive pharmacokinetic and biodistribution studies in living organism are possible using proteins conjugated with near-infrared dyes. In the present study we designed a highly efficient probe based on fluorescent dye self-quenching for monitoring of *in vivo* biodegradation of recombinant human butyrylcholinesterase. The maximum enhancement of integral fluorescence in response to degradation of an intravenously administered enzyme was observed 6 h after injection. Importantly, excessive butyrylcholinesterase labeling with fluorescent dye results in significant changes in the pharmacokinetic properties of the obtained conjugate. This fact must be taken into consideration during future pharmacokinetic studies using *in vivo* bioimaging.**

KEYWORDS **fluorescent probe, biodegradation, pharmacokinetics, *in vivo* bioimaging, self-quenching, butyrylcholinesterase, proteolysis.**

ABBREVIATIONS **SPECT – single-photon emission computed tomography; PET – positron emission tomography; HIV – human immunodeficiency virus; rhBChE – tetrameric recombinant human butyrylcholinesterase; PRAD – proline-rich attachment domain; MMP – matrix metalloproteinase; sCy5 – Sulfo-Cyanine5; sCy7 – Sulfo-Cyanine7; F_{max} – relative fluorescence intensity enhancement; F_{enz} – fluorescence intensity enhancement after proteolytic digestion; F_0 – fluorescence intensity before proteolytic digestion; N – modification degree of pharmaceuticals; rhBChE-sCy7 ON – fluorescent rhBChE-sCy7 conjugate having no self-quenching effect; rhBChE-sCy7 OFF – nonfluorescent rhBChE-sCy7 conjugate having a quenching effect; BSA – bovine serum albumin; KLH – hemocyanin.**

INTRODUCTION

Modern pharmacokinetics is a technology-intensive field that utilizes cutting-edge noninvasive approaches, such as single-photon emission computed tomography (SPECT), positron emission tomography (PET), and *in vivo* bioimaging not only for determining pharmacokinetic parameters but also for studying biodistribution and evaluating the accumulation profiles of pharmaceuticals [1]. Since recombinant protein-based pharmaceuticals are widely used in treatment of serious diseases such as cancer [2, 3], autoimmune diseases [4], and blood disorders [5], it is extremely important to examine

their biodistribution and biodegradation during preclinical studies. The new infrared fluorescent dyes with a high brightness allow working in the tissue transparency window (700–900 nm), are commercially available, safe, and efficient, which makes fluorescence bioimaging one of the most widely used imaging techniques [6, 7]. The imaging data can reveal pharmaceutical accumulation compartment [8] and pharmacokinetic parameters of elimination [9]. The relationship between accumulation and biodegradation is especially crucial for the recombinant protein-based pharmaceuticals with specific activity. The knowledge about pharmaceutical biodegradation is also of great interest as it allows one to determine the main elimination routes.

The aim of this study was to design a probe that enables determination of the main biodegradation compartments of a recombinant protein. Recombinant human butyrylcholinesterase, a bioscavenger of organophosphorus agents, was used as an example of the protein-based biological antidote against nerve-agent poisoning [10, 11]. The approach employed is based on self-quenching of fluorophores [12]. The essence of this phenomenon is that fluorescence quenching is typical of fluorophore molecules characterized by a small Stokes' shift (~20–30 nm) and situated at a distance of less than 10 nm from one another. Quenching effectiveness depends, among other factors, on the aggregation tendency of fluorophore molecules due to their π-π and hydrophobic interactions [13]. Thus, excessive modification of a protein-based pharmaceutical with an infrared fluorophore having the self-quenching effect gives rise to a conjugate with "switched off" fluorescence, while its degradation and the formation of peptide products enhances the integral fluorescence. This approach is currently used for tumor imaging based on the presence of MMP activity or presence of specific or hyperexpressed receptors [14–18] and to detect the activity of proteolytic antibodies against HIV surface protein, gp120 [19]. In this study, we proposed excessive labeling of recombinant butyrylcholinesterase to visualize the compartments responsible for biodegradation and elimination of the pharmaceutical *in vivo* and to evaluate the parameters of enzyme biodistribution and biodegradation.

MATERIALS AND METHODS

Protein-based pharmaceuticals

Tetrameric recombinant human butyrylcholinesterase (rhBChE) was produced in CHO-K1 cells transfected with a pFUSE PRAD-F2A-BChE construct, which results in simultaneous expression of the PRAD tetramerization peptide gene and the human butyrylchoninesterase gene. rhBChE was purified by affinity chromatography on a procainamide-Sepharose XK10/50 column (GE Healthcare, USA) followed by ion exchange chromatography on a MonoQ 5/50 column (GE Healthcare, USA). Polyacrylamide gel electrophoresis followed by Coomassie staining and Karnovsky and Roots's staining to detect specific butyrylcholinesterase activity [20] showed 95% protein purity. Commercially available KLH and BSA proteins were purchased from Sigma Aldrich.

Synthesis of pharmaceuticals based on fluorescently labeled proteins

The proteins were labeled with various NHS-activated fluorophores of the cyanine family: Sulfo-Cyanine5 (sCy5) and Sulfo-Cyanine7 (sCy7) (Lumiprobe). The conjugation procedure was performed in 0.1 M $NaHCO_3$ in accordance with the manufacturer's protocol. Reaction products were removed from the fluorescently labeled proteins by gel filtration chromatography on a HiTrap Desalting column (GE Healthcare, USA). The fluorescence of the pharmaceuticals was measured on a Varioscan Flash instrument (Thermo Scientific). To determine the maximum relative fluorescence enhancement, the protein-based pharmaceuticals were subjected to proteolysis with a solution containing a protease mixture (1 mg/ml proteinase K (Fermentas) and 2 mg/ml subtilisin Carlsberg) in phosphate buffered saline pH 7.4 at 37°C for 4 h. The completeness of proteolysis was monitored fluorimetrically according to saturation attainment on the fluorescence intensity (RFU) vs. time curve. The relative fluorescence enhancement (F_{max}) was calculated as the ratio between the difference of fluorescence intensity after proteolytic digestion (F_{enz}) and fluorescence intensity before proteolytic digestion (F_0): $F_{max} = (F_{enz} - F_0)/F_0 * 100\%$. The modification degree of the samples (N), i.e., the number of fluorophore groups per protein molecule, was determined by the absorbance measurements of the solutions at 280 nm ($E^{1\%}$=18) and 760 nm; the molar extinction coefficient of sCy7 was assumed to be 240600 $M^{-1}cm^{-1}$.

Determination of the pharmacokinetic parameters of rhBChE-sCy7 conjugates

rhBChE samples (without a fluorescent label, low-labeled rhBChE-sCy7 ON and excessively conjugated rhBChE-sCy7 OFF) were intravenously injected at a dose of 200 μg/mouse into three groups of BALB/c mice with 6 animals per group to assess blood concentrations of rhBChE conjugates. rhBChE concentration in mouse blood serum was determined according to its activity using the Ellman's method [21]. The pharmacokinetic characteristics of rhBChE samples were obtained from fitting the serum rhBChE vs time curve using the two-compartment model [10].

In vivo imaging experiments

The biodistribution and the degradation pattern of rhBChE were determined using rhBChE-sCy7 OFF and rhBChE-sCy7 ON. The rhBChE-sulfo-Cyanine7 conjugates were intravenously injected into BALB/c mice at a dose of 500 μg/mouse. An In Vivo MS FX PRO small animal imaging system (Bruker) was used to visualize the distribution of BChE and its degradation products. The excitation (730 nm) and emission (790 nm) filters were used to detect the fluorescence of sCy7.

RESULTS AND DISCUSSION

The application of excessively labeled protein fluorescence quenching with subsequent fluorescence enhancement via proteolytic degradation has been successfully demonstrated in studies with a low level of proteolytic activity [22] or by analyzing low enzyme levels [23]. It is evident that fluorescein cannot be used as a source of analytical signal in *in vivo* studies, since organs and tissues provide a high background signal. To eliminate this disadvantage, we conjugated protein molecules to sCy5 and sCy7 dyes under various conditions. We also suggested that the use of red and near-infrared fluorophores results in more sensitive probes for proteolytic activity as fluorescence enhancement would be more efficient. We used the conventional substrate proteins utilized to analyze nonspecific proteolytic activity (bovine serum albumin (BSA)) and hemocyanin (KLH)) and butyrylcholinesterase—a pharmaceutical utilized as a biological antidote against nerve-agent poisoning. As a result, KLH-sCy5, BSA-sCy5, rhBChE-sCy5, BSA-sCy7, rhBChE-sCy7 ON and rhBChE-sCy7 OFF specimens were obtained (Table 1).

The conjugates were subjected to proteolysis to determine the fluorescence enhancement efficiency. All the fluorescent substrates exhibited high levels of maximum enhancement of fluorescence (F_{max}) (Table 1), which exceeded those of the conventional BSA–FITC substrate. The rhBChE-sCy5 specimen showed the highest efficiency (fluorescence increased over 700-fold).

The fluorescence of the rhBChE-sCy7 ON specimen remained unchanged before and after proteolytic digestion, while the fluorescence of the rhBChE-sCy7 OFF specimen was significantly quenched and increased 220-fold after proteolytic digestion. Thus, the rhBChE-sCy7 OFF specimen can act as a probe to assess the proteolytic degradation of rhBChE in pharmacokinetic experiments. We analyzed several variants of excessively labeled butyrylcholinesterase to design a fluorescent probe with maximum efficiency. We relied on two selection criteria: relative fluorescence intensity enhancement and specific activity of the modified enzyme (*Fig. 1*). The variant with a modification degree N=32 was eventually chosen, since more than 70% of its specific activity was retained.

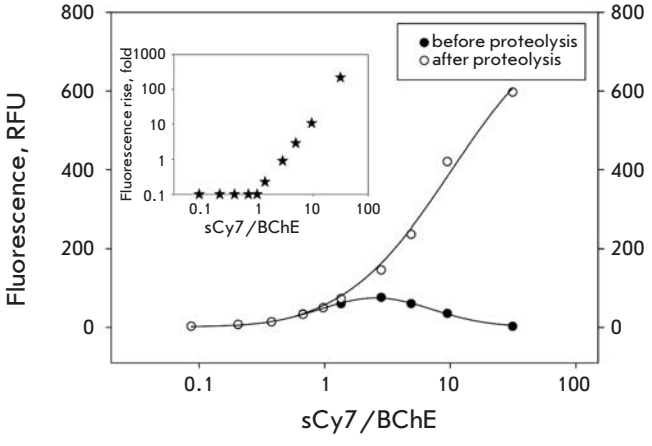

Fig. 1. Analysis of rhBChE-sCy7 conjugates with different modification degrees

Table 1. Properties of the fluorescent dye labeled proteins used in the present study

Conjugate	*N*	F_0, RFU	F_{enz}, RFU	F_{max}
BSA-FITC (Voss et al.)	25	-	-	3450
KLH-sCy5	380-750	6.25	1140	18100
BSA-sCy5	6.7	2.37	1680	70800
rhBChE-sCy5	30	6.17	1750	28300
BSA-sCy7	6.5	1.8	660	36500
rhBChE-sCy7 OFF	32	2.71	597	21900
rhBChE-sCy7 ON	1	50	50.05	0.1

N – modification degree; F_0 – fluorescence before proteolytic digestion; F_{enz} – fluorescence after proteolytic digestion.

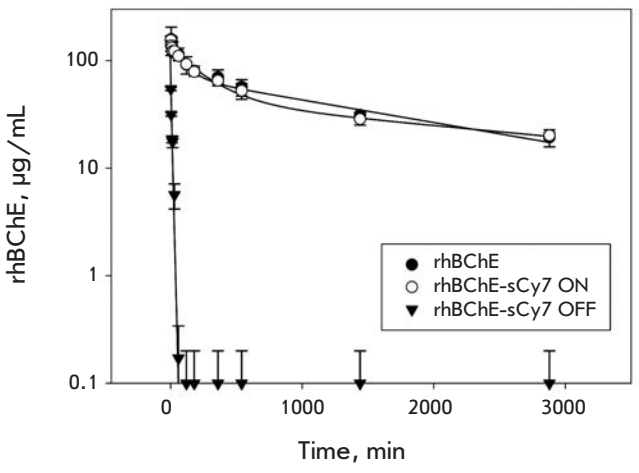

Fig. 2. Analysis of the pharmacokinetic parameters of elimination of rhBChE and rhBChE-sCy7 conjugates from serum

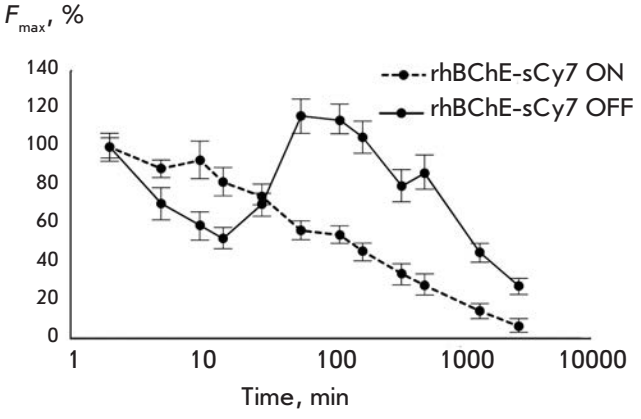

Fig. 3. Analysis of the elimination kinetics of rhBChE-sCy7 conjugates observed by sCy7 fluorescence

Pharmacokinetic studies of rhBChE-sCy7 ON and rhBChE-sCy7 OFF specimens

Studying the pharmacokinetic parameters of the rhBChE-sCy7 ON and rhBChE-sCy7 OFF specimens, we used a unique opportunity to assess the butyrylcholinesterase level in the blood flow simultaneously using the kinetic and fluorescent methods. Indeed, the pharmacokinetic parameters of protein-based pharmaceuticals are usually assessed using either a direct radioactive method or indirect methods (e.g., ELISA). However, all these methods often indicate only that there is a protein fragment (containing a radioactive label or specific antibody–epitope binding, respectively) but do not prove the presence of an active protein-based pharmaceutical. In the case of butyrylcholinesterase, only the active enzyme acts as a biological antidote; hence, the actual pharmacokinetic parameters of the pharmaceutical can be evaluated by observing the changes in its activity in the blood. The fluorescent probe shows the existence of the integral protein as well as its fragments. Hence, comparison of the elimination profiles observed using two different methods demonstrates pharmaceutical degradation against a background of elimination from the organism.

Figure 2 and Table 2 show the identity of the elimination pattern and parameters of rhBChE-sCy7 ON to the respective unmodified enzyme, while the rhBChE-sCy7 OFF specimen is characterized by drastic changes in its behavior in the organism. The elimination rate greatly increases (Table 2).

It was found by analyzing the elimination profiles observed by fluorescence in different time points after the pharmaceutical had been administered (*Fig. 3*) that the maximum fluorescence level is observed 1.5–8 h after administration. It is fair to say that within this period pharmaceutical accumulation reaches the highest level in liver where the enzyme is actively degraded, which results in an increase in fluorescence (*Fig. 4*). The pharmacokinetics of elimination of rhBChE-sCy7 ON with fluorescent detection (*Fig. 3*) does not significantly differ from a similar elimination curve for rhBChE-sCy7 ON detected according to the enzymatic activity (*Fig. 2*). Hence, fluorescent detection of enzyme distribution adequately shows the accumulation of rhBChE in a certain compartment. Meanwhile, the comparison of these curves for the rhBChE-sCy7 OFF specimen clearly indicates that two different processes take place: 1 – rapid elimination of rhBChE-sCy7 OFF from

Table 2. Pharmacokinetic parameters of rhBChE and rhBChE-sCy7 conjugates

Parameter	rhBChE	rhBChE-sCy7 ON	rhBChE-sCy7 OFF
$\tau_{1/2}$ disr, min	100±40	140±50	6±2
$\tau_{1/2}$ el, min	1600±300	2200±400	
MRT, min	2400±600	2700±700	9±3

the blood flow (which is unrelated to the degradation of rhBChE-sCy7 OFF and results in a rapid decrease in rhBChE activity in blood but is not accompanied by fluorescence intensity enhancement); 2 – slow degradation of rhBChE-sCy7 OFF in the accumulation area (fluorescence increases to attain its maximum while zero activity of rhBChE in blood is detected).

The results of an *in vivo* biodistribution of rhBChE-sCy7 ON and rhBChE-sCy7 OFF specimens in mouse organs are shown in *Fig. 4*. Both specimens mainly accumulate in the liver, kidneys, and bladder. The liver is the main organ responsible for degradation of the enzyme; maximum enhancement of integral fluorescence indicating enzyme biodegradation is observed 6 h after intravenous injection. The degradation products enter the blood flow and are eliminated mostly by the kidneys. Hence, *in vivo* distribution data of a protein-based pharmaceutical mainly confirm the findings obtained at the previous stages (see *Fig. 2, 3* and *Table 2*).

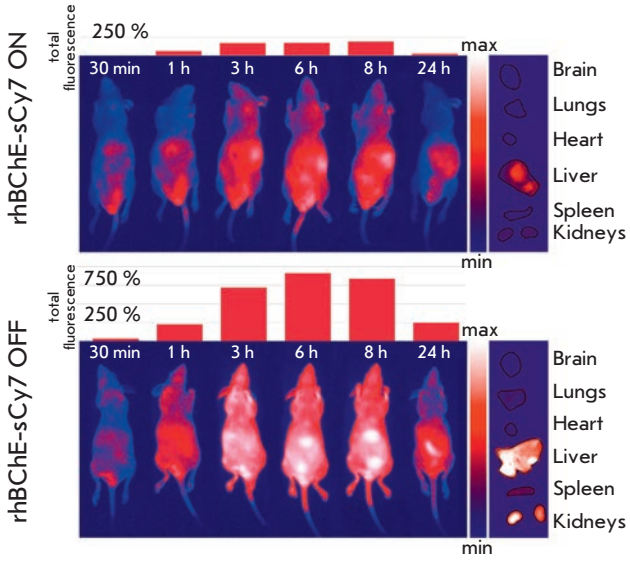

Fig. 4. Biodistribution analysis of rhBChE-sCy7 conjugates using fluorescent bioimaging

CONCLUSIONS

Fluorescent probes are a simple and very sensitive method to detect proteolytic activity. The advances in the chemistry of fluorescent dyes have made it possible to design substrates with a high fluorescence intensity and low background signal. We designed a panel of fluorescent substrates based on proteins excessively labeled with sulfo-Cyanine5 and sulfo-Cyanine7 fluorophores and attained a 700-fold enhancement of fluorescence after proteolysis. The application of an excessively labeled specimen for *in vivo* imaging of the organs and tissues responsible for degradation and elimination of pharmaceuticals enable one to characterize the behavior of therapeutic protein-based pharmaceuticals in the organism more thoroughly. It is evident that researchers should take into account the pattern and site of degradation of a potential pharmaceutical when attempting to improve its pharmacokinetic parameters. The methods increasing blood retention together with the liver accumulation rate reduction may contribute to the design of pharmaceuticals with prolonged half-life. It should be mentioned that this approach is universal allowing one to perform *in vivo* degradation studies of any protein or peptide. However, excessive labeling may drastically change the pharmacokinetic properties and the elimination route of a certain protein-based pharmaceutical [24], which should be taken into consideration when choosing a fluorescent bioimaging technique during pharmacokinetic studies. The proposed approach may prove to be extremely topical during comparative preclinical studies using a panel of similar protein-based pharmaceuticals and selecting the optimal candidate that would exhibit the targeted effect. ●

This work was supported by the Ministry of Education and Science of the Russian Federation (project ID RFMEFI57614X0184), the Presidium of the Russian Academy of Sciences (program "Molecular and Cellular Biology"), State Contract with the Ministry of Industry and Trade of the Russian Federation (№ 13411.1008799.13.128, ID "2.1 Antidot 2013"), Presidential Scholarship SP-2477.2013.4 (I.S.), Presidential Grant for the support of leading scientific schools NSh-2064.2014.14 "Chemical Foundations of Biocatalysis", and program of basic research of the Presidium of the Russian Academy of Sciences № 24 "Foundations of Basic Research in Nanotechnologies and Nanomaterials" (project "Nanopharmaceuticals based on myelin basic protein fragments compartmentalized into lyposome containers for treating neurodegenerative diseases"). RFBR grants (14-04-00647 A, 14-04-31207 mol_a), Russian Science Foundation project 14-24-00106. The work was carried out under the state program to improve competitiveness of the Kazan (Volga) Federal University among the world's leading research and educational Centers.

REFERENCES

1. Hoppin J., Orcutt K.D., Hesterman J.Y., Silva M.D., Cheng D., Lackas C., Rusckowski M. // JPET. 2011. V. 337 № 2 P. 350–358.
2. Yuskevich V., Khodarovich Y., Kagarliskiy G., Stremovskiy O., Maksimenko O., Lukash S., Polanovsky O., Deyev S. // Biochimie. 2011 V. 93 №3 P. 628-630.
3. Sreenivasan V.K., Stremovskiy O.A., Kelf T.A., Heblinski M., Goodchild A.K., Connor M., Deyev S.M., Zvyagin A.V. // Bioconjugate Chem. 2011. V.22 № 9 P. 1768-1775.
4. Stepanov A.V., Belogurov A.A. Jr., Ponomarenko N.A., Stremovskiy O.A., Kozlov L.V., Bichucher A.M., Dmitriev S.E., Smirnov I.V., Shamborant O.G., Balabashin D.S. // PLoS One. 2011. V. 6 №6 P. e20991.
5. Orlova N.A., Kovnir S.V., Vorobiev I.I., Gabibov A.G., Vorobiev A.I. // Acta Naturae. 2013. V. 5 № 2 P. 19-39.
6. Yi X.M., Wang F.L., Qin W.J., Yang X.J., Yuan J.L. // International Journal of Nanomedicine. 2014. V. 9 № 1 P. 1347–1365.
7. Vonwil D., Christensen J., Fischer S., Ronneberger O., Shastri V. P. // Molecular Imaging and Biology. 2013. V. 16 № 3 P. 350–361.
8. Satoa K., Watanabea R., Hanaokaa H., Haradaa T., Nakajimaa T., Kimb I., Paikc C.H., Choykea P.L., Kobayashi H. // Molecular Oncology 2014. V. 8 № 3 P. 620–632.
9. Dobosz M., Strobel S., Stubenrauch K.-G., Osl F., Scheuer W. // Journal of Biomedical Optics. 2014. V. 19 № 1 P. 16022.
10. Ilyushin D.G., Smirnov I.V., Belogurov A.A., Dyachenko I.A., Zharmukhamedova T.Iu., Novozhilova T.I., Bychikhin E.A., Serebryakova M.V., Kharybin O.N., Murashev A.N. et al. // PNAS. 2013. V. 110 № 4 P. 1243-1248.
11. Ilyushin D.G., Haertley O.M., Bobik T.V., Shamborant O.G., Surina E.A., Knorre V.D., Masson P., Smirnov I.V., Gabibov A.G., Ponomarenko N.A. // Acta Naturae. 2013 V. 5 № 1 P. 73-84.
12. Kobayashi H., Choyke P.L. // Acc Chem Res. 2011. V. 44 № 2 P. 83–90.
13. Zhegalova N. G., He S., Zhou H., Kim D.M., Berezin M.Y. // Contrast Media & Molecular Imaging. 2014. V. 9 № 5 P. 355–362.
14. Moin K., Sameni M., Victor B.C., Rothberg J.M., Mattingly R.R., Sloane B.F. // Methods in Enzymology. 2012. V. 506 P. 175–194.
15. Hama Y., Urano Y., Koyama Y., Kamiya M., Bernardo M., Paik R.S., Shin I.S., Paik C.H., Choyke P.L., Kobayashi H. // Cancer Research. 2007. V. 67 № 6 P. 2791-2799.
16. Akers W.J., Xu B., Lee H., Sudlow G.P., Fields G.B., Achilefu S., Edwards W.B. // Bioconjugate Chem. 2012. V. 23 № 3 P. 656–663.
17. Vinita A.M., Sano K., Yu Z., Nakajima T., Choyke P.L., Ptaszek M., Kobayashi H. // Bioconjugate Chem. 2012. 23 № 8 P. 1671-1679.
18. Springa B.Q., Abu-Yousifa A.O., Palanisamia A., Rizvia I., Zhenga X., Maia Z., Anbila S., Searsa R. B., Mensaha L.B., Goldschmidta R. et al. // PNAS. 2014. V. 111 № 10 P. E933-E942.
19. Ponomarenko N.A., Vorobiev I.I., Alexandrova E.S., Reshetnyak A.V., Telegin G.B., Khaidukov S.V., Avalle B., Karavanov A., Morse H.C. 3rd, Thomas D., // Biochemistry. 2006. V. 45 № 1 P. 324-330.
20. Karnovsky M.J., Roots L. // J Histochem Cytochem. 1964 V. 12 P. 219–221.
21. Ellman G.L., Courtney K.D., Andres V. Jr., Feather-Stone R.M. // Biochem Pharmacol. 1961. V. 7 P. 88–95.
22. Ponomarenko N.A., Pillet D., Paon M., Vorobiev I.I., Smirnov I.V., Adenier H., Avalle B., Kolesnikov A.V., Kozyr A.V., Thomas D. et al. // Biochemistry. 2007. V. 46 № 50 P. 14598–14609.
23. Voss E.W., Workman C.J., Mummert M.E. // Biotechniques. 1996. V. 20 №2 P. 286-291.
24. Sano K., Mitsunaga M., Nakajima T., Choyke P.L., Kobayashi H. // Breast Cancer Research. 2012. V. 14 № 2 R61.

Human SLURP-1 and SLURP-2 Proteins Acting on Nicotinic Acetylcholine Receptors Reduce Proliferation of Human Colorectal Adenocarcinoma HT-29 Cells

E. N. Lyukmanova[1,2,*], M. A. Shulepko[1,2], M. L. Bychkov[1,2], Z. O. Shenkarev[1,2], A. S. Paramonov[1,2], A. O. Chugunov[1,2], A. S. Arseniev[1,3], D. A. Dolgikh[1,2], M. P. Kirpichnikov[1,2]

[1]Shemyakin and Ovchinnikov Institute of Bioorganic Chemistry, Russian Academy of Sciences, Miklukho-Maklaya str., 16/10, Moscow, 117997, Russian Federation

[2]Biological Department, Lomonosov Moscow State University, Vorobievy Gory, 1, Moscow, 119991, Russia

[3]Moscow Institute of Physics and Technology (State University), Institutskii per., 9, Dolgoprudny, Moscow Region, 141700, Russia

*E-mail: ekaterina-lyukmanova@yandex.ru

ABSTRACT **Human secreted Ly-6/uPAR related proteins (SLURP-1 and SLURP-2) are produced by various cells, including the epithelium and immune system. These proteins act as autocrine/paracrine hormones regulating the growth and differentiation of keratinocytes and are also involved in the control of inflammation and malignant cell transformation. These effects are assumed to be mediated by the interactions of SLURP-1 and SLURP-2 with the α7 and α3β2 subtypes of nicotinic acetylcholine receptors (nAChRs), respectively. Available knowledge about the molecular mechanism underling the SLURP-1 and SLURP-2 effects is very limited. SLURP-2 remains one of the most poorly studied proteins of the Ly-6/uPAR family. In this study, we designed for the first time a bacterial system for SLURP-2 expression and a protocol for refolding of the protein from cytoplasmic inclusion bodies. Milligram quantities of recombinant SLURP-2 and its ^{13}C-^{15}N-labeled analog were obtained. The recombinant protein was characterized by NMR spectroscopy, and a structural model was developed. A comparative study of the SLURP-1 and SLURP-2 effects on the epithelial cell growth was conducted using human colorectal adenocarcinoma HT-29 cells, which express only α7-nAChRs. A pronounced antiproliferative effect of both proteins was observed. Incubation of cells with 1 μM SLURP-1 and 1 μM SLURP-2 during 48 h led to a reduction in the cell number down to ~ 54 and 63% relative to the control, respectively. Fluorescent microscopy did not reveal either apoptotic or necrotic cell death. An analysis of the dose-response curve revealed the concentration-dependent mode of the SLURP-1 and SLURP-2 action with EC_{50} ~ 0.1 and 0.2 nM, respectively. These findings suggest that the α7-nAChR is the main receptor responsible for the antiproliferative effect of SLURP proteins in epithelial cells.**

KEYWORDS **nicotinic acetylcholine receptor; bacterial expression; refolding; Lynx; colon cancer.**

ABBREVIATIONS **nAChR – nicotinic acetylcholine receptor; SLURP – secreted Ly-6/uPAR related protein; ws-Lynx1 – water-soluble domain of human Lynx1.**

INTRODUCTION

The nicotinic acetylcholine receptor (nAChR) is a ligand-gated ion channel found both in the central and peripheral nervous systems and in many other human tissues, including the epithelium [1, 2]. During last decade, in higher animals, proteins were found that belong to the Ly-6/uPAR family and have a modulating effect on nAChRs (Lynx1, Lynx2, Lypd6, SLURP-1, and SLURP-2) [3–7]. A conserved location of Cys residues (*Fig. 1*), forming disulfide bonds, indicates the homology of the spatial structure of the Lynx and SLURP proteins to the three-finger structure of snake venom α-neurotoxins, which are highly efficient and specific nAChR inhibitors [8].

SLURP-1 and SLURP-2 are secreted proteins found in many human tissues, including the epithelium, as well as the immune and nervous systems [5, 6, 9, 10]. SLURPs affect the growth, migration, and differentiation of epithelial cells, and they are involved in the control of inflammation and tumors [6, 11, 12]. With the Het1A keratinocyte line, it was demonstrated that SLURP-1 exhibits antiproliferative activity and pro-

motes apoptotic cell death [11], while SLURP-2 accelerates keratinocyte growth, delaying their differentiation and reducing the response to proapoptotic signals [6]. In addition, SLURPs regulate wound healing in the skin and mucous membranes [13] and are involved in the protection of skin cells from the oncogenic transformation caused by nitrosamines (nicotine derivatives) [14, 15]. Probably, SLURP-1 and SLURP-2 act as auto/paracrine regulators and their effects are mediated by the interaction with the nAChRs presented on the cell membrane surface of keratinocytes and immune cells [10, 16]. α7 and α3β2 nAChRs are the putative targets for SLURP-1 and SLURP-2, respectively [6, 11]. Recently, SLURP-1 expression was detected in HT-29 human colorectal adenocarcinoma cells and the level of endogenous production of SLURP-1 in these cells was demonstrated to decrease significantly when the cells are treated with nicotine [17]. At the same time, HT-29 cells were shown to be able to express only the α7 type of nAChRs [18].

Currently, the structural and functional properties of human SLURP-1 and SLURP-2, as well as their mechanism of action, remain poorly studied. The main stumbling stones in studying SLURP-1 and SLURP-2 are related to the inability to produce adequate amounts of protein samples from natural sources, as well as to the problems of recombinant production of these proteins with a native sequence and spatial structure. As a consequence, the majority of previously published results were obtained using hybrid constructs containing, along with the SLURP protein sequence, additional polypeptide sequences that can significantly affect resultant activity. For example, in the study [6], a construct fused with the SUMO protein (the total protein weight was 22 kDa, of which only ~ 8 kDa accounted for SLURP-2) was used to investigate SLURP-2.

In the present study, an efficient bacterial system for human SLURP-2 production in the form of cytoplasmic inclusion bodies was developed for the first time and protein refolding protocol was proposed. The resulting recombinant analog differs from the wild type protein by the presence of one additional residue (N-terminal Met). A high-expression yield (~ 5 mg of the refolded protein per 1 L of the bacterial culture) enabled production of milligram quantities of the recombinant protein and its $^{13}C^{15}N$-labeled analog. The development of this system of recombinant production opens up new perspectives for structural and functional studies of SLURP-2. For example, in this paper, we demonstrated for the first time a significant antiproliferative effect of SLURP-1 and SLURP-2 on HT-29 line cells. This suggests that α7-nAChR plays the main role in transduction of SLURP-induced signals resulting in the reduction of growth of epithelial cells.

EXPERIMENTAL

Cloning and bacterial production of SLURP-2.

The *slurp-2* gene encoding 75 amino acid residues of the human SLURP-2 protein (*Fig. 1A*) was constructed from overlapping synthetic oligonucleotides using PCR and with allowance for the codon frequency in *E. coli* (Evrogen, Moscow, Russia). The *slurp-2* gene was cloned into the *pET-22b(+)* expression vector (Novagen) at NdeI and BamHI restriction sites. BL21 (DE3) *E. coli* cells transformed with the *pET-22b(+)/slurp-2* vector were cultured at 37 ^{0}C on a TB medium (12 g of bacto-tryptone, 24 g of yeast extract, 4 mL of glycerol, 2.3 g of KH_2PO_4, 12.5 g of K_2HPO_4 per 1 L of the medium, pH 7.4) in a Bioflo 3000 fermentor (New Brunswick Scientific) under automatically maintained conditions of a relative oxygen content in the system of not less than 30% of the maximum achievable value. The *slurp-2* gene expression was induced by adding isopropyl β-D-1-thiogalactopyranoside (IPTG) to the final concentration of 0.05 mM at an optical density of the cell culture of 1.0 OD. After the induction, the cells were cultured for 8 h.

In order to produce the ^{13}C-^{15}N-labeled SLURP-2 analogue, 1 L of the cell culture, which had been preliminarily grown on a TB medium in flasks to a cell density of 1.0 OD, was centrifuged at 1,000 g for 20 min. The cell pellet was aseptically re-suspended in 1 L of the M9 minimal medium (6 g of Na_2HPO_4, 3 g of KH_2PO_4, 0.5 g NaCl, 2 g of NH_4Cl, 240 mg of anhydrous $MgSO_4$, 11 mg of $CaCl_2$, 3 g of glucose, 2 mg of yeast extract, 200 μL of 5% thiamine chloride per 1 L of the medium, pH 7.4) containing ^{13}C-glucose and ^{15}N-NH_4Cl (CIL) as a source of glucose and nitrogen, respectively. Induction and further growth were carried out similarly to growth on the TB medium.

Purification and refolding of recombinant SLURP-2.

Inclusion bodies containing SLURP-2 were isolated and washed according to the protocols described previously for SLURP-1 [19]. The washed inclusion bodies were re-suspended in 30 mM Tris-HCl, pH 8.7, containing 8 M urea, 0.4 M sodium sulfite, 0.15 M sodium tetrathionate in the amount of 10 mL of the buffer per 1 g of inclusion bodies. The suspension was disintegrated by ultrasound (Branson Digital Sonifier) at an output power of 50 W and 4 ˚C for 1 min and left for 8 h under mild stirring. The suspension was then centrifuged at 36,000 g, 4 ˚C, for 30 min, and the supernatant was diluted 10 times with 2 M urea. Afterwards, the sulfited SLURP-2 sample was loaded onto a column of DEAP-sferonit-OH (joint development by the Institute of Highly Pure Biopreparations, St. Petersburg, and the Institute of Bioorganic Chemistry, Moscow, Russia) preliminarily

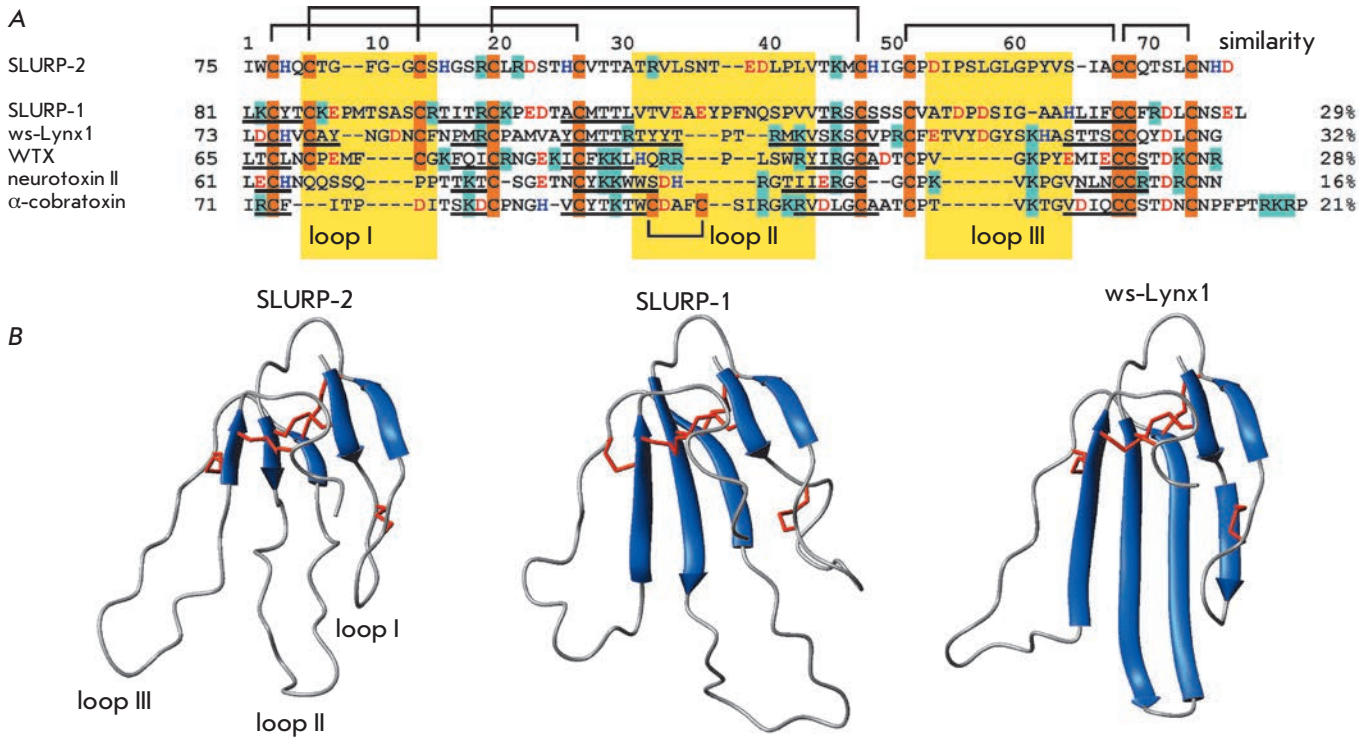

Fig. 1. Comparison of the structures of three-finger proteins of the Ly-6/uPAR family. (A). Amino acid sequence alignment of human SLURP-1, SLURP-2, and a water-soluble domain of human Lynx1 (ws-Lynx1), the WTX neurotoxin from *Naja kaouthia*, the neurotoxin II from *Naja oxiana*, and the α-cobratoxin from *Naja kaouthia*. The positively charged (Arg/Lys), negatively charged (Asp/Glu), His and Cys residues are highlighted by color, the disulfide bonds are shown. The protein fragments forming β-strands are underlined. The loop regions are highlighted by a yellow background. The amino acid sequence homology between SLURP-2 and other three-finger proteins was calculated using the CLUSTAL W2 software. (B). Comparison of the SLURP-2 structure model with the spatial structures of SLURP-1 (Shenkarev *et. al*, submitted, PDB 2MUO) and ws-Lynx1 ([23], PDB 2L03)

equilibrated with the buffer A (30 mM Tris-HCl, pH 8.0). After loading of the protein, the column was sequentially washed with the buffer A, with the buffer A supplemented with 1 M NaCl, and with the buffer A supplemented with 8 M urea. The sulfited SLURP-2 was eluted with the buffer A supplemented with 8 M urea and 0.5 M NaCl. Fractions containing SLURP-2 were added with a 1,000-fold (relative to the protein) molar excess of DTT. Reduced SLURP-2 was purified by HPLC (Jupiter C4, A300, 10×250 mm, Phenomenex). SLURP-2 was eluted with the acetonitrile gradient (20 – 45%) in the presence of 0.1% TFA for 40 min. The resulting reduced SLURP-2 sample was lyophilized and dissolved in the refolding buffer containing 50 mM Tris-HCl, pH 9.0, 2 M urea, 0.5 M L-arginine, 2 mM GSH, and 2 mM GSSG to a final protein concentration of 0.1 mg/mL. Refolding was performed at 4 °C for three days. Analysis and purification of SLURP-2 after refolding was performed by HPLC (Jupiter C4, A300, 4.6x250 mm, Phenomenex). The resulting refolded SLURP-2 sample was lyophilized.

NMR spectroscopy and modeling of the structure of SLURP-2.

NMR spectra of ^{13}C-^{15}N-labeled and unlabelled SLURP-2 (sample concentration was 0.5 mM) were acquired on an AVANCE-700 spectrometer (Bruker) at 30 °C.

To model the structure of SLURP-2, the ws-Lynx1 protein (PDB 2L03) was used as a template. Alignment of amino acid sequences was performed on the Clustal web server (www.clustal.org). The model was constructed using the Modeller V8.2 software [20].

Working with the HT-29 cell line.

HT-29 colorectal adenocarcinoma cells (Institute of Cytology of the Russian Academy of Sciences, St. Petersburg, Russia) were maintained in a RPMI-1640 medium (PanEco, Moscow, Russia) supplemented with 5% fetal bovine serum (Hyclone, Thermo Fisher Scientific). The cells were maintained in a humidified atmosphere (37 °C, 5% CO_2) and were passaged every 48 h. Sixteen hours before the experiment, the cells

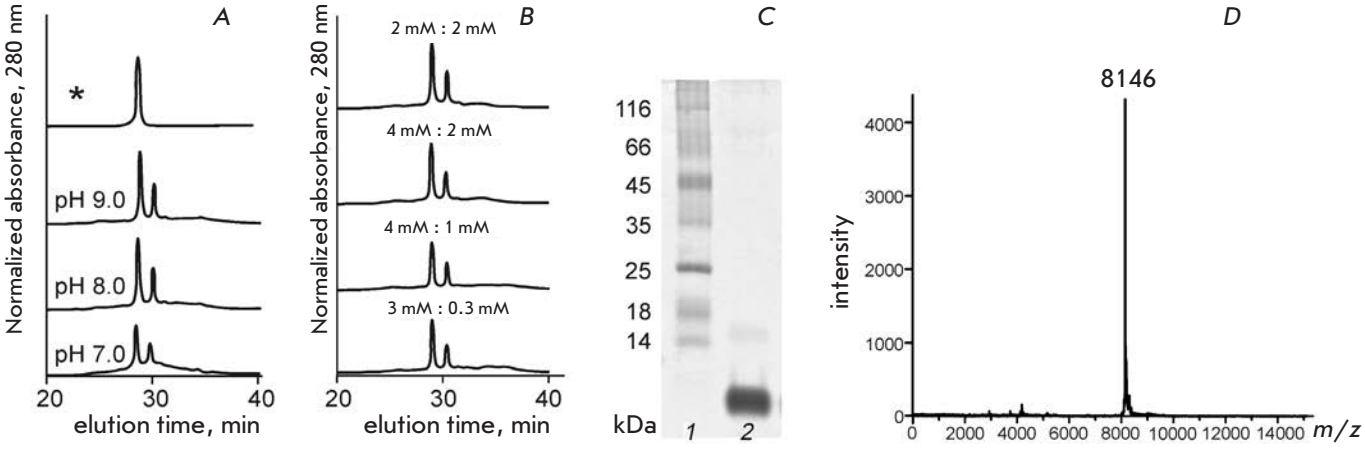

Fig. 2. Analysis of recombinant SLURP-2. (A–B). The SLURP-2 refolding efficiency depends on the pH of the refolding buffer (A) and the concentration of the reduced (GSH) and oxidized (GSSG) forms of glutathione (B). The peak corresponding to the refolded SLURP-2 is denoted by an asterisk. (C). SDS-PAGE analysis of the refolded SLURP-2 after purification by HPLC. (D). Mass-spectrum of the refolded SLURP-2

were seeded in 96-well culture plates at a density of 10^4 cells per well. After adsorption of cells, they were added with SLURP-1 and SLURP-2 samples (the recombinant SLURP-1 sample was prepared according to the protocol described in [19]). All sample dilutions were performed in the culture medium. The cells were incubated with SLURP-1 and SLURP-2 samples for 48 h. Cell proliferation was studied using a WST-1 reagent (water soluble tetrazolium salt 1, Santa Cruz). WST-1 was dissolved in 20 mM HEPES (pH 7.4), and an electron transport reagent, 1-m-PMS (1-methoxy-5-methylphenazinium methyl sulfate, Santa Cruz), was dissolved in deionized water, after which the solutions were mixed and added to plate wells in the amount of 0.5 mM WST-1 and 20 μM 1-m-PMS per well. After 3 h incubation with WST-1, cell viability was evaluated spectrophotometrically by absorbance at 450 nm with alignment of the background at 655 nm (BioRad Spectrophotometer 680, BioRad Laboratories).

Fluorescence microscopy.

To study the morphology of tumor cell nuclei, the Hoechst 33342 dye (Sigma) was used. Necrotic cell death was determined by staining the cells with propidium iodide (Sigma). The cells were treated in the same manner as for the proliferation assay, but after incubation with SLURP-1 and SLURP-2 samples, the cells were stained with 1 μM Hoechst 33342 dye and 0.5 μM propidium iodide, and then the nuclei were analyzed using a Nikon Eclipse TS100-f microscope (Nikon Corp) with a 40x lens.

RESULTS AND DISCUSSION

Bacterial production and refolding of SLURP-2.

Previously, using the example of the weak toxin WTX from *Naja kaouthia* venom [21], ws-Lynx1 modulating the nAChR activity [22], and the human SLURP-1 [19], it was demonstrated that the optimal way for the production of recombinant three-finger containing the fifth disulfide bond in the first loop (*Fig. 1A*) is production in the form of cytoplasmic inclusion bodies, followed by refolding. This approach was also used for the recombinant production of SLURP-2. The yield of the SLURP-2 with reduced disulfide bonds was approximately 40 mg and 15 mg per 1 L of the bacterial culture on rich (TB) and minimal (M9) media, respectively. However, the refolding protocols developed earlier for other three-finger proteins [19, 21, 22] were ineffective for the refolding of SLURP-2.

To optimize conditions for the refolding of SLURP-2, different pH values (7.0–9.0) of the refolding buffer and different concentrations of the reduced (GSH) and oxidized (GSSG) forms of glutathione (4:1 mM, 4:2 mM, 2:2 mM, and 3:0.3 mM) were tested (*Figs. 2A and B*). Under the optimum conditions (see Experimental section), the yield of refolded SLURP-2 and ^{13}C-^{15}N-labeled analog was 4.6 and 3 mg per 1 L of the bacterial culture, respectively. The homogeneity of the refolded SLURP-2 was confirmed by SDS electrophoresis (*Fig. 2C*), HPLC (*Fig. 2A*) and mass spectrometry (*Fig. 2D*). The molecular weight of the recombinant protein was 8146 Da, which, with allowance for the experimental error, was in accordance with the predicted weight of

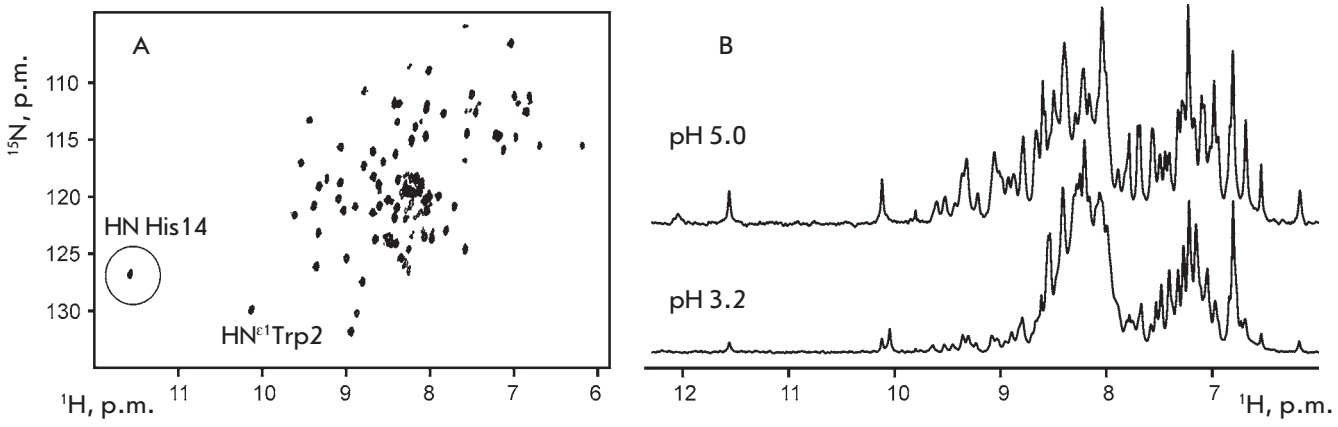

Fig. 3. NMR analysis of recombinant SLURP-2. (A). 2D ^{1}H-^{15}N HSQC spectrum of 0.5 mM ^{13}C-^{15}N-labeled SLURP-2 (30 °C, pH 5.0). (B). Fragments of 1D ^{1}H spectra of unlabeled SLURP-2 at pH 5.0 and 3.2

SLURP-2 (8145 Da) with five closed disulfide bonds and an additional N-terminal methionine residue. The formation of disulfide bonds was also confirmed by the Ellman's reagent.

NMR spectra and modeling of the structure of SLURP-2.

An analysis of the 2D ^{1}H-^{15}N correlation NMR spectrum of recombinant SLURP-2 (*Fig. 3A*) confirmed the homogeneity and purity of the obtained sample. A considerable dispersion of the $^{1}H^{N}$ backbone signals (7 to 9.7 ppm) indicated the presence of β-structural regions in the protein. A single set of signals was observed in the NMR spectra, which indicated a lack of conformational heterogeneity due to *cis-trans* isomerization of Xxx-Pro peptide bonds. In this aspect, the SLURP-2 protein is similar to ws-Lynx1, which has a single structural form in the solution [23], and differs from SLURP-1, which in the solution forms two equally populated structural states due to slow (on the NMR timescale) isomerization of the Tyr39-Pro40 peptide bond [19]. In this regard, it should be noted that, according to the amino acid sequence analysis, SLURP-2 has greater homology with ws-Lynx1 than with the SLURP-1 (32 and 29%, respectively, *Fig. 1A*). Interestingly, human Lynx1 and SLURP-2 proteins are the products of a single gene located on the chromosome 8 that arise during alternative splicing.

The similarity of the SLURP-2 and ws-Lynx1 structures is also indicated by the presence of the characteristic downfield $^{1}H^{N}$ signal at 11.6 ppm (circled, *Fig. 3A*). According to the published spatial ws-Lynx1 structure [23], a significant downfield shift of the $^{1}H^{N}$ Asn15 signal is caused by the formation of a hydrogen bond with a side chain of His4. A similar hydrogen bond in the structure of SLURP-2 can be formed between the side chain of His4 and the backbone amide group of His14. A reduction in the pH value of the SLURP-2 sample from 5 to 3 resulted in a significant decrease in the signal intensity in the downfield region (8.7–9.7 ppm) of the ^{1}H NMR spectrum with a simultaneous increase in the signal intensity around 8 ppm (*Fig. 3B*). This indicated partial disruption of the spatial structure of the protein, accompanied by transitions of individual fragments from the β-structural conformation to the random coil conformation. Similar pH-induced denaturation was previously observed for ws-Lynx1 but not for SLURP-1 (Shenkarev et al., unpublished data).

Taking into account this indirect evidence of the spatial structure similarity, a model of SLURP-2 was built (*Fig. 1B*) based on the known structure of the ws-Lynx1 protein. The resulting model shows the typical three-finger fold with β-structural core enclosing two antiparallel β-sheets formed by five β-strands.

Effects of SLURP-1 and SLURP-2 on the HT-29 cells

Incubation of colorectal adenocarcinoma HT-29 cells with the SLURP-1 and SLURP-2 at a concentration of 1 μM for 48 h resulted in a significant decrease in the cell number to 54 ± 2% and 63 ± 2% relative to the control, respectively. An analysis of cell nuclei morphology by fluorescence microscopy demonstrated that neither SLURP-1 nor SLURP-2 causes apoptotic or necrotic death of HT-29 cells (*Fig. 4*). For example, a reduction in the cell density was not accompanied by a change in the morphology of most of the cell nuclei compared to the control, and staining of cells with propidium

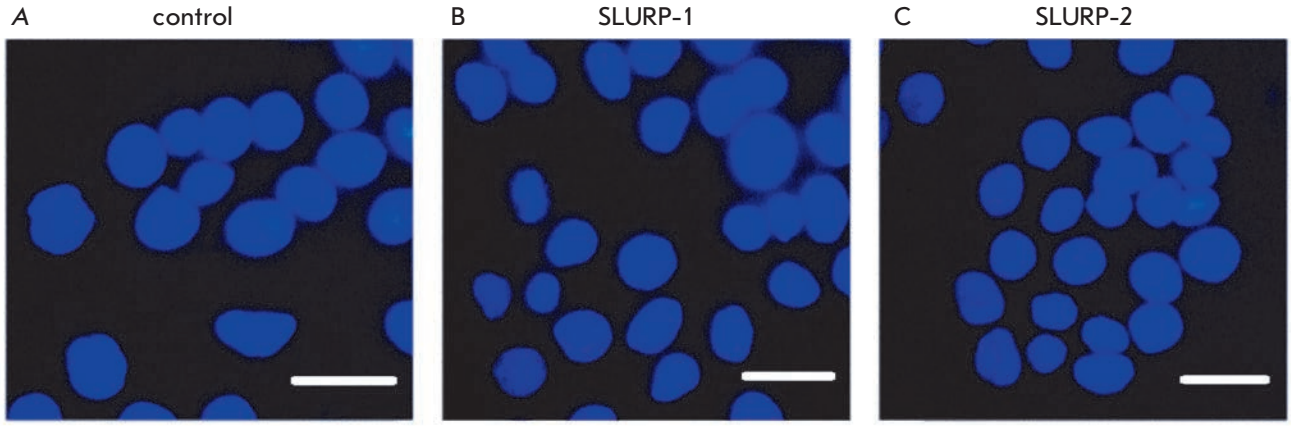

Fig. 4. Effect of SLURP-1 and SLURP-2 on the morphology of colorectal adenocarcinoma HT-29 cell nuclei. (A). Cells without SLURP proteins. (B–C). Cells after 48 h incubation with 1 μM SLURP-1 and 1 μM SLURP-2, respectively. Cell nuclei were stained with Hoechst 33342 and propidium iodide. Bar scale is 10 microns

iodide showed no increase in the fraction of necrotic cells (3 ± 1% in the control and in wells containing 1 μM SLURP-1 and SLURP-2). Therefore, the observed effects of SLURP-1 and SLURP-2 are associated with inhibition of HT-29 cell's proliferation.

A comparative analysis of results of WST-1 test revealed that SLURP-1 and SLURP-2 significantly inhibit the growth of HT-29 tumor cells. An analysis of the dose-effect curve showed that the inhibitory effect of SLURP-1 and SLURP-2 depends on their concentration (*Fig. 5*). The half maximal effective concentration (EC_{50}) was ~ 0.1 nM for SLURP-1 and ~ 0.2 nM for SLURP-2. The maximum inhibitory effect was achieved at a protein concentration of about 1 μM (*Fig. 5*).

HT-29 cells were demonstrated to contain mRNAs encoding only α4, α5, α7 and β1 subunits of the nAChR [18]. Due to the fact that only α7 subunits of this set can form functional receptors [1], the authors suggested that the α7-nAChR is the only nicotinic acetylcholine receptor presented in HT-29 cells [18]. Perhaps, this is the receptor that is involved in the regulation of interleukin-8 release by HT-29 cells exposed to nicotine [18]. Based on these data, we may assume that α7-nAChR is the target of SLURP-1 and SLURP-2 proteins in HT-29 cells.

Previously, based on experiments on the competition between ^{3}H-nicotine and ^{3}H-epibatidine in Het1A keratinocytes, which, contrary to HT-29 cells, express different types of nAChR [24], it was suggested that the target of SLURP-1 is α7-nAChR and that SLURP-2 affects primarily α3β2-nAChR [6, 11]. In this case, SLURP-1 reduced the proliferation of keratinocytes [11], while SLURP-2, instead, increased it [6]. Therefore, it may be assumed that the inhibitory effect of SLURP-1 and SLURP-2 observed on Het1A and HT-29 cells is mediated by the interaction with α7-nAChR. In this case, the activating effect of SLURP-2 observed on keratinocytes could be due to the interaction with α3β2-nAChR. The lower antiproliferative activity of SLURP-2 compared to that of SLURP-1 on HT-29 cells is probably associated with lower affinity of this protein to the α7-nAChR.

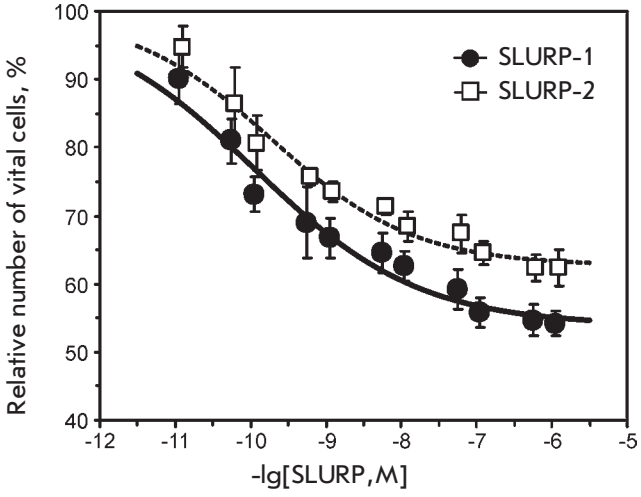

Fig. 5. Effect of SLURP-1 and SLURP-2 on the growth of colorectal adenocarcinoma HT-29 cells as determined by the WST-1 test. Each point is the mean ± S.E. of 3 independent experiments. Dose-effect curves of SLURP-1 and SLURP-2 (the percentage ratio of viable cells to the control) were fitted to the Hill equation ($y=A1+(100\%-A1)/(1+([SLURP]/EC_{50})^{nH})$). The calculated parameters EC_{50}, nH, and A1 were 0.11 ± 0.05 nM, 0.4 ± 0.1, and 54 ± 2%, respectively, for SLURP-1, and 0.19 ± 0.07 nM, 0.5 ± 0.1, and 63 ± 2%, respectively, for SLURP-2

CONCLUSIONS

In this study, an efficient system for the production of the human SLURP-2 was developed for the first time and milligram quantities of the recombinant protein and its ^{13}C-^{15}N-labeled analogue were obtained. Recombinant SLURP-2 differs from the wild type protein by the presence of an additional N-terminal Met residue. The development of this system opens up new opportunities for structure-function studies of SLURP-2, including by site-directed mutagenesis. The antiproliferative effect of the SLURP-1 and SLURP-2 on the human colorectal adenocarcinoma HT-29 cell line has been described for the first time, and this effect is assumed to be mediated by the interaction with α7-nAChR. These findings provide a fresh look at the role of the nicotinic acetylcholine receptor and its distinct subtypes in the regulation of epithelial cell growth. ●

The development of the system for recombinant SLURP-2 production, the production of recombinant SLURP-2, and the structural and functional studies of SLURP-2 were performed with the financial support of the Russian Science Foundation (agreement #14-14-00255). The production of recombinant SLURP-1 and its functional studies were performed with the support of the Russian Academy of Sciences ("Molecular and Cell Biology" program) and the Russian Foundation for Basic Research (grant #12-04-01639).

REFERENCES

1. Papke R.L. // Biochem. Pharmacol. 2014. V. 89. № 1. P. 1–11.
2. Sharma G., Vijayaraghavan S. // J. Neurobiol. 2002. V. 53. № 4. P. 524–534.
3. Miwa J.M., Ibanez-Tallon I., Crabtree G.W., Sánchez R., Sali A., Role L.W., Heintz N. // Neuron. 1999. V. 23. № 1. P. 105–114.
4. Tekinay A.B., Nong Y., Miwa J.M., Lieberam I., Ibanez-Tallon I., Greengard P., Heintz N. // Proc. Natl. Acad. Sci. USA. 2009. V. 106. P. 4477–4482.
5. Chimienti F., Hogg R.C., Plantard L., Lehmann C., Brakch N., Fischer J., Huber M., Bertrand D., Hohl D. // Hum. Mol. Genet. 2003. V. 12. P. 3017–3024.
6. Arredondo J., Chernyavsky A.I., Jolkovsky D.L., Webber R.J., Grando S.A. // J. Cell. Physiol. 2006. V. 208. P. 238–245.
7. Darvas M., Morsch M., Racz I., Ahmadi S., Swandulla D., Zimmer A. // Eur. Neuropsychopharmacol. 2009. V. 19. P. 670–681.
8. Tsetlin V., Utkin Y., Kasheverov I. // Biochem. Pharmacol. 2009. V. 78. P. 720–731.
9. Moriwaki Y., Watanabe Y., Shinagawa T., Kai M., Miyazawa M., Okuda T., Kawashima K., Yabashi A., Waguri S., Misawa H. // Neurosci. Res. 2009. V. 64. P. 403–412.
10. Moriwaki Y., Yoshikawa K., Fukuda H., Fujii Y.X., Misawa H., Kawashima K. // Life Sci. 2007. V. 80. P. 2365–2368.
11. Arredondo J., Chernyavsky A.I., Webber R.J., Grando S.A. // J. Invest. Dermatol. 2005. V. 125. P. 1236–1241.
12. Chernyavsky A.I., Galitovskiy V., Shchepotin I.B., Grando S.A. // Biomed. Res. Int. 2014. V. 2014. P. 609086.
13. Chernyavsky A.I., Kalantari-Dehaghi M., Phillips C., Marchenko S., Grando S.A. // Wound Repair Regen. 2012. V. 20. № 1. P. 103–113.
14. Arredondo J., Chernyavsky A.I., Grando S.A. // Life Sci. 2007. V. 80. P. 2243–2247.
15. Arredondo J., Chernyavsky A.I., Grando S.A. // Biochem. Pharmacol. 2007. V. 74. № 8. P. 1315–1319.
16. Chernyavsky A.I., Marchenko S., Phillips C., Grando S.A. // Dermatoendocrinol. 2012. V. 4. № 3. P. 324–330.
17. Pettersson A., Nylund G., Khorram-Manesh A., Nordgren S., Delbro D.S. // Auton. Neurosci. 2009. V. 148. P. 97–100.
18. Summers A.E., Whelan C.J., Parsons M.E. // Life Sci. 2003. V. 72. № 18–19 P. 2091–2094.
19. Shulepko M.A., Lyukmanova E.N., Paramonov A.S., Lobas A.A., Shenkarev Z.O., Kasheverov I.E., Dolgikh D.A., Tsetlin V.I., Arseniev A.S., Kirpichnikov M.P. // Biochemistry (Mosc). 2013. V. 78. P. 204–211.
20. Webb B., Sali A. // Current Protocols in Bioinformatics. 2014. V. 47 №:5.6 P. 1–32.
21. Lyukmanova E.N., Shulepko M.A., Tikhonov R.V., Shenkarev Z.O., Paramonov A.S., Wulfson A.N., Kasheverov I.E., Ustich T.L., Utkin Y.N., Arseniev A.S., et al. // Biochemistry (Mosc). 2009. V. 74. P. 1142–1149.
22. Shulepko M.A., Lyukmanova E N., Kasheverov I.E., Dolgikh D.A., Tsetlin V.I., Kirpichnikov M.P. // Russian J. Bioorg. Chem. 2011. V. 37. P. 43–549.
23. Lyukmanova E.N., Shenkarev Z.O., Shulepko M.A., Mineev K.S., D'Hoedt D., Kasheverov I.E., Filkin S., Janickova H., Dolezal V., Dolgikh D.A., et al. // J. Biol.Chem. 2011. V. 286. P. 1061–810627.
24. Grando S.A. // J. Investig. Dermatol. Symp. Proc. 1997. V. 2. № 1. P. 41–48.

Investigation of Channel-Forming Activity of Polyene Macrolide Antibiotics in Planar Lipid Bilayers in the Presence of Dipole Modifiers

S. S. Efimova*, L. V. Schagina, O. S. Ostroumova
Institute of Cytology, Russian Academy of Sciences, Tikhoretsky Ave., 4, St. Petersburg, 194064, Russia
*E-mail: ssefimova@mail.ru
Received 29.04.2014

ABSTRACT **The role of membrane components, sterols, phospholipids and sphingolipids in the formation and functioning of ion-permeable nanopores formed by antifungal macrolide antibiotics, amphotericin B, nystatin and filipin in planar lipid bilayers was studied. Dipole modifiers, flavonoids and styryl dyes, were used as a tool to study the molecular mechanisms of polyene channel-forming activity. The introduction of dipole modifiers into the membrane bathing solutions was shown to change the conductance of single channels and the steady-state transmembrane current induced by polyene antibiotics in the sterol-containing phospholipid-bilayers. The conductance of single amphotericin B channels was found to depend on the dipole potential of the membrane. The experiments with various phospholipids, sterols, and polyenes led to the assumption that the shape of a phospholipid molecule, the presence of double bonds at the positions 7 and 22 of a sterol molecule, the number of conjugated double bonds, and the presence of an amino sugar in the polyene antibiotic molecule are important factors impacting the stability of polyene-lipid complexes forming ion-permeable pores. Experimental and literature data presented in the paper suggest that the channel-forming activity of polyene antibiotics is also affected by the physicochemical properties of polyene-enriched ordered membrane domains.**
KEYWORDS **planar lipid bilayers, polyene antibiotics, sterols, styryl dyes, sphingolipids, flavonoids, phospholipids.**
ABBREVIATIONS **AMB – amphotericin B; NYS – nystatin; FIL – filipin; DPhPC – 1,2-diphytanoyl-*sn*-glycero-3-phosphocholine; DPhPS – 1,2-diphytanoyl-*sn*-glycero-3-phospho-L-serine; DOPC – 1,2-dioleoyl-*sn*-glycero-3-phosphocholine; POPC – 1-palmitoyl-2-oleoyl-*sn*-glycero-3-phosphocholine; DOPS – 1,2-dioleoyl-*sn*-glycero-3-phospho-L-serine; DOPE – 1,2-dioleoyl-*sn*-glycero-3-phosphoethanolamine; Rh-DPPE – 1,2-dipalmitoyl-*sn*-glycero-3-phosphoethanolamine-N-(lissamine rhodamine); Chol – cholesterol, Erg – ergosterol; DhChol – 7- dehydrocholesterol; Stigm – stigmasterol; PhSG – N-stearoyl-phytosphingosine (*Saccharomyces cerevisiae*); SM – porcine brain sphingomyelin; SG – N-stearoyl-D-erythro-sphinganine.**

INTRODUCTION

Polyene macrolide antibiotics are among the most effective drugs against fungal infections and deep systemic mycoses. They have been widely used in clinical medicine for many decades. Polyene macrolides also attract attention due to their anti-tumor and antiviral activity [1–3]. In spite of side effects, such as nephrotoxicity, anemia, and cardiac arrhythmia [4, 5], polyene macrolide remains the drug of choice for treatment of immunosuppressed patients [6, 7]. Pharmaceutical technologies develop innovative formulations that aim at reducing the concentration of free AMB in patients' serum without compromising its therapeutic efficacy.

The main representatives of non-aromatic polyene macrolide antibiotics are amphotericin B (AMB) [8], nystatin (NYS) [9, 10], and filipin (FIL) [11]. The lactone ring of amphotericin B contains 38 carbon atoms (*Fig. 1*). Hydrophilic and heptaenic chains in the AMB macrolactone ring include C_1–C_{15} and C_{20}–C_{33} carbon atoms, respectively. These chains are arranged parallel to each other. The C_{20}–C_{33} heptaenic chain is a rigid system consisting of seven double bonds. The hydrophilic chain of AMB contains hydroxyl and carbonyl groups. The hydroxyl groups in the hydrophilic region of the molecule are arranged in one plane. A carboxyl group and a mycosamine residue are located at positions 6 and 19,

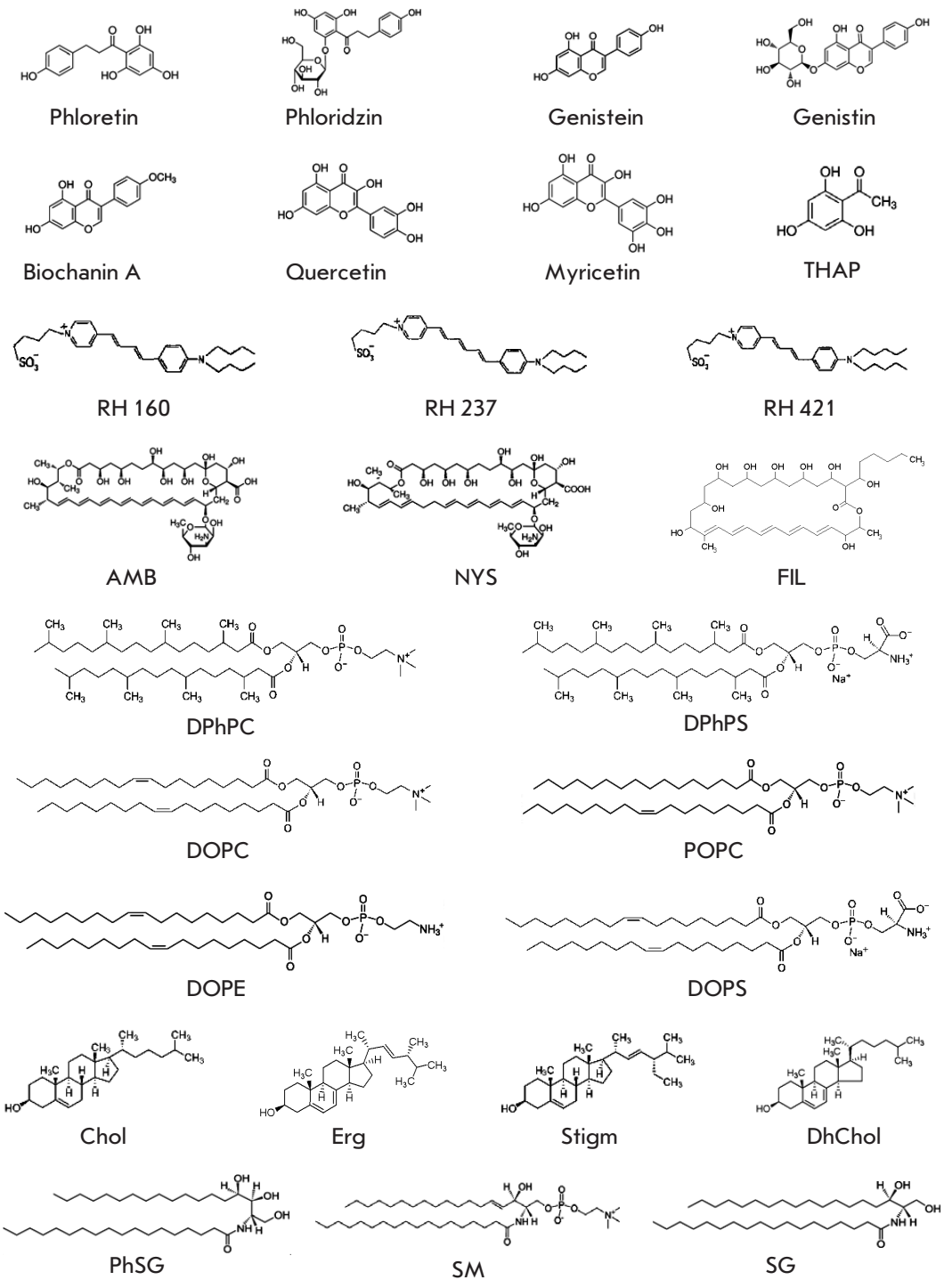

Fig. 1. Chemical structures of flavonoids (phloretin, phloridzin, genistein, genistin, biochanin A, quercetin, myricetin and THAP), styryl dyes (RH 160, RH 237 and RH 421), polyenes (AMB, NYS and FIL), phospholipids (DPhPC, DPhPS, DOPC, POPC, DOPE and DOPS), sterols (Chol, Erg, DhChol and Stigm) and sphingolipids (PhSG, SM and SG)

respectively. Another hydroxyl group is located in the hydrophobic portion of the molecule at position 35. The chemical structure of nystatin, a tetraene, is similar to that of AMB. Nystatin differs from AMB in the positions of hydroxyl groups in the hydrophilic chain and discontinuity of the conjugated double bond system. A saturated bond divides the chromophore into the diene and tetraene portions. Filipin belongs to methylpentaens and has a smaller polyene fragment and no amino sugar residue as compared to AMB and NYS [12].

It is widely accepted that polyene antibiotics bind to the plasma membranes of the target cells, participate in formation of transmembrane pores and disrupt the water-electrolyte balance in cells, leading to cell death. The

presence of sterols in the target cell membranes is a prerequisite for pore formation [8, 13, 14]. Despite 40 years of research into the molecular mechanisms of formation and functioning of the AMB channel, its precise molecular architecture is still under debate. Various models of AMB channels have been proposed. The most popular one is the sterol-dependent model, where the channel, in case of a two-sided (in respect to the membrane) addition of the antibiotic, is formed via association of two "half-pores" formed by polyene-sterol complexes located in opposite monolayers [8, 13, 15]. The cylindrical half-pore is formed by the same number (7 to 10) of antibiotic and sterol molecules, which are oriented perpendicular to the membrane plane. The cavity of the pores is lined with hydrophilic chains of lactone rings. A transmembrane pore is formed via hydrogen bonds between the hydroxyl groups of AMB molecules that are present in the interacting half-pores [12].

The sterol-dependent membrane activity of amphotericin B indicates that the therapeutic efficacy of AMB is primarily related to its differential preference for various sterols in cell membranes. It is well known that cholesterol (Chol) is the major membrane sterol in mammalian cells, whereas ergosterol (Erg) is the major sterol in fungi. It is still unclear whether the specificity of interaction of various polyenes with cell membranes is due to better stability of the AMB–Erg complex as compared to the AMB–Chol one or if the observed effects are mediated by different impacts of these sterols on structural and dynamic properties of membranes [16, 17].

The data reported by Neumann *et al.* [18, 19] support the first hypothesis. The more rigid and extended molecular shape of Erg, compared to Chol, facilitates Erg interaction with AMB. Since van der Waals interactions between rod-shaped molecules depend on their relative orientation and reach the maximum when two molecules lie in one plane and are parallel to each other, the π-π-electron interaction between a double bond in Erg side chain and AMB polyene chromophore may be an additional site required for stabilizing the proper orientation of the complex (*Fig. 2 A, B*) [20]. In case of Chol, not only is the energy of the complex formation higher (no double bond in the side chain of the sterol molecule), but in addition there is a need to compensate for entropic losses associated with a decrease in conformational flexibility of the sterol side chain. The results of the studies of mobility of AMB and sterols molecules in phospholipid bilayers by ^{2}H NMR conducted by Matsumori et al. [21] confirmed the hypothesis of stronger intermolecular interaction between AMB and Erg compared to Chol.

Sterols are responsible for membrane fluidity and are predominantly located in the more ordered membrane domains, lipid rafts, which may be considered as an argument in favor of the second hypothesis. It has been shown that AMB has higher affinity for sterol-containing ordered phase and hence it can, like sterols, be accumulated in lipid rafts [17, 22]. Several studies indicate that the presence of AMB increases orderding of Chol-containing membranes and that no such effect is observed in case of Erg-containing membranes [17, 23, 24].

Czub and Baginski [17] demonstrated that the negatively charged carboxyl group (COO^-) in AMB molecule is shifted towards the aqueous phase compared with the protonated amine group (NH_3^+). The authors suggested that the dipole of the polar head of AMB ($COO^- \rightarrow NH_3^+$) tends to be oriented parallel to the dipoles of phosphatidylcholine polar heads, thus increasing the dipole potential of the membrane. This jump in the potential occurs at the bilayer–solution interface as a result of specific mutual orientation of the lipid membrane dipoles and the adjacent water dipoles [25–27] and plays an essential role in regulation of transport across the membrane.

As mentioned before, polyene macrolide antibiotics exhibit their antifungal effect by binding to membrane sterols, but little information is available on the role of other membrane components, in particular, phospholipids and sphingolipids. There is some evidence to suggest that phospholipids affect the activity of polyene antifungals. According to the published data, polyene antibiotics can form transmembrane pores in the bilayer even in the absence of sterols [28–32]. Fujii et al. [33] have shown that AMB can specifically interact with phospholipid molecules. In the ^{2}H NMR studies of liposomes made of dimyristoyl-phosphatidylcholine with AMB, Dufourc *et al.* [34] have noted the improved ordering of acyl chains of this lipid molecule in its interaction with AMB. Furthermore, based on the analysis of circular dichroism spectra of AMB in liposomes in the absence of sterol, Balakrishnan and Easwaran [35] have suggested the presence of a multi-molecular organized structure in the bilayer, in which AMB interacts with acyl chains of the dipalmitoyl-phosphatidylcholine molecule at a 1:1 ratio. The differential scanning calorimetry studies by Fournier *et al.* [36] showed that AMB induces phase separation in the membrane; namely, that three phases of dipalmitoyl-phosphatidylcholine liposomes are simultaneously detected in the presence of AMB. The first phase corresponds to pure phospholipid, the second and the third phases are characterized by phase transition in a wide range of temperatures above the phase transition point of pure phospholipid. Furthermore, Paquet *et al.* [23] demonstrated a dose-dependent increase in the lipid phase transition point from gel to the liquid crystal state in

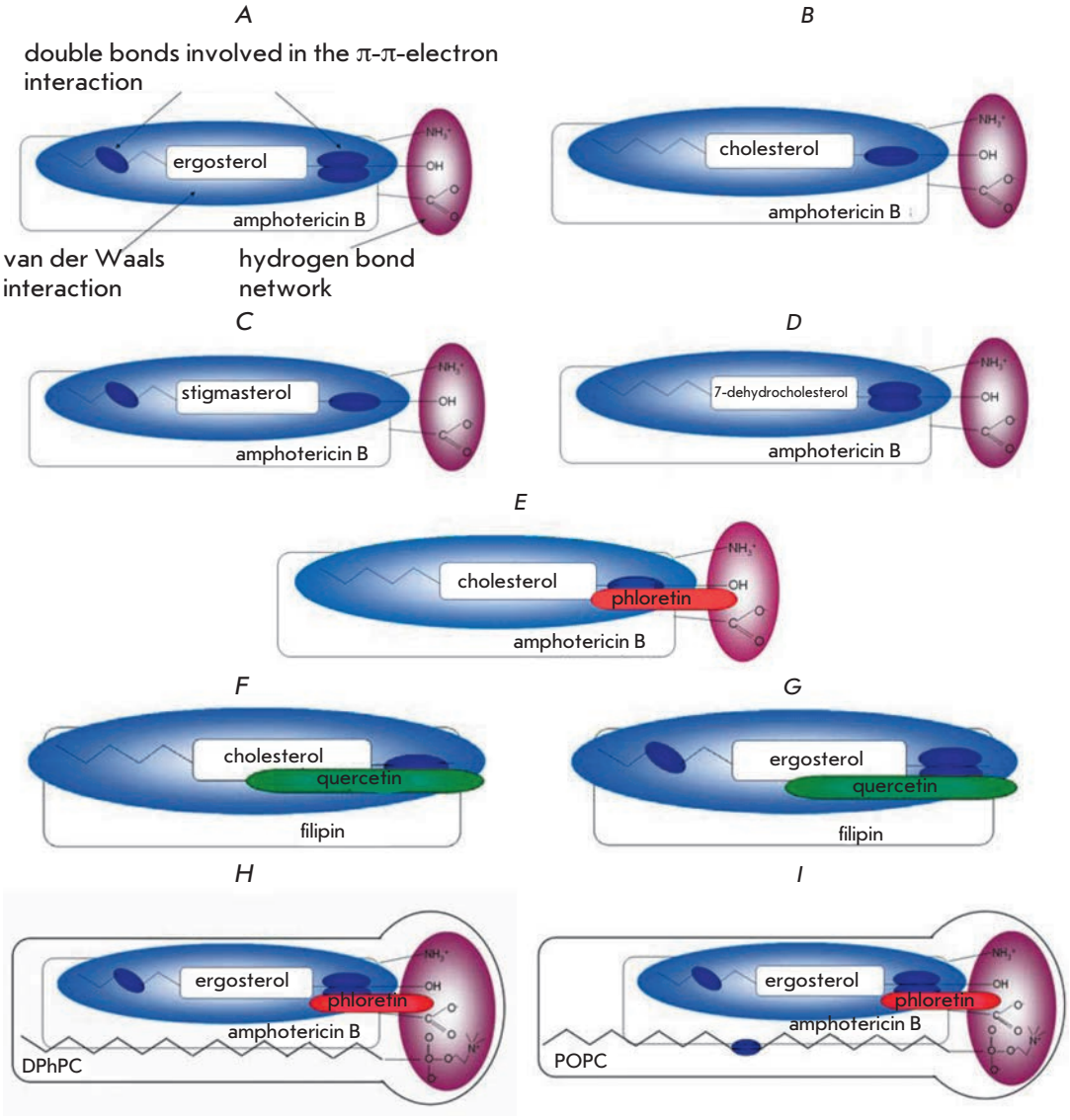

Fig. 2. Schematic representation of intermolecular bonds in the complexes of AMB-Erg (*A*), AMB-Chol (*B*), AMB-Stigm (*C*), AMB-DhChol (*D*), AMB-Chol with phloretin (*E*), FIL-Chol with quercetin (*F*), the FIL-Erg with quercetin (*G*), AMB-Erg-DPhPC with phloretin (*H*) and AMB-Erg-POPC with phloretin (*I*). AMB-Chol and AMB-Erg complexes as shown in [20] with some changes

the presence of AMB. Milhaud *et al.* [37] suggested that AMB interacts with multi-molecular phospholipid ensembles. The results obtained by Sternal *et al.* [38] using the molecular dynamics methods do not contradict the hypothesis of interaction between polar heads of AMB and dimyristoyl-phosphatidylcholine. Such interaction was observed, in particular, between the carboxyl group of AMB and the amino group of a lipid. Herec *et al.* [39] suggested that hydrogen bonds between the horizontally oriented AMB molecules and polar groups of a lipid lead to condensation of the bilayer.

We have found only indirect evidence of possible interactions between polyene macrolides and membrane sphingolipids. For example, Zager [40] showed that polyene antibiotics affect the concentration of phospholipids and ceramides in the plasma membrane. Nagiec *et al.* [41] found that a mutant strain of *Saccharomyces cerevisiae*, capable of growth without producing sphingolipids, is more susceptible to AMB than wild-type cells. Studies of the effect of the sphingolipid composition of a membrane on the activity of polyene macrolides are also interesting because sphingolipids, as well as sterols and polyenes, are located in lipid rafts [17].

The aim of the present work was to determine the molecular mechanisms of the formation of polyene transmembrane pores in membranes containing various phospholipids, sterols, and sphingolipids. Dipole modifiers, namely flavonoids and styryl dyes, which are capable of altering the dipole potential of membranes, were used as a research tool. The choice of dipole modifiers was based on their successful application in the studies focused on formation and functioning of ion channels in model and cell membranes [42–51].

MATERIALS AND METHODS

Materials

The following reagents were used: KCl, HEPES, pentane, ethanol, chloroform, dimethyl sulfoxide (DMSO), hexadecane and squalene, phloretin, phloridzin, genistin, genistein, quercetin, myricetin, biochanin A, 2 ', 4', 6'-trihydroxyacetophenone monohydrate (THAP), RH 421, amphotericin B (AMB), nystatin (NYS) and filipin (FIL) (Sigma, USA); RH 160 and RH 237 (Molecular Probes, USA); 1,2-diphytanoyl-*sn*-glycero-3-phosphocholine (DPhPC), 1,2-diphytanoyl-*sn*-glycero-3-phospho-L-serine (DPhPS), 1,2-dioleoyl-*sn*-glycero-3-phosphocholine (DOPC) 1-palmitoyl-2-oleoyl-*sn*-glycero-3-phosphocholine (POPC), 1,2-dioleoyl-*sn*-glycero-3-phospho-L-serine (DOPS), 1,2-dioleoyl-*sn*-glycero-3-phosphoethanolamine (DOPE), cholesterol (Chol), ergosterol (Erg), 7-dehydrocholesterol (DhChol), stigmasterol (Stigm), N-stearoyl-phytosphingosine from *S. cerevisiae* (PhSG), porcine brain sphingomyelin (SM), a synthetic sphingolipid N-stearoyl-D-*erythro*-sphinganine (SG) and 1,2-dipalmitoyl-*sn*-glycero-3-phosphoethanolamine-N-(lissamine rhodamine) (Rh-DPPE) (Avanti Polar Lipids, USA). Chemical structures of flavonoids, styryl dyes, polyenes, phospholipids, sterols and sphingolipids are shown in *Fig. 1*.

Measurement of currents flowing through the planar lipid bilayers

The bilayer lipid membranes were formed using the Montal and Mueller method [52] by combining the condensed lipid monolayers on the aperture in a Teflon film dividing the experimental chamber into two (*cis*- and *trans*-) compartments. The volume of each compartment was 1.5 ml, the thickness of the Teflon film was 10 μm, and the aperture diameter was ~ 50 μm. Before the membrane formation process was started, the aperture in the Teflon film had been pretreated with hexadecane. Monolayers were formed on the air–water interface of the solution of 1 mg/ml lipid in pentane. The phospholipid:sterol and phospholipid:ergosterol:sphingolipid mixtures were used to form monolayers (the molar ratios were 67:33 mol % and 53:27:20 mol %, respectively). The channel-forming activity of polyenes was measured under the same ionic composition of aqueous electrolyte solution (2.0 M KCl). The acidity of the solution (pH 7.0) was maintained with a 5 mM HEPES-KOH buffer mixture.

Polyene antibiotics were added to the aqueous phase in both compartments: AMB and NYS as DMSO solution (10^{-4} to 10^{-3} M, respectively), and FIL as ethanol solution (10^{-4} M) to a final concentration of 10^{-8}–10^{-6} M in the membrane bathing solution. The two-side administration of polyene antibiotics was chosen, because according to [8, 13, 15] the channels are formed by two associated half-pores. The final concentration of ethanol or DMSO in the chamber did not exceed 0.1% and did not cause any changes in the consistency of the membrane conductance.

Flavonoids phloretin, phloridzin, genistin, genistein, quercetin, myricetin, biochanin A and THAP were added in both compartments of the chamber as millimolar solutions in ethanol or DMSO to a final concentration of 20 μM in the membrane bathing solutions; and styryl dyes RH 160, RH 237, and RH 421, to a concentration of 5 μM.

The current flowing through the lipid bilayer membrane was measured in voltage clamp mode. Ag/AgCl electrodes with 1.5% agarose/2 M KCl bridges were used to apply the transmembrane voltage (V) and measure the transmembrane current. Positive voltage refers to the potential initiating flow of cations from the *cis*-compartment to the *trans*- one. Electrophysiological measurements were performed at room temperature.

Transmembrane currents were measured and digitized in a voltage clamp mode using Axopatch 200V and Digidata 1440A systems (Axon Instruments, USA). The data were processed using an 8-pole Bessel filter (Model 9002, Frequency Devices) and filtering frequency of 1 kHz. The data were processed using the Clampfit 9.0 software package (Axon Instruments, USA). Statistical analysis of the data was performed using Origin 8.0 software (OriginLab, USA).

The average ratio (I_∞/I_∞^0) of the steady-state integral transmembrane current, induced by a channel-forming agent (AMB, NYS and FIL) in the presence (I_∞) and in the absence (I_∞^0) of dipole modifiers, was defined as the arithmetic mean of I_∞/I_∞^0 measured in three to nine bilayers (mean ± SE). The steady-state number of channels operating in the membrane was defined as a ratio between the steady-state transmembrane current (I_∞^0) and the current flowing through a single channel (i).

Single-channel conductance (g) was defined as the ratio between the current flowing through a single channel (i) and the transmembrane potential difference (V). To construct histograms of current fluctuations, the transmembrane current values were determined by changes in the amplitude of currents at opening (or closing) of single channels. The total number of events (N) used for the analysis at a fixed value of the transmembrane potential ranged from 100 to 5000. Relative frequencies of the transmembrane current values are plotted along the Y axis . All peaks in the histograms were approximated using the normal density distribution. The distribution hypothesis was verified using $\chi 2$ ($P<0.05$).

Measurements of channel selectivity

To measure the cation-anion selectivity of the channel, a 10-fold concentration gradient of KCl electrolyte has been created in the membrane. The selectivity of AMB channels was measured at solution concentrations of 0.2 and 2.0 M KCl in the *cis*- and *trans*-compartments of the experimental chamber, respectively. The anion transference number (t^-) ($t^- + t^+ = 1$) was calculated using the Henderson equation [53]:

$$V^{rev} = (RT/F)(1-2t^-)\ln(C_{cis}/C_{trans}), \quad (1)$$

where V^{rev} is the reversal potential corresponding to zero transmembrane current at a given ratio between concentrations of ions penetrating from the *cis*- and *trans*-sides of the membrane (C_{cis}/C_{trans}); R is the universal gas constant (R = 8.31 J/(mol K)); T is thermodynamic temperature (T = 294 K); and F is the Faraday constant (F = 96485 C/mol).

Confocal microscopy of giant unilamellar vesicles

Giant unilamellar vesicles were produced by electroformation using Nanion Vesicle Prep Pro workstation (Germany) (standard protocol, 3 V, 10 Hz, 1 h, 25°C). The lateral phase separation was visualized by introducing a fluorescent Rh-DPPE probe into the source lipid solution of POPC in chloroform (11 mM). Rh-DPPE concentration in the sample was 1 mol %. The resulting liposome suspension was divided into aliquots. An aliquot without AMB was used a control. The experimental samples contained 100 or 300 μM of AMB. Vesicles were observed through immersion lenses 100.0×/1.4 HCX PL on an Apo Leica TCS SP5 confocal laser system (Leica Microsystems, Germany). The preparations were studied at 25°C. Rh-DPPE was excited by 543 nm light (He-Ne laser). It is known that Rh-DPPE in a bilayer with phase separation is preferably incorporated into the disordered liquid phase [54], while the ordered liquid and solid (gel) phases remain unstained [55]. At least four independent experiments have been performed for each system.

RESULTS AND DISCUSSION

The influence of dipole modifiers on conductance of single amphotericin channels

Figure 3 shows the examples of fluctuations in transmembrane current flowing through the single AMB channels in DPhPC:Chol membranes (*Fig. 3, left column)* and DPhPC:Erg bilayers (*Fig. 3, right column*), before and after the addition of dipole modifiers, flavonoids (phloretin and quercetin) and styryl dyes (RH 160, RH 237 and RH 421). *Figure 3 A, B* shows that the current flowing through single AMB channels in the absence of dipole modifiers does not depend on sterol type (Chol or Erg) in the membrane. The addition of phloretin to the membrane bathing solutions reduces the transmembrane current through single AMB channels, both in DPhPC:Chol membranes and in DPhPC:Erg bilayers (*Fig. 3 C, D*). However, the addition of

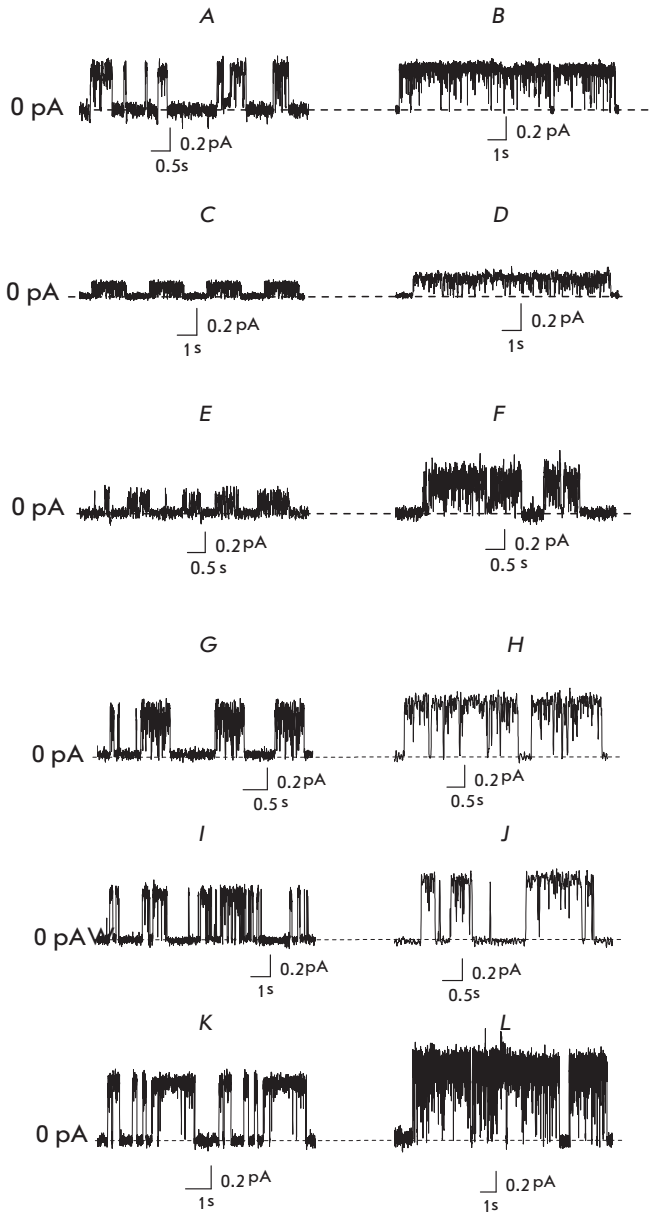

Fig. 3. Fluctuations of transmembrane current through the single AMB channels in the lipid bilayers. Membranes were made from DPhPC:Chol (67:33 mol %) and DPhPC:Erg (67:33 mol %) and bathed in 2.0 M KCl (pH 7.0). *A*, *B* – control (no dipole modifiers). Membrane bathing solution contains (μM): 20 phloretin (*C*, *D*), 20 quercetin (*E*, *F*), 5 RH 160 (*G*, *H*), 5 RH 237 (*I*, *J*), 5 RH 421 (*K*, *L*). Dashed lines correspond to 0 pA. V = 50 mV

Table 1. Ratios between the conductances of single amphotericin channels in the absence and in the presence of various dipole modifiers at V = 50 mV ($g/g_{V=50}$). Membranes were made from DPhPC:Chol (67:33 mol %) and DPhPC: Erg (67:33 mol %) and bathed in 2.0 M KCl (pH 7.0)

Dipole modifier		Membrane-forming solution	
		DPhPC:Chol	DPhPC:Erg
Flavonoid	Phloretin	3.30 ± 0.21	2.20 ± 0.41
	Phloridzin	1.00 ± 0.10	1.00 ± 0.10
	Quercetin	1.72 ± 0.21	0.95 ± 0.15
	Genistein	0.98 ± 0.09	–
	Genistin	0.96 ± 0.08	–
	Biochanin A	0.89 ± 0.11	–
	THAP	0.91 ± 0.15	–
Styryl dyes	RH 421	0.69 ± 0.07	0.49 ± 0.06
	RH 237	0.71 ± 0.08	0.61 ± 0.05
	RH 160	0.80 ± 0.09	0.63 ± 0.06

Table 2. Changes in the dipole potential ($\Delta\varphi_d$, mV) of DPhPC:Chol (67:33 mol %)* or DPhPC:Erg (67:33 mol %)* membranes in the presence of different dipole modifiers

Dipole modifier		Membrane-forming solution	
		DPhPC:Chol	DPhPC:Erg
Flavonoid, 20 μM	Phloretin	-75 ± 10	-150 ± 5
	Phloridzin	-45 ± 10	-50 ± 10
	Quercetin	-110 ± 10	-105 ± 15
	Genistein	-35 ± 5	-40 ± 10
	Genistin	-30 ± 5	–
	Biochanin A	-75 ± 15	-80 ± 15
	THAP	-40 ± 10	-40 ± 10
Styryl dyes, 5μM	RH 421	50 ± 8	57 ± 9
	RH 237	75 ± 10	85 ± 5
	RH 160	55 ± 10	45 ± 5

* Results are taken from [69].

quercetin reduces the transmembrane current through AMB channels only in DPhPC:Chol membranes but does not affect the transmembrane current through AMB channels in DPhPC:Erg membranes (*Fig. 3 E, F*). The introduction of styryl dyes of the RH series into the membrane bathing solutions increases the transmembrane current through single AMB channels. The current rises in the series RH 160 < RH 237 < RH 421 both for DPhPC:Chol membranes (*Fig. 3 G, I, K*) and for DPhPC:Erg bilayers (*Fig. 3 H, J, L*).

Table 1 presents the ratios between conductance of single AMB channels in the absence and in the presence of dipole modifiers at the transmembrane potential of 50 mV ($g/g_{V=50}$). The results shown in *Table 1* reveal that phloretin reduces the conductance of single AMB channels in DPhPC:Chol and DPhPC:Erg membranes by a factor of 3 and 2, respectively. However, the addition of quercetin reduces the conductance of single AMB channels by a factor of 1.7 in DPhPC:Chol membranes but basically does not change *g* in the case of DPhPC:Erg bilayers. The introduction of other flavonoids to the membrane bathing solutions, such as phloridzin, biochanin A, THAP, genistin or genistein, do not practically affect the conductance of AMB channels. The addition of styryl dye to the membrane bathing solutions increases *g* in the series RH 160, RH 237 and RH 421 in DPhPC:Chol membranes by factors of 1.3, 1.4 and 1.5 and in DPhPC:Erg bilayers by factors of 1.6, 1.7 and 2.1, respectively.

Table 2 presents changes in the dipole potential of DPhPC:Chol and DPhPC:Erg bilayers in the presence of dipole modifiers in the membrane bathing solutions. For example, phloretin reduces the dipole potential of DPhPC:Chol membranes by 75 ± 10 mV, and that of DPhPC:Erg bilayers by 150 ± 5 mV. The addition of quercetin to the membrane bathing solutions leads to an almost identical reduction in φ_d in Chol- and Erg-containing DPhPC-bilayers by 100 ± 15 mV. The introduction of genistin and THAP into the membrane bathing solutions has little effect on the φ_d of DPhPC:Chol and DPhPC:Erg bilayers. The addition of styryl dyes of the RH series to the membrane bathing solutions increases the dipole potential of the membrane. The ability to increase the dipole potential of sterol-containing membranes increases in the series RH 421 ≈ RH 160 < RH 237. The addition of styryl dye RH 237 to the membrane bathing solutions increases φ_d of sterol-containing bilayers by 80 ± 10 mV, regardless of sterol composition of the membrane. Meanwhile, the presence of RH 421 or RH 160 in the membrane bathing solutions increases the dipole potential of DPhPC:Chol and DPhPC:Erg membranes by 55 ± 10 mV and 50 ± 10 mV, respectively. Comparison of the values in *Tables 1* and *2* suggests a correlation between the changes in the conductance of single AMB channels and the dipole potential of sterol-containing DPhPC-bilayers upon introduction of dipole modifiers. These results suggest that the change in *g* with introduction of phloretin or styryl dyes into the solutions bathing the Chol- and Erg-containing DPhPC-membranes and quercetin into the solutions bathing the DPhPC:Chol bilayer may be associated with a change in the membrane dipole po-

tential. The discrepancies between the changes in the conductance of single AMB channels and dipole potential of sterol-containing DPhPC-bilayers caused by introduction of dipole modifiers suggest that the change in *g* is caused not only by the changes in the membrane dipole potential, but may also result from interaction of dipole modifiers (phloretin, quercetin and/or styryl dyes) with the AMB-Chol and/or AMB-Erg complexes.

Fig. 2 shows schematic representation of intermolecular bonds in the polyene-sterol complexes. It is known that polyene-sterol complexes are formed by van der Waals interactions [19]. The strength of interaction in this case depends on the coplanarity and parallelism of polyene and sterol molecules. The relative orientation of molecules occurs through the formation of hydrogen bonds between the OH group of the sterol molecule and the amino sugar of the polyene molecule. The presence of extra (compared with Chol) double bonds in the steroid core and in the side chain of the Erg molecule leads to the formation of a stable AMB-Erg complex through additional points of π-π-electron interaction compared to AMB-Chol complex [20] (*Fig. 2 A, B*). Therefore, AMB-Erg and AMB-Chol complexes may interact with the dipole modifiers in a different manner.

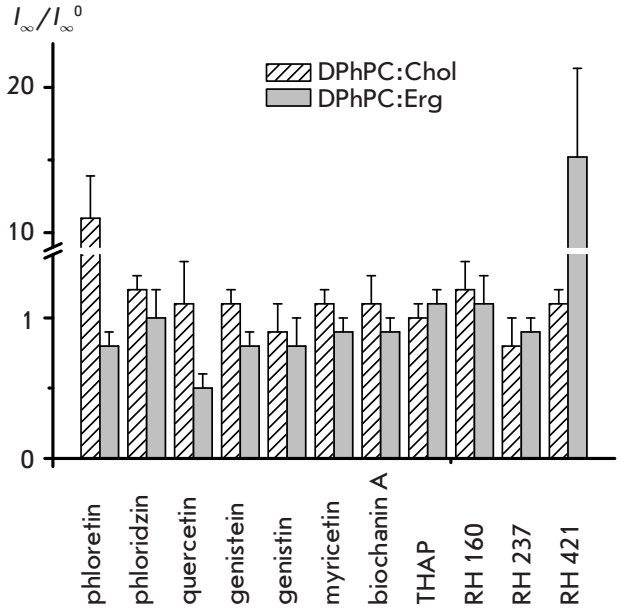

Fig. 4. The ratio between the steady-state transmembrane currents induced by amphotericin B in sterol-containing bilayers before and after the introduction of various dipole modifiers (I_∞/I_∞^0). Membranes were made from DPhPC:Chol (67:33 mol %) or DPPhC:Erg (67:33 mol %) and bathed in 2.0 M KCl (pH 7.0)

INFLUENCE OF DIPOLE MODIFIERS ON MULTICHANNEL MEMBRANE CONDUCTANCE INDUCED BY POLYENE ANTIFUNGALS

Influence of sterol composition

To test the hypothesis about the interaction between dipole modifiers and polyene-sterol complexes, we have studied the effect of dipole modifying agents on the steady-state transmembrane current induced by amphotericin B. The mean ratio between the steady-state transmembrane currents induced by AMB in Chol- and Erg-containing DPhPC bilayers before and after the introduction of various dipole modifiers (I_∞/I_∞^0) at a transmembrane voltage of 50 mV is presented as diagram in *Fig. 4*. The addition of phloretin to the membrane bathing solutions caused a significant increase in the steady-state transmembrane current induced by AMB in DPhPC:Chol bilayers. No such influence of phloretin on I_∞ was observed in case of DPhPC:Erg membranes. The introduction of quercetin to the membrane bathing solutions does not affect I_∞ in DPhPC:Chol membranes and reduces I_∞ in DPhPC:Erg bilayers. Such flavonoids as phloridzin, genistein, genistin, biochanin A, myricetin and THAP do not impact I_∞ in Chol- and Erg-containing DPhPC-membranes. The introduction of RH 421 to the solution bathing DPhPC:Chol bilayers does not practically affect I_∞, and the addition of the modifier to the solution bathing DPhPC:Erg membrane increases I_∞. However, other styryl dyes, such as RH 160 and RH 237, have no effect on the multi-channel activity of AMB in Chol- and Erg-containing DPhPC membranes. It seems likely that in the case of the less energetically favorable AMB-Chol complex, phloretin, due to its "hairpin" conformation, can become a mediator between the polyene and sterol molecules and can stabilize the AMB-Chol complex (*Fig. 2 E*), which is expressed as an increase in AMB channel-forming activity in the presence of this dipole modifier in Chol-containing membranes. Quercetin, due to the greater depth of immersion into the bilayer compared with phloretin [56], can compete with sterols for the interaction with AMB and destabilize the most energetically favorable AMB-Erg complex, which expressed by a reduction of channel-forming activity of polyene (*Fig. 4*). Considering the fact that RH 421 styryl dye is characterized by intermediate chromophore immersion depth in the bilayer compared with RH 160 and RH 237 and has near-normal orientation on the membrane surface [57], we can assume its colocalization with the AMB-Erg complex. In this case, styryl dyes can be regarded as a third party to van der Waals interactions, which acts as an additional orienting factor via its participation in the π-π-electron interactions.

Since the main difference between Erg and Chol molecules is the presence of two double bonds at the posi-

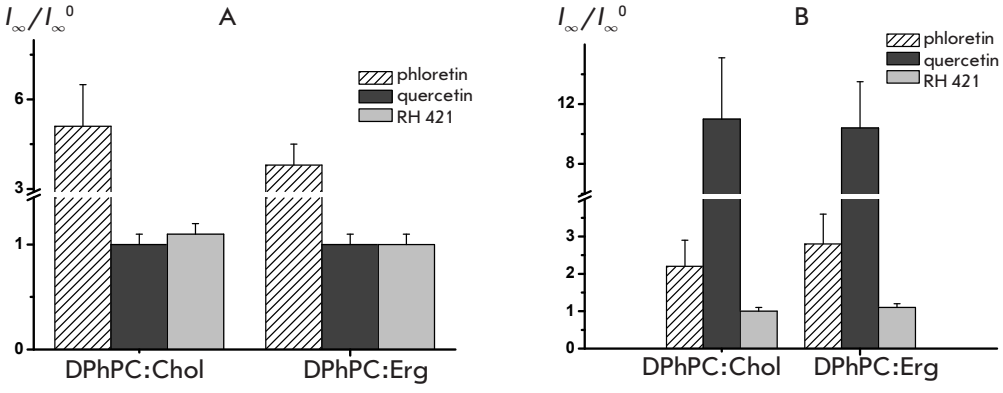

Fig. 5. The ratios between the steady-state transmembrane currents induced by nystatin (*A*) and filipin (*B*) in sterol-containing bilayers before and after the introduction of various dipole modifiers (I_∞/I_∞^0). Membranes were made from DPhPC:Chol (67:33 mol %) or DPPhC:Erg (67:33 mol %) and bathed in 2.0 M KCl (pH 7.0)

tion 7 in the steroid core and at the position 22 in the side hydrocarbon chain, the choice of sterols included those that differ from cholesterol in having one double bond at the position 7 or 22, 7-dehydrocholesterol (DhChol) and stigmasterol (Stigm), respectively (*see Fig. 1*). It has been determined that the addition of phloretin to the membrane bathing solution leads to a greater increase in the steady-state transmembrane current through DPhPC:Stigm membranes ($I_\infty/I_\infty^0 = 5.3 \pm 3.1$), compared with DPhPC:DhChol bilayers ($I_\infty/I_\infty^0 = 1.7 \pm 0.3$). The strength of phloretin effect on AMB-modified DPhPC:Chol and DPhPC:Stigm membranes, as well as its absence in DPhPC:Erg bilayers and its weakness in the case DPhPC:DhChol membranes, indicates similar geometry of AMB-Chol and AMB-Stigm complexes and AMB-Erg and AMB-DhChol complexes, respectively. Schematic representation of intermolecular bonds in AMB-DhChol and AMB-Stigm complexes is shown in *Fig. 2 C, D*. Since the similarity between Chol and Stigm molecules and DhChol and Erg molecules is the absence or presence of a double bond at the position 7, respectively, one can suggest that the decisive role of electrical density distribution in the steroid core area (near the position 7), which can affect the possible formation of a hydrogen bond between the hydroxyl group of the sterol molecule and the OH groups of phloretin. The introduction of RH 421 to the solutions bathing DPhPC:DhChol and DPhPC:Stigm bilayers does not significantly effect on I_∞ ($I_\infty/I_\infty^0 = 1.1 \pm 0.1$). As RH 421 is only effective in case of DPhPC:Erg membranes and does not affect AMB-modified DPhPC:DhChol bilayers, and Erg differs from DhChol in the presence of a double bond at the position 22, the results suggest that RH 421 is a more sensitive tool for studying AMB-sterol complexes than phloretin, and the double bond at position 22 still has an effect on the geometry and energy of the complex.

Influence of the type of polyene antibiotic

Since polyene molecules can also interact with dipole modifiers, their effect on the steady-state transmembrane current induced by nystatin and filipin (*Fig. 1*) has been studied in sterol-containing bilayers. NYS molecule differs from AMB molecule in the absence of a double bond in the middle of the polyene fragment, which may affect π-π-electron interactions in polyene-sterol complexes. FIL molecule, unlike AMB and NYS, does not contain an amino sugar residue. This structural difference should affect the formation of the network of hydrogen bonds between the polyene and sterol molecules. In the case of nystatin, I_∞ increases with addition of phloretin both in DPhPC:Chol and in DPhPC:Erg containing membranes, while introduction of quercetin does not affect I_∞ if the membrane contains either Chol or Erg (*Fig. 5 A*). Both flavonoids (phloretin and quercetin) increase the steady-state equilibrium transmembrane current induced by filipin, regardless of the type of the membrane-forming sterol, by a factor of 2 and 10 for DPhPC:Chol and DPhPC:Erg membranes, respectively (*Fig. 5 B*). However, the addition of RH 421 to the solutions bathing DPhPC:Chol and DPhPC:Erg membranes does not change the steady-state transmembrane current induced by both nystatin and filipin (*Fig. 5 A, B*). Disruption of double bond conjugation in NYS molecule may destabilize the polyene-sterol complex and increase the depth of sterol immersion in the bilayer, pushing it away from the polar "head" of polyene molecules. Phloretin may be able to stabilize such NYS-sterol complexes. The absence of amino sugars in filipin molecule changes the hydrogen bond network in the polyene-sterol complexes and destabilize them. It is possible that localization of quercetin in the hydrocarbon region of the bilayer allows its interaction with a more hydrophobic polyene filipin (*Fig. 2 F, G*), thus significantly increasing the steady-state transmembrane FIL-induced current in the Chol- and Erg-containing DPhPC-bilayers.

Influence of phospholipid composition

The channel-forming activity of AMB in lipid bilayers that comprise, in addition to sterols, various phospho-

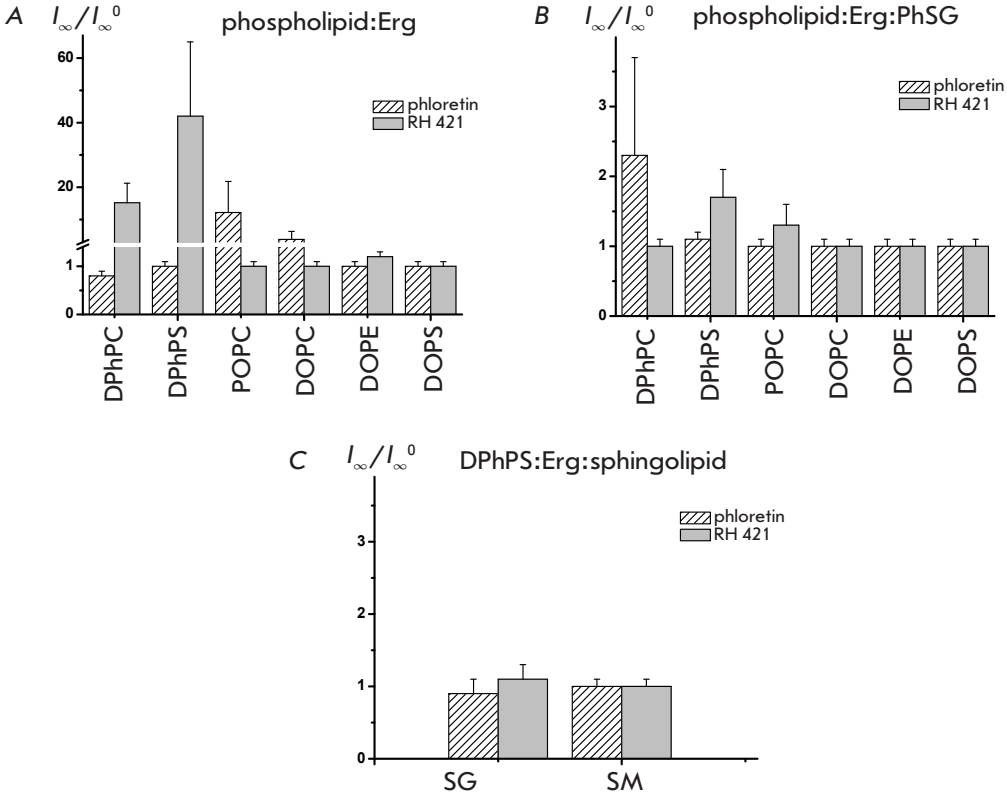

Fig. 6. The ratios between the steady-state transmembrane currents induced by amphotericin B in ergosterol-containing bilayers before and after the introduction of the dipole modifiers (I_∞/I_∞^0). Membranes were made from phospholipid:Erg (67:33 mol %) (*A*), phospholipid:Erg:PhSG (53:27:20 mol %) (*B*) and DPhPS:Erg:sphingolipid (53:27:20 mol %) (*C*) and bathed in 2.0 M KCl (pH 7.0)

lipids and sphingolipids was studied in the presence of phloretin and RH 421 to investigate the interaction of polyenes with other membrane components. The average ratio between the steady-state transmembrane currents induced by AMB in Erg-containing phospholipid bilayers before and after the introduction of dipole modifiers (I_∞/I_∞^0) at a transmembrane voltage of 50 mV is shown in *Fig. 6 A*. It has been established that the introduction of phloretin into the membrane bathing solution leads to a significant increase in the AMB channel-forming activity in Erg-containing POPC (12-fold) and DOPC (4-fold) bilayers, while this dipole modifier does not affect the AMB-modified Erg-containing membranes formed with by DPhPC, DPhPS, DOPE and DOPS. The introduction of RH 421 to the membrane bathing solutions causes a manifold increase in I_∞ through Erg-containing DPhPC (15-fold) and DPhPS (42-fold) bilayers, but does not affect the steady-state transmembrane current induced by AMB in Erg-containing membranes, including POPC, DOPC, DOPE and DOPS. Given that DPhPC, DPhPS, DOPE and DOPS molecules have a conical shape and DOPC and POPC molecules have a cylindrical shape [58, 59], we can assume that the latter are better fit for a rigid AMB molecule. Schematic representation of intermolecular bonds in AMB-Erg-DPhPC and AMB-Erg-POPC complexes is shown in *Fig. 2 H, I*. It is possible that strong "polyene-phospholipid" interaction weakens "polyene-ergosterol" interaction. Such polyene-sterol complex can be stabilized by phloretin molecules, which, due to their high conformational mobility and four functional hydroxyl groups, are able to act as intermediaries in the formation of hydrogen bond network between sterol and AMB. Differences between rigid rod-shaped AMB molecules and conical phospholipids (DPhPC, DPhPS, DOPE and DOPS) prevent strong "polyene-phospholipid" interaction and therefore there is no destabilization of the polyene-sterol complexes. Previously, we have assumed that RH 421 increases the channel-forming activity of AMB in Erg-containing DPhPC-membranes as this dipole modifier takes part in both hydrogen bonds network and in π-π-electron interactions between Erg and AMB molecules. Probably, similar processes take place in AMB-modified Erg-containing DPhPS bilayers.

Influence of sphingolipid composition

The introduction of sphingolipids into the membrane-forming solutions significantly affects the interaction between AMB molecules and phospholipids. It was established that phloretin is responsible for a 2-fold increase in I_∞ in case of DPhPC:Erg:PhSG membranes and that RH 421 leads to a 1.7-fold increase in case of DPhPS:Erg:PhSG bilayers. Replace-

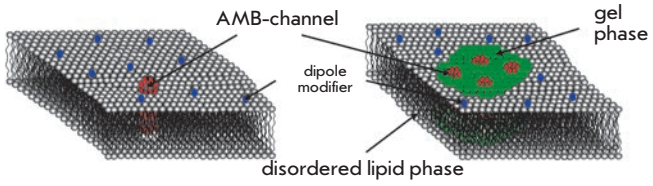

Fig. 7. Schematic representation of the microenvironment of AMB channels in membranes with different concentrations of polyene antimycotics, corresponding to the functioning of single channels (*A*) and integral multi-channel current (*B*). High concentrations (*B*) of AMB provoke the formation of a more ordered lipid phase in the membrane (shown in green)

ment of sphingolipid (PhSG to SG or SM (*Fig. 6 C*)) or phospholipid (DPhPC to DPhPS, POPC, DOPC, DOPE or DOPS in case of phloretin and DPhPS to DPhPC, POPC, DOPC, DOPE, DOPS in the case of RH 421 (*Fig. 6 B*)) component in the aforementioned mixtures does not increase I_∞ in the presence of dipole modifiers. These results indicate that the sphingolipids introduced to the membrane-forming solution play an important role in the interaction of AMB with phospholipids and sterols.

Since phloretin reduces the conductance of single AMB channels in DPhPC:Erg membranes, the lack of effect of this dipole modifier on the steady-state transmembrane current induced by AMB must indicate a jump in the number of open AMB channels. Lack of evidence for such a conclusion suggests two hypotheses: 1) differences in the properties of single AMB channels, in particular, the lack of selectivity of AMB channels responsible for integral current; in this case the conductance of the channels should not be a function of the membrane dipole potential; 2) differences in properties of the channel microenvironment in the membrane, i.e. single AMB pores and channels that are responsible for integral current are localized in the membrane regions with different properties, including those with different values of the membrane dipole potential (*Fig. 7*).

Cation-anion selectivity of amphotericin channels

To test the first hypothesis, we have measured the cation-anion selectivity of the single AMB channel and the integral transmembrane current. The results showed that AMB channels in sterol-containing bilayers are predominantly anion-selective, regardless of the degree of modification of the AMB membrane. The anion transference number for the single AMB channels $t^- = 0.9 \pm 0.1$, while t^- for the integral current induced by AMB is 0.8 ± 0.1. The data obtained indicate that due to the high selectivity the conductance of the AMB channels that are responsible for integral current is expected to depend on the membrane dipole potential.

Amphotericin channels in membranes with phase separation

There is some evidence in favor of the second hypothesis. For example, a dose-dependent increase in the phase transition point of lipids from the gel phase to the liquid crystal one has been demonstrated in the presence of AMB [23]. It implies that AMB triggers the formation of a more ordered phase in the membrane. Moreover, as mentioned earlier, AMB molecules have higher affinity to ordered lipid domains (rafts) [17]. Since ordered lipid domains are rich in sphingolipids and sterols, their physicochemical properties are defined by the lipid composition of the membrane. It is known that the degree of ordering of lipid molecules and the likelihood of rafts formation depend on the type of sterol incorporated into bilayer [60–62]. Sphingolipid composition of the membrane is also important. In particular, PhSG is different from SG in having a hydroxyl group at the C_4 position. Idkowiak-Baldys et al. demonstrated that C_4-hydroxylation significantly affects the physical and structural properties of lipid microdomains [63]. The additional hydroxyl group most likely promotes condensation of lipid molecules by increasing the number of hydrogen bonds [64]. Plasma membranes of fungal cells contain phytosphingosine

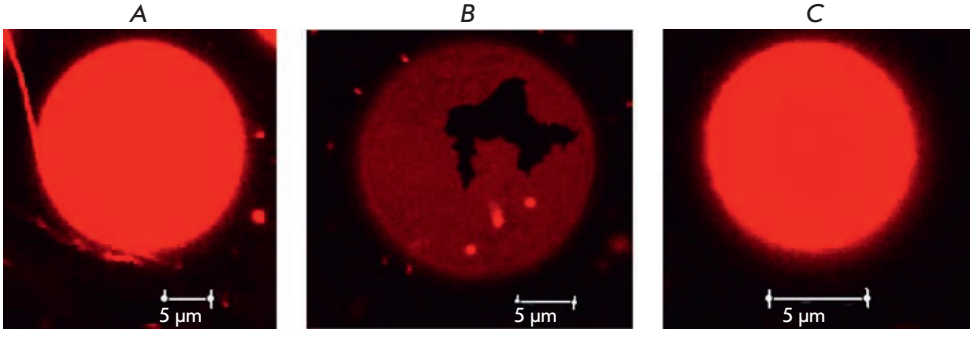

Fig. 8. Photomicrographs of unilamellar POPC vesicles in the absence of polyene antibiotics (*A*) and in the presence of 300 μM AMB in the membrane bathing solutions (*B*) and a combination of 300 μM AMB and 400 μM phloretin (*C*)

and ergosterol [65], and plasma membranes of mammalian cells contain sphingomyelin and cholesterol [66]. Evolutionary preference for these combinations can be attributed to the properties of ordered lipid domains formed by them. Moreover, some phospholipids with a low melting temperature, which are not localized in the ordered membrane domains, can induce the formation of these domains. Therefore, the ability to stabilize lipid rafts depends on phospholipid structure and decreases for the series DPhPC, DPhPS, POPC (DOPC) [67].

Fluorescent confocal microscopy of giant unilamellar vesicles demonstrated that dipole modifiers affect phase separation in liposomes [68]. Flavonoids biochanin A and phloretin lead to liquefaction of solid crystalline regions in liposome membranes and promote the formation of membrane rafts, while myricetin causes bilayer condensation. The data obtained by differential scanning calorimetry confirm the effect of flavonoids on phase separation in liposomes [68].

Our results show that liposomes from POPC are homogeneously stained in the absence of AMB; lateral heterogeneity of the membrane is not observed (*Fig. 8 A*). The addition of 300 μM AMB induces the formation of unstained dendritic domains in liposomes, which can be attributed to the solid lipid phase (*Fig. 8 B*). Phloretin in a concentration of 400 μM liquefies gel domains in AMB-modified vesicles and liposomes become homogeneously dyed (*see Fig. 8 C*). These data indicate that dipole modifiers influence the formation and dynamics of polyene-enriched ordered membrane domains.

CONCLUSION

It has been established that the channel-forming activity of polyene antibiotics in lipid bilayers is defined by the superposition of several factors: the membrane dipole potential, stability of the polyene-lipid complexes, and physicochemical properties of ordered lipid domains. ●

The authors are grateful to E.G. Chulkov for his participation in some experiments.
This work was supported by the Russian Foundation for Basic Research (grant № 12-04-33121), the program of the Presidium of the Russian Academy of Sciences "Molecular and Cell Biology" and the Scientific School grant NSh-1721.2014.4.

REFERENCES

1. Malewicz B., Momsen M., Jenkin H.M. // Antimicrob. Agents Chemother. 1983. V. 23. P. 119–124.
2. Kuwano M., Akiyama S., Endo H., Kohga M. // Biochem. Biophys. Res. Commun. 1972. V. 49. P. 1241–1248.
3. Medoff G., Kwan C.N., Schlessinger D., Kobayashi G.S. // Cancer Res. 1973. V. 33. P. 1146–1149.
4. Craven P.C., Gremillion D.H. // Antimicrob. Agents Chemother. 1985. V. 27. P. 868–871.
5. Shigemi A., Matsumoto K., Ikawa K., Yaji K., Shimodozono Y., Morikawa N., Takeda Y., Yamada K. // Int. J Antimicrob Agent. 2011. V. 38. P. 417–420.
6. Guinet R., Chanas J., Goullier A., Bonnefoy G., Ambroise-Thomas P. J. // Clin. Microbiol. 1983. V. 18. P. 443–444.
7. Hawkins J.L., Baddour L.M. // Clin. Infect. Dis. 2003. V. 36. P. 14–18.
8. Andreoli T. // Ann. N. Y. Acad. Sci. 1974. V. 235. P. 448–468.
9. González-Damián J., Ortega-Blake I. // Membr. Biol. 2010. V. 237. P. 41–49.
10. Récamier K.S., Hernández-Gómez A., González-Damián J., Ortega-Blake I. // J. Membr. Biol. 2010. V. 237. P. 31–40.
11. Samedova A.A., Kasumov Kh.M. // Antibiot. Khimioter. 2009. V. 54. P. 44–52.
12. Kasumov Kh.M. Structure and function of membrane polyene macrolide antibiotics. Nauka, Moscow, 2009. 512 pp.
13. de Kruijff B., Gerritsen W.J., Oerlemans A., Demel R.A., van Deenen L.L. // Biochim. Biophys. Acta. 1974. V. 339. P. 30–43.
14. Baginski M., Resat H., Borowski E. // Biochim. Biophys. Acta. 2002. V. 1567. P. 63–78.
15. Marty A., Finkelstein A. // J. Gen. Physiol. 1975. V. 65. P. 515–526.
16. Venegas B., Gonzalez-Domian J., Celis H., Ortega-Blake I. // Biophys. J. 2003. V. 85. P. 2323–2332.
17. Czub J., Baginski M. // J. Phys. Chem. B 2006. V. 110. P. 16743–16753.
18. Neumann A., Czub J., Baginski M. // J. Phys. Chem. B. 2009. V. 113. P. 15875–15885.
19. Neumann A., Baginski M., Czub J. // J. Am. Chem. Soc. 2010. V. 132. P. 18266–18272.
20. Baran M., Borowski E., Mazerski J. // Biophys. Chem. 2009. V. 141. P. 162–168.
21. Matsumori N., Tahara K., Yamamoto H., Morooka A., Doi M., Oishi T., Murata M. // J. Am. Chem. Soc. 2009. V. 131. P. 11855–11860.
22. Hamilton K.S., Barber K.R., Davis J.H., Neil K., Grant C.W. // Biochim. Biophys. Acta. 1991. V. 1062. P. 220–226.
23. Paquet M.J., Fournier I., Barwicz J., Tancrede P., Auger M. // Chem. Phys. Lipids. 2002. V. 119. P. 1–11.
24. Gabrielska J., Gagoś M., Gubernator J., Gruszecki W.I. // FEBS Lett. 2006. V. 580. P. 2677–2685.
25. Liberman E.A., Topaly V.P. // Biofizika (Russian). 1969. V. 4. P. 452–461.
26. Hladky S.B., Haydon D.A. // Biochim. Biophys. Acta. 1973. V. 318. P. 464–468.
27. Brockmann H. // Chem. Phys. Lipids. 1994. V. 73. P. 57–79.
28. Hsuchen C.C., Feingold D. // Antimicrob. Agents Chemother. 1973. V. 4. P. 316–319.
29. Vertut-Croquin A., Bolard J., Chabbert M., Gary-Bobo C. Biochemistry. 1983. V. 22. P. 2939–2944.
30. Hartsel S.C., Perkins W.R., McGarvey G.J., Cacso D.S. // Biochemistry. 1988. V. 27. P. 2656–2660.
31. Cohen B.E. // Biochim. Biophys. Acta. 1992. V. 1108. P. 49–58.
32. Ruckwardt T., Scott A., Scott J., Mikulecky P., Hartsel S.C. // Biochim. Biophys. Acta. 1998. V. 1372. P. 283–288.
33. Fujii G., Chang J.E., Coley T., Steere B. Biochemistry. 1997. V. 36. P. 4959–4968.
34. Dufourc E.J., Smith I.C.P., Jarell H.C. // Biochim. Biophys. Acta. 1984. V. 778. P. 435–442.

35. Balakrishnan A.R., Easwaran K.R.K. // Biochemistry. 1993. V. 32. P. 4139–4144.
36. Fournier I., Barwicz J., Tancrede P. // Biochim. Biophys. Acta. 1998. V. 1373. P. 76–86.
37. Milhaud J., Ponsinet V., Takashi M., Michels B. // Biochim. Biophys. Acta. 2002. V. 1558. P. 95–108.
38. Sternal K., Czub J., Baginski M. // J. Mol. Model (Online). 2004. V. 10. P. 223–232.
39. Herec M., Dziubinska H., Trebacz K., Morzycki J.W., Gruszecki W.I. // Biochem. Pharmacol. 2005. V. 70. P. 668–675.
40. Zager R.A. // Am. J. Kidney Dis. 2000. V. 36. P. 238–249.
41. Nagiec M.M., Young C.L., Zaworski P.G., Kobayashi S.D. // Biochem. Biophys. Res. Commun. 2003. V. 307. P. 369–374.
42. Sun X., Garlid K.D. // J. Biol. Chem. 1992. V. 267. P. 19147–19154.
43. Rokitskaya T.I., Kotova E.A., Antonenko Y.N. // Biophys. J. 2002. V. 82. P. 865–873.
44. Hwang T.C., Koeppe R.E., Andersen O.S. // Biochemistry. 2003. V. 42. P. 13646–13658.
45. Ostroumova O.S., Kaulin Y.A., Gurnev P.A., Schagina L.V. // Langmuir. 2007. V. 23. P. 6889–6892.
46. Asandei A., Mereuta L., Luchian T. // Biophys. Chem. 2008. V. 135. P. 32–40.
47. Ostroumova O.S., Schagina L.V. // Biological membrane (Moscow). 2009. V. 26. P. 287–292.
48. Apetrei A., Mereuta L., Luchian T. // Biochim. Biophys. Acta. 2009. V. 1790. P. 809–816.
49. Ostroumova O.S., Malev V.V., Ilin M.G., Schagina L.V. // Langmuir. 2010. V. 26. P. 15092–15097.
50. Ostroumova O.S., Efimova S.S., Schagina L.V. // Biochim. Biophys. Acta Biomembr. 2011. V. 1808. P. 2051–2058.
51. Mereuta L., Asandei A., Luchian T. // PLoS One. 2011. V. 6. P. e25276.
52. Montal M., Muller P. // Proc. Nat. Acad. Sci. USA. 1972. V. 65. P. 3561–3566.
53. Morf W.E. // Analyt. Chem. 1977. V. 49. P. 810–813.
54. Juhasz J., Davis J.H., Sharom F.J. // Biochem. J. 2010. V. 430. P. 415–423.
55. Muddana H.S., Chiang H.H., Butler P.J. // Biophys. J. 2012. V. 102. P. 489–497.
56. Tarahovsky Y.S., Muzafarov E.N., Kim Y.A. // Mol. Cell Biochem. 2008. V. 314. P. 65–71.
57. Passechnik V.I., Sokolov V.S. // Bioelectrochemistry. 2002. V. 55. P. 47–51.
58. Bezrukov S.M. // Current Opinion in Colloid Interface Sci. 2000. V. 5. P. 237–243.
59. Sakuma Y., Taniguchi T., Imai M. // Biophys. J. 2010. V. 99. P. 472–479.
60. Hsueh Y.W., Chen M.T., Patty P.J., Code C., Cheng J., Frisken B.J., Zuckermann M., Thewalt J. // Biophys. J. 2007. V. 92. P. 1606–1615.
61. Cournia Z., Ullmann G.M., Smith J.C. // J. Phys. Chem. 2007. V. 111. P. 1786–1801.
62. Róg T., Pasenkiewicz-Gierula M., Vattulainen I., Karttunen M. // Biochim. Biophys. Acta. 2009. V. 1788. P. 97–121.
63. Idkowiak-Baldys J., Grilley M.M., Takemoto J.Y. // FEBS Lett. 2004. V. 569. P. 272–276.
64. Lofgren H., Pascher I. // Chem. Phys. Lipids. 1977. V. 20. P. 273–284.
65. Rest M.E., Kamminga A.H., Nakano A., Anraku Y., Poolman B., Konings W.N. // Microbiol. Rev. 1995. V. 59. P. 304–322.
66. Simons K., Toomre D. // Nat. Rev. Mol. Cell Biol. 2000. V. 1. P. 31–39.
67. Bakht O., Pathak P., London E. // Biophys. J. 2007. V. 93. P. 4307–4318.
68. Ostroumova O.S., Chulkov E.G., Stepanenko O.V., Schagina L.V. // Chem. Phys. Lipids. 2014. V. 178. P. 77–83.
69. Efimova S.S., Ostroumova O.S. // Langmuir. 2012. V. 28. P. 9908–9914.

A Cytofluorometric Study of Membrane Rafts in Human Monocyte Subsets in Atherosclerosis

M. A. Chelombitko[1,2*], V. S. Shishkina[1,2], O. P. Ilyinskaya[1], A. I. Kaminnyi[2], T. O. Pavlunina[2], N. N. Samovilova[2], E. V. Gracheva[2], E. M. Tararak[2], N. V. Prokazova[2]

[1]Biological Faculty, Lomonosov Moscow State University, Leninskie Gory 1, Bldg. 12, Moscow, 119991, Russia

[2]Russian Cardiology Research and Production Complex, 3rd Cherepkovskaya Str., 15A, Moscow, 121552, Russia

E-mail: atma69@yandex.ru

Received 05.05.2014

ABSTRACT **The peripheral blood monocytes of atherosclerotic patients are pre-activated and have some of the features of tissue macrophages. Their adhesion to the endothelium is 1.5 times higher than that of monocytes from healthy subjects, and they express a number of receptors and antigens typical of tissue macrophages. Additionally, earlier we showed that the biosynthesis of gangliosides, whose main function is the formation of membrane rafts, is significantly activated in blood monocytes from atherosclerotic patients, as well as during the *in vitro* differentiation of normal monocytes into macrophages. In this study, we investigated the expression of membrane rafts on various monocyte subsets from healthy subjects and atherosclerotic patients. Based on flow cytometry results, the monocytes in the examined atherosclerotic patients were found to differ from those in healthy subjects by a twofold increase in the proportion of the intermediate subset ($CD14^{++}/CD16^{+}$) and by enhancement in the expression of the fractalkine receptor CX3CR1 on the intermediate and non-classical subsets ($CD14^{++}/CD16^{+}$ and $CD14^{+}/CD16^{++}$) (2.3 and 1.8 times, respectively). This suggests a pre-activated state of monocytes in atherosclerotic patients. At the same time, the expression of the membrane raft marker on the monocyte subsets was similar in both studied groups. However, a study of the *in vitro* differentiation of monocytes into macrophages showed that the membrane raft expression increased 2 times as early as on the 1st day of culturing and 3 times on the 7th day compared to that in freshly isolated monocytes. Therefore, it is suggested that monocytes in atherosclerosis accumulate gangliosides that are used to form membrane rafts during the macrophage differentiation after the migration of monocytes into the arterial intima.**

KEYWORDS **monocyte subsets, macrophages, membrane rafts, flow cytometry, atherosclerosis.**

INTRODUCTION

Monocytes are immune system cells that play a key role in the formation of innate and adaptive immunity. Human blood monocytes are morphologically and functionally heterogeneous; several subsets can be distinguished based on the differential expression of CD14 (a component of the receptor complex that recognizes bacterial lipopolysaccharides) and CD16 (FcγRIII, the low affinity receptor for the Fc-fragment of IgG) [1, 2]. Recently, the Committee on Nomenclature of the International Union of Immunological Societies and the WHO adopted an official nomenclature, according to which monocytes are divided into three subsets: a classical ($CD14^{++}/CD16^{-}$), an intermediate ($CD14^{++}/CD16^{+}$), and a non-classical ($CD14^{+}/CD16^{++}$) (percentage of subsets is 83–85, 4–5, and 7–11%, respectively) [3, 4].

Clinical and experimental studies have shown that there is a significant increase in the number of monocytes in intermediate and non-classical subsets in infectious, autoimmune and inflammatory diseases, which may be an indication of the proinflammatory nature of their activity [5]. Furthermore, the monocytes of these populations are the main producers of proinflammatory cytokines: the tumor necrosis factor (TNF) and interleukin-12 (IL-12) [6]. Monocytes play a critical role in the pathogenesis of atherosclerosis, because after they are attracted to the lipid and lipoprotein-enriched intimal areas of the arteries, they differentiate into macrophages under the influence of the macrophage colony-stimulating factor (M-CSF) produced by the activated endothelium. Macrophages absorb oxidized lipoproteins and other lipids and form lipid saturated foam cells,

which are the main cells of atherosclerotic plaques [7]. It is also obvious that the relative level of monocytes of minor subsets is significantly increased in atherosclerosis [8, 9]. In the peripheral blood of atherosclerotic patients, monocytes have been found to be preactivated and to exhibit some macrophage features. Their adhesion to the endothelium is 1.5 times higher than that of monocytes in healthy subjects. They express a number of receptors (Fcγ-receptor type I and II, ICAM) and an increased level of MHC II, which is typical of tissue macrophages [10–12]. In addition, we demonstrated previously that the biosynthesis and level of gangliosides in the circulating monocytes of atherosclerotic patients are significantly higher than those in the monocytes of healthy subjects, similar to upon the *in vitro* differentiation of monocytes into macrophages [13, 14].

Gangliosides are sialic acid-containing glycosphingolipids that play an active role in the formation, stabilization, dynamics, and biological functions of membrane rafts. Due to the amide bond and bulk carbohydrate moiety in their molecule, gangliosides form in cell membranes, through a large number of hydrogen bonds, and conglomerate with cholesterol, sphingomyelin, and receptor proteins, the so-called membrane microdomains (rafts) that can move easily in the plane of the phospholipid membrane layer [15]. Therefore, raft gangliosides are involved in the processes of reception, adhesion, cell motility, and apoptosis. Their qualitative and quantitative composition changes dramatically during cell differentiation and transformation.

It is known that upon activation of lymphocytes, many receptors are transported into the rafts, where they acquire an active conformation and form complexes with other co-receptors and auxiliary proteins. Receptor phosphatidylinositol-anchored proteins, similarly to myristoylated and palmitoylated proteins, are permanent components of these membrane structures that are enriched in sphingolipids and cholesterol. Furthermore, transmembrane proteins are inductively involved in the rafts, thereby forming reception and adhesion foci [16].

In this paper, we conducted a comparative study of the expression of membrane rafts in different subsets of monocytes from the blood of atherosclerotic patients and healthy subjects, using flow cytometry, to elucidate the monocyte pre-activation mechanism in atherosclerosis.

EXPERIMENTAL

The study object

In this study, peripheral blood samples were used that were obtained at the Russian Cardiology Research and Production Complex of the Russian Ministry of Health from patients with angiographically confirmed coronary atherosclerosis (n = 25) and apparently healthy donors (n = 15). In all cases, an informed patient consent was obtained. The mean age of the healthy subjects was 25 ± 3 years; the mean age of the patients was 55 ± 8 years. Since atherosclerosis is typical of almost all elderly people, the control group (healthy subjects) was composed of younger people.

Isolation and flow cytometry analysis of human peripheral blood mononuclear leukocytes

Mononuclear leukocytes were isolated from the peripheral blood by a traditional method in the Ficoll-Paque™ PLUS (Amersham Biosciences, USA) density gradient (1.077 g/L). The venous blood collected into tubes with 6% sodium EDTA (0.5 mL of EDTA per 10 mL of blood) was centrifuged at 400 g for 30 min. The blood cell pellet at the tube's bottom was combined with phosphate buffered saline (PBS) to the original volume and carefully re-suspended. The resulting suspension was gently layered on Ficoll-Paque ™ PLUS at a 2.5 : 1 ratio and was centrifuged at 400 g for 30 min. The interphase layer containing the blood mononuclear cells was harvested and washed twice in PBS.

The expression of the surface markers of mononuclear leukocytes was analyzed by triple immunofluorescence staining. Membrane rafts were detected with the cholera toxin B subunit conjugated with Alexa Fluor 488 (Vybrant® Lipid Raft Labeling Kit, Molecular Probes, Inc.). Surface receptors were identified with specific, fluorescently labeled mouse monoclonal antibodies: CD14-PC5 (Beckman Coulter Inc.), CD16-PE (Beckman Coulter Inc.), CD16-FITC (Beckman Coulter Inc.), CCR5-PE (eBioscience Inc.), CX3CR1-PE (R & D Systems), and TLR-4-PE (eBioscience). After washing, the resultant precipitate was added with PBS (pH 7.2) containing 1% bovine serum albumin (BSA) in the amount of 100 μL of solution per sample. Cells were re-suspended, and 100 μL aliquots of the suspension were transferred into 2 mL microtubes. Samples containing the cholera toxin B subunit (CTB) conjugated with Alexa Fluor 488 were incubated for 10 min; the remaining samples were incubated in the dark at 4 °C for 30 min. Further, each sample was added with 300 μL of 1% formalin, and the suspension was analyzed by flow cytometry. As the isotype control, mouse IgG isotype immunoglobulins labeled with dyes identical to labels of the monoclonal antibodies were used.

Flow cytometric studies were performed on a FACSCalibur flow laser cytometer (Becton Dickinson, USA) using identical instrument settings for all samples. The Summit V3.1 Built 844 (Cytomation Inc., USA) software was used for the analysis and visualization of the flow cytometry data. The monocyte region was identified

based on the forward (FSC) and side (SSC) scatter parameters. The total monocyte population was identified based on CD14, in combination with SSC. Based on the expression level of CD14 and CD16 receptors, monocytes were divided into three subsets: $CD14^{++}/CD16^{-}$, $CD14^{++}/CD16^{+}$, and $CD14^{+}/CD16^{++}$. Separately, each subset was evaluated for the expression level of CCR2, TLR4, and CX3CR1 receptors using the mean fluorescence intensity (MFI).

Culturing and immunocytochemical analysis of mononuclear cells in healthy subjects

A portion of the isolated mononuclear cells from healthy subjects was plated on the bottom or glass of Petri dishes (ø 60 mm) at a concentration of 2–2.5 million/mL in a X-VIVO-10 culture medium (Lonza Biosciences, USA) containing 2 mM *L*-glutamine, 0.01 % fungizone, 1% penicillin/streptomycin mixture (Sigma reagents), and 10 ng/mL of M-CSF (Biosource) [13].

The dynamic pattern of co-expression of membrane rafts and various monocyte markers (CD14 and CD16) and the marker of differentiation of monocytes into macrophages (CD206) were analyzed at different stages of culturing (1st, 4th, and 7th day) by triple immunofluorescence staining using specific, fluorescently labeled mouse monoclonal antibodies: CD14-PC5, CD16-PE, and CD206-PE (Beckman Coulter, USA). Rafts were identified using the cholera toxin B subunit conjugated with Alexa Fluor 488. For this, cells were detached from the plastic support by a rubber scriber and centrifuged at 400 g for 10 min. Then, the cells were stained as described above and analyzed on a FACSCalibur flow cytometer (Becton Dickinson).

The dynamic pattern of co-expression of membrane rafts with different markers of monocytes and macrophages at different stages of culturing (4th, 7th, and 12th day) was analyzed by double immunofluorescence staining. For this, the cells plated on glass were stained using the cholera toxin B subunit conjugated with Alexa Fluor 488 and antibodies conjugated to phycoerythrin (PE) (to detect CD14-, CD16- and CD206-positive cells) and incubated at 37 ^{0}C in 5% CO_2 for 30 min. Thereafter, the cells were washed three times with a warm medium and fixed in 10% formalin for 10 min. Then the samples were embedded in glycerin-gelatin and analyzed using a Leica DM 5000B fluorescence microscope (filters BP 450-490, LP 515 and BP 515-560, and LP 590) equipped with a DC 420 digital camera and an image analysis system. R-PE conjugated IgGs of the same subclass as the specific antibodies were used as the isotype control.

Statistical analysis

The statistical analysis of the data was performed using the Excel and Statistica 7.0 software. The two-sided Mann-Whitney U-test was used to estimate the statistical significance of intergroup differences. The differences were considered statistically significant at $P < 0.05$. The data are presented as the arithmetic mean and its standard deviation (M ± SD).

RESULTS AND DISCUSSION

Flow cytometry analysis of the monocyte subsets of patients and healthy subjects

The monocytes and their subsets were identified by flow cytometry using the forward and side scatter parameters and the expression level of the surface markers CD14 and CD16. A gating strategy used to identify the classical ($CD14^{++}/CD16^{-}$), intermediate ($CD14^{++}/CD16^{+}$), and non-classical ($CD14^{+}/CD16^{++}$) monocyte subsets is presented in *Figs. 1A–C*. The obtained cytofluorograms and percentage ratio of the subsets are consistent with published data [3, 4].

Figures 1D–F present the results of the flow cytometry analysis of the membrane rafts on monocyte subsets using monoclonal antibodies to CD14 and CD16 and the cholera toxin B subunit, which identifies membrane rafts. To detect rafts on the membranes of whole cells, a commonly used method based on the very high affinity (10^{-12} M) of the cholera toxin B subunit to the GM1 ganglioside was utilized. The method is based on their interactions on the cell membrane, although the level of this ganglioside compared to that of other gangliosides in the plasma membrane of blood cells is low [17]. Therefore, the use of GM1 as a raft marker is related not so much to its significance for the raft structure as to its availability as a reactant [18]. The analysis of the results by the Summit V3.1 Built 844 software demonstrated that all of the monocyte subsets expressed GM1, a marker of membrane rafts (*Figs. 1D–F*).

Interestingly, our data are partly inconsistent with the results obtained previously by Moreno-Altamirano *et al.* [19], who divided the monocytes of healthy subjects into two populations based on the expression of rafts: $CD14^{+}/GM1^{+}$ (95.5% with a low raft expression) and $CD14^{+}/GM1^{++}$ (2.5% with a high raft expression). To analyze the rafts, they, like us, used a fluorescently labeled cholera toxin B subunit. We observed a different pattern (*Figs. 1D–F*): the classical and intermediate monocyte subsets had the same raft expression; the low expression was typical of the non-classical subset only. This contradiction may be due to the different gating strategy used by Moreno-Altamirano *et al.* Indeed, as seen from the data in *Figs. 2A* and *B*, based on the granularity (SSC) and size (FSC) parameters, which were different from those of the monocytes in the gate, we identified the so-called non-gate classical ($CD14^{++}/CD16^{-}$) and intermediate ($CD14^{++}/CD16^{+}$)

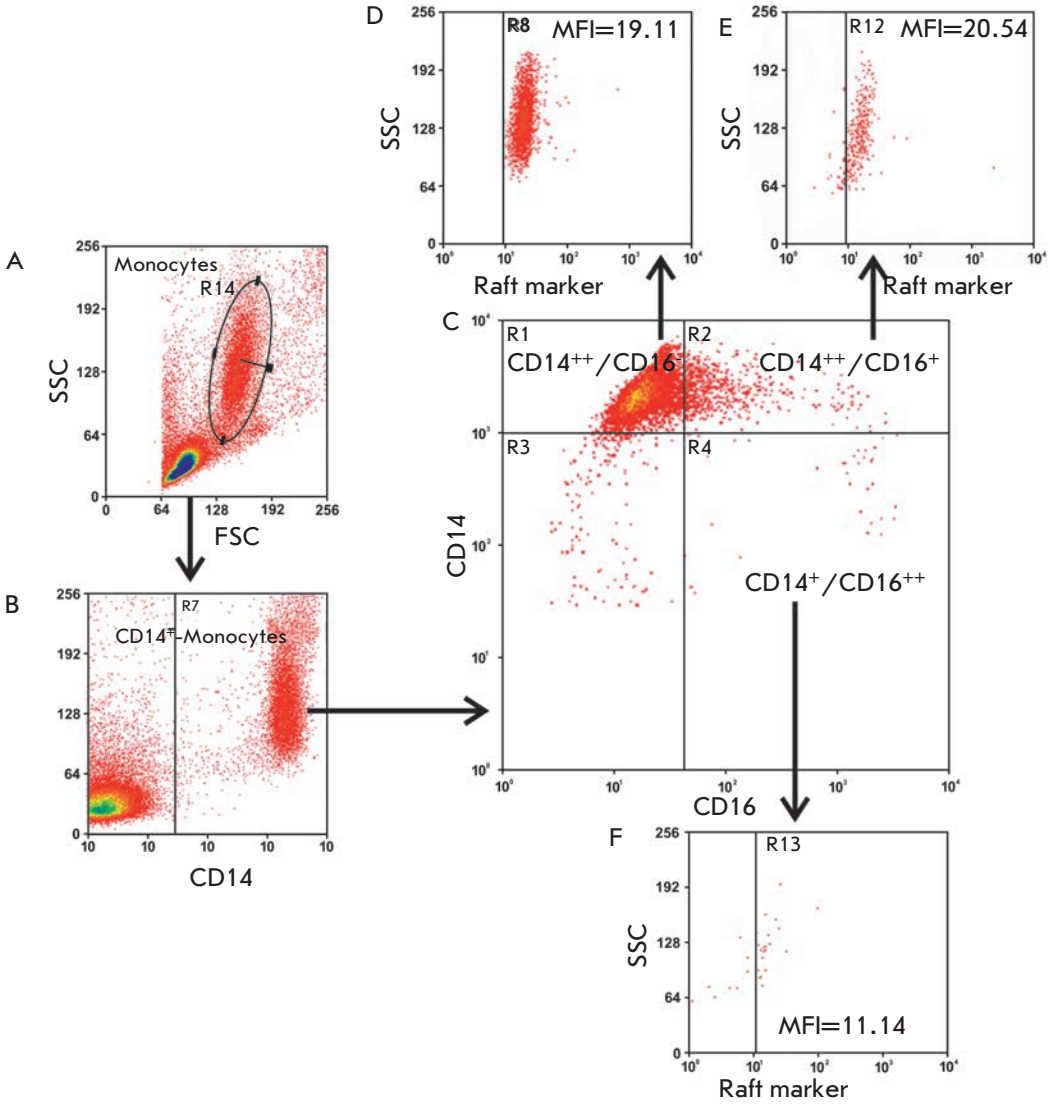

Fig. 1. Multistep gating of monocyte subsets. (A) Identification of the monocyte region based on the forward scatter (FSC) and side scatter (SSC) parameters; (B) Gating of the total population based on CD14 positive events; (C) Identification of monocyte subsets by the expression level of the surface markers CD14 and CD16; (D–F) Gating in the analysis of the expression of various receptors and membrane rafts on monocyte subsets based on the SSC parameters and positive events (illustrated by an example of the GM1 raft marker)

monocyte subsets. In this case, the latter subset had a higher expression of the marker rafts than the classical one. It is most likely that Moreno-Altamirano *et al.* [19], contrary to us, probably took into account the cells of non-gated subsets. We observed the monocytes of non-gated subsets in equal amounts both in patients and in healthy subjects (*Fig. 2B*). The properties and functions of this population need to be further studied.

Figures 3A and *B* provide the typical cytofluorograms of the monocyte subsets of a healthy subject and an atherosclerotic patient. The data in *Fig. 3B* demonstrate that the percentage of intermediate subset monocytes is significantly increased (20.7 ± 7.0%) and the percentage of classical subset monocytes is decreased (68.6 ± 7.9%) in patients with atherosclerosis compared to those of healthy subjects (12.8 ± 3.4 and 74.8 ± 7.6%, respectively). Therefore, atherosclerosis is apparently accompanied by a redistribution of monocyte subsets: the proportion of monocytes with an intermediate phenotype ($CD14^{++}/CD16^{+}$) is increased due to the reduction in the proportion of the main subset of classical monocytes ($CD14^{++}/CD16^{-}$). The level of non-classical subset monocytes was identical in patients and healthy subjects.

These findings are consistent with the results of a series of studies that explored monocyte subsets in atherosclerosis. For example, the high level of intermediate subset monocytes ($CD14^{++}/CD16^{+}$) was found to be associated with an increase in the body mass index and thickening of the intima-media complex. Clinical data indicate a higher level of $CD14^{++}/CD16^{+}$ monocytes and the total population of $CD16^{+}$ monocytes in patients with coronary heart disease compared to healthy subjects. An increase in the number of monocytes of the $CD16^{+}$ subsets was associated with the predominance of unstable plaques in the coronary arteries and

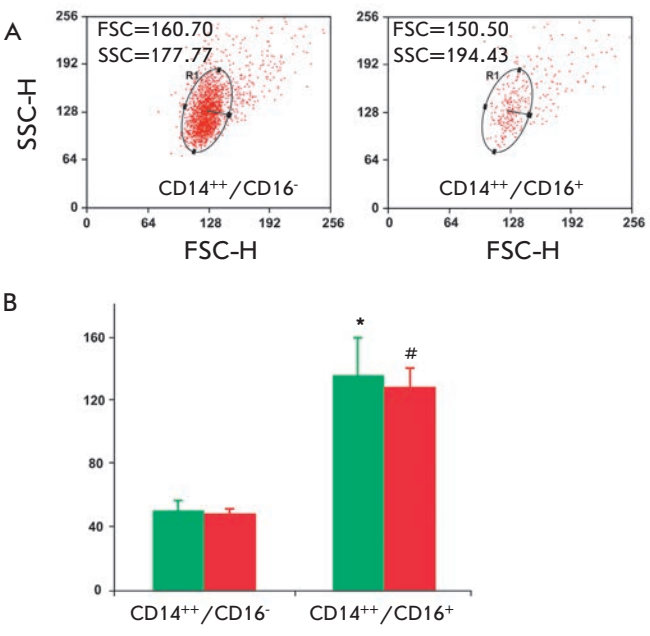

Fig. 2. Blood cell subsets from a healthy subject located outside a monocyte gate. (A) Characteristics of $CD14^{++}/CD16^{-}$ and $CD14^{++}/CD16^{+}$ cell subsets based on their granularity (SSC) and size (FSC); (B) Cumulative data on the fluorescence intensity of the raft marker (GM1) on $CD14^{++}/CD16^{-}$ and $CD14^{++}/CD16^{+}$ cells in 15 healthy subjects (green bars) and 25 atherosclerotic patients (red bars). Values are presented as M ± SD. $^{*,\#}P<0.5$

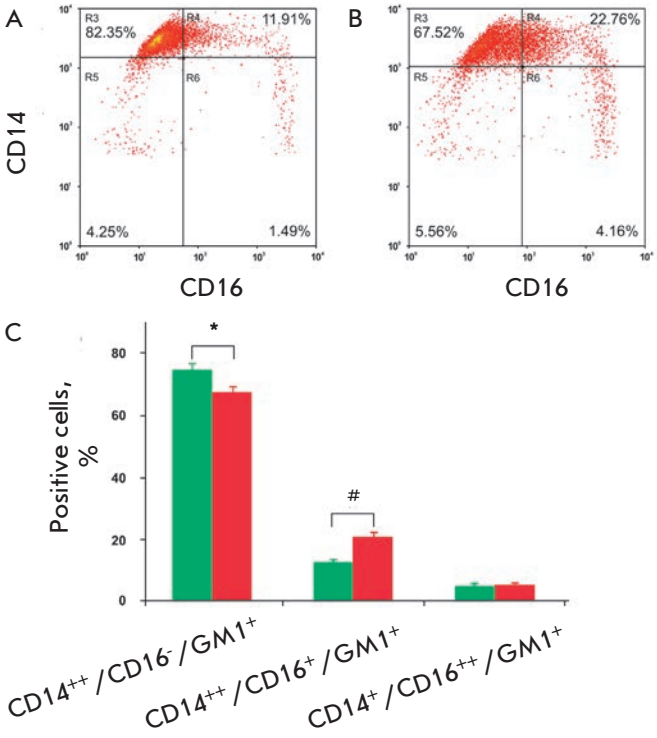

Fig.3. Monocyte subsets from healthy subjects and atherosclerotic patients. Typical cytofluorograms of monocyte subsets from a healthy subject (A) and an atherosclerotic patient (B); (C) Cumulative data on the percentage ratio of monocyte subsets in 15 healthy subjects (green bars) and 25 atherosclerotic patients (red bars). Values are presented as M ± SD. $^{*,\#}P<0.05$

an unfavorable prognosis in the coronary heart disease [3, 6, 20]. It should also be noted that, until recently, the $CD14^{++}/CD16^{+}$ and $CD14^{+}/CD16^{++}$ monocyte subsets were analyzed together in many clinical studies, because a standard gating protocol was not adopted in the analysis of flow cytometry data to identify monocyte subsets. This did not allow researchers to draw an unambiguous conclusion on the role of individual $CD16^{+}$ subsets in the pathogenesis of atherosclerosis. As seen from *Fig. 3B*, no significant differences in the percentage of non-classical subset monocytes in healthy subjects and in atherosclerotic patients were found.

Expression of cytokine receptors on monocyte subsets

The function of chemokines and their receptors is to attract specifically different monocyte subsets to the inflammatory area [21]. Monocyte populations are known to differ in their expression of chemokine receptors [22]. For example, the classical $CD14^{++}/CD16^{-}$ subset is characterized by a high level of CCR2, the receptor of the monocyte chemoattractant protein-1 (MCP-1), a moderate expression of CX3CR1, the fractalkine receptor, and a low level of CCR5, the receptor of the inflammatory cytokines CCL3, CCL4, CCL8, and CCL3. The $CD16^{+}$ subsets are CCR2 negative and express a high level of the CX3CR1 and CCR5 receptors. These two receptors were also found to play a prominent role in the formation of atherosclerotic lesions, because their ligands are found in the atherosclerotic plaques and are expressed by endothelial cells after their activation by cytokines [23, 24]. In connection with this, the expressions of CCR5, CX3CR1, and the LPS receptor (TLR4), which is common to all monocytes, were studied on the monocytes of healthy subjects and arteriosclerotic patients using flow cytometry with triple staining by monoclonal antibodies. No significant differences in the CCR5 and TLR4 expression by the monocytes of atherosclerotic patients and healthy subjects were found among all the subsets (data not shown).

The expression of CX3CR1 (fractalkine receptor) on the intermediate and non-classical subsets was higher than that on classical monocytes, which is consistent with the concept of its localization on $CD16^{+}$ monocytes [23]. In this case, both $CD16^{+}$ monocyte subsets in pa-

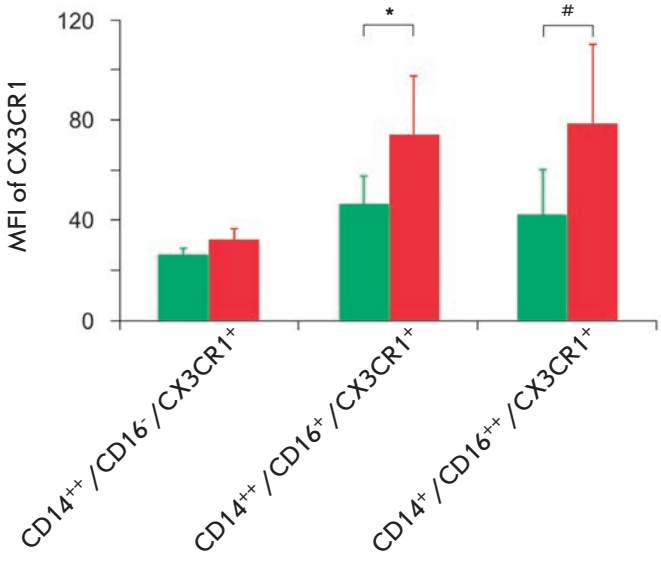

Fig. 4. Fractalkine receptor (CX3CR1) expression on monocyte subsets in 15 healthy subjects and 25 atherosclerotic patients. The differences are statistically significant for the $CD16^+$ cells of healthy subjects (green bars) and atherosclerotic patients (red bars). Values are presented as M ± SD. $P<0.05$

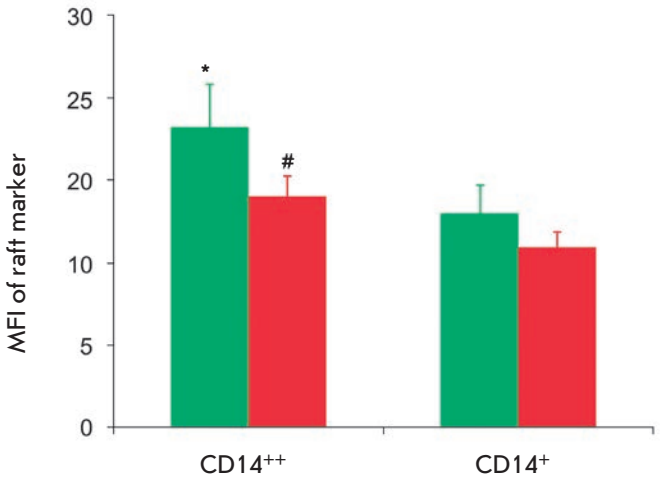

Fig. 5. Cumulative data on the mean fluorescence intensity (MFI) of the raft marker (GM1) on monocyte subsets in 15 healthy subjects (green bars) and 25 atherosclerotic patients (red bars). Values are presented as M ± SD. $^{*,\#}P<0.05$

tients had a CX3CR1 fluorescence intensity 2 times higher than that of the monocytes in healthy subjects (*Fig. 4*).

An unambiguous role of CX3CR1/CX3CL1 in the formation of atherosclerotic lesions in human vessels was also demonstrated in experimental atherosclerosis in mice [24]. Therefore, our findings confirm the results of previous studies.

Expression of lipid rafts on monocyte subsets

Previously, we found that the biosynthesis of gangliosides whose main function is the formation of lipid rafts is significantly activated in the blood monocytes of patients with atherosclerosis [15]. On this basis, we suggested that pre-activation of circulating monocytes in atherosclerosis is accompanied by an increase in the number of the lipid rafts necessary for the functioning of membrane proteins.

Many antigens and receptors of monocytes, such as CD14, CD32, CD64, CD11/CD18, and the major histocompatibility complex class II (MHC II), were previously demonstrated to be permanent components of membrane rafts [25, 26]. When monocytes are activated, additional protein molecules are transported to the plasma membrane. For example, under certain conditions, CD16 are mobilized from cytosol depots to membrane rafts [27]. Activation and functioning of monocytes require the integration of individual rafts into large platforms with the involvement of additional protein components [28, 29]. Disruption of rafts through treatment of cells with nystatin or methyl cyclodextrin (cholesterol binding compounds), conversely, results in a loss of the association of receptors in lipid platforms and, consequently, in a disruption of signal transduction and cellular responses to specific ligands [10].

As seen from the data shown in *Fig. 3B*, the percentage ratio among the subsets of monocytes expressing $GM1^+$ rafts ($CD14^{++}/CD16^-/GM1^+$, $CD14^{++}/CD16^+/GM1^+$, and $CD14^+/CD16^{++}/GM1^+$) in healthy subjects and in atherosclerotic patients did not differ; however, a redistribution of monocytes among the subsets of $CD14^{++}/CD16^-$, $CD14^{++}/CD16^+$ and $CD14^+/CD16^{++}$ occurred in atherosclerosis (see above).

The analysis of fluorescence after triple staining with antibodies to CD14 and CD16 and the cholera toxin B subunit demonstrated that the mean fluorescence intensity (MFI) of rafts on monocytes with a high expression of CD14 was higher than that on monocytes with a low expression of CD14 both in patients and in healthy subjects (1.4 and 1.27 times, respectively) (*Fig. 5*). Based on these data, it may be concluded that the direct relationship between the accumulation of gangliosides in monocytes in atherosclerosis and an increase in the number of rafts in the membranes of these cells is not obvious. We assumed that this ganglioside pool may be realized in the form of lipid rafts as a result of the differentiation of pre-activated monocytes in the arterial intima during the atherogenesis.

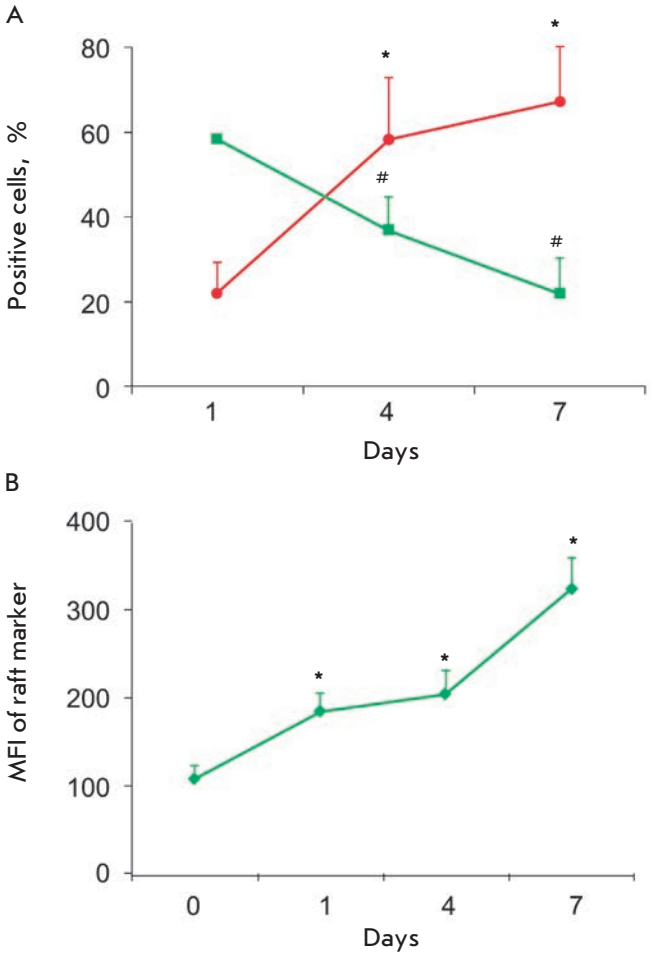

Fig. 6. Cytofluorometric analysis of the *in vitro* differentiation of cultured monocytes from healthy subjects. (A) Change in the proportion of $CD14^+/CD16^+$ (■) and $CD14^+/CD206^+$ cells (•) during the differentiation (n=3). *,#The differences are statistically significant between the 1st and the 4th day and the 1st and 7th day; (B) Change in the raft marker expression on $CD14^+/CD206^+$ cells during the differentiation (n=3). *The difference is significant between the reference point and 1st day, and the 1st and 7th day. Values are presented as M ± SD. *,#P<0.05

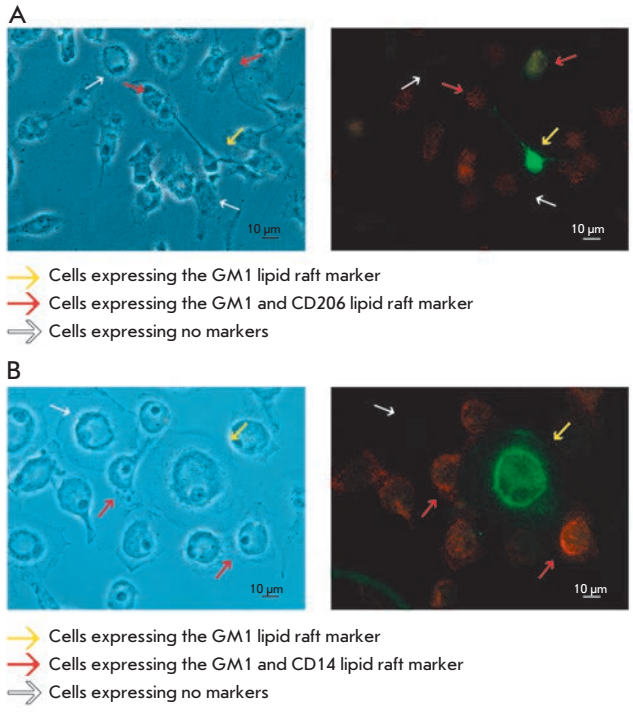

Fig. 7. Double immunofluorescence staining of cultured monocytes/macrophages from a healthy subject. Double staining with the cholera toxin B-subunit, which reveals GM1ganglioside, and monoclonal antibodies, which recognize the differentiation marker CD206 (A) or the monocyte/macrophage marker CD14 (B). The left images are obtained by phase contrast microscopy of the same cells. The length of the bar is 10 μm

Flow cytometry analysis of the membrane rafts of cultured monocytes/macrophages in healthy subjects. Previously, we observed a significant increase in the synthesis of gangliosides during the *in vitro* differentiation of human monocytes into macrophages [14]. We also found that the mRNA level of GM3 synthase (a key enzyme of the ganglioside synthesis) was significantly higher in cultured monocytes/macrophages than in freshly isolated monocytes and in the intima of an atherosclerotic plaque compared to the intima of unaffected regions of the human aorta [30]. It should be noted that macrophages are the main cells in the intima of the atherosclerotic arteries, whereas they are actually absent in the normal intima.

This study demonstrated, using the flow cytometry analysis of cultured monocytes of healthy subjects, a reduction in the proportion of $CD14^+/CD16^+$ cells and an increase in the proportion of $CD14^+/CD206^+$ cells (*Fig. 6A*), which indicates a differentiation of monocytes into macrophages [30]. Increasing MFI of rafts by 2 times as early as after 24 h and by 3 times on the 7th day of culturing compared to freshly isolated monocytes (*Fig. 6B*) was revealed by triple staining with antibodies to CD14 and CD206 (macrophage differentiation marker) and the fluorescently labeled cholera toxin B subunit.

These findings, in conjunction with our earlier results [13, 14, 30], indicate a probable relationship between biosynthesis activation and, as a consequence, an increase in the level of gangliosides and a higher

expression of lipid rafts in cultured macrophages compared to freshly isolated monocytes. An increasing amount of data confirms that monocytes are already pre-activated, circulating before their migration to inflammation areas during inflammatory pathologies accompanied by an increased production of cytokines, such as TNF-α, M-CSF, or IL-6 [10–12]. In this regard, it seems likely that the previously found accumulation of gangliosides in the activated monocytes of atherosclerotic patients [13] is necessary for the formation of membrane rafts after the infiltration of monocytes into the vascular wall intima with their subsequent differentiation into macrophages.

In previous studies, we found, using methods of immunocytochemistry with specific antibodies to the main ganglioside of monocytes/macrophages, that the intima of human atherosclerotic lesions contains a large number of cells with a high expression of this ganglioside. The study of the phenotype of these cells demonstrated that the majority of them were macrophages [31,32].

A study of the expression of differentiation and lipid raft markers using double staining of monocytes/macrophages revealed that a significant portion of $CD14^+$/$SD206^+$ cells was raft-positive (*Figs. 7A* and *B*). A small number of cells of different morphologies with a high expression of the raft marker were present at all stages of culturing. Among these cells, cells expressing and non-expressing markers of macrophages were present.

CONCLUSION

The flow cytometry study based on a single strategy of gating monocyte subsets demonstrated that three monocyte subsets (classical, intermediate, and non-classical) can be identified in the peripheral blood of both atherosclerotic patients and healthy subjects. In patients with atherosclerosis, an increase in the proportion of the intermediate subset ($CD14^{++}$/$CD16^+$) and a decline in the proportion of the classical subset ($CD14^{++}$/$CD16^-$) of monocytes were observed compared to healthy subjects. In them, the monocytes of the intermediate subset were characterized by a higher expression of the fractalkine receptor CX3CR1 compared to healthy subjects. The monocytes of patients and healthy subjects did not differ in the expression of membrane rafts. However, $CD14^{++}$ monocytes differed from $CD14^+$ monocytes by a higher expression of rafts. In addition, the so-called non-gate classical ($CD14^{++}$/$CD16^-$) and intermediate ($CD14^{++}$/$CD16^+$) monocyte subsets were identified in both of the studied groups, with the latter subset having a higher expression of the raft marker. During culturing of monocytes/macrophages in the presence of M-CSF, their activation with further differentiation accompanied by a threefold increase in the expression of membrane rafts occurred. In conjunction with our previous data, it may be concluded that the accumulation of gangliosides, which are essential components of rafts, in pre-activated monocytes of atherosclerotic patients did not result in an increase in the expression of membrane rafts. However, the data obtained in this work suggest that during the differentiation of monocytes into macrophages, an accumulated pool of gangliosides is realized in macrophages in the form of the rafts required for activating the adhesion and phagocytosis. ●

The authors are grateful to Prof. Yu.A. Romanov (Russian Cardiology Research and Production Complex of the Ministry of Health of the Russian Federation) for help with the flow cytometry analysis.

This work was supported by the Russian Foundation for Basic Research (grants 10-04-00888a and 12-04-31639).

REFERENCES

1. Zawada A.M., Rogacev K.S., Rotter B., Winter P., Marell R.R., Fliser D., Heine G.H. // Blood. 2011. V.118. № 12. P. 50-61.
2. Ancuta P., Liu K.Y., Misra V., Wacleche V.S., Gosselin A., Zhou X., Gabuzda D. // BMC Genomics. 2009. V. 10. P. 403-422.
3. Ziegler-Heitbrock L., Hofer T.P.J. // Frontiers in Immunology. 2013. V. 4. P. 1-5.
4. Hristov M., Schmitz S., Nauwelaers F., Weber C. // J. Immunol. Methods. 2012. V. 38. № 1. P. 9-13.
5. Merino A., Buendia P., Martin-Malo A., Aljama P., Ramirez R., Carracedo J. // J. Immunol. 2011. V.186. № 3. P. 1809-15.
6. Wong K.L., Yeap W.H., Tai J.J., Ong S.M., Dang T.M., Wong S.C. // Immunol. Res. 2012. V. 53. № 1-3. P. 41-57.
7. Tabas I., Williams K.J., Borén J. // Circulation. 2007. V. 116. № 16. P. 1832-44.
8. Zawada A.M., Rogacev K.S., Schirmer S.H., Sester M., Böhm M., Fliser D., Heine G.H. // Immunobiology. 2012. V. 217. № 12. P. 1273-84.
9. Gleissner C.A., Leitinger N., Ley K. // Hypertension. 2007. V. 50. № 2. P. 276-283.
10. Murphy A.J., Woollard K.J., Hoang A., Mukhamedova N., Stirzaker R. A., McCormick S.P., Remaley A.T., Sviridov D, Chin-Dusting J. // Arterioscler. Thromb. Vasc. Biol. 2008. V. 28. № 11. P. 2071-2077.
11. Ziegler-Heitbrock H.W., Fingerle G., Ströbel M., Schraut W., Stelter F., Schütt C., Passlick B., Pforte A. // Eur. J. Immunol. 1993. V. 23. № 9. P. 2053-2058.
12. Luu N.T., Madden J., Calder P.C., Grimble R.F., Shearman C.P., Chan T., Tull S.P., Dastur N., Rainger G.E., Nash G.B.// Atherosclerosis. 2007. V. 193. № 2. P. 259-268.
13. Gracheva E.V., Samovilova N.N., Golovanova N.K., Andreeva E.R., Andrianova I.V., Tararak E.M., Prokazova N.V.

// Biochemistry (Moscow). 2007. V. 72. № 3. P. 948-954 (In Russian).
14. Gracheva E.V., Samovilova N.N., Golovanova N.K., Piksina G.F., Shishkina V.S., Prokazova N.V. // Biomed. Khim.. 2013. V. 59. №. 4. P. 459-468 (In Russian).
15. Schmitz G., Orsó E. // Curr. Opin. Lipidol. 2002. V. 13. № 5. P. 513-521.
16. Sonnino S., Mauri L., Chigorno V., Prinetti A. // Glycobiology. 2007. V. 17. № 1. P. 1R-13R.
17. Hollenberg M., Fishman P.H., Bennet V., Cuatrecasas P. // Proc. Nat. Acad. Sci. 1974. Vol. 71. № 10. P. 4224-4228.
18. Parton R.G., Richards A.A. // Traffic. 2003. V. 4. № 11. P. 724–738.
19. Moreno-Altamirano M.M.B., Aguilar-Carmona I., Sánchez-García F.J. // Immunology. 2007. V. 120. №4. P. 536-43.
20. Hristov M., Weber C. // Thromb Haemost. 2011. V. 106. № 5. P. 757-62.
21. Weber C., Belge K.U., von Hundelshausen P., Draude G., Steppich B., Mack M., Frankenberger M., Weber K.S., Ziegler-Heitbrock H.W. // J. Leukoc. Biol. 2000. V. 67. № 5. P. 699-704.
22. Pandzić Jaksić V., Gizdić B., Miletić Z., Ostović K.T., Jaksić O. // Coll. Antropol. 2010. V. 34. № 1. P. 319-25.
23. Ancuta P., Rao R., Moses A., Mehle A., Shaw S.K., Luscinskas F.W., Gabuzda D. // J. Exp. Med. 2003. V. 197. № 12. P. 1701-1707.
24. Koenen R.R., Weber C. // EMBO Mol. Med. 2011. V. 3. № 12. P. 713-725.
25. Zilber M.T., Setterblad N., Vasselon T., Doliger C., Charron D., Mooney N., Gelin C. // Blood. 2005. V. 106. № 9. P. 3074-3081.
26. Pfeiffer A., Boettcher A., Orso E., Kapinsky M., Nagy P., Bodnar A., Spreitzer I., Liebisch G., Drobnik W., Gempel K., et al. // Eur. J. Immunol. 2001. V. 31. № 11. P. 3153–3164.
27. Cuschieri J., Sakr S., Bulger E., Knoll M., Arbabi S., Maier R.V. // Shock. 2009. V. 32. № 6. P. 572-577.
28. Triantafilou M., Triantafilou K. // J. Endotoxin Res. 2003. V. 9. № 5. P. 331-335.
29. Triantafilou M., Morath S., Mackie A., Hartung T., Triantafilou K. // J. Cell Sci. 2004. V. 117. № 17. P. 4007–4014.
30. Gracheva E.V., Samovilova N.N., Golovanova N.K., Kashirina S.V., Shevelev A., Rybalkin I., Gurskaya T., Vlasik T.N., Andreeva E.R., Prokazova N.V. // Mol. Cell Biochem. 2009. V. 330. № 1-2. P. 121-129.
31. Bobryshev Y.V., Lord R.S., Golovanova N.K., Gracheva E.V., Zvezdina N.D., Sadovskaya V.L., Prokazova N.V. // Biochim. Biophys. Acta. 1997. V. 1361. № 3. P. 287-294.
32. Bobryshev Y.V., Lord R.S., Golovanova N.K., Gracheva E.V., Zvezdina N.D., Prokazova N.V. // Biochim. Biophys. Acta. 2001. V. 1535. № 2. P. 87-99.

Hct-A Is a New Actinoporin Family from the *Heteractis Crispa* Sea Anemone

E. V. Leichenko*, M. M. Monastirnaya, E. A. Zelepuga, E. S. Tkacheva, M. P. Isaeva, G. N. Likhatskaya, S. D. Anastyuk, E. P. Kozlovskaya
Elyakov Pacific Institute of Bioorganic Chemistry, Far Eastern Branch of the Russian Academy of Sciences, 100 Let Vladivostoku Prosp., 159, Vladivostok, 690022, Russia
*E-mail: 969844@gmail.com
Received 25.09.2014

ABSTRACT **Several new actinoporin isoforms with molecular weights of 18995.5 to 19398.7 Da exhibiting a high hemolytic activity were isolated from the tropical sea anemone *Heteractis crispa* using a combination of liquid chromatography techniques. The actinoporins were demonstrated to occur as mono-, di-, and trimers in aqueous solutions. The sequences of the genes encoding actinoporins were identified, and the amino acid sequences of the new polypeptides belonging to the Hct-A actinoporin family were obtained. The new acinoporins differ in their isoelectric points, the number and localization of charged amino acid residues at the functionally important N-terminal fragment of the molecule, as well as in the charge of a tetrapeptide (amino acid residues 74–77) involved in an electrostatic interaction with the cytoplasmic membrane. A recombinant actinoporin, rHct-A2, with a molecular weight of 19141 Da, pI of 9.64, and hemolytic activity of 4.0×10^4 HU/mg, was obtained. The conductivity of the ion channels formed by rHct-A2 in the BLM was demonstrated to be similar to that of the native actinoporin from *H. crispa*. The obtained data expand knowledge on the structural and functional relationships of actinoporins and contribute to our understanding of the functioning mechanism of these molecules, which is the basis for the development of compounds with a high biomedical potential. Currently, they are considered as models for obtaining antitumor, antibacterial, and cardiac-stimulating agents.**
KEYWORDS **sea anemone; actinoporins; hemolytic activity; lipid membrane conductivity; structural and functional analysis.**
ABBREVIATIONS **PFT – pore-forming toxins; BLM – bilayer lipid membrane; aa – amino acid residue; GST – glutathione S-transferase; IPTG – isopropyl-β-D-1-thiogalactopyranoside.**

INTRODUCTION

The reason for the close attention paid by researchers to sea anemones, marine coelenterates, is their toxins that are complex mixtures of biologically active compounds of a protein nature. Neurotoxins (modulators of Nav, ASICs and Kv ion channels), proteinase inhibitors differing in their structure and mechanism of action, and actinoporins belonging to the α-pore-forming toxin (α-PFT) family are of great interest for future use as pharmacological agents [1–3]. Actinoporins have a unique spatial structure that allows them to exist both in the water-soluble and in membrane-bound states and determines their ability to bind to sphingomyelin-containing membranes and to form ion channels or pores in them [4]. A wide range of pharmacological activities exhibited by these polypeptides, such as anti-tumor, anti-parasitic, dermatonecrotic, and cardiac stimulatory [5–7] activities is associated with the pore formation. It was found that EqtII actinoporin from *Actinia equina* at a concentration of 0.1–1 nM has a cardiotoxic effect, but at higher concentrations it stimulates platelet aggregation [8]. Tenebrosins (actinoporins from *A. tenebrosa*) at low concentrations (~ 10^{-9} M) were demonstrated to also act as cardiac stimulants [9]. EqtII and Bc2 actinoporins from *Bunodosoma caissarum* [10] were found to be effective anticancer agents affecting fibrosarcoma and glioblastoma [11]. Recently, using HeLa, THP-1, MDA-MB-231, and SNU-C4 cells, we demonstrated that RTX-A actinoporin from *Heteractis crispa*, at nontoxic concentrations, exhibits antitumor effect and suppresses the epidermal-growth-factor-induced tumor transformation of JB6P+Cl41 mouse epithelial cells [7]. This effect was found to be due to the induction of p53-independent apoptosis and inhibition of the activity of the oncogenic nuclear factors AP-1 and NF-κB.

In recent years, α-pore-forming toxins from sea anemones have been used to develop pharmaceutical drugs on the basis of immunoconjugates of actinoporins with ligands, such as monoclonal antibodies, hormones,

or growth factors, whose action is directed at the cytoplasmic membranes of tumor and/or parasitic cells [6]. In this regard, investigation of the molecular basis of the actinoporin pharmacological effects seems to be of interest.

This work continues the structural and functional studies of actinoporins. It describes the isolation of actinoporins from the *H. crispa* sea anemone, identification of the sequences of the genes encoding them, production of recombinant analogues, and investigation of some aspects of the mechanism for interaction of actinoporins with biological targets.

EXPERIMENTAL

Reagents from the following companies were used in the study: Reanal, Hungary; Whatman, UK; ICN Biochemicals, Sigma, Invitrogen, and Thermo Scientific, USA; Fermentas, Lithuania; Merk, Germany; Kriohrom, SibEnzyme, Helicon, and Evrogen, Russia.

Biological material

H. crispa sea anemones were collected in the intertidal zone of the South China Sea during a scientific expedition on the Akademik Oparin research vessel in 2007. The species of the sea anemone were identified by E.E. Kostina (Institute of Marine Biology, Far Eastern Branch of the Russian Academy of Sciences, Vladivostok, Russia). The sea anemone samples were frozen and stored at −20 ˚C.

Isolation and purification of polypeptides

Preparation of an aqueous extract and precipitation of the total fractions of water-soluble proteins with acetone (63%) were performed as described previously [12]. All manipulations were performed at 4 ˚C.

Ion exchange chromatography of the polypeptides was performed on a CM-32 cellulose column (2.6 × 50 cm) equilibrated with a 0.01-M ammonium acetate buffer, pH 6.0, with a linear concentration gradient of NaCl (0–0.5 M, total volume of 2 L) in the working buffer. The elution rate was 20 mL/h; the fraction volume was 5 mL.

Gel filtration of the polypeptides was conducted on a Superdex Peptide 10/30 column equilibrated with a 0.1-M ammonium acetate buffer, pH 6.0, using FPLC (AKTA System Pharmacia, Sweden). Elution was performed at a rate of 3 mL/min. The fraction volume was 1.5 mL.

HPLC of the polypeptides was performed on a Nucleosil C_{18} reversed phase column (4.6 × 250 mm) equilibrated with 10% acetonitrile in 0.1% trifluoroacetic acid using an Agilent 1100 chromatograph (Agilent Technologies, USA). Elution was performed with a concentration gradient of acetonitrile from 10 to 90% in 0.1% trifluoroacetic acid at pH 2.2 for 60 min. The elution rate was 0.5 mL/min. A Concentrator 5301 vacuum concentrator (Eppendorf, Germany) was used for the evaporation of acetonitrile.

The protein concentration was determined by the Lowry method [13]; bovine serum albumin was used as a standard.

Cloning of actinoporin genes

cDNA was synthesized based on the total mRNA isolated from tentacles of the *H. crispa* sea anemone [14]. Nucleotide sequences encoding mature actinoporins were amplified using the gene-specific primers 5'-TCGTTACc/aATGATA-3' (*hct_sign*) and 5'-GATTCTCTATTTGTCTTC-3' (*hct_notransl*) constructed with the Vector NTI 8 software (Invitrogen, USA) based on the sequences of known actinoporin genes. The primers were synthesized at Evrogen (Moscow, Russia). PCR was performed on a GeneAmp® PCR System 2700 thermocycler (Applied Biosystems, USA) under the following conditions: 94 ˚C for 5 min; followed by 28 cycles of 94 ˚C for 30 s, 59 ˚C for 45 s, and 72 ˚C for 45 s; followed by 72 ˚C for 15 min. PCR fragments (650 bp) were isolated from agarose gel with a DNA Extraction Kit (Thermo Scientific, USA) and cloned into pTZ57R/T using a T/A cloning system (Thermo Scientific, USA). Recombinant plasmids were transformed into DH5 *Escherichia coli* cells. Clones were selected using moderately blue selection on a LB medium containing X-Gal and IPTG. The presence of a desired insert in selected clones was determined by colony PCR with standard primers.

Determination and analysis of nucleotide and amino acid sequences

Plasmid DNA was isolated by the alkaline lysis method [15]. Determination of the nucleotide sequences of inserts was performed on an ABI3130xl genetic analyzer (Applied Biosystems, USA) [16]. The nucleotide and deduced amino acid sequences were analyzed using the Vector NTI 8 software package (Invitrogen, USA).

Expression of actinoporin genes

To generate an expression construct, an actinoporin encoding a DNA fragment was amplified using Vent DNA polymerase (SibEnzyme, Russia) and the gene-specific primers: *hct-a(f)* (5'-GGCTTTAGCTGGTACAATTATCGCGGGTGCA-3') and *hct-a(r)* (5'-CCCCAAGCTTAGCGTGAGATCTTAATTTGCAGTAT-3'). To preserve the endopeptidase site and to insert correctly the gene into the pET-41a(+) vector (Novagen, USA), the 5'-end of the forward primer was added with dGMP, and the reverse primer was introduced with the restriction site

for HindIII, combined with the stop codon, and with four additional nucleotides for efficient restriction enzyme activity. PCR was conducted under the following conditions: 94 ˚C for 5 min; then 30 cycles of 94 ˚C for 30 s, 65 ˚C for 45 s, and 72 ˚C for 45 s; followed by 72 ˚C for 15 min. pTZ57R/T with the *hct-a2* gene insert was used as the template. The PCR fragment was treated with the HindIII restriction enzyme and cloned into the pET-41a(+) vector at the PshAI and HindIII restriction sites. Recombinant plasmids were isolated and sequenced. Plasmids with the correct insert were used to transform Rosetta (DE3) *E. coli* cells by electroporation on a Multiporator device (Eppendorf, Germany). The transformed cells were cultured in a 2xYT medium containing antibiotics kanamycin (50 μg/mL) and chloramphenicol (34 μg/mL) overnight, after which the culture was grown in a volume of 100 mL until a absorbance A_{600} = 0.5–0.6. To induce expression, IPTG was added (Fermentas, Lithuania) to the final concentration of 0.1 mM and the cells were further grown at 30 ^{0}C for 3 h to obtain a fusion protein in soluble form. The cells were then centrifuged (8000 rpm) and washed with a 1× PBS buffer.

Isolation of recombinant actinoporin

Cells containing the fusion protein were re-suspended in 1× PBS (1 : 5 by volume) and sonicated on a Sonopuls HD 2070 device (Bandelin Electronic, Germany) to destroy the cell membrane. After centrifugation (10000 rpm), the cell lysate was loaded onto a Ni^{2+}-CAM agarose, incubated for 10 min (4 ^{0}C) with constant stirring for the binding of the fusion protein to the carrier. To remove cell lysate proteins, Ni^{2+}-CAM agarose with the fusion protein was washed with a buffer solution (50 mM NaH_2PO_4, 300 mM NaCl, 10 mM imidazole, pH 8.0) and then with an enteropeptidase reaction buffer solution (20 mM Tris-HCl, 50 mM NaCl, 2 mM $CaCl_2$, pH 8.0). The fusion protein was added with enteropeptidase (New England BioLabs, UK) in the amount of 1 enzyme unit per 20 μg of the fusion protein, and the mixture was incubated at room temperature with constant stirring overnight. After sedimentation of Ni^{2+}-CAM agarose by centrifugation at 3000 rpm, the recombinant actinoporin containing the fraction was collected and incubated with STI agarose to remove enteropeptidase.

Electrophoretic analysis

Electrophoresis was performed according to the Laemmli method [17] in vertical plates (9 × 12 × 1 mm) in a 15% polyacrylamide gel in the presence of 0.1% sodium dodecyl sulfate (SDS). Molecular weights were estimated using a PageRuler™ Unstained protein ladder (a set protein markers, 10–200 kDa, (Fermentas, Lithuania)).

Mass spectrometric analysis

The molecular weights of the polypeptides were determined on an Ultraflex III TOF/TOF (time of flight) mass spectrometer (Bruker Daltonics, Germany). Time of flight mass spectra was recorded in the linear and reflector modes.

Hemolytic activity

The hemolytic activity was detected in mouse erythrocytes in a medium containing 0.9% NaCl. The hemoglobin level in the supernatant was measured spectrophotometrically at 540 nm after preliminary rapid cooling of the reaction mixture and its centrifugation to precipitate erythrocytes and their shadows. The amount of protein causing 50% hemolysis of red blood cells in 1 mL of 0.7% suspension at 37 ˚C for 30 min was taken as one hemolytic unit (HU).

The results processed according to the variation statistics rules using the MS Office Excel 2007 software package are presented as the mean values of six independent experiments ± standard deviation. The statistical significance of the differences among the indicators was assessed by the ANOVA one parameter test.

Determination of the N-terminal amino acid sequence

The amino acid sequence of the recombinant actinoporin N-terminal fragment was determined on a Procise 492 cLC automatic solid-phase protein sequencer (Applied Biosystems, USA) according to the manufacturer's program using a protein sample on the PVDF membrane. The recombinant protein was transferred from a polyacrylamide gel to a 0.45 μm PVDF membrane (Millipore, USA) in a buffer solution containing 25 mM Tris, 192 mM glycine, 20% methanol, 0.1% SDS, pH 8.3, at 26 V and 60 mA, overnight, using a Mini Trans-Blot® camera (Bio-Rad, USA). The membrane was stained with 0.04% Coomassie Brilliant Blue G-250 in 10% (by volume) glacial acetic acid and then washed free of dye with 50% (by volume) methanol and dried in a thermostat at 37 ˚C.

Preparation of bilayer lipid membranes

Bilayer lipid membranes (BLMs) were formed on the 0.25 mm aperture of a Teflon cup by the Muller method [18] using a 1% solution of monoolein in n-heptane containing predetermined concentrations of sphingomyelin. Aqueous phase: 0.1 M or 1 M NaCl, 10 mM Hepes, pH 7.5. Actinoporins RTX-A (5 ng/mL) and Hct-A2 (50 ng/mL) were added to the aqueous phase until the BLM formation.

Measurement of BLM electrical characteristics

The current through the BLM was measured by a VK2-16 high resistance voltmeter-electrometer in

the membrane voltage clamp mode using silver/silver chloride electrodes (asymmetry potential of 2.3 mV). Current recording at the amplifier output was performed by means of a KPS-4 potentiometer.

Homology modeling of actinoporins

Actinoporins spatial structure models were generated by homology modeling using the SWISS-MODEL web server [19] and Swiss-PdbViewer software [20]. The spatial structure of StnII sticholysin (PDB ID 1GWY) [21] from the *Stichodactyla helianthus* sea anemone, received from the Protein Data Bank, was used as a prototype in constructing the model [22]. Evaluation of the electrostatic properties of the molecular surface in the Amber ff12 force field and visualization of the structures were performed using the MOE software [23].

RESULTS AND DISCUSSION

According to published data, native actinoporins are usually isolated from the aqueous extracts of whole animals and their further purification is carried out by a combination of various methods of liquid chromatography [4, 12, 24, 25]. In this study, to isolate individual actinoporins, their precipitation from an aqueous extract of the *H. crispa* (=*Radianthus macrodactylus*) sea anemone with acetone and separation of the components of the total protein sample by cation exchange chromatography, FPLC gel filtration, and RP-HPLC were used.

Figure 1A presents the elution profile of the total protein sample obtained by chromatography on CM-32 cellulose. The polypeptides of fraction 2 had a high hemolytic activity, and those of the fractions 1 and 3 had a lower activity. The fraction 2 polypeptides were rechromatographed under the same conditions. Subsequent purification of actinoporins was performed by gel filtration (*Fig. 1B*). In result the hemolitic active fractions containing 50 to 500 μg of the protein were obtained. According to the electrophoretic analysis, these fractions contained polypeptides with a molecular weight of about 19–20 kDa. The polypeptides of fractions 1–3 were subjected to reverse phase HPLC on a Nucleosil C_{18} column (*Figs. 1C–E*, respectively). Based on this, both fractions of the homogeneous polypeptides (*Fig. 1D*) and fractions containing several polypeptides (*Figs. 1C, E*) with a molecular weight of 18995.5 to 19398.7 Da, according to the mass spectrometric analysis, were obtained. Obviously, actinoporins in the combined fractions are presented as multiple isoforms with very similar physicochemical properties, which is likely the reason for the peak broadening during chromatographic separation of polypeptides.

Previously, from *H. crispa*, we isolated and characterized actinoporins RTX-A, RTX-S, and RTX-SII as well as identified the sequences of the genes and deduced amino acid sequences for 18 actinoporins of the Hct-S family that contain the N-terminal serine residue [12, 14, 25, 26]. The experimental values of the molecular weights of the isolated actinoporins range from 18995.5 to 19398.7 and are consistent with the calculated values for the Hct-S family (from 19338 to 19518 Da) that indicates the existence of many actinoporin isoforms not only at the genomic or transcriptomic, but also at the translational levels. The presence of lower intensity signals in the regions of 38543 and 57950 m/z in the mass spectra demonstrates that actinoporins exist in aqueous solutions likewise in the form of dimers and/or trimers, respectively, which is consistent with the experimental data obtained previously for StnII from *S. helianthus* [27].

It should be noted that the absence of the first two N-terminal amino acid residues is a distinctive feature of the primary structure of RTX-A actinoporin isolated from *H. crispa* (19273 Da) [12]. According to the calculated molecular weights of actinoporins of the Hct-S family (from 19338 to 19518 Da) and the values determined for actinoporins by MALDI TOF mass spectrometry (18995.5 to 19398.7 Da), the existence of another family of actinoporins with smaller molecular weights and, probably, with an alanine residue at the N-terminus of the molecule, may be assumed.

Cloning of actinoporin genes

To determine the sequences of the genes encoding mature actinoporins of the *H. crispa* sea anemone, the forward (*hct_sign*) and reverse (*hct_notransl*) primers were constructed. The *hct_sign* primer was constructed on the basis of the signal sequence analysis of known actinoporins, and the gene-specific reverse *hct_notransl* primer was constructed on the basis of previously obtained information on the 3'-untranslated region of *rtx-a* and *rtx-sii* from *H. crispa* [28].

With the use of PCR, cloning, sequencing, and analysis of PCR fragments, 17 sequences of the actinoporin genes were obtained, five of which encoded actinoporins of the new Hct-A family (Hct-A2–Hct-A6), and 12 were actinoporins of the Hct-S family established by us previously (*Fig. 2*) [26]. The identity of the nucleotide sequences ranged from 93 to 99%, and that of amino the acid sequences ranged from 88 to 99%. Hct-A2–Hct-A4, Hct-S3, Hct-S5, and Hct-S6 were the most represented.

The calculated molecular weights of the actinoporins of the Hct-A and Hct-S families ranged from 19158 to 19518 Da, which corresponds to the native actinoporins from *H. crispa*, *A. equina*, *S. helianthus*, *H. magnifica*, and *Phyllodiscus semoni* [12, 24–32]. All members of

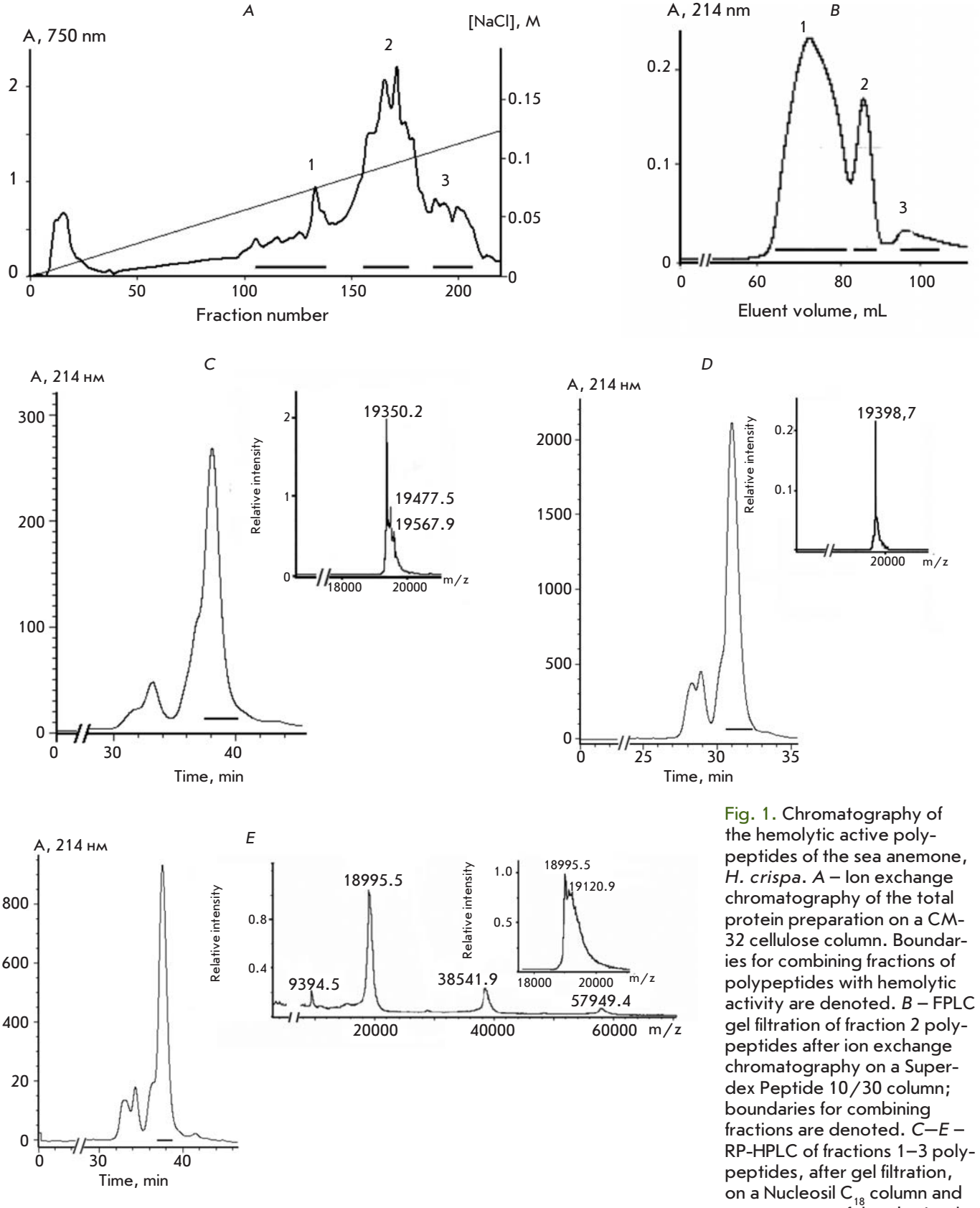

Fig. 1. Chromatography of the hemolytic active polypeptides of the sea anemone, *H. crispa*. *A* – Ion exchange chromatography of the total protein preparation on a CM-32 cellulose column. Boundaries for combining fractions of polypeptides with hemolytic activity are denoted. *B* – FPLC gel filtration of fraction 2 polypeptides after ion exchange chromatography on a Superdex Peptide 10/30 column; boundaries for combining fractions are denoted. *C*–*E* – RP-HPLC of fractions 1–3 polypeptides, after gel filtration, on a Nucleosil C_{18} column and mass spectra of the obtained compounds

```
                β1          α1             β2            β3                  β4   β5                 β6
                SSS HHH  HHHHH HHHHH       SSSSSSSSS     SSSSSS SS S         SS   SS SSSSSS          SSSSS
                 10         20         30         40         50         60         70         80         90
RTX-A       --ALAGAIIA GASLTFQILD KVLAELGQVS RKIAIGIDNE SGGSWTAMNA YFRSGTTDVI LPEFVPNQKA LLYSGRKNRG PDTTGAVGAL
Hct-A2      --....T... ....G..... ...G...K.. ......V... .......L.. .......... .......... .......DT. .VA....A.F
Hct-A3      --....T... ....G..... ...G...K.. ....V..... .......L.. .......... .......... .......DT. .VA....A.F
Hct-A4      --....T... ......K... E..G...K.. ....V.V... .......L.. .......... .......... .......... .EA....A.F
Hct-A6      --....T... ......K... E..G...K.. ....V.A... .......L.. .......... .......... .......... .EA....A.F
Hct-A5      --....T... ......K... E..G...K.. ....V.V... .......L.. .......... .......... .......... .EA....A.F
Hct-S3      SA....T..E ....G..... ...G...K.. ......V... .......L.. .......... .......... .......DT. .VA....A.F
Hct-S5      SA....T... ......K... E..G...K.. ....V.V... .......L.. .......... .......... .......... .EA....A.F
Hct-S6      SA....T... ......K... E..G...K.. ....V.V... .......L.. .......... .......... .......... .EA....A.F
Hct-S7      SA....T.TE ....G..... ...G...K.. ......V... .......L.. .......... .......... .......DT. .VA....A.F
HMgIII      SA....T..E ....G..... ...G...K.. ....V.V... .......L.. .......... .......... .......DT. .VA....A.F
StnI        -SE...T..D ......EV.. ...G...K.. ....V..... ...T...L.. .......... ...V...T.. .......SS. .VA....A.F
StnII       --....T... .......V.. ...E...K.. ....V..... ...T...L.. .......... .......T.. .......DT. .VA....A.F
EqtII       SADV...V.D ....S.D..K T..EA..N.K ....V.V... ..KT...L.T ......S.IV ..HK..HG.. ...N.Q.D.. .VA.....V
EqtIV       SV.V.....K ..A...NV.Q T..KA..DI. ....V.V... ..KT...L.T ......S.IV ..HK..HG.. ...N.Q.D.. .VA.....V.
EqtV        SV.V.....K ..A...NV.Q T..KA..DI. ....V.V... ..KT...L.T ......S.IV ..HK..HG.. ...N.Q.D.. .VA.....V.

                β7                  β8                α2          β9    β10        β11          β12
            SSSS   SSS SSSSSS          SSSSS SSS      H HHHHHHH      SS    SS SSSSS  SSS SSSS    SS SSSSSS
                    100        110        120        130        140        150        160        170        180
RTX-A       AYYMSNGNTL GVMFSVPFDY NLYSNWWDVK VYSGKRRADQ AMYEDLYY-S NPYRGDNGWH QKNLGYGLKM KGIMTSAGEA IMEIRISR- [175]
Hct-A2      .......H.. .......... .F........ .......... G....M..-G .......... ........RV .......... .LQ.K...- [175]
Hct-A3      .......H.. .......... .F........ .......... G....M..-G .......... ........R. R......... .LQ.K...- [175]
Hct-A4      .....D.... .......S.. .......... I......... G....M..-G .......... .......... .......... .LQ.K...- [175]
Hct-A6      .....D.... .......... .......... I......... ........-G .......... .......... .......... .LQ.K...- [175]
Hct-A5      .....D.... .......... .......... I......... ........-G .......... .......... .......... .LQ.K...- [175]
Hct-S3      .......H.. .......... .F........ .......... G....M..-G .......... ........R. .......... .LQ.K...- [177]
Hct-S5      .....D.... .......... .......... I......... ........-G .......... .......... .......... .LQ.K...- [177]
Hct-S6      .....D.... .......... .......... I......... ........-G .......... .......... .......... MLQ.K...- [177]
Hct-S7      .......H.. .......... .F........ .......... G....M..-G .......... ........R. .......... .LQ.K...- [177]
HMgIII      .......H.. .......... .F........ .......... G....M..-G .......... ........R. .......... .LQ.....- [177]
StnI        .......... .......... .W........ I.P....... G....M..-G .........Y ........R. .......... K.Q.K...- [176]
StnII       .....S.... .......... .W........ I......... G.......-G .......... E.......R. .......... K.Q.K...- [175]
EqtII       ..L..D.... A.L....Y.. .W.....N.R I.K....... R...E...NL S.F....... TR.......S R.F.N.S.H. .L..HV.KA [179]
EqtIV       ..A..D.... A.L....Y.. .W.....N.R IFK.R..... R...Q...YL S.F....... ERH......S R.F.N.G.Q. .L..HVTKA [179]
EqtV        ..A..D.... A.L....Y.. .W.....N.R IFK.R..... R...Q...YL S.F....... ERH......S R.F.N.G.Q. .L..HVTKA [179]
```

Fig. 2. Multiple alignment of actinoporin amino acid sequences. RTX-A, RTX-SII, Hct-As, and Hct-Ss are actinoporins of *H. crispa*; HMgIII is magnificalysin of *Heteractis magnifica* (Swiss-Prot, Q9U6X1); StnI and StnII are sticholysins of *S. helianthus* (Swiss-Prot, P81662, P07845); EqtII, EqtIV, and EqtV are equinatoxins of *A. equina* (Swiss-Prot, P61914, Q9Y1U9, Q93109). Identical residues are marked by points; the length of α-helices and β-strands corresponds to the StnII structure and is denoted by H and S, respectively

the Hct-A and Hct-S families are highly basic polypeptides; the calculated values of their isoelectric points are in the range of 9.10–9.74, which is typical of actinoporins from *H. crispa*, as well as of the majority of well-known members of actinoporins from other species of sea anemones.

According to the obtained data, a number of actinoporin isoforms encoded by multigene families are synthesized in the tentacle tissue of *H. srispa* as well as the sea anemones *A. equina* [29, 33], *H. magnifica* [34], and *S. helianthus* [24, 35]. Actinoporins differ by single amino acid substitutions (*Fig. 2*), most of which are located in the functionally important amphiphilic N-terminal fragment of the molecule (1–27 aa) that is involved in the pore formation and is associated with the β-core by the highly charged S/KRK30 loop [21, 28, 36]. All actinoporins are characterized by a high conservation of amino acid residues within the aromatic phosphorylcholine (POC) membrane binding site (104–137 aa) as well as the Lys77 residue localized in the loop connecting the β5- and β6-strands (76–79 aa). This residue, as demonstrated for EqtII, is involved in the monomers oligomerization [37].

In silico analysis of charged amino acid residues in the area of interaction of actinoporins with the membrane

To date, it has been established that the molecular mechanism of pore formation is based on the electrostatic attraction between a positively charged actinoporin molecule and the oppositely charged cytoplasmic membrane and on the specific interaction between the POC binding site and the phosphorylcholine head of sphingomyelin [5, 21, 28, 36]. Subsequent conforma-

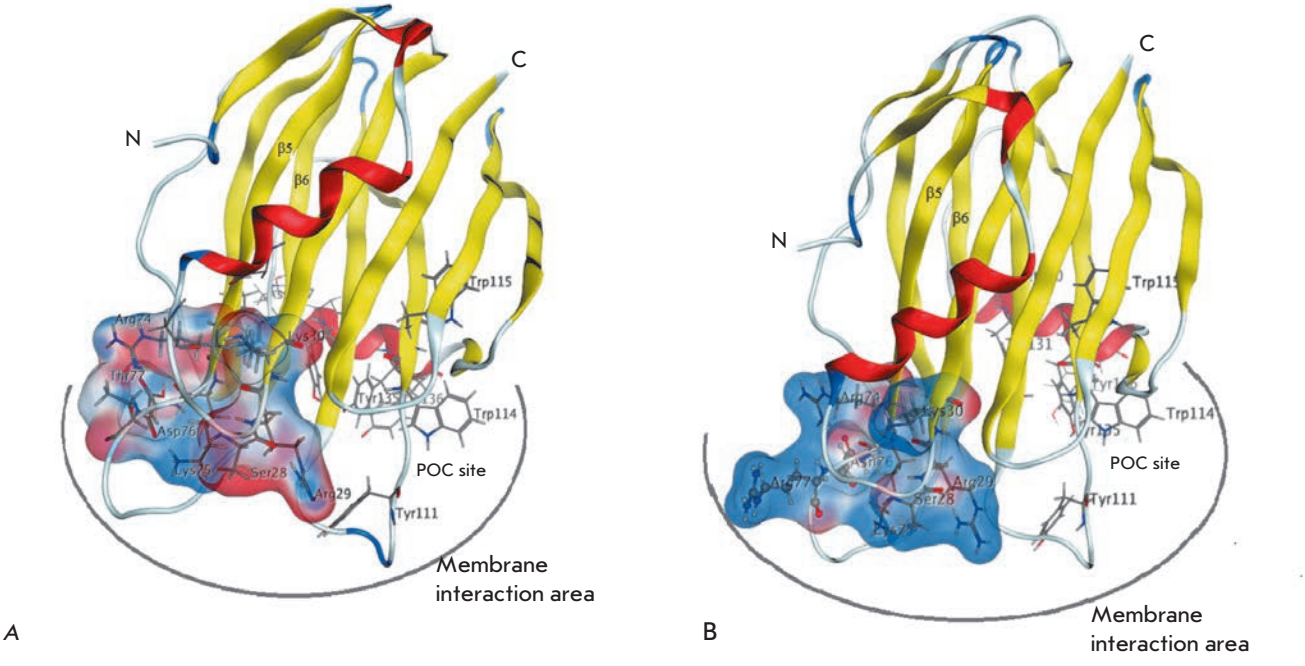

Fig. 3. Spatial structure models of Hct-A2 and Hct-A6 actinoporins. The spatial structure models of Hct-A2 (*A*) and Hct-A6 (*B*) actinoporins are presented as a ribbon diagram and colored according to the secondary structure elements. The amino acid residues forming the POC binding site and "pseudorigid" 28SRK30 loop as well as residues with a charged side chain in the loop connecting the β5- and β6-strands are presented as a sticks; the amino acid residues Arg77 and Asn76 of the Hct-A6 actinoporin are presented as a ball-and-sticks. The variable regions of the molecular surface are colored according to electrostatic properties: positively charged residues are in blue, and negatively charged ones are in red. Visualization was performed using the MOE software [23]

tional rearrangement of the N-terminal fragment of the molecule leads first to its transition to the water-lipid interface and then to its inclusion into the membrane hydrophobic core. The process is accompanied by oligomerization of three, or four, or nine monomer molecules [27, 38–40].

To determine the localization of the functionally important sites of actinoporins of the Hct-A family (Hct-A2–Hct-A6), models of their spatial structures were built. The crystal structure of StnII (PDB, 1gwyA) with the highest resolution of 1.71 Å (sequence identity ranging from 90.29 to 99.43%) was used as a prototype. The resulting 3D actinoporin structure models contain 12 β-strands, which form the β-core, and two α-helices located at the N- and C-termini of the molecule. The antiparallel β-strands are connected to each other and to the α-helices by different-length loops (*Fig. 3*), which are included into the membrane interface during the pore formation [40]. The RMSD value for 175 Cα atoms of the model relative to the prototype was 0.27 Å.

In this study, an analysis of variations in charged residues in the area of interaction of the actinoporins with the membrane was performed. Mapping the molecular surface of these molecules with the changes in their electrostatic properties demonstrated that despite high conservation of the location of charged residues in the structure of the actinoporins, the 74–83 loop connecting the β5- and β6-strands contains a variable region (*Figs. 2* and *3*). According to cryoelectron microscopy, this loop is localized, like the POC binding site, on the surface of the contacts between the actinoporins and the lipid interface and plays an important role both in the recognition and in interaction with the membrane [21]. Substitution of the neutral Thr residue with the positively charged Arg residue at position 77 and the negatively charged Asp with Asn at position 76 in three members of the Hct-A4–Hct-A6 family was demonstrated to increase significantly the positive charge density in this region (*Fig. 3*). In our opinion, this should lead to a strong electrostatic interaction of both this loop and the adjacent, highly charged, "pseudorigid" SRK loop (28–30 aa) with the membrane surface. Obviously, these are electrostatic interactions that facilitate, in turn, the conformational reorganization of the N-terminal fragment and its subsequent dislocation and integration into the membrane.

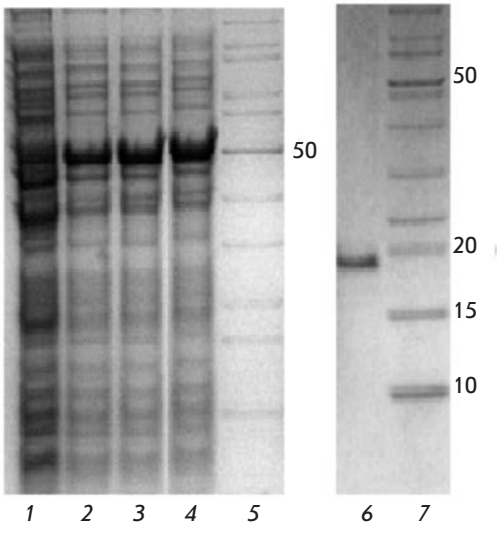

Fig. 4. Electrophoregrams of cell lysate proteins after expression of pET41a(+)-*hct-a2* without addition of IPTG (*1*); after expression of pET41a(+)-*hst-a2* with addition of IPTG at concentrations of 0.1, 0.5, and 1.0 mM (*2–4*, respectively); and the recombinant rHct-A2 actinoporin (*6*); *5*, *7* – molecular weight markers, kDa

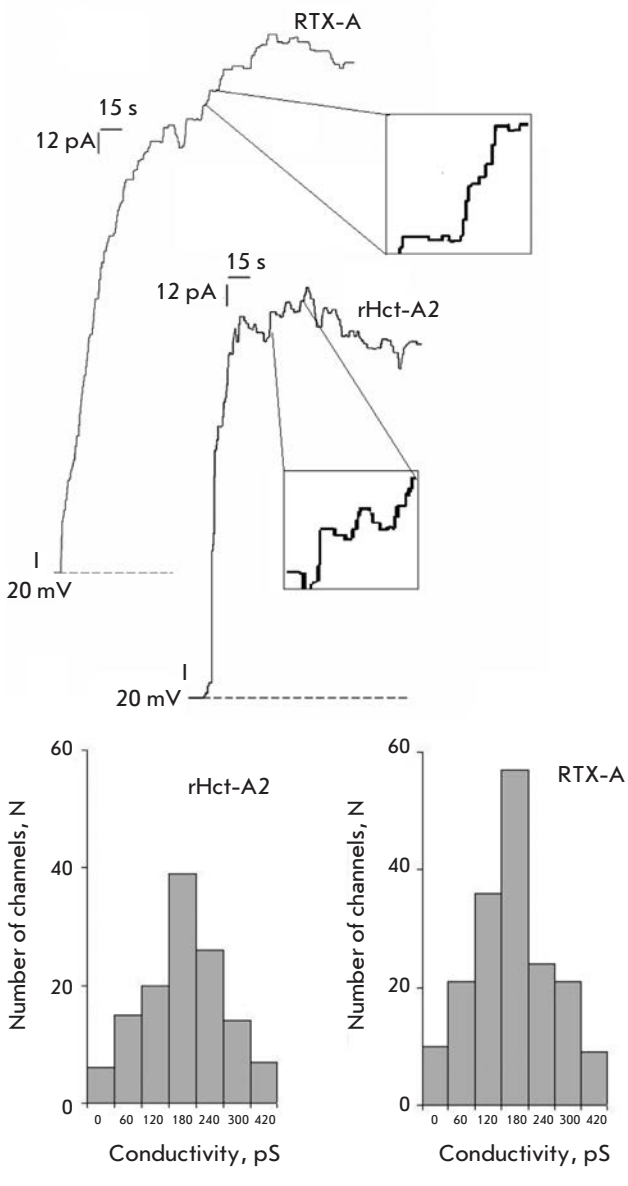

Fig. 5. The results of the analysis of the channel-forming activity of actinoporins on the BLM. A – BLM conductivity induced by actinoporins from *H. crispa*: rHct-A2 (50 ng/mL) and RTX-A (5 ng/mL). The membrane potential is 20 mV. *B* – conductivity histograms of membranes modified with rHct-A2 and RTX-A actinoporins

Obtaining of recombinant actinoporin and study of its properties

A large number of actinoporin isoforms in a single producer species creates certain difficulties in producing homogeneous polypeptides in an amount sufficient in order to conduct structural and functional studies. In order to obtain individual actinoporins, conditions for the expression of their genes in a bacterial system were selected and a scheme of their isolation in the recombinant form was developed.

To generate a construct expressing the actinoporin gene, the pET system was chosen; in particular, the pET-41a(+) plasmid vector designed for *E. coli* expression of target proteins fused with a carrier protein, glutathione S-transferase (GST). Based on the sequences of genes encoding mature actinoporins of the Hct-A family, the gene-specific primers *hct-a(f)* and *hct-a(r)* flanking the *hct-a2* gene at the 5'- and 3'-termini, respectively, were constructed. The recombinant pTZ57R plasmid containing the *hct-a2* gene was used as a template for PCR. A 550 bp fragment was obtained using PCR that was inserted into the plasmid at the PshAI and HindIII sites. Recombinant plasmids with the desired insert were used to transform the Rosetta (DE3) *E. coli* strain. The recombinant actinoporin was obtained as a GST-fused protein with a polyhistidine tag (GST–His6–rHct-A2). According to the electrophoretic analysis, the molecular weight of the fusion protein was slightly above 50 kDa (*Fig. 4*), which is consistent with the calculated data (~52 kDa). GST–His6–rHct-A2 was also detected in the culture medium, but in smaller quantities. IPTG concentration of 0.1–1.0 mM had practically no effect on the recombinant protein yield. The recombinant rHct-A2 actinoporin with a molecular weight of approximately 20 kDa was isolated from the

cell lysate by affinity chromatography under native conditions (*Fig. 4*). The actinoporin yield was 4 mg/L, on average. The N-terminal amino acid sequence (15 aa) was determined by sequencing that fully corresponded to that deduced from the nucleotide sequence. The calculated molecular weight of rHct-A2 was 19141 Da, and the isoelectric point was 9.64. The hemolytic activity of rHct-A2 was 4.0×10^4 HU/mg, which is comparable to that of actinoporins both from *H. crispa* [12, 25, 26] and from other species of sea anemones [4, 5, 9, 24, 29].

Based on the analysis of the recombinant actinoporin channel activity on the monoolein : sphingomyelin (1 : 3) BLM, it was found that rHct-A2 at a concentration of 50 ng/mL causes discrete current fluctuations in the membrane, which indicates the formation of conductive structures in the membrane – ion channels (*Fig. 5A*). The most probable conductivity value of the rHct-A2-induced channels in 0.1 M NaCl at pH 7.5 was 180 ± 30 pS, which corresponds to the conductivity of the channels formed by native RTX-A (*Fig. 5B*).

CONCLUSION

According to pharmacological studies of actinoporins, their biological activity is determined by a nonspecific effect that leads to an increase in the membrane permeability, which can stimulate a variety of toxic effects in cells. In fact, an increase in the actinoporin-induced cell permeability leads to profound changes in the morphology of the cell and its organelles, cell fragmentation [5], as well as to an increase in cell size and to cell death [41, 42]. Structural and functional studies of actinoporins, as well as many other toxins, are ultimately aimed at determining their pharmacological activity and therapeutic potential. Currently, α-PFTs of sea anemones are considered as models for the designing of anticancer, antibacterial, and cardiac-stimulating agents [43, 44]. These natural, unique compounds may find successful application as pharmaceuticals (or the basis for developing drugs) in a combined therapy of cancer diseases and/or various cardiac and cytological pathologies. ●

The authors are grateful to the members of the Pacific Institute of Bioorganic Chemistry, Far Eastern Branch of the Russian Academy of Sciences, O.V. Chernikov for sequencing of the N-terminal amino acid sequence and K.V. Guzev for sequencing of the nucleotide sequences.

This work was supported by the Far East 42P comprehensive program of basic research of the Far Eastern Branch of the Russian Academy of Sciences. Obtaining and investigation of the properties of recombinant actinoporin were performed using funds from the Russian Science Foundation (project 14-25-00037).

REFERENCES

1. Parker M.W., Feil S.C. // Prog. Biophys. Mol. Biol. 2005. V. 88. № 6202. P. 91–142.
2. Chi V., Pennington M.W., Norton R.S., Tarcha E.J., Londono L.M., Sims-Fahey B., Upadhyay S.K., Lakey J.T., Iadonato S., Wulff H., et al. // Toxicon. 2012. V. 59. № 4. P. 529–546.
3. Frazão B., Vasconcelos V., Antunes A. // Mar. Drugs. 2012. V. 10. № 8. P. 1812–1851.
4. Turk T.J. // Toxicol. Toxin. Rev. 1991. V. 10. P. 223–262.
5. Anderluh G., Maček P. // Toxicon. 2002. V. 40. № 2. P. 111–124.
6. Tejuca M., Anderluh G., Dalla Serra M. // Toxicon. 2009. V. 54. № 8. P. 1206–1214.
7. Fedorov S., Dyshlovoy S., Monastyrnaya M., Shubina L., Leychenko E., Kozlovskaya E., Jin J.-O., Kwak J.-Y., Bode A.M., Dong Z., et al. // Toxicon. 2010. V. 55. № 4. P. 811–817.
8. Batista U., Maček P., Sedmak B. // Cell Biol. Int. Rep. 1990. V. 14. № 11. P. 1013-1024.
9. Norton R.S., Bobek G., Ivanov J.O., Thomson M., Beer E.F., Mortiz R.L., Simpson R.J. // Toxicon. 1990. V. 28. № 1. P. 29–41.
10. Migues P.V., Leal R.B., Mantovanni M., Nicolau M., Gabilan N.H. // NeiroReport. 1999. V. 10. № 1. P. 67-70.
11. Soletti R.C., Alves T., Vernal J., Terenzi H., Anderluh G., Borges H.L., Gabilan N.H., Moura-Neto V. // Anticancer Res. 2010. V. 30. № 4. P. 1209–1215.
12. Monastyrnaya M.M., Zykova T.A., Apalikova O.V., Shwets T.V., Kozlovskaya E.P. // Toxicon. 2002. V. 40. № 8. P. 1197–1217.
13. Lowry O.H., Rosebrough N.J., Fearr A.L., Randall R.J. // J. Biol. Chem. 1951. V. 193. № 1. P. 265–275.
14. Il´ina A., Lipkin A., Barsova E., Issaeva M., Leychenko E., Guzev K., Monastyrnaya M., Lukyanov S., Kozlovskaya E. // Toxicon. 2006. V. 47. № 5. P. 517–520.
15. Sambrook J., Russel D.W. Molecular cloning. Laboratory Manual. 3rd ed. New York: Cold Spring Harbor Laboratory Press, 2001. P. 1.31–1.58.
16. Sanger F., Nicklen S., Coulson A.R. // Proc. Natl. Acad. Sci. USA. 1977. V. 74. № 12. P. 5463-5467.
17. Laemmli U.K. // Nature. 1970. V. 227. № 5259. P. 680–685.
18. Muller P., Rudin D.O., Tien H.T., Wescott W.C. // J. Phys. Chem. 1963. V. 67. P. 534-535.
19. Guex N., Peitsch M.C. // Electrophoresis. 1997. V. 18. № 15. P. 2714–2723.
20. Guex N., Peitsch M.C., Schwede T. // Electrophoresis. 2009. V. 30. Suppl 1. P. S162–173.
21. Mancheño J.M., Martín-Benito J., Martínez-Ripoll M., Gavilanes J.G., Hermoso J.A. // Structure. 2003. V. 11. № 11. P. 1319–1328.
22. http://www.rcsb.org/
23. Molecular Operating Environment (MOE), 2013.08; Chemical Computing Group Inc., 1010 Sherbooke St. West, Suite #910, Montreal, QC, Canada, H3A 2R7, 2014.

24. Lanio M.E., Morera V., Alvarez C., Tejuca M., Gómez T., Pazos F., Besada V., Martínez D., Huerta V., Padrón G., et al. // Toxicon. 2001. V. 39. № 2–3. P. 187–194.
25. Klyshko E.V., Issaeva M.P., Monastyrnaya M.M., Il´ina A.P., Guzev K.V., Vakorina T.I., Dmitrenok P.S., Zykova T.A., Kozlovskaya E.P. // Toxicon. 2004. V. 44. № 3. P. 315–324.
26. Tkacheva E.S., Leychenko E.V., Monastyrnaya M.M., Issaeva M.P., Zelepuga E.A., Anastyuk S.D., Dmitrenok P.S., Kozlovskaya E.P. // Biochemistry. 2011. V. 76. № 10. P. 1387–1397.
27. Alegre-Cebollada J., Cunietti M., Herrero-Galán E., Gavilanes J.G., Martínez-del-Pozo A. // J. Mol. Biol. 2008. V. 382. № 4. P. 920-930.
28. Monastyrnaya M., Leychenko E., Issaeva M., Likhatskaya G., Zelepuga E., Kostina E., Trifonov E., Nurminski E., Kozlovskaya E. // Toxicon. 2010. V. 56. № 8. P. 1299-1314.
29. Maček P., Lebez D. // Toxicon. 1981. V. 19. № 2. P. 233–240.
30. Anderluh G., Pungerčar J., Štrukelj B., Maček P., Gubenšek F. // Biochem. Biophys. Res. Commun. 1996. V. 220. № 2. P. 437–442.
31. Samejima Y., Yanagisaws M., Aoki-Tomomutsu Y., Iwasaki E., Ando J., Mebs D. // Toxicon. 2000. V. 38. № 2. P. 259–264.
32. Nagai H., Oshiro N., Takuwa-Kuroda K., Iwanaga S., Nozaki M., Nakajima T.A. // Biosci. Biotechnol. Biochem. 2002. V. 66. № 12. P. 2621–2625.
33. Wang Y., Yap L.L., Chua K.L., Khoo H.E. // Toxicon. 2008. V. 51. № 8. P. 1374–1382.
34. Anderluh G., Križaj I., Štrukelj B., Gubenšek F., Maček P., Pungerčar J. // Toxicon. 1999. V. 37. № 10. P. 1391–1401.
35. Blumenthal K.M., Kem W.R. // J. Biol. Chem. 1983. V. 258. № 9. P. 5574–5581.
36. Kristan K., Podlesek Z., Hojnik V., Gutierrez-Aguirre I., Gunčar G., Turk D., Gonzalez-Manas J.M., Lakey J.H., Maček P., Anderluh G. // J. Biol. Chem. 2004. V. 279. № 45. P. 46509–46517.
37. Anderluh G., Barlič A., Potrich C., Macek P., Menestrina G. // J. Membrane Biol. 2000. V. 173. № 1. P. 47-55.
38. Mechaly A.E., Bellomio A., Gil-Cartón D., Morante K., Valle M., González-Mañas J.M., Guérin D.M. // Structure. 2011. V. 19. № 2. P. 181-191.
39. Bakrač B., Gutiérrez-Aguirre I., Podlesek Z., Sonnen A.F.-P., Gilbert R.J.C., Macek P., Lakey J.H., Anderluh G. // J. Biol. Chem. 2009. V. 283. № 27. P. 18665–18677.
40. Rojko N., Kristan K.C., Viero G., Zerovnik E., Maček P., Dalla Serra M., Anderluh G. // J. Biol. Chem. 2013. V. 288. № 33. P. 23704–23715.
41. Zorec R., Tester M., Maček P., Mason W.T. // J. Membrane Biol. 1990. V. 118. № 3. P. 243–249.
42. Meunier F.A., Frangez R., Benoit E., Ouanounou G., Rouzaire-Dubois B., Suput D., Molgo J. // Toxicon. 2000. V. 38. № 11. P. 1547-1560.
43. Lewis R.J., Garcia M.L. // Nat. Rev. Drug Discov. 2003. V. 2. № 10. P. 790–802.
44. Takagi J. // Biochem. Soc. Transactions. 2004. V. 32. № 3. P. 403–406.

Acipensins – Novel Antimicrobial Peptides from Leukocytes of the Russian Sturgeon *Acipenser gueldenstaedtii*

O. V. Shamova[1,3], D. S. Orlov[1,3], S. V. Balandin[2,4], E. I. Shramova[2], E. V. Tsvetkova[3], P. V. Panteleev[2], Yu. F. Leonova[2], A. A. Tagaev[2], V. N. Kokryakov[1,3], T. V. Ovchinnikova[2,4,*]

[1]Institute of Experimental Medicine, Northwest Branch of the Russian Academy of Medical Sciences, Academician Pavlov Street, 12, Saint-Petersburg 197376, Russia

[2]Shemyakin and Ovchinnikov Institute of Bioorganic Chemistry, Russian Academy of Sciences, Miklukho-Maklaya Street, 16/10, Moscow 117997, Russia

[3]Saint-Petersburg State University, Universitetskaya Embankment, 7/9, Saint-Petersburg 199034, Russia

[4]Moscow Institute of Physics and Technology (State University), Department of Physicochemical Biology and Biotechnology, Institutskii Pereulok, 9, Dolgoprudny 141700, Moscow Region, Russia

*E-mail: ovch@ibch.ru

Received 11.10.2014

ABSTRACT **Antimicrobial peptides (AMPs) play an important role in the innate defense mechanisms in humans and animals. We have isolated and studied a set of antimicrobial peptides from leukocytes of the Russian sturgeon *Acipenser gueldenstaedtii* belonging to a subclass of chondrosteans, an ancient group of bony fish. Structural analysis of the isolated peptides, designated as acipensins (Ac), revealed in leukocytes of the Russian sturgeon six novel peptides with molecular masses of 5336.2 Da, 3803.0 Da, 5173.0 Da, 4777.5 Da, 5449.4 Da, and 2740.2 Da, designated as Ac1–Ac6, respectively. Complete primary structures of all the isolated peptides were determined, and the biological activities of three major components – Ac1, Ac2, and Ac6 – were examined. The peptides Ac1, Ac2, Ac3, Ac4, and Ac5 were found to be the N-terminal acetylated fragments 1–50, 1–35, 1–49, 1–44, and 1–51 of the histone H2A, respectively, while Ac6 was shown to be the 62–85 fragment of the histone H2A. The peptides Ac1 and Ac2 displayed potent antimicrobial activity towards Gram-negative and Gram-positive bacteria (*Escherichia coli* ML35p, *Listeria monocytogenes* EGD, MRSA ATCC 33591) and the fungus *Candida albicans* 820, while Ac6 proved effective only against Gram-negative bacteria. The efficacy of Ac 1 and Ac2 towards the fungus and MRSA was reduced upon an increase in the ionic strength of the solution. Ac1, Ac2, and Ac6, at concentrations close to their minimum inhibitory concentrations, enhanced the permeability of the *E.coli* ML35p outer membrane to the chromogenic marker, but they did not affect appreciably the permeability of the bacterial inner membrane in comparison with a potent pore-forming peptide, protegrin 1. Ac1, Ac2, and Ac6 revealed no hemolytic activity against human erythrocytes at concentrations of 1 to 40 μM and had no cytotoxic effect (1 to 20 μM) on K-562 and U-937 cells *in vitro*. Our findings suggest that histone-derived peptides serve as important anti-infective host defense molecules.**

KEYWORDS **innate immunity; antimicrobial peptides; sturgeon leukocytes; histone H2A derivatives; acipensin.**

ABBREVIATIONS **Ac – acipensin, AMP – antimicrobial peptides, CFU – colony forming units, EDTA – ethylenediaminetetraacetic acid, HNP – human neutrophil peptide (alpha-defensin), MIC – minimum inhibitory concentration, MRSA – methicillin resistant *Staphylococcus aureus*, ONPG – ortho-nitrophenyl β-*D*-galactopyranoside, PAGE – polyacrylamide gel electrophoresis, PBS – phosphate buffered saline, PCR – polymerase chain reaction, PG-1 – protegrin 1, SDS – sodium dodecyl sulfate, TFA – trifluoroacetic acid, TSB – trypticase soy broth; MALDI-TOF-MS – matrix-assisted laser desorption ionization time of flight mass spectrometry; Tris – tris (hydroxymethyl) aminomethane.**

INTRODUCTION

Antimicrobial peptides (AMPs) of the innate immune system play an essential role in the anti-infective protection of humans and animals [1]. These molecular factors of innate immunity are of particular importance in providing protective functions to lower vertebrates (fish, amphibians), because the system of adaptive immunity in poikilothermic animals cannot ensure a sufficiently rapid and effective response (antibody formation) to infection at a low temperature in the environment. Therefore, an investigation of the antimicrobial peptides of fish phagocytes and mucous coats is

important for explaning the biological role of this group of physiologically active substances in anti-infective immunity.

To date, the AMPs (defensins, cathelicidins, etc) of phagocytes and barrier epithelium of various mammals, birds, and amphibians have been described. Information on fish AMPs remains limited and mostly relates to investigation of the compounds isolated from the mucus, skin, gills, kidneys, spleen, and gastrointestinal tract [2]. For example, pleurocidins [3, 4], which are a group of linear antimicrobial peptides with an α-helix conformation and a positive charge of the molecule, were isolated from the mucus of the *Pleuronectes americanus* flounder. A peptide called pardaxin was isolated from the mucous secretions of another flounder species, *Pardachirus marmoratus* [5]. The peptide hepcidin containing four intramolecular disulfide bridges was isolated from the gills of the hybrid striped bass [6]. Later, hepcidins were found in other fishes. An antimicrobial peptide, misgurin, with broad-spectrum microbicidal activity was obtained from the skin mucus of the loach (mudfish) *Misgurnus anguillicaudatus* [7].

Peptides of the α-defensin family have not yet been found in fish. However, in recent years, data on β-defensins of bony fish have appeared: these peptides were found in epithelial cells of the digestive tract, gills, and spleen of the Chinese perch *Siniperca chuatsi* [8], in the liver of the orange-spotted grouper *Epinephelus coioides* [9], and in the skin and gills of the carp *Cyprinus carpio* L. [10]. Peptides of the cathelicidin family have been found in the rainbow trout and other salmon and cod species [11–15].

Peptides that are histone derivatives have been found in the skin and mucous coats of some fishes. For example, antimicrobial peptides that are N-terminal parts of histone H2A were isolated from the skin mucus of the Atlantic halibut (*Hippoglossus hippoglossus* L.) and the Amur catfish *Parasilurus asotus* and called hipposin [16] and parasin 1 [17], respectively. An antimicrobial protein (SAM) with a molecular weight of 20,734 Da that appeared to be histone H1 was isolated from the liver of the *Salmo salar* salmon [18].

Therefore, to date, a number of antimicrobial peptides have been described that were isolated from the mucous coats, skin, digestive tract, gills, liver, and spleen of fish. However, there is actually a scarcity of data on AMPs from fish blood leukocytes. Therefore, the aim of this study was to investigate the structural properties and biological activity of antimicrobial peptides from blood leukocytes of the Russian sturgeon *Acipenser gueldenstaedtii*, a member of the subclass Chondrostei, the oldest group of bony fish (Osteichthyes).

EXPERIMENTAL

Reagents

We used acrylamide, N,N'-methylene-bis-acrylamide (Sigma, USA), urea, sodium chloride, tris(hydroxymethyl)aminomethane, MTT (3-[4,5-dimethyl-2-thiazolyl]-2,5-diphenyl-2H-tetrazolium bromide), agarose, trypticase soy broth, trifluoroacetic acid, heptafluorobutyric acid, o-nitrophenyl-β-D-galactopyranoside (Sigma, USA); acetic acid (Vekton, Russia); media and sera for cell cultures (Biolot, Russia); Saburo medium (Pharmacotherapy Research Center, Russia); and enzymes and buffers for PCR and genetic engineering (Thermo Fisher Scientific, USA). Antimicrobial peptides were used as standards: chemically synthesized protegrin 1 kindly provided by Professor Robert Lehrer (University of California, Los Angeles, USA), human defensin HNP-1 and bactenecin 5 isolated from human and goat blood leukocytes, respectively, using the method described previously [19].

Isolation and purification of antimicrobial peptides from leukocytes of the Russian sturgeon

Blood from *A. gueldenstaedtii* sturgeons, caught in the Volga delta (Alexandrovskiy sturgeon plant), was stabilized by heparin and kept in vessels for 6 h for delamination, after which the buffy coat was pipetted off and washed twice with saline, followed by centrifugation at 400 g for 5 min. The resulting precipitate was homogenized. Extraction of proteins from the leukocyte-rich suspension was carried out in 20% acetic acid at 4 °C under magnetic stirring for 20 h. The homogenate was then centrifuged at 15,000 g for 1 h. The supernatant was collected and subjected to ultrafiltration through the YM-10 membrane using a device from Amicon (USA). The resulting material containing peptides and low-molecular-weight proteins with molecular weights under 10–12 kDa was concentrated to 1 mL by ultrafiltration through the YM-0.5 membrane and loaded onto an electrophoretic column (a sample was preliminarily added with urea to a concentration of 3 M) for separation of the proteins by preparative electrophoresis (EP). Preparative EP with continuous elution of proteins was performed in a 12.5% polyacrylamide gel (PAAG) in an acidic buffer system in the presence of urea [20] using a Bio-Rad cell (USA). Protein fractions eluted from the column were analyzed in the presence of sodium dodecyl sulfate [21] by analytical EP, which was carried out in PAAG plates on a Hoeffer device (USA). The solution absorbance of each fraction was measured at 280 nm, and the antimicrobial activity was determined. The fractions with antimicrobial activity were collected, and the peptides present in them were separated by means of several successive cycles of reverse phase

high-performance liquid chromatography (RP-HPLC) on a Gold System instrument (Beckman, USA) using Vydac C-18 columns (4.6 × 250 mm; 10 × 250 mm, the diameter of sorbent particles was 5 μm), eluting peptides with the gradient of acetonitrile concentration using different counterions (0.1% trifluoroacetic acid or 0.13% heptafluorobutyric acid). The fractions obtained by RP HPLC were lyophilized by centrifugation under vacuum using a SpeedVac device (Savant, USA). Evaluation of the purity was performed by analytical EP, MALDI TOF mass spectrometry, and analytical RP HPLC. The protein concentration in the extracts from sturgeon leukocytes and in the purified peptide samples was determined by the Bradford method and the Wolf method using the following equation: peptide concentration (μg/mL) = $(A_{215} - A_{225}) \times 144$ [22].

Evaluation of peptide antimicrobial activity by radial diffusion in agarose gels

The antibiotic effect of the peptides isolated from leukocytes was measured by the method proposed by Lehrer *et al.* [23]. The antimicrobial activity of the samples towards a number of Gram-negative and Gram-positive bacteria, as well as one of the fungi, was determined. The following strains of bacteria were used: Gram-negative bacterium *Escherichia coli* ML-35p, Gram-positive bacteria: *Listeria monocytogenes* EGD and MRSA ATCC 33591 (methicillin resistant *Staphylococcus aureus*), and fungus *Candida albicans* 820. The bacteria were grown on a solid medium containing a 3% trypticase soy broth (Sigma, USA); the fungi were grown in a medium containing 3% Saburo. When *E. coli* ML-35P was cultured, the medium was supplemented with 100 μg/mL ampicillin and the medium for MRSA ATCC 33591 was supplemented with 6 μg/mL oxacillin. Microorganism strains were kindly provided by Professor Robert Lehrer (University of California, Los Angeles, USA).

The microorganisms were cultured for 16–18 h in a medium containing a 3% trypticase soy broth (TSB) solution at 37 ˚C. Bacterial suspension aliquots were taken from the resulting culture, transferred to the fresh 3% TSB solution, and incubated at 37 ˚C for 2.5 h to obtain microorganisms in the logarithmic growth phase. The overnight culture was used in experiments with the fungus *C. albicans*. Microorganism suspensions were further centrifuged at 400 g for 10 min, the precipitate was washed twice with a 10 mM sodium phosphate buffer (PBS), pH 7.4, and re-suspended in 3 mL of the same buffer. To prepare agarose gels containing microorganisms, the volume of the suspension with 4×10^6 cells was calculated [23]. The number of bacterial cells was evaluated by measuring the suspension optical density at 620 nm (it was assumed that the optical density of 0.2 corresponds to 5×10^7 CFU/mL). Another equation was used for fungi: the optical density of 1 at 450 nm corresponds to 2.86×10^7 CFU/mL [23]. The calculated amount of microorganism suspension was added to 8 mL of a sterile 1% agarose solution in a 10 mM sodium phosphate buffer (in some experiments, 100 mM NaCl), pH 7.4, at a temperature of 43 ˚C. The resulting mixture was poured into a sterile plastic Petri dish with a diameter of 90 mm, wherein the mixture was solidified to form an agarose gel. Holes with a diameter of 2 mm were perforated in the agarose gels. Wells were filled with the analyzed samples (serial (two-fold) dilutions of the peptides in a 0.01% aqueous acetic acid solution and a control, 0.01% acetic acid without peptides) and incubated at 37 ˚C for 3 h. During incubation, the peptides diffused from the wells into the agarose gels. After completing incubation, a 1% agarose solution containing a 6% trypticase soy broth was applied to the agarose gel surface. The dishes were then incubated for more 20 h at 37 ˚C. To quantify the peptide antibiotic activity, the diameter of the microbial growth inhibition zone around the wells was measured, taking 0.1 mm as the unit, and 20 units were subtracted, which corresponded to the well diameter, from the measured value. The minimum inhibitory concentration (MIC) was determined for each peptide by plotting the dependence of the peptide antimicrobial activity on their concentration. The value obtained for the intersection of the plot of the linear regression of each peptide with the X axis (peptide concentration in μM) was taken as the MIC. Two parallel samples were tested in each experiment. Experiments were performed in triplicate, and the arithmetic mean of the obtained MIC ± standard deviation was calculated.

Evaluation of the peptide's effect on the permeability of the outer and cytoplasmic membranes of *E. coli* ML35p

The *E. coli* ML35p strain used in this method is characterized by a lack of lactose permease (enzyme transporting lactose into the cell), with the synthesis of β-galactosidase in the bacterium cytoplasm being constitutive, not inducible as in most bacteria. Furthermore, the β-lactamase enzyme is present in the periplasmic space of *E. coli* ML35p [24]. The state of the cytoplasmic and outer membranes of *E. coli* ML35p was judged by their permeability to chromogenic markers, o-nitrophenyl-β-*D*-galactopyranoside (ONPG) and nitrocefin, which are substrates of β-galactosidase and β-lactamase, respectively. A modification of the previously described procedure was used [25]. If the medium surrounding the bacteria contains substrates of β-galactosidase or β-lactamase, the enzymatic reaction involving these substrates can occur only if they are able to penetrate through the bacterial membranes. If the outer

and cytoplasmic membranes of the bacteria, under the action of some damaging agent, such as an antimicrobial peptide, become permeable to the substrates, then the chromogenic products of substrate hydrolysis by intracellular enzymes pass into the incubation medium. The optical density of the medium at 496 or 420 nm (absorption maximum of the chromogenic products of hydrolysis of nitrocefin or ONPG, respectively) increases, which enables monitoring, in real time, of the process of damage to the outer and cytoplasmic membranes of the bacteria by the antimicrobial agent. Sample composition (100 μL): 2.5 mM ONPG or 20 μM nitrocefin; 2.5×10^7 CFU/mL of bacteria; 0.01 M Na-phosphate buffer, pH 7.4; 0.03% TSB; the peptides at a concentration that is equal to their minimum inhibitory concentration under these conditions and is measured by a standard colony count method. The controls contained equal volumes of the solvent (0.01% acetic acid) instead of preparations. The samples were added into the wells of a 96-well plate, and the solution absorbance was measured at 496 and 420 nm using a SpectraMax 250 spectrophotometer (Molecular Devices, USA) at 37 ˚C and under periodic shaking of the plates for 2 h. The data were processed with the Sigma Plot 11 software. The plots present the results of a typical experiment: each point is the average of two values obtained for duplicate samples. The experiments were performed in triplicate, and the curve pattern was similar for all three series.

Analysis of peptide hemolytic activity

Blood from healthy donors was collected in plastic tubes, using heparin as an anticoagulant and centrifuged at 250 g, 4 ˚C, for 10 min. The supernatant was removed, and the pellet was added with 10 mL of buffered saline (PBS), pH 7.4, with 4 mM EDTA and centrifuged at 250 g, 4 ˚C, for 10 min. The precipitate was washed 3 times with PBS using centrifugation as described above. 280 μL of the erythrocyte precipitate (the precipitate was assumed to be 100% red blood cells) was adjusted to 10 mL with cold PBS to obtain a 2.8% suspension. The analyzed samples were added with 27 μL of the erythrocyte suspension and 3 μL of the test peptide at various concentrations in PBS. To prepare a positive control (100% erythrocyte lysis), 27 μL of the erythrocyte solution was added with 3 μL of a surfactant (10% Triton X-100). To prepare a negative control (0% erythrocyte lysis), 27 μL of the erythrocyte solution was added with 3 μL of PBS. Samples in triplicate were incubated at 37 ˚C for 30 min, and the reaction was terminated by adding 75 μL of ice-cold PBS. The samples were centrifuged at 5,000 g, 4 ˚C, for 4 min, and the supernatant was collected and added to the wells of a 96-well plate (Corning, USA). The sample's optical densities at 540 nm were measured on a SpectraMax 250 spectrophotometer (Molecular Devices, USA). The erythrocyte hemolysis parameters were calculated as a percentage according to the equation:

$$\% \text{ Hemolysis} = ((A_{exper} - A_{control})/(A_{total} - A_{control})) \times 100\%,$$

where A_{exper} and $A_{control}$ are the supernatant absorbance obtained for treated with the peptides and untreated (0% lysis) erythrocytes, respectively, and A_{total} is the supernatant absorbance for red blood cells treated with Triton X-100 (100% lysis).

MTT test

The effect of the peptides on cell viability was examined by the MTT assay [26]. This test is based on the ability of dehydrogenases from living cells to reduce colorless forms of 3-(4,5-dimethylthiazol-2-yl)-2,5-diphenyltetrazolium bromide (MTT reagent) or 3-(4,5-dimethylthiazol-2-yl)-2,5-diphenyl-2H-tetrazolium bromide to a blue formazan crystal. The cultured cell lines K-562 (human erythroleukemia cells) and U-937 (human histiocytic lymphoma cells) were used in the experiments. The cell suspensions were placed into the wells of 96-well plates (Orange Scientific, Belgium) in a RPMI-1640 medium, 20,000 cells per well. The cells were added with 10 μL of a peptide solution (in RPMI-1640 medium) at various concentrations in quadruplicate. Control samples were added with 10 μL of the medium instead of the peptides. The plates were then placed in a CO_2 incubator for 20 h. Three hours before the end of incubation, the plate wells were added with 10 μL of the MTT solution (5 mg/mL in PBS). After incubation, the wells were added with 100 μL of isopropanol with 0.04 M HCI, stirred, and the optical density of the solution in plate wells was measured at 540 nm (subtracting the absorbance at 690 nm as a background) on a Spectra Max 250 spectrophotometer (Molecular Devices, USA). The significance of the differences between groups was evaluated using the Wilcoxon-Mann-Whitney U-test. In all calculations, the 95% confidence level ($P<0.05$) was considered as significant.

Mass Spectrometry

The molecular weights of the isolated peptides were determined on a Reflect III MALDI-TOF mass spectrometer (Bruker, Germany) equipped with a UV-laser with a wavelength of 336 nm. 2,5-dihydroxybenzoic acid (Sigma, Germany) in 20% acetonitrile and 0.1% TFA at a concentration of 10 mg/mL was used as a matrix.

Determination of the N-terminal amino acid sequence

The amino acid sequence was determined by using a Procise cLC 491 protein sequencing system (Applied

Biosystems, USA). The phenylthiohydantoin derivatives of amino acid residues were identified on a 120A PTH analyzer (Applied Biosystems, USA).

Deblocking of N-terminal amino acid residues

Deacylation of the N-terminal acetylserine residue was performed according to the procedure in [27] on an inert carrier, Immobilon, used for automatic protein sequencing. A peptide sample was applied to Immobilon, placed in a 500 μL test tube, damped with 30 μL of 25% TFA solution, and then incubated in a sealed test tube at 45 ˚C for 4 min. Peptide-coated Immobilon was dried in an open test tube at 20 ˚C for 5 min and at 45 ˚C for another 10 min and then incubated in a sealed test tube at 45 ˚C for 72 h. The resulting sample was used for automated sequencing of the peptide.

Isolation of genomic DNA

Sturgeon tissue fragments were incubated in the TNES buffer (10 mM Tris-HCl, pH 7.5; 400 mM NaCl; 100 mM EDTA, 0.6% SDS) with 10 mg/mL proteinase K at 55 ˚C for 16 h. After centrifugation at 12,000 g for 10 min, the supernatant was added with a 0.25 volume of 5M NaCl and DNA was precipitated by adding one volume of 95% ethanol. The precipitate was washed with 80% ethanol, dried in an open test tube, and dissolved in water. Then, a single purification of DNA was performed with the phenol : chloroform mixture (1 : 1, v/v); the remaining phenol was extracted with an equal volume of chloroform, and DNA was precipitated with 95% ethanol.

Amplification of nucleotide sequences

To amplify an internal region of the sturgeon histone H2A gene, degenerate primers №1 (ATGTGTGGACG(A,C)GG(C,T)AA(A,G)AC(A,C,T)GG) and №2 (GTCTTCTTGGG(C,G)AG(C,T)AG(C,T)AC(G,T)GCC) were used. PCR was performed with a stepwise reduction in temperature at the stage of primer annealing: 94 ˚C – 1 min; 5 × (94 ˚C – 30 s, 61 ˚C – 40 s, 68 ˚C – 60); 5 × (94 ˚C – 30 s, 58 ˚C – 40 s, 68 ˚C – 60); 30 × (94 ˚C – 30 s, 55 ˚C – 40 s, 68 ˚C – 60 s).

Prior to inverse PCR, the sturgeon genomic DNA was treated with BglII restrictase. Composition of the reaction mixture: 1 × buffer O (Thermo Fisher Scientific), 50 ng/μL DNA, 40 units of BglII (Thermo Fisher Scientific). The reaction was conducted in a volume of 50 μL at 37 ˚C for 16 h. The reaction products were diluted 25 times with water (2 ng/μL of DNA), followed by the ligation reaction conducted in the presence of 10 mM ATP at 4 ˚C for 16 h. Then, DNA was precipitated with 95% ethanol: the precipitate was dissolved in water and used as a template for inverse PCR.

Inverse PCR was conducted using two primer pairs in two stages. At the first stage, primers №3 (GAGCACAGCGGCCAGATAGA) and №4 (CTGAAATCCTGGAGCTGGC) and the following amplification program were used: 94 ˚C – 5 min; 35 × (94 ˚C – 30 s, 58 ˚C – 60 s, 72 ˚C – 120 s). The resulting product was diluted with water (1:100) and used as a template for nested PCR with primers №5 (CACGCTGGGCATAGTTTCC) and №6 (GAATCATCCCGCGTCACCTG) under the following conditions: 94 ˚C – 5 min; 35 × (94 ˚C – 30 s, 62 ˚C – 60 s, 72 ˚C – 120 s).

Cloning and sequencing of PCR products

PCR products were eluted from low-melting-point agarose and ligated into the pGEM-T vector at sticky T/A ends (Promega, USA). Manipulations with recombinant DNA were performed according to the reference procedures [28]. Competent cells of the *Escherichia coli* DH-10B strain (Life Technologies, USA) were used for transformation. The plasmid DNA was isolated by alkaline lysis. DNA sequencing was performed using the ABI PRISM BigDye Terminator v. 3.1 reagent kit, followed by an analysis of the reaction products on a 3730 DNA Analyzer automatic sequencer (Applied Biosystems, USA).

Statistical analysis of results

Data obtained in the study of peptide antimicrobial activity are presented as an arithmetic mean ± standard deviation. The arithmetic mean was calculated based on three independent experiments, each of which was performed in duplicate. The data were processed with the Statistica 6 software.

RESULTS

Structural study of AMPs from leukocytes of the Russian sturgeon

To isolate the antimicrobial peptides from Russian sturgeon leukocytes, a procedure for isolation and purification was used that involved acid extraction of proteins and peptides from leukocytes, ultrafiltration, preparative EP, and reverse-phase high-performance liquid chromatography [29]. The use of this set of methods yielded six purified AMPs with molecular weights of 5,448.8 Da, 5,336.0 Da, 5,174.0 Da, 4,777.6 Da, 3,804.0Da, and 2,741.7 Da determined using MALDI TOF mass spectrometry, with the three peptides with molecular weights of 5,336.0 Da, 3,804.0 Da, and 2,741.7 Da accounting for the predominant peptide fractions. The described isolation procedure was repeated several times using the blood leukocytes of sturgeons that were caught at different times and were of different ages and genders, with each cycle of isolation resulting in a similar spectrum of the antimicrobial peptides. In some

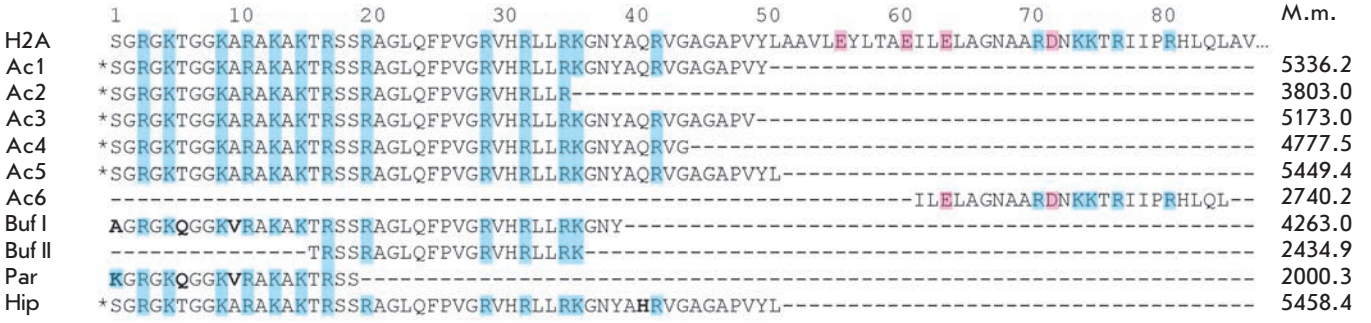

Fig. 1. The structure of acipensins and related AMPs. Histone H2A N-terminal amino acid sequence (*A. gueldenstaedtii*) and Ac1–Ac6 acipensins are presented. Buf I and Buf II – buforins I and II (*Bufo bufo gargarizans*); Par – parasin 1 (*Parasilurus asotus*); Hip – hipposin (*Hippoglossus hippoglossus* L.). The asterisk (*) denotes acetylated N-terminal amino acid residues. M.m. – calculated molecular weights of AMPs, Da. Lys and Arg residues are highlighted with blue; Asp and Glu residues are highlighted with pink. The single amino acid differences between AMP sequences and sturgeon histone H2A are shown in bold

experiments, during preparation of the leukocyte-rich suspension and extraction, the serine protease inhibitor, phenylmethylsulfonyl fluoride, was used which did not lead to a significant change in the spectrum of the isolated antimicrobial peptides. The objectives of this study included the structural analysis of the selected peptides and investigation of their biological activity.

A partial N-terminal amino acid sequence of the isolated peptides was established by automated microsequencing. In some cases, sequencing was possible after the chemical reaction of deblocking of the N-terminal amino acid residues. Removal of the acetyl group of the N-terminal acetylserine residue was carried out in an acidic medium using a 25% solution of TFA. After the removal of the acetyl protection, the N-terminal amino group was easily modified with phenylisothiocyanate, which allowed stepwise degradation of the peptides by the Edman method using a Procise cLC 491 protein sequencing system and identification of the obtained phenylthiohydantoin derivatives of the amino acid residues.

The analysis of the N-terminal peptide sequences from the Russian sturgeon *Acipenser guldenstaedtii*, which we named acipensins 1–5, using the BLAST software (http://blast.ncbi.nlm.nih.gov/Blast.cgi) demonstrated that they were the N-terminal fragments of a histone of the H2A family, while another peptide, acipensin 6, was a fragment of the central part of the histone molecule of the same family. These AMPs constitute the dominant part of acid-soluble peptides with antimicrobial activity from sturgeon leukocytes.

To determine the complete primary structure of the acipensins, cloning and sequencing of encoding nucleotide sequences was performed. It is known that the genes of canonical histones, which are most widely present in eukaryotic cells, lack introns, and that their mRNAs lack the 3'-terminal polyA sequence [30]. Only mRNAs of specialized histone variants constituting a minor fraction of these proteins are subjected to polyadenylation. Another feature of the canonical histones is the presence of multiple copies of their genes in the genome. All this makes it preferable to use genomic DNA as a template for the amplification of nucleotide sequences encoding histones. Based on the assumption that the isolated AMPs were products of the partial proteolysis of the dominant fraction of the sturgeon histone H2A, it was decided to amplify a region of the genomic DNA encoding this histone. Due to the low evolutionary conservation of the untranslated regions flanking this site, the experiment was carried out in two stages. The internal part of the gene with degenerate primers selected for conserved segments of the translated region were first amplified. Cloning and sequencing of the resulting amplicon about 300 bp in length enabled selection of the structure of primers for inverse PCR that was used to amplify the nucleotide sequence of the regions immediately adjacent to the fragment sequenced at the first stage. The amplicon size in this case was about 400 bp. The data obtained by DNA sequencing (GenBank KP059880) in combination with the data of the N-terminal amino acid analysis and mass spectrometry allowed us to determine the complete amino acid sequence of acipensins 1–6 (*Fig. 1*). It was found that Ac1, Ac2, Ac3, Ac4, and Ac5 are the N-terminal acetylated fragments 1–50, 1–35, 1–49, 1–44, and 1–51 of histone H2A, respectively, and Ac6 is the fragment 62–85 of histone H2A. The structural analysis of acipensins 1–6 showed the presence of

Table 1. Antimicrobial activity of acipensins Ac1, Ac2, and Ac6*

	Minimum Inhibitory Concentration, μM							
	E.coli **ML35p**		*Listeria monocytogenes* **EGD**		MRSA ATCC 33591		*Candida albicans* **820**	
	without NaCl	100 mM NaCl	without NaCl	100 mM NaCl	without NaCl	100 mM NaCl	without NaCl	100 mM NaCl
Ac1	0.7 ± 0.1	0.4 ± 0.1	1.1 ± 0.2	2.3 ± 0.4	0.9 ± 0.2	>40	1 ± 0.2	>40
Ac2	0.3 ± 0.1	1.1 ± 0.2	1.0 ± 0.2	2.7 ± 0.3	0.6 ± 0.1	>40	0.9 ± 0.1	>40
Ac6	2.5 ± 0.3	>40	>40	>40	>40	>40	>40	>40
HNP-1	0.8 ± 0.1	>50	1.0 ± 0.3	1.1 ± 0.2	1.7 ± 0.3	>50	2.1 ± 0.4	>50
PG-1	0.2 ± 0.1	0.2 ± 0.1	0.3 ± 0.05	0.3 ± 0.1	0.4 ± 0.1	0.4 ± 0.2	0.4 ± 0.1	1.2 ± 0.4
ChBac5	0.4 ± 0.1	0.3 ± 0.1	0.6 ± 0.1	1.5 ± 0.7	0.8 ± 0.3	>40	0.9 ± 0.2	>40

* Data are presented as the minimum inhibitory concentration of peptides in μM; the peptides were incubated with microorganisms in a 10 mM sodium phosphate buffer, pH 7.4, in one case, and in a 10 mM sodium phosphate buffer, pH 7.4, containing 100 mM NaCl, in another case. The comparison peptides were porcine protegrin 1 (PG-1), human alpha-defensin HNP-1, and goat bactenecin ChBac5.

peptides with calculated molecular weights of 5,336.2 Da, 3,803.0 Da, 5,173.0 Da, 4,777.5 Da, 5,449.4 Da, and 2,740.2 Da, respectively, in sturgeon leukocytes. The calculated molecular weights of acipensins 1–6 were in good agreement with the experimental data of mass-spectrometry analysis (5,336.0 Da, 3,804.0 Da, 5,174.0 Da, 4,777.6, 5,448.8 Da, and 2,741.7 Da, respectively).

The literature data indicate that histone H2A derivatives have already been isolated from the skin and mucus of lower vertebrates (fish and amphibians). In particular, buforins [31] that are structurally similar to acipensins (*Fig. 1*) were isolated from the gastric mucosa of the Asian toad *Bufo bufo gargarizans* and characterized. As previously mentioned, the antimicrobial peptides hipposin and parasin that appeared to be the N-terminal fragments of histone H2A were isolated from the mucous coats of bony fishes, the halibut *Hippoglossus hippoglossus* L. [16], and the Amur catfish *Parasilurus asotus* [17], respectively.

Analysis of acipensin antimicrobial activity

Antimicrobial activity is believed to be a central functional property of AMPs. The peptides described in the literature (defensins, cathelicidins, etc) have it to different extents: the mechanism of their antibacterial action is diverse. The antimicrobial activity of three major fractions of acipensins (Ac1, Ac2, Ac6) was evaluated by radial diffusion, with experiments being conducted under various conditions: in a medium containing only a 10 mM sodium phosphate buffer with no added salts and in the same medium but with 100 mM sodium chloride (close to the physiological concentration of sodium chloride). This approach aimed at evaluating the impact of an increase in the solution's ionic strength on the efficiency of the antimicrobial activity of peptides was used in many experimental studies of the antimicrobial properties of natural AMPs described in the literature, and its use enables a comparison of the activity of the isolated peptides with the antibiotic effects of other AMPs. The results of the analysis of the acipensin's antimicrobial activity against bacteria *Escherichia coli* ML-35p, *Listeria monocytogenes* EGD, methicillin-resistant *Staphylococcus aureus* (MRSA) ATCC 33591, and the fungus *Candida albicans* 820 are presented in Table 1. The activity of acipensins was studied in comparison with three other AMPs with a different structure and mechanism of antimicrobial action: porcine protegrin 1, human alpha-defensin HNP-1, and goat bactenecin ChBac5. Alpha-defensins are the main antimicrobial peptides, along with cathelicidin LL-37, of human neutrophilic granulocytes. Proline-rich bactenecins are the dominant family of the AMPs of goat and sheep neutrophils. Protegrin 1 (PG-1) of porcine leukocytes, which has a beta-hairpin conformation, is one of the most active peptides, described to date, of animal leukocytes that exhibits a broad spectrum of antimicrobial activity based on its ability to damage the membranes of microorganisms.

As seen from the Table, in a medium with a low ionic strength, acipensins 1 and 2 demonstrate a broad spectrum of action and exhibit a high antimicrobial activity against both Gram-negative and Gram-positive bacteria, as well as the fungus. However, the spectrum of Ac1 and Ac2 activity changes with increasing medium ionic strength: the efficiency of their effect against the Gram-positive bacterium MRSA ATCC 33591 and the fungus *Candida albicans* 820 is significantly reduced. Ac6 demonstrates an antimicrobial effect only against

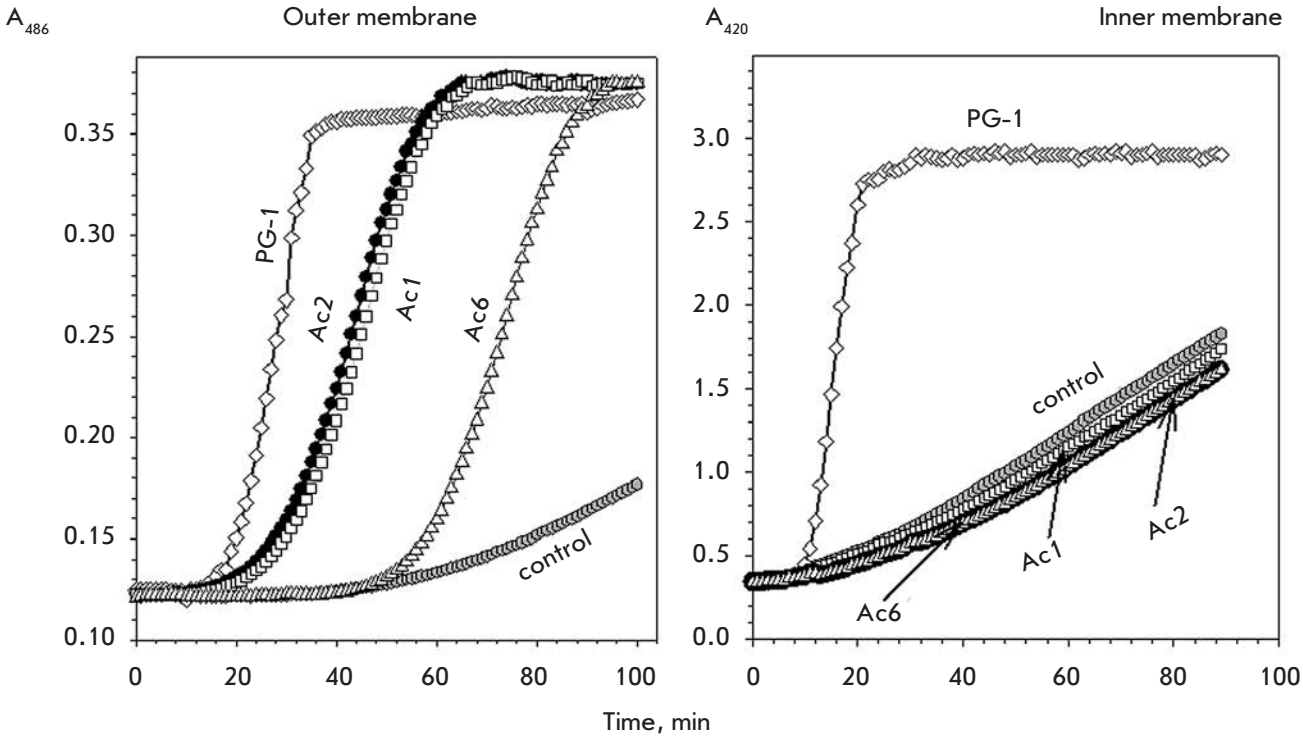

Fig. 2. Kinetics of the changes in the *E.coli* ML35p membrane permeability to chromogenic markers under the action of antimicrobial peptides. X axis – time of incubation of peptides and bacteria, min. Y axis – optical density of a solution containing chromogenic markers: the nitrocefin hydrolysis product (left panel displaying the outer membrane permeability) and the ONPG hydrolysis product – o-nitrophenol (right panel displaying the inner membrane permeability). The peptides were applied at concentrations equal to their MICs for *E.coli* ML35p under similar conditions

the Gram-negative bacterium *E.coli* in a low-ionic-strength medium. The antimicrobial effect of Ac1 and Ac2 differs from that of membrane-active PG-1 and is similar to the effects of bactenecin ChBac5. Bactenecins are known to exhibit antibacterial action mainly against Gram-negative bacteria, and this action is exerted without significant damage to the bacterial membranes and is directed against intracellular targets [14]. Although acipensins do not have a structural similarity with proline rich bactenecins, it may be assumed that the prime targets of their antibacterial action, similarly to bactenecins, are not bacterial membranes. Investigation of the effects of Ac1, Ac2, and Ac6 on the barrier function of bacterial membranes was the next objective of this study.

The effect of acipensins on the permeability of the outer and cytoplasmic membranes of *E.coli* ML35p to chromogenic markers

Figure 2 presents the kinetics of the action of acipensins 1, 2, and 6 (at a concentration equal to their minimum inhibitory concentration (MIC) against this bacterium) on the outer and inner (cytoplasmic) membranes of *E.coli* ML35p. The membrane-active peptide PG-1 was used as a standard. Acipensins 1 and 2 have a distinct effect on the permeability of the outer membrane of the bacterium to a chromogenic marker, nitrocefin (as evidenced by an increase in the solution's optical density due to the appearance of a colored product of the nitrocefin cleavage (see Experimental section)), although to a lesser extent than PG-1. An increase in the outer membrane permeability was observed 15–29 min after the addition of Ac1 and Ac2 to bacteria and 50 min in the case of Ac6. However, an action of all three studied acipensins on the cytoplasmic membrane of *E.coli* ML35p, evaluated by this method, was hardly observed 90 min after the start of the experiment: the membrane permeability to the chromogenic marker ONPG was unchanged compared to the control values (indicators in samples without peptides). Therefore, these data suggest that the main target of acipensins at concentrations close to the MIC are not the bacterial membranes but intracellular components.

Apart from the antimicrobial activity, most AMPs are known to exhibit a variety of effects on the host cells, including a cytotoxic effect, causing cell death.

We investigated the possibility of acipensin's toxic effect on cells of a macroorganism.

Acipensin cytotoxic activity against human cells *in vitro*

As in most published studies on the cytotoxic activity of various AMPs, human cells are the main subject of the investigation of this peptide's activity, because natural AMPs are considered as promising prototypes of new drugs for use in medicine, and elucidation of the toxicity of these compounds, especially against human cells, is of great importance. We investigated the hemolytic activity of acipensins 1, 2, and 6 against human erythrocytes. Erythrocyte hemolysis was found not to be observed for the studied peptides at concentrations of 1–40 μM (*Fig. 3*). As in previous experiments, PG-1, which has a high hemolytic activity contrary to that of sturgeon peptides, was used as a positive control. A study of the acipensin effect on the cultured human cell lines K-562 (human erythroleukemia cells) and U-937 (human histiocytic lymphoma cells) revealed that the peptides at concentrations of 1–20 μM did not exert toxic effects on the target cells: the proportion of viable cells after their incubation with each of the studied acipensins for 20 h did not differ from the proportion of viable cells in the control samples.

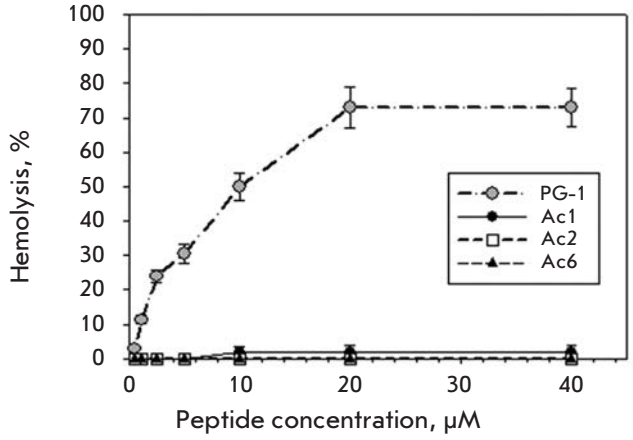

Fig. 3. Hemolytic activity of acipensins. X axis – peptide concentration, μM. Y axis – percentage of erythrocyte hemolysis calculated by the following equation: % Hemolysis = $((A_{exper} - A_{control})/(A_{total} - A_{control})) \times 100\%$, where A_{exper} and $A_{control}$ are the supernatant absorbance obtained for treated and untreated red cells, respectively, and A_{total} is the supernatant absorbance for red cells treated with 1% Triton X-100. A strong hemolytic activity of the peptide PG-1 was used as a positive control

DISCUSSION

The discovery, in fish and amphibians, of cationic peptides that exhibit antimicrobial activity and are histone fragments allowed a number of researchers to suggest that these histone derivatives might have a non-nuclear localization and function as antimicrobial protectors [18, 32, 33]. This hypothesis is supported by data on the detection of histone H1 in the cytosol of human intestinal villus cells [34]. In mice, H1 was found on the macrophage surface, where it acts as a thyroglobulin receptor [35]. Histones H1 (MUMP-1 and MUMP-2) and H2B (MUMP-3) were isolated from the granular fraction of mouse macrophages [36]. In addition, histone H1 was found on the surface of mouse neurons [37], human monocytes [38], and the nonspecific cytotoxic cells of channel catfish (similar to natural killer cells of mammals) [39]. The importance of histones in the course of immune processes became apparent when information about their involvement in the functioning of neutrophil extracellular traps (NETs) emerged [40, 41]. The formation of these structures, first identified in 2004, is the third, along with phagocytosis and secretion of antimicrobial compounds, mechanism of neutrophil killing activity [42]. Extracellular traps are formed during NETosis (controlled cell death, significantly different from necrosis and apoptosis) and are a decondensed chromatin network that includes antimicrobial factors of both granular (proteases, AMPs) and nuclear (histones and products of their partial proteolysis) origin. Extracellular traps ensure capture and destruction of pathogenic microorganisms that, for some reason, cannot be neutralized by phagocytosis. Due to the structuring role of DNA, diffusion of antimicrobial factors from the trap is slowed, which enables achievement of high local concentrations of these substances and a reduction in their harmful effect on healthy tissues.

The obtained data on the structural and functional properties of antimicrobial peptides from leukocytes of the Russian sturgeon, acipensins, as histone H2A derivatives confirm the hypothesis that during evolution, derivatives of proteins that usually have a nuclear localization might be selected as endogenous antibiotic peptides in separate groups of animals. This demonstrates a surprising variety of structural AMP families among members of different taxa of the animal world. The most common group of AMPs is known to be members of the defensin family, whose functional activity is realized in phagocytes (neutrophils and macrophages of vertebrates, and amoebocytes and coelomocytes of invertebrates) and at the level of barrier epithelia of the integument and mucosae of animals. However, peptides of the defensin family were not found in sturgeon leukocytes. Defensins are also absent in the phagocytes of certain mammalian species (mouse, cat, dog, sheep and goat). In these species, the function of molecules inactivating phagocytized microbes is performed by

peptides of the cathelicidin family (bactenecins, protegrins, etc). The peculiarity of the species pattern of the antimicrobial peptides of Russian sturgeon leukocytes is that they are dominated by peptides, histone H2A derivatives, that had not previously been found in fish phagocytes.

Acipensins have a broad spectrum of antimicrobial action like other, currently known histone H2A derivatives: buforin, parasin, hipposin, abhizin (peptide from the Haliotis mollusc) [16, 17, 31, 43]. Unlike parasin and buforin 1, acipensins 1–5 are molecules with an acetylated N-terminus. The hipposin molecule has the same property [16]. Acetylation of the N-terminus was found not to be necessary for the exhibition of antimicrobial activity, because synthetic non-acetylated hipposin turns out to be active [16].

The observed decrease in the antimicrobial activity of acipensins with an increase in the solution ionic strength is characteristic of many AMPs described in the literature: e.g., human alpha-defensins and goat bactenecins. The antimicrobial activity of defensins is known to be able to recover in media containing physiological concentrations of sodium chloride, which results from synergistic action with other AMPs of human neutrophils, in particular, cathelicidin LL-37 [44]. It may be assumed that, along with the constitutively synthesized acipensins, sturgeon leukocytes contain inducible antimicrobial factors whose synthesis is increased during the infectious process, and that can act together with acipensins, which increases the efficiency of the antimicrobial action of AMPs.

The data on the low antimicrobial activity of Ac6 compared to that of Ac1 and Ac2 suggest that these are N-terminal derivatives of histone H2A that play a key role in anti-infective protection.

The mechanisms of action of AMP derivatives of histone H2A described in the literature are slightly different: the main mechanism of antimicrobial action of buforin 2 is associated with its ability to penetrate into bacterial cells without significant damage to their membranes and to interact with nucleic acids, which leads to inhibition of vital processes in microbial cells and to their death [45, 46]. However, another peptide, parasin, exerts a pronounced damaging effect on the bacterial membranes [47]. A synthetic analog of hipposin was demonstrated also to have the ability to increase the permeability of bacterial membranes (*E. coli* ATCC 25922) [48]. Although acipensins have a significant structural similarity to hipposin, no appreciable increase in the permeability of the cytoplasmic membrane of *E. coli* ML35p under the action of acipensins was observed in our experiments. On the one hand, it may be assumed that the difference in the results is related to the fact that other bacterial strains and permeability markers were used in our study. On the other hand, the decisive role is probably played by the peptide concentration. For example, the dual mode of action [49] was established for proline-rich peptides, in particular bactenecins: at concentrations close to the MIC, the peptides did not have a damaging effect on the membranes, their effects were associated with the impact on intracellular targets, while at concentrations above the MIC, these AMPs, in addition to the inhibition of intracellular processes, disturbed the structural integrity of the membrane. Because concentrations close to the MIC were used in experiments on the evaluation of the acipensin effect on the permeability of bacterial membranes, we may assume that acipensins at higher concentrations, like bactenecin and hipposin, can also disturb the barrier function of bacterial membranes. Finally, it cannot be excluded that the observed discrepancy in the results may be due to those few amino acid substitutions that distinguish Ac1 and Ac2 from the hipposin analog used in [48]. A more detailed investigation of the effect of acipensins on bacterial membranes will be conducted in our future studies using recombinant acipensin analogs.

Similarly to other natural AMP derivatives of histone H2A, all three studied acipensins (Ac1, Ac2, and Ac6) exhibited no significant cytotoxic activity against the cultured human cells. Further investigation of the interaction of acipensins and their structural analogs with the cells will establish whether they possess the potential to translocate across the eukaryotic cell membranes, as it was demonstrated for buforins [46]. Having similar properties opens prospects for the practical application of the peptides in antitumor therapy as vectors for the delivery of drugs into malignant cells.

CONCLUSION

A set of antimicrobial peptides called acipensins that are histone H2A fragments were for the first time isolated from leukocytes of the Russian sturgeon *A. gueldenstadti*. These peptides have a broad spectrum of antibacterial activity and do not exhibit toxic properties towards host cells. The obtained data contribute to the development of ideas regarding the evolution of the molecular factors of innate immunity and support the assumption of the biological role of histones as protective molecules involved in the implementation of the anti-infective function of the immune system. ●

This work was supported by a grant from the Federal Target Program "Research and Development on Priority Directions of Scientific-Technological Complex of Russia for 2014–2020" (agreement #14.604.21.0104). Unique identifier for Applied Scientific Research (project) RFMEFI60414X0104.

REFERENCES

1. Kokryakov V.N. Ocherki o vrozhdennom immunutete (Essays on the innate immunity). St-Petersburg: Nauka. 2006. 261 pp. In Russian.
2. Rieger A.M, Barreda D.R. // Dev. Comp. Immunol. 2011. V. 35. № 12. P. 1238–1245.
3. Cole A.M., Weis P., Diamond G. // J. Biol. Chem. 1997. V. 272. № 18. P. 12008–12013.
4. Douglas S.E., Gallant J.W., Gong Z., Hew C. // Dev. Comp. Immunol. 2001. V. 25. № 2. P. 137–147.
5. Shai Y., Fox J., Caratsch C., Shih Y.L., Edwards C., Lazarovici, P. // FEBS Lett. 1988. V. 242. P. 161–166.
6. Shike H., Lauth X., Westerman M.E., Ostland V.E., Carlberg J.M., Van Olst J.C., Shimizu C., Bulet P., Burns J.C // Eur. J. Biochem. 2002. V. 269. P. 2232–2237.
7. Park C., Lee J., Park I., Kim M., Kim S. // FEBS Lett. 1997. V. 411. № 2–3. P. 173–178.
8. Wang G., Li J., Zou P., Xie H., Huang B., Nie P., Chang M. // Fish Shellfish Immunol. 2012. V. 33. № 3. P. 522–531.
9. Guo M., Wei J., Huang X., Huang Y., Qin Q. // Fish Shellfish Immunol. 2012. V. 32. № 5. P. 828–838.
10. Marel Mv., Adamek M., Gonzalez S.F., Frost P., Rombout J.H., Wiegertjes G.F., Savelkoul H.F., Steinhagen D. // Fish Shellfish Immunol. 2012. V. 32. № 3. P. 494–501.
11. Maier V.H., Dorn K.V., Gudmundsdottir B.K., Gudmundsson G.H. // Molecular Immunology. 2008. V. 45. P. 3723–3730.
12. Chang C., Pleguezuelos O., Zhang Y., Zou J., Secombes C. // Infection and Immunity. 2005. V. 73. P. 5053–5064.
13. Chang C., Zhang Y., Zou J., Nie P., Secombes C. // Antimicrobial Agents and Chemotherapy. 2006. V. 50. P. 185–195.
14. Scocchi M., Pallavicini A., Salgaro R., Bociek K., Gennaro R. // Comp. Biochem. Physiol. B Biochem. Mol. Biol. 2009. V. 152. № 4. P. 376–381.
15. Bridle A., Nosworthy E., Polinski M., Nowak B. // PLoS One. 2011. V. 6. №8. e23417.
16. Birkemo G. A., Lüders T., Andersen Ø., Nes I.F., Nissen-Meyer J. Hipposin, a histone-derived antimicrobial peptide in Atlantic halibut (*Hippoglossus hippoglossus*). // Biochimica et Biophisica Acta. 2003. V. 1646. P. 207–215.
17. Park I.Y., Park C.B., Kim M.S., Kim S.C. // FEBS Lett. 1998. V. 437. P. 258–262.
18. Richards R.C., O'Neil D.B., Thibault P., Ewart K.V. // Biochem. Biophis. Res. Commun. 2001. V. 284. P. 549–555.
19. Shamova O., Orlov D., Stegemann C., Czihal P., Hoffmann R., Brogden K., Kolodkin N., Sakuta G., Tossi A., Sahl H-G. et al. // International Journal of Peptide Research and Therapeutics. 2009. V. 15. № 1. P. 31–35.
20. Harwig S.S., Chen N.P., Park A.S.K., Lehreer R.I. // Anal. Biochem. 1993. V. 208. P. 382–346.
21. Schagger H., von Jagow G. // Anal. Biochem. 1987. V. 166. P. 368–379.
22. Wolf P. // Anal. Biochem. 1983. V. 129. № 1. P. 145–155.
23. Lehrer R.I., Rosenman M., Harwig S.S., Jackson R., Eisenhauer P. // J. Immunol. Methods. 1991. V. 137. № 2. P. 167–73.
24. Lehrer R., Barton A., Ganz T. // J. Immunol. Methods. 1988. V. 108. P. 153–158.
25. Artamonov A.Yu., Shamova O.V., Kokryakov V.N., Orlov D.S. // Vestnik Sankt-Peterburgskogo Universiteta. 2008. Ser. 3, N. 2. P. 139–142. In Russian.
26. Mosmann T. // Journal of Immunological Methods. 1983. V. 65. P. 55–63.
27. Wellner D., Panneerselvam C., Horecker B.L. // Proc. Nat. Acad. Sci. 1990. V. 87. P. 1947–1949.
28. Sambrook J., Fritsch E.F., Maniatis T. Molecular Cloning: a laboratory manuals. 2nd ed. New York: Cold Spring Harbor Laboratory Press, 1989. 1626 p.
29. Shamova O.V., Orlov D.S., Ovchinnikova T.V., Sal Kh-G., Tver'yanovich I.A., Popova V.A., Dyubin V.A., Kokryakov V.N. // Fundamentalnye Issledovaniya. 2006. № 1. P. 10–13. In Russian.
30. Marzluff W.F., Wagner E.J., Duronio R.J. // Nat. Rev. Genet. 2008. V. 9. № 11. P. 843–54.
31. Kim H.S., Park C.B., Kim M.S., Kim S.C. // Biochem. Biophys. Res. Commun. 1996. V. 229. № 2. P. 381–7.
32. Kawasaki H., Iwamuro S. // Infect. Disord. Drug Targets. 2008. V. 8. № 3. P. 195–205.
33. Parseghian M., Luhrs K. // Biochem. Cell Biol. 2006. V. 84. № 4. P. 589–604.
34. Rose F.R., Bailey K., Keyte J.W., Chan W.C., Greenwood D., Mahida Y.R.. // Infect. Immun. 1998. V. 66. P. 3255–3263.
35. Brix K., Summa W., Lottspeich F., Herzog V. // J. Clin. Invest. 1998. V. 102. P. 283–293.
36. Hiemstra P.S., Eisenhauer P.B., Harwig S.S., van den Barselaar M.T., van Furth R., Lehrer R.I. // Infect. Immun. 1993. V. 61. P. 3038–3046.
37. Bolton S.J., Perry V.H. // J. Neurocytol. 1997. V. 26. P. 823–831.
38. Holers V.M., Kotzin B.L. // J. Clin. Invest. 1985. V. 76. P. 991–998.
39. Evans D.L., Kaur H., Leary J. 3rd, Praveen K., Jaso-Friedmann L. // Dev Comp Immunol. 2005. V. 29. № 12. P. 1049–64.
40. Nauseef W.M., Borregaard N. // Nat. Immunol. 2014. V. 15. № 7. P. 602–11.
41. Zawrotniak M., Rapala-Kozik M. // Acta Biochim Pol. 2013. V. 60. № 3. P. 277–84.
42. Brinkmann V., Reichard U., Goosmann C., Fauler B., Uhlemann Y., Weiss D.S., Weinrauch Y., Zychlinsky A. // Science. 2004. V. 303. № 5663. P. 1532–5.
43. De Zoysa M., Nikapitiya C., Whang I., Lee J.S., Lee J. // Fish Shellfish Immunol. 2009. V. 27. № 5. P. 639–46.
44. Nagaoka I., Hirota S., Yomogida S., Ohwada A., Hirata M. // Inflamm Res. 2000. V. 49. № 2. P. 73–9.
45. Park C.B., Kim H.S., Kim S.C. // Biochem Biophys Res Commun 1998. V. 244. № 1. P. 253–257.
46. Cho J.H., Sung B.H., Kim S.C. // Biochim Biophys Acta. 2009. V. 1788. № 8. P. 1564–9.
47. Koo Y.S., Kim J.M., Park I.Y., Yu B.J., Jang S.A., Kim K.S., Park C.B., Cho J.H., Kim S.C., // Peptides. 2008. V. 29. P. 1102–1108.
48. Bustillo M.E., Fischer A. L., LaBouyer M.A., Klaips J. A., Webb A.C., Elmore D.E. // Biochim. Biophys. Acta. 2014. V.1838. № 9. P. 2228–2233.
49. Podda E., Benincasa M., Pacor S., Micali F., Mattiuzzo M., Gennaro R., Scocchi M. // Biochim. Biophysi. Acta. 2006. V. 1760. P. 1732–1740.

The Mechanism of Choline-Mediated Inhibition of Acetylcholine Release in Mouse Motor Synapses

A. E. Gaydukov*, P. O. Bogacheva, E. O. Tarasova, O. P. Balezina
Lomonosov Moscow State University, Faculty of Biology, Department of Human and Animal Physiology, Leninskie Gory, 1, build. 12, Moscow, 119234, Russia
*E-mail: gaydukov@gmail.com
Received 12.05.2014

ABSTRACT **The mechanism of action of tonically applied choline, the agonist of α7 nicotinic acetylcholine receptors (nAChRs), to the spontaneous and evoked release of a neurotransmitter in mouse motor synapses in diaphragm neuromuscular preparations using intracellular microelectrode recordings of miniature endplate potentials (MEPPs) and evoked endplate potentials (EPPs) was studied. Exogenous choline was shown to exhibit a presynaptic inhibitory effect on the amplitude and quantal content of EPPs for the activity of neuromuscular junction evoked by single and rhythmic stimuli. This effect was inhibited either by antagonists of α7-nAChRs, such as methyllycaconitine and α-cobratoxin, or by blocking SK-type calcium-activated potassium (K_{Ca}) channels with apamin or blocking intraterminal ryanodine receptors with ryanodine. A hypothesis was put forward that choline in mouse motoneuron nerve terminals can activate presynaptic α7-nAChRs, followed by the release of the stored calcium through ryanodine receptors and activation of SK-type K_{Ca} channels, resulting in sustained decay of the quantal content of the evoked neurotransmitter release.**
KEYWORDS **quantal content, ryanodine receptors, choline, α7-nicotinic acetylcholine receptors, SK channels.**
ABBREVIATIONS **ACh – acetylcholine; MEPP – miniature endplate potential; nAChRs – nicotinic acetylcholine receptors; EPP – endplate potential.**

INTRODUCTION

Although postsynaptic nAChRs in the motor synapses of the skeletal muscles of vertebrates have been thoroughly studied [1–3], data on presynaptic ones is rather scarce and contradictory. Immunohistochemical and pharmacologic tests demonstrate that there are several types of presynaptic nAChRs in motor synapses [4–7]. At the same time, the location and functions of the specific nAChRs remain poorly studied, especially those of α7-nAChRs [8, 9] that are characterized by a comparatively high calcium-ion conductivity [10–12]. In contrast to the central nervous system where activation of presynaptic α7-nAChRs with ACh or selective agonists (choline, nicotine) typically facilitates neurotransmitter release [13–16], inhibition of the release in peripheral motor synapses has been reported [5, 17]. In our previous research, activation of α7-nAChRs with small doses of nicotine triggered calcium-dependent inhibition of the evoked release of acetylcholine in rhythmically stimulated neuromuscular junctions of mouse, which could be prevented by using methyllycaconitine, a selective antagonist of α7-nAChRs [18]. The mechanisms of this inhibition remain unclear. Due to this fact, presynaptic α7-nAChRs in the present work were activated by their selective agonist choline in order to assess its ability to suppress the evoked ACh release and to study the mechanisms of this effect.

EXPERIMENTAL

Object of research

Experiments were carried out using isolated neuromuscular preparations of the diaphragm *(m. diaphragma – n. phrenicus)* of mature (30) male mice of the 129/Sv line provided by the Anokhin Institute of Normal Physiology of the Russian Academy of Sciences (Moscow, Russia). A total of 27 animals were used. The mice were managed in accordance with the Directive 86/609/EEC regulating the use of laboratory animals. The procedure was approved by the Bioethics Commission of the Department of Biology of the Moscow State University. The mice were euthanized by quick decapitation.

Electrophysiology

The dissection of muscle fiber allowing one to simultaneously record both a spontaneous and non-reduced evoked release of the neurotransmitter was performed

according to the standard protocol [5, 17, 18]. The left half of the diaphragm with the phrenic nerve was put into a 3-mL camera and rinsed with an oxygenated (95% O_2, 5% CO_2) Liley buffer (pH 7.2–7.4, 135 mM NaCl, 4 mM KCl, 0.9 mM NaH_2PO_4, 2 mM $CaCl_2$, 1 mM $MgCl_2$, 16.3 mM $NaHCO_3$, 11 mM glucose) at room temperature. All experiments were carried out at 20–22 °C. MEPPs and EPPs were recorded using intracellular glass microelectrodes filled with 2.5 M KCl (resistance at the microelectrode tip was 15–20 MΩ). Single EPPs were detected upon stimulation of the phrenic nerve with suprathreshold impulses of 0.3 Hz frequency (at least 30 stimuli). When studying the rhythmic synaptic activity, the phrenic nerve was stimulated with short trains of stimuli (50 stimuli 0.1 ms long each, frequency of 50 Hz). Signals were registered by an Axoclamp-2B amplifier (Molecular Devices) and recorded using an L-Card E-154 analog-to-digital converter (with PowerGraph interface) into the PC hard drive. The data were processed using the MiniAnalysis software (Synaptosoft). Controls included MEPP and EPP recordings from 5 or more different synapses under normal conditions and after the substances under study had been administered in a certain order. The synaptic activity was registered during 1–1.5 h. At least 3 neuromuscular preparations were used in each series of experiments.

Substances and solutions

Choline, methyllycaconitine, apamin (Sigma, USA), and ryanodine (Enzo Life Sciences, USA) were used. A high-affinity blocker of α7-nAChRs, namely the long-chain α-cobratoxin (extracted from *Naja naja kaouthia*) [19–21], was kindly provided by Yu.N. Utkin, the head of the Laboratory of Molecular Toxicology of the Shemyakin–Ovchinnikov Institute of Bioorganic Chemistry, Russian Academy of Sciences (Moscow, Russia).

Data analysis and statistics

We estimated the amplitude, variation of MEPPs and EPPs with time, the MEPP frequency, and the quantal content of EPP (the latter was calculated as the ratio between the mean EPP amplitude corrected for non-linear summation [22] to the mean MEPP amplitude). The statistical significance of the difference between sample groups was assessed using the Student's t-test and Mann–Whitney test. The significance level of the differences between two sample groups was 0.05 (n – being the number of synapses studied).

RESULTS

In the first series of experiments, the muscle was rinsed with a 100-μM choline solution for 40 min. The characteristics of MEPPs and the single-evoked EPPs were analyzed. No statistically significant changes in the membrane potential (MP) in the postsynaptic membrane were revealed during choline perfusion ((the average MP in the controls was −39.16 ± 1.13 mV (n = 18) and −40.06 ± 1.18 (n = 19) in the presence of choline). Choline reduced the EPP amplitude by over 25% on average as compared to the control *(Fig. 1A)*. The effect developed within 10–15 min after the administration of choline and remained unchanged during the next 30 min. The changes in amplitude, temporal characteristics, and MEPP frequency were not statistically significant; the decline in the EPP amplitude was caused by a decrease in the quantal content of EPPs from 34.20 ± 2.56 in the control to 25 ± 2.56 in the presence of choline ($p < 0.05$) *(Fig. 1B)*. In additional experiments on intact (non-dissected) neuromuscular preparations, 100-μM choline caused no significant changes in the MEPP amplitude (1.49 ± 0.07 mV in controls (n = 17) and 1.52 ± 0.11 (n = 17, $p < 0.05$) in the presence of choline). Compared with the controls, the MEPP frequency

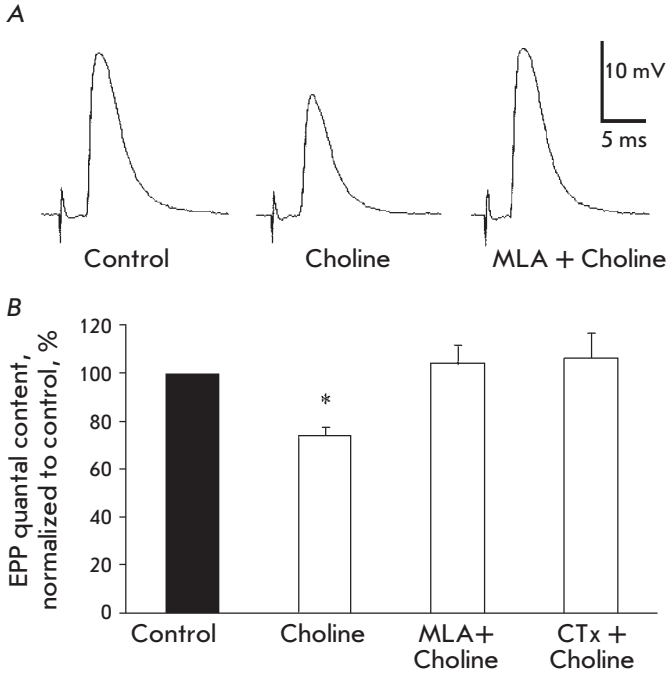

Fig. 1. Inhibitory effect of exogenous choline on the single (0.3 Hz) evoked release of neurotransmitter mediated by its influence on α7-nAChRs. *A* – averaged recordings of single EPPs in controls, in the presence of choline (100 μM) and in the presence of both choline (100 μM) and MLA (20 nM). *B* – quantal content of single EPPs in controls, in the presence of choline and in the presence of choline and previously administered MLA and CTx (5 nM). The Y axis shows the quantal content of EPPs (% compared to the control), *$p < 0.05$ compared to the controls

and its variation with time in the presence of choline were not significantly different. Thus, the decline in the quantal content of EPPs in the presence of choline at the same MP and MEPP values indicates that choline has a presynaptic inhibitory effect on the evoked quantal release of ACh.

Choline-induced inhibition of the quantal content of the single EPP could be prevented by a selective blocker of α7-nAChRs, methyllycaconitine (MLA), administered in a concentration of 20 nM. When administered for 15–30 min, MLA caused no statistically significant changes in MEPPs and EPPs; however, the amplitude and quantal content of single EPPs did not decrease in the presence of methyllycaconitine choline, either (*Fig*. 1A,B). A similar result—the prevention of the inhibitory effect of exogenous choline on the quantal content of single EPPs—was obtained with the aid of another selective blocker of α7-nAChRs, the long-chain α-cobratoxin (CTx) administered in a concentration of 5 nM *(Fig. 1B)*. This means that choline, when administered tonically, facilitates the inhibition of the evoked release of ACh precisely by activating α7-nAChRs.

The following series of experiments was aimed at investigating choline-induced responses to short trains consisting of 50 EPPs (50 Hz, 1s). Administration of 100-μM choline for 40 min showed the same decrease in the amplitude and quantal content as that observed for single-evoked EPPs; this effect was recorded for the first and all following EPPs in the train. It developed during the first 10–15 min of choline administration and remained unchanged for the next 30 min. There, the EPP train pattern did not change: identically to the controls, we observed short-term facilitation of the synaptic transmission in the beginning of the train, which was followed by the depression continuing into a lower stable level of EPPs compared to the first one (a plateau) *(Fig. 2A)*. Preliminary administration of selective blockers of α7-nAChRs, 20nM MLA (*Fig. 2B*) or 5 nM CTx, to the neuromuscular preparation changed neither the MEPP parameters nor quantal content of EPP of the high-frequency short train. Meanwhile, choline administered alongside the mentioned blockers of α7-nAChRs had no inhibitory effect on the quantal content of EPP in trains *(Fig. 2B)*.

To elucidate the mechanism of the inhibitory effect of choline, an assumption was made that choline-induced activation of α7-nAChRs letting calcium in the terminal generates a calcium signal that can activate SK K_{Ca} channels similar to the pathway of the inhibitory effect of ACh on the impulse activity of some other excitable cells [23, 24]. A selective blocker of SK K_{Ca} channels, apamin, was administered to the muscle in a concentration of 200 nM to verify this hypothesis. Apamin alone provided no statistically significant changes in the amplitude and quantal content of the single or rhythmically generated EPPs, but 100-μM choline administered along with it lost its ability to inhibit the quantal content of EPPs in trains *(Fig. 3A)*. All these facts allowed us to assume that the inhibitory effect of exogenous choline depends on calcium and is based on the choline-induced activation of the calcium influx into the terminal via channels of α7-nAChRs, which activates potassium SK-channels and the outgoing potassium current. The ensuing membrane hyperpolarization suppresses the voltage-dependent calcium channels in active zones, thus diminishing the possibility of the evoked ACh release.

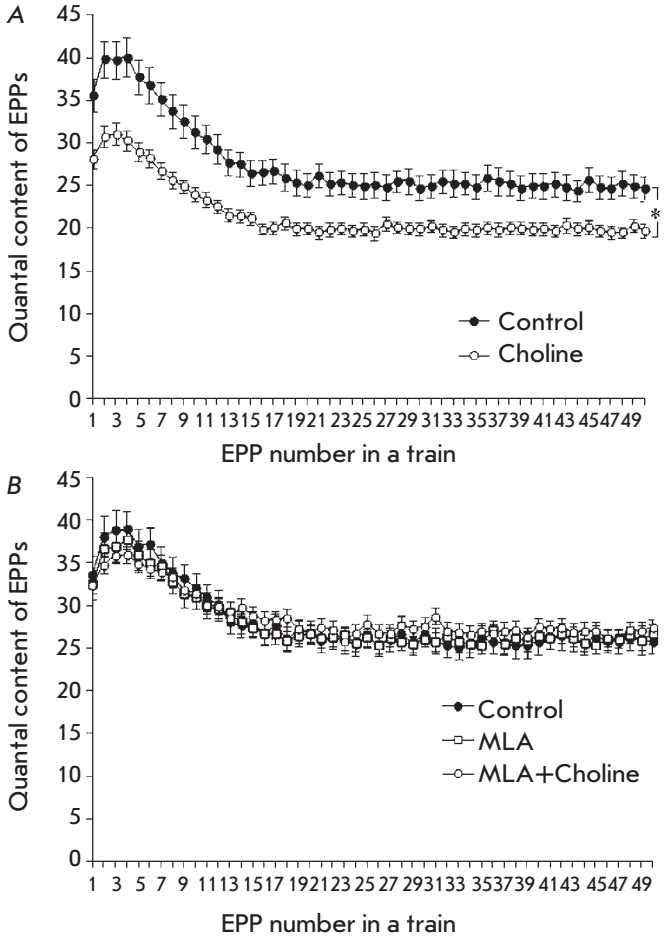

Fig. 2. Change in the quantal content of EPPs during the short train of stimuli at a rhythmical activity of synapses of 50 Hz. *A* – in controls and upon administration of 100 μM choline. *B* – in controls, in the presence of 20 nM MLA and upon administration of choline subsequent to MLA. The Y axis shows the quantal content of EPP; the X axis shows the number of EPPs in the train, *$p < 0.05$ compared to controls

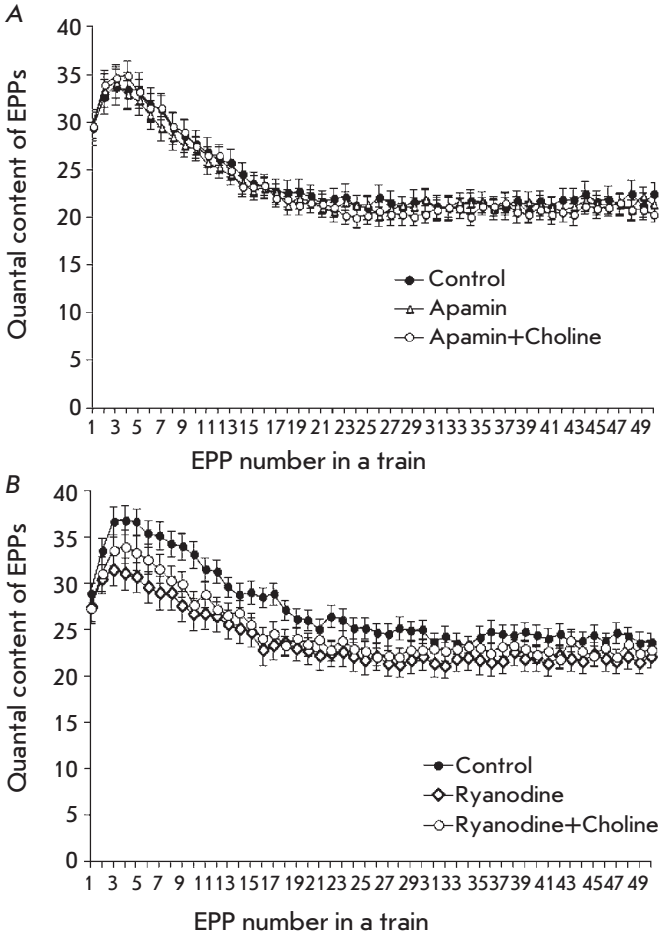

Fig. 3. Change in the quantal content of EPPs during the short train of stimuli at a frequency of 50 Hz. *A* – in controls, in the presence of 200 nM apamin, and in the presence of both 100 μM choline and apamin. *B* – in controls, in the presence of 3 μM ryanodine, and in the presence of both 100 μM choline and ryanodine. The Y axis shows the quantal content of EPPs; the X axis shows the number of EPPs in the train

According to publications, SK channels can be activated by calcium from different sources [25]. Thus, for instance, the activity of SK channels in certain hippocampal synapses [24] rises due to the calcium-triggered release of calcium from stores caused by the influx of calcium from the outside through the channels of α7-nAChRs. That is why the next series of experiments were aimed at elucidating the possible involvement of ryanodine receptors and the release of calcium from the calcium stores of motor terminals in the mechanisms of the calcium-dependent inhibitory effects of choline employing SK potassium channels.

Application of ryanodine in a concentration that reciprocally blocks ryanodine receptors (3 μM) to the muscle showed no statistically significant changes in the amplitude and quantal content of EPPs but insignificantly worsened the transmission in the beginning of the short train of EPPs (*Fig. 3B)*. With a ryanodine presence (3 μM), the subsequent application of choline did not decrease the amplitude or quantal content of EPPs in the train (*Fig. 3B)*. This fact demonstrates that calcium-dependent choline-induced inhibition of the evoked release of ACh requires not only α7-nAChRs, but also the release of calcium from stores.

DISCUSSION

The effects discovered by administering exogenous choline (100 μM) and selective blockers of α7-nAChRs (methyllycaconitine and a-CTx), along with the impact of an inhibitor of SK channels (apamin) and that of the blocker of ryanodine receptors (ryanodine), elucidated the mechanism of the inhibitory effect of choline on the evoked ACh release.

The ability of certain endogenous and exogenous agonists of neuronal nAChRs when applied briefly (several seconds) and in high (millimolar) concentrations to inhibit ACh release in motor synapses has been reported earlier in a number of studies [5, 8, 17]. However, those studies specified neither the type of presynaptic nAChRs mediating these effects nor the mechanism of the latter. Choline is known to be a full selective agonist of α7-nAChRs and at the same time an activator of the M_1-choline receptors located on the terminals and motor synapses of Schwann cells [26]. However, the publications state that choline activates these receptors when administered in doses that are considerably higher than those used in our study [27, 28]. Apart from that, the selective activation of the M_1-choline receptors of motor synapses facilitates the release of neurotransmitter [29, 30] and, thus, cannot be a reason for the discovered inhibitory effect of exogenous choline on ACh release. That is why in our attempts to explain the discovered choline effects we relied on the well-documented and widely known facts of choline ability to selectively activate the α7-nAChRs of nerve terminals [31, 32].

According to the protocol used, choline was applied tonically (during several dozens of minutes) at a low concentration of 100 μM, which does not reach EC_{50} for activating α7-nAChRs (0.5–1.5 mM) [31, 33]. It is commonly known that α7-nAChRs belong to the family of rapidly desensitizing choline receptors [34]. However, according to the desensitization model of α7-nAChRs, low (not exceeding EC_{50}) concentrations of agonists lead to prolonged opening of the channel of α7-nAChRs with insignificant desensitization or blockage of the open channel at negative (hyperpolarized) MP values [32]. The fact that choline-induced decay of the

quantal content of EPPs can be prevented by blockers of α7-nAChRs means that the effect of choline in this particular concentration (100 μM) is mediated by the activation, not desensitization, of neuronal nAChRs on the presynaptic membrane. The prolonged effects of choline might be due to the processes taking place upon activation of α7-nAChRs. It has recently been shown on preterminal axons of hippocampal neurons that even short-term activation (10 min) of nAChRs with exogenous agonists may lead (after the immediate effects) to a long-term (30 min and more) intracellular rise in the calcium content, activation of CaMKII and other enzymes, accompanied by a long-term increase of the neurotransmitter release [35].

In our study of peripheral synapses, attempts to activate presynaptic α7-nAChRs with choline revealed another effect, namely the long-term inhibition of the neurotransmitter release caused by the involvement of SK K_{Ca} channels. These channels have been described for motoneuron nerve terminals in rodents [36]. It also has been shown that they might be involved in the regulation of the spontaneous MEPP frequency [37]. Our work is the first to report the activation of SK channels and their involvement in the possibly mediation of the inhibitory impact of choline on the evoked ACh release. Similar examples of the response of SK channels to the activation of α7-nAChRs have been described for the central synapses of hair cells [23] and hippocampal neurons [24].

Administering ryanodine as a blocker of ryanodine receptors demonstrated another necessary component that mediates the inhibitory effects of choline — ryanodine-dependent release of calcium from stores. In the central nervous system, functional coupling of α7-nAChRs to ryanodine receptors strengthens the calcium signal in terminals and facilitates the release of ACh and other neurotransmitters [14, 38, 39]. We were first to demonstrate that in peripheral synapses, on the contrary, functional interaction between α7-nAChRs and the ryanodine receptors of calcium stores decreases the evoked neurotransmitter release due to the activation of SK K_{Ca} channels. α7-nAChRs are apparently located in the terminals of motoneurons, far from the exocytosis sites, but spatially close to certain perimembrane cisterns of ryanodine calcium stores; thus, the entire complex can activate SK potassium channels. A similar interaction between α7-nAChRs, ryanodine receptors, and SK channels was described for hippocampal interneurons at the postsynaptic level [24] and in hair cells [40]. In both cases, it slowed down the neuronal activity.

It is widely known that spatial diffusion of the combined action of extracellular ACh and its derivate, choline, in the central nervous system may regulate the activity of the extrasynaptic and perisynaptic α7-nAChRs located on preterminal axons, neuronal dendrites, and bodies of glial cells [41]. For peripheral axons and the terminals of motoneurons, a regulation that would employ ACh and choline has not been reported yet. In neuromuscular junctions, the rate of ACh release and the level of AChE activity are significantly higher compared to those in the central cholinergic synapses [41]. Therefore, the prolonged activity of synapses and ACh hydrolysis must significantly increase the level of endogenous choline in the synaptic cleft. Its diffusion from the cleft and the activation of presynaptic α7-nAChRs might serve as a negative feedback mechanism of endogenous auto-regulation of ACh release. Nevertheless, we were not successful in establishing a response by endogenous choline to the ACh release upon single and short-train stimulation of synapses. Contrary to expectations, administration of blockers of α7-nAChRs failed to cause any changes in the quantal content of the single EPPs and short trains of EPPs(50 EPP, 50 Hz). A longer and more intensive action of motor synapses is probably required to accumulate endogenous choline. The same relates to its diffusion (spillover) from the cleft and development of an inhibitory effect, especially when presynaptic α7-nAChRs are distanced from the exocytosis sites (e.g., preterminal α7-nAChRs in central synapses) [42]. This concept was confirmed by the results of experiments on the rat diaphragm, where the ability of blockers of α7-nAChRs to prevent a decline in the quantal content of EPPs could be detected only on condition that it was evolving during a prolonged (several hours) low-frequency activity of synapses [17].

CONCLUSIONS

Our study has demonstrated the tonic effect of choline administered in concentrations relatively low on the activation of α7-nAChRs to cause long-term inhibition of the ACh release.

We were the first to reveal the mechanism of this inhibition. It consists in the activation of presynaptic axonal α7-nAChRs with choline, the subsequent release of calcium from stores through ryanodine receptors, and activation of SK K_{Ca} channels in mouse motor terminals. We cannot rule out other possible participants in this mechanism; such as certain calcium-dependent enzymes. However, further research is required to elucidate this point. It is also interesting to test whether choline-dependent inhibition of the neurotransmitter release can contribute to the fatigue of neuromuscular transmission at a prolonged intensive work of motor synapses in mammals. ●

This present work was supported by the Russian Foundation for Basic Research (grant No 13-04-00413a).

REFERENCES
1. Katz B., Miledi R. // J. Physiol. 1973. V. 231. № 3. P. 549-574.
2. Albuquerque E.X., Pereira E.F., Alkondon M., Rogers S.W. // Physiol. Rev. 2009. V. 89. № 1. P. 73-120.
3. Sine S.M. // Physiol. Rev. 2012. V. 92. № 3. P. 1189-1234.
4. Vizi E.S., Somogyi G.T. // Br. J. Pharmacol. 1989. V. 97. № 1. P. 65-70.
5. Tian L., Prior C., Dempster J., Marshall I.G. // J. Physiol. 1994. V. 476. № 3. P. 517-529.
6. Tsuneki H., Kimura I., Dezaki K., Kimura M., Sala C., Fumagalli G. // Neurosci. Lett. 1995. V. 196. № 1-2. P. 13-16.
7. Faria M., Oliveira L., Timoteo M.A., Lobo M.G., Correia-De-Sa P. // Synapse. 2003. V. 49. № 2. P. 77-88.
8. Tian L., Prior C., Dempster J., Marshall I.G. // Br. J. Pharmacol. 1997. V. 122. № 6. P. 1025-1034.
9. Dehkordi O., Haxhiu M.A., Millis R.M., Dennis G.C., Kc P., Jafri A., Khajavi M., Trouth C.O., Zaidi S.I. // Respir. Physiol. Neurobiol. 2004. V. 141. № 1. P. 21-34.
10. Castro N.G., Albuquerque E.X. // Biophys. J. 1995. V. 68. № 2. P. 516-524.
11. Fucile S. // Cell Calcium. 2004. V. 35. № 1. P. 1-8.
12. Uteshev V.V. // Adv. Exp. Med. Biol. 2012. V. 740. P. 603-638.
13. Gray R., Rajan A.S., Radcliffe K.A., Yakehiro M., Dani J.A. // Nature. 1996. V. 24. V. 383. № 6602. P. 713-716.
14. Sharma G., Vijayaraghavan S. // Neuron. 2003. V. 38. № 6. P. 929-939.
15. Jiang L., Role L.W. // J. Neurophysiol. 2008. V. 99. № 4. P. 1988-1999.
16. Kalappa B.I., Feng L., Kem W.R., Gusev A.G., Uteshev V.V. // Am. J. Physiol. Cell Physiol. 2011. V. 301. № 2. P. C347-361.
17. Prior C., Singh S. // Br. J. Pharmacol. 2000. V. 129. № 6. P. 1067-1074.
18. Balezina O.P., Fedorin V.V., Gaydukov A.Ye. // Bulletin of experimental biology and medicine. 2006. V. 142. *No* 1. P. 17-21.
19. Alkondon M., Albuquerque E.X. // Eur. J. Pharmacol. 1990. V. 191. № 3. P. 505-506.
20. Servent D., Antil-Delbeke S., Gaillard C., Corringer P.J., Changeux J.P., Menez A. // Eur. J. Pharmacol. 2000. V. 393. № 1-3. P. 197-204.
21. Tsetlin V.I., Hucho F. // FEBS Lett. 2004. V. 557. № 1-3. P. 9-13.
22. McLachlan E.M., Martin A.R. // J. Physiol. 1981. V. 311. P. 307-324.
23. Yuhas W.A., Fuchs P.A. // J. Comp. Physiol A. 1999. V. 185. № 5. P. 455-462.
24. Griguoli M., Scuri R., Ragozzino D., Cherubini E. // Eur. J. Neurosci. 2009. V. 30. № 6. P. 1011-1022.
25. Adelman J.P., Maylie J., Sah P. // Annu. Rev. Physiol. 2012.
V. 74. P. 245-269.
26. Wright M.C., Potluri S., Wang X., Dentcheva E., Gautam D., Tessler A., Wess J., Rich M.M., Son Y.J. // J. Neurosci. 2009. V. 29. № 47. P. 14942-14955.
27. Ulus I.H., Millington W.R., Buyukuysal R.L., Kiran B.K. // Biochem. Pharmacol. 1988. V. 37. № 14. P. 2747-2755.
28. Fischer V., Both M., Draguhn A., Egorov A.V. // J. Neurochem. 2014. V. 129. № 5. P. 792-805.
29. Minic J., Molgo J., Karlsson E., Krejci E. // Eur. J. Neurosci. 2002. V. 15. № 3. P. 439-448.
30. Santafe M.M., Lanuza M.A., Garcia N., Tomas J. // Eur. J. Neurosci. 2006. V. 23. № 8. P. 2048-2056.
31. Alkondon M., Pereira E.F., Cortes W.S., Maelicke A., Albuquerque E.X. // Eur. J. Neurosci. 1997. V. 9. № 12. P. 2734-2742.
32. Papke R.L., Bencherif M., Lippiello P. // Neurosci. Lett. 1996. V. 213. № 3. P. 201-204.
33. Papke R.L., Porter Papke J.K. // Br. J. Pharmacol. 2002. V. 137. № 1. P. 49-61.
34. Giniatullin R., Nistri A., Yakel J.L. // Trends Neurosci. 2005. V. 28. № 7. P. 371-378.
35. Zhong C., Talmage D.A., Role L.W. // PLoS One. 2013. V. 8. № 12. P. e82719.
36. Roncarati R., Di Chio M., Sava A., Terstappen G.C., Fumagalli G. // Neuroscience. 2001. V. 104. № 1. P. 253-262.
37. Balezina O.P., Bukiya A.N., Lapteva V.I. // Russian Journal of Physiology. 2005. V. 91. № 1. P. 61-70.
38. Dickinson J.A., Kew J.N., Wonnacott S. // Mol. Pharmacol. 2008. V. 74. № 2. P. 348-359.
39. Shen J.X., Yakel J.L. // Acta Pharmacol. Sin. 2009. V. 30. № 6. P. 673-680.
40. Lioudyno M., Hiel H., Kong J.H., Katz E., Waldman E., Parameshwaran-Iyer S., Glowatzki E., Fuchs P.A. // J. Neurosci. 2004. V. 24. № 49. P. 11160-11164.
41. Descarries L., Gisiger V., Steriade M. // Prog. Neurobiol. 1997. V. 53. № 5. P. 603-625.
42. Jones I.W., Wonnacott S. // J. Neurosci. 2004. V. 24. № 50. P. 11244-11252.

Phosphoryl Guanidines: A New Type of Nucleic Acid Analogues

M. S. Kupryushkin, D. V. Pyshnyi, D. A. Stetsenko*
Institute of Chemical Biology and Fundamental Medicine, Siberian Branch of the Russian Academy of Sciences, Lavrentiev Ave. 8, Novosibirsk 630090, Russia
*E-mail: dast@niboch.nsc.ru
Received 28.09.2014

ABSTRACT **A new type of nucleic acid analogues with a phosphoryl guanidine group is described. Oxidation of polymer-supported dinucleoside 2-cyanoethyl phosphite by iodine in the presence of 1,1,3,3-tetramethyl guanidine yields a dinucleotide with an internucleoside tetramethyl phosphoryl guanidine (Tmg) group as the main product. The Tmg group is stable under conditions of solid-phase DNA synthesis and subsequent cleavage and deprotection with ammonia. Oligonucleotides with one or more Tmg groups bind their complementary DNA or RNA with affinity similar to that of natural oligodeoxyribonucleotides.**
KEYWORDS **nucleic acid analogue; modified oligonucleotide; solid-phase synthesis; tetramethylguanidine; phosphoryl guanidine; phosphite.**
ABBREVIATIONS **MALDI-TOF – matrix-assisted laser-desorption ionization time-of-flight, RP-HPLC – reverse-phased high-performance liquid chromatography, TMG – 1,1,3,3-tetramethyl guanidine.**

Nucleic acid analogues of various structures are widely used in molecular biology and are regarded as promising therapeutic agents and probes for molecular diagnostics [1, 2]. The main impediment to the widespread application of nucleic acid derivatives for therapy is their generally poor cell uptake in the absence of specific transfection agents or delivery systems. The relative inefficiency of oligonucleotide penetration into cells can be at least partly attributed to their large net negative charge.

Only two types of nucleic acid analogues with theoretically charge-neutral backbones have been reasonably well studied over the past 20 years: peptide nucleic acids (PNA) [3] and phosphorodiamidate morpholino oligomers (PMO) [4]. Both types of analogues can bind natural DNA and RNA sequence-specifically and therefore they have found applications both in molecular biology and, in particular, in medicine as potential drugs [5, 6]. Taking this into account, the search for new nucleic acid analogues that could be used for development of oligonucleotide therapeutics capable of efficient cell penetration in the absence of transfection agents or other delivery means remains a highly relevant and challenging task.

We have shown that oxidation of 3',5'-dithymidine-β-cyanoethyl phosphite by iodine in pyridine in the presence of 1,1,3,3-tetramethyl guanidine (TMG) yields a dinucleotide with an internucleotide tetramethyl phosphoryl guanidine group (Tmg) as the main product (*Figure A*) (similarly, oxidation of trialkylphosphite with iodine in pyridine in the presence of a primary amine yields phosphoramidates [7]). Solid-phase oligonucleotide synthesis was carried out until hexathymidylate was formed. The oligonucleotide was cleaved from the polymer using a 25% aqueous ammonia solution at room temperature for 1 h; ammonia was subsequently removed in vacuo, and the solution containing the oligonucleotide was analyzed by RP-HPLC and MALDI-TOF mass spectrometry.

The elution profile of the reaction mixture (*Figure B*) showed that the main product is an oligonucleotide 5'-d(T_5p*T), where p* indicates the position of the Tmg group. Two main peaks with τ_R 16.7 and 17.6 min corresponded to the modified oligonucleotides; they were assigned to individual diastereomers resulting from chirality of the internucleotide phosphoryl guanidine group. The unmodified oligonucleotide dT_6 (τ_R 14.3) was also present as a by-product that most likely was formed via hydrolysis of the intermediate reactive iodophosphonium derivative by traces of moisture. The Tmg group exhibits pronounced hydrophobic properties: it is characterized by a longer retention time (τ_R) of the Tmg group-containing oligonucleotides compared with that of the unmodified oligonucleotide. Other modified oligothymidylates up to 20 nucleotide long have been synthesized, featuring one or two Tmg groups at various positions in the oligonucleotide chain. The presence of tetramethyl phosphoryl guanidine

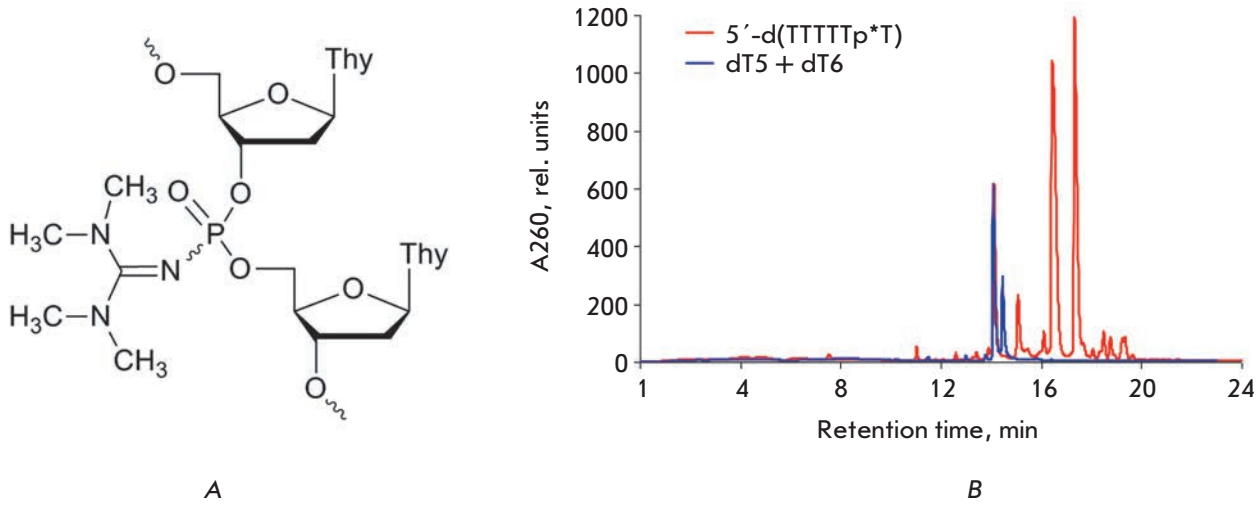

A *B*

Fig. *A* – Structure of an oligonucleotide with an internucleotide tetramethyl phosphoryl guanidine group (Tmg). *B* – Elution profile of an oligonucleotide 5'-d(T_5p*T), where p* indicates the position of the Tmg group. RP-HPLC was carried out on an Agilent 1200 HPLC system (USA) using a Zorbax SB-C18 (5 μm) 4.6 × 150 mm column with a gradient of acetonitrile (0 → 40%) in 20 mM triethylammonium acetate (pH 7) for 30 min; flow rate 2 mL/min

Table. Structures and molecular masses of phosphoryl guanidine oligonucleotide derivatives with the Tmg group

№	Oligonucleotide sequence, 5' → 3'	Molecular mass#		
		Calculated [M]	Experimental	
			$[M + H]^+$	$[M-H]^-$
1	d(TTTTTp*T)	1860.39	1860.35	1857.54
2	d(Tp*TTTTT)	1860.39	1860.34	1858.63
3	d(TCp*A)	941.80	942.17	938.97
4	d(TTTTTTTTTTTTTTTTTTTp*T)	6119.16	6121.13	6113.80
5	d(TTTTTTTTTTp*TTTTTTTTT)	6119.16	6121.54	–
6	d(TTp*TTTTTTTTTTTTTTTTT)	6119.16	6120.01	6114.19
7	d(TTp*TTTTTTTTTTTTTTTTTp*T)	6216.33	–	6221.11

p* indicates the position of the Tmg group.
#Positive or negative ion MALDI-TOF spectra were recorded on a Bruker Reflex III Autoflex Speed mass spectrometer (Germany) using 3-hydroxypicolinic acid as a matrix.

groups in the oligonucleotides was confirmed by MALDI-TOF mass spectrometry (*Table*).

Thermal denaturation experiments with optical registration of signal carried out at 10^{-5} M concentrations of each oligonucleotide in a 10 mM Na-cacodylate buffer (pH 7.2) containing 100 mM NaCl and 5 mM $MgCl_2$ showed a relatively small effect of an isolated Tmg group at the 3'-end or in the middle of the chain on the stability of the complementary complex formed by the modified oligodeoxyribonucleotides with poly(dA) or poly(rA) templates as compared with the unmodified oligonucleotide dT_{20}. The melting temperatures (T_m) for the complexes formed with a poly(rA) template were 48°C for 5'-d(T_{19}p*T) and 46.5°C for 5'-d(T_{11}p*T_9); for those formed with a poly(dA) template, the T_ms were 54 and 52.5°C, respectively, which was sufficiently close to the T_m of the complexes formed by the unmodified dT_{20} oligonucleotide with the same templates (48 and 55°C, respectively). Individual d(T_{19}p*T) diastereomers, which could be separated by RP-HPLC, showed only slightly different T_m values with the $dC_2A_{20}C_2$ template: 45.8°C for the diastereomer with a shorter retention time and 45.1°C for the diastereomer with a longer retention time, compared with 45.1°C for the unmodified dT_{20} oligonucleotide. The complex of an oligonucleotide d(T_{11}p*T_9) with the modification in the middle of the

chain, obtained as a mixture of diastereomers, melted at 44.7°C. These results are quite surprising, since a replacement of an internucleotide phosphate with the tetramethyl phosphoryl guanidine group leads to the substitution of a 20-atom group (including hydrogens) for one oxygen atom. The data indicated that oligodeoxyribonucleotides modified with Tmg groups can bind their complementary DNA and RNA to form stable complexes that differ only slightly in their thermal stability from the natural duplexes, a property which is a prerequisite for their therapeutic application.

To conclude, we have described a new type of nucleic acid analogues, phosphoryl guanidines [8], which is a third class of the formally charge-neutral oligonucleotide derivatives described so far in addition to known peptide nucleic acids (PNA) and morpholino oligomers (PMO). Our results indicate that oxidation of an internucleotide phosphite triester by iodine in pyridine in the presence of 1,1,3,3-tetramethylguanidine is a convenient method for obtaining oligonucleotide derivatives with the tetramethyl phosphoryl guanidine (Tmg) group. It is noteworthy that, unlike the previously described oligonucleotide analogues such as PNA or PMO, phosphoryl guanidine derivatives can be synthesized by conventional phosphoramidite chemistry using a standard DNA synthesizer. Therefore, it becomes possible to obtain various phosphoryl guanidine oligomers using a wide range of commercially available phosphoramidites, including those modified at the sugar residue and/or heterocyclic base.

We have shown that the Tmg group is stable under solid-phase oligonucleotide synthesis conditions, subsequent deprotection and cleavage from their polymer support of mixed-sequence oligodeoxyribonucleotides using standard 25% aqueous ammonia treatment at 55°C for 16 h. Oligonucleotides containing one or more Tmg groups are able to bind their complementary DNA and RNA sequences with affinity that is only slightly different from that of natural oligodeoxyribonucleotides, despite the steric bulk of the Tmg group. In our opinion, the results obtained indicate that this novel class of phosphoryl guanidine nucleic acid analogues may be quite promising for the designing of new biologically active oligonucleotide derivatives. ●

The authors are grateful to M. Kassakin for recording mass spectra and to Dr A. Lomzov for conducting thermal denaturation experiments.

This work was partly carried out with support of the Government of the Russian Federation for research projects implemented under supervision of world leading scientists (agreement No. 14.B25.31.0028 with S. Altman as a leading scientist) and the Russian Foundation for Basic Research (grant № 13-04-01176).

REFERENCES

1. Therapeutic Oligonucleotides: Methods and Protocols. Methods Mol. Biol. / Ed. Goodchild J. N.Y.: Humana Press, 2011. V. 764. 340 p.
2. Bell N.M., Micklefield J. // ChemBioChem. 2009. V. 10. № 17. P. 2691-2703.
3. Egholm M., Buchardt O., Nielsen P.E., Berg R.H. // J. Am. Chem. Soc. 1992. V. 114. № 5. P. 1895-1897.
4. Summerton J., Weller D. // Antisense Nucleic Acid Drug Dev. 1997. V. 7. № 3. P. 187-195.
5. Nielsen P.E. // Mol. Biotechnol. 2004. V. 26. № 3. P. 233-248.
6. Karkare S., Bhatnagar D. // Appl. Microbiol. Biotechnol. 2006. V. 71. № 5. P. 575-586.
7. Jäger A., Levy M.J., Hecht S.M. // Biochemistry. 1988. V. 27. № 19. P. 7237-7246.
8. Stetsenko D.A., Kupryushkin M.S., Pyshnyi D.V. WO patent application PCT/RU2014/000647, priority from 22.08.2014.

GENERAL RULES

Acta Naturae publishes experimental articles and reviews, as well as articles on topical issues, short reviews, and reports on the subjects of basic and applied life sciences and biotechnology.

The journal is published by the Park Media publishing house in both Russian and English.

The journal *Acta Naturae* is on the list of the leading periodicals of the Higher Attestation Commission of the Russian Ministry of Education and Science

The editors of *Acta Naturae* ask of the authors that they follow certain guidelines listed below. Articles which fail to conform to these guidelines will be rejected without review. The editors will not consider articles whose results have already been published or are being considered by other publications.

The maximum length of a review, together with tables and references, cannot exceed 60,000 symbols (approximately 40 pages, A4 format, 1.5 spacing, Times New Roman font, size 12) and cannot contain more than 16 figures.

Experimental articles should not exceed 30,000 symbols (20 pages in A4 format, including tables and references). They should contain no more than ten figures. Lengthier articles can only be accepted with the preliminary consent of the editors.

A short report must include the study's rationale, experimental material, and conclusions. A short report should not exceed 12,000 symbols (8 pages in A4 format including no more than 12 references). It should contain no more than four figures.

The manuscript should be sent to the editors in electronic form: the text should be in Windows Microsoft Word 2003 format, and the figures should be in TIFF format with each image in a separate file. In a separate file there should be a translation in English of: the article's title, the names and initials of the authors, the full name of the scientific organization and its departmental affiliation, the abstract, the references, and figure captions.

MANUSCRIPT FORMATTING

The manuscript should be formatted in the following manner:

- Article title. Bold font. The title should not be too long or too short and must be informative. The title should not exceed 100 characters. It should reflect the major result, the essence, and uniqueness of the work, names and initials of the authors.
- The corresponding author, who will also be working with the proofs, should be marked with a footnote *.
- Full name of the scientific organization and its departmental affiliation. If there are two or more scientific organizations involved, they should be linked by digital superscripts with the authors' names. Abstract. The structure of the abstract should be very clear and must reflect the following: it should introduce the reader to the main issue and describe the experimental approach, the possibility of practical use, and the possibility of further research in the field. The average length of an abstract is 20 lines (1,500 characters).
- Keywords (3 – 6). These should include the field of research, methods, experimental subject, and the specifics of the work. List of abbreviations.
- INTRODUCTION
- EXPERIMENTAL PROCEDURES
- RESULTS AND DISCUSSION
- CONCLUSION

  The organizations that funded the work should be listed at the end of this section with grant numbers in parenthesis.
- REFERENCES

  The in-text references should be in brackets, such as [1].

RECOMMENDATIONS ON THE TYPING AND FORMATTING OF THE TEXT

- We recommend the use of Microsoft Word 2003 for Windows text editing software.
- The Times New Roman font should be used. Standard font size is 12.
- The space between the lines is 1.5.
- Using more than one whole space between words is not recommended.
- We do not accept articles with automatic referencing; automatic word hyphenation; or automatic prohibition of hyphenation, listing, automatic indentation, etc.
- We recommend that tables be created using Word software options (Table → Insert Table) or MS Excel. Tables that were created manually (using lots of spaces without boxes) cannot be accepted.
- Initials and last names should always be separated by a whole space; for example, A. A. Ivanov.
- Throughout the text, all dates should appear in the "day.month.year" format, for example 02.05.1991, 26.12.1874, etc.
- There should be no periods after the title of the article, the authors' names, headings and subheadings, figure captions, units (s – second, g – gram, min – minute, h – hour, d – day, deg – degree).
- Periods should be used after footnotes (including those in tables), table comments, abstracts, and abbreviations (mon. – months, y. – years, m. temp. – melting temperature); however, they should not be used in subscripted indexes (T_m – melting temperature; $T_{p.t}$ – temperature of phase transition). One exception is mln – million, which should be used without a period.
- Decimal numbers should always contain a period and not a comma (0.25 and not 0,25).
- The hyphen ("-") is surrounded by two whole spaces, while the "minus," "interval," or "chemical bond" symbols do not require a space.
- The only symbol used for multiplication is "×"; the "×" symbol can only be used if it has a number to its right. The "·" symbol is used for denoting complex compounds in chemical formulas and also noncovalent complexes (such as DNA·RNA, etc.).
- Formulas must use the letter of the Latin and Greek alphabets.

- Latin genera and species' names should be in italics, while the taxa of higher orders should be in regular font.
- Gene names (except for yeast genes) should be italicized, while names of proteins should be in regular font.
- Names of nucleotides (A, T, G, C, U), amino acids (Arg, Ile, Val, etc.), and phosphonucleotides (ATP, AMP, etc.) should be written with Latin letters in regular font.
- Numeration of bases in nucleic acids and amino acid residues should not be hyphenated (T34, Ala89).
- When choosing units of measurement, SI units are to be used.
- Molecular mass should be in Daltons (Da, KDa, MDa).
- The number of nucleotide pairs should be abbreviated (bp, kbp).
- The number of amino acids should be abbreviated to aa.
- Biochemical terms, such as the names of enzymes, should conform to IUPAC standards.
- The number of term and name abbreviations in the text should be kept to a minimum.
- Repeating the same data in the text, tables, and graphs is not allowed.

GUIDENESS FOR ILLUSTRATIONS

- Figures should be supplied in separate files. Only TIFF is accepted.
- Figures should have a resolution of no less than 300 dpi for color and half-tone images and no less than 500 dpi.
- Files should not have any additional layers.

REVIEW AND PREPARATION OF THE MANUSCRIPT FOR PRINT AND PUBLICATION

Articles are published on a first-come, first-served basis. The publication order is established by the date of acceptance of the article. The members of the editorial board have the right to recommend the expedited publishing of articles which are deemed to be a priority and have received good reviews.

Articles which have been received by the editorial board are assessed by the board members and then sent for external review, if needed. The choice of reviewers is up to the editorial board. The manuscript is sent on to reviewers who are experts in this field of research, and the editorial board makes its decisions based on the reviews of these experts. The article may be accepted as is, sent back for improvements, or rejected.

The editorial board can decide to reject an article if it does not conform to the guidelines set above.

A manuscript which has been sent back to the authors for improvements requested by the editors and/or reviewers is reviewed again, after which the editorial board makes another decision on whether the article can be accepted for publication. The published article has the submission and publication acceptance dates set at the beginning.

The return of an article to the authors for improvement does not mean that the article has been accepted for publication. After the revised text has been received, a decision is made by the editorial board. The author must return the improved text, together with the original text and responses to all comments. The date of acceptance is the day on which the final version of the article was received by the publisher.

A revised manuscript must be sent back to the publisher a week after the authors have received the comments; if not, the article is considered a resubmission.

E-mail is used at all the stages of communication between the author, editors, publishers, and reviewers, so it is of vital importance that the authors monitor the address that they list in the article and inform the publisher of any changes in due time.

After the layout for the relevant issue of the journal is ready, the publisher sends out PDF files to the authors for a final review.

Changes other than simple corrections in the text, figures, or tables are not allowed at the final review stage. If this is necessary, the issue is resolved by the editorial board.

FORMAT OF REFERENCES

The journal uses a numeric reference system, which means that references are denoted as numbers in the text (in brackets) which refer to the number in the reference list.

For books: the last name and initials of the author, full title of the book, location of publisher, publisher, year in which the work was published, and the volume or issue and the number of pages in the book.

For periodicals: the last name and initials of the author, title of the journal, year in which the work was published, volume, issue, first and last page of the article. Must specify the name of the first 10 authors. Ross M.T., Grafham D.V., Coffey A.J., Scherer S., McLay K., Muzny D., Platzer M., Howell G.R., Burrows C., Bird C.P., et al. // Nature. 2005. V. 434. № 7031. P. 325–337.

References to books which have Russian translations should be accompanied with references to the original material listing the required data.

References to doctoral thesis abstracts must include the last name and initials of the author, the title of the thesis, the location in which the work was performed, and the year of completion.

References to patents must include the last names and initials of the authors, the type of the patent document (the author's rights or patent), the patent number, the name of the country that issued the document, the international invention classification index, and the year of patent issue.

The list of references should be on a separate page. The tables should be on a separate page, and figure captions should also be on a separate page.

The following e-mail addresses can be used to contact the editorial staff: vera.knorre@gmail.com, actanaturae@gmail.com, tel.: (495) 727-38-60, (495) 930-87-07